

INVESTIGATING *MYCOBACTERIUM TUBERCULOSIS* PH-DEPENDENT ADAPTATIONS

By

Benjamin K. Johnson

A DISSERTATION

Submitted to
Michigan State University
in partial fulfillment of the requirements
for the degree of

Microbiology and Molecular Genetics – Doctor of Philosophy

2016

ABSTRACT

INVESTIGATING *MYCOBACTERIUM TUBERCULOSIS* PH-DEPENDENT ADAPTATIONS

By

Benjamin K. Johnson

Mycobacterium tuberculosis (Mtb) is now classified by the World Health Organization as the number one killer in the world by a single infectious agent. Mtb is a successful pathogen because of its ability to overcome obstacles raised by the immune system. Sensing and responding to host cues is essential for Mtb pathogenesis. During infection, Mtb encounters a variety of anti-microbial environmental stresses including acidic pH. The two-component regulator system (TCS) PhoPR has been implicated in sensing and responding to acidic pH. Loss of this TCS results in severe attenuation during infection. Therefore it follows, that identification of inhibitors that disrupt this TCS-mediated adaptive response to acidic pH will provide therapeutic leads for further development of novel Mtb treatments and chemical probes to provide a deeper understanding of Mtb physiology at acidic pH.

To identify small molecule inhibitors of PhoPR-mediated signaling and Mtb growth at acidic pH, I have taken a high-throughput screening approach using a fluorescent reporter as a synthetic phenotype for PhoPR signaling activity. To analyze this large amount of data I have developed the *High throughput screening Automated Analysis and Retrieval of Putative hits* (HAARP) custom software suite to provide diagnostic plots and positive hit information. Using this tool, I identified the FDA-approved carbonic anhydrase inhibitor ethoxzolamide (ETZ) as a potent inhibitor of the PhoPR-regulon that attenuates Mtb virulence. Discovery of ETZ established a previously unrecognized link between carbonic anhydrase activity and PhoPR-signaling. We also identified a compound that targets Mtb thiol pools and demonstrated the

essentiality of maintaining redox homeostasis through these pools is required for resistance to oxidative stress at acidic pH. These findings highlight that modulation of processes Mtb uses to adapt to acidic environments can provide additional insight into physiological requirements and novel therapeutic targets.

While characterizing candidate inhibitors of the PhoPR-regulon and Mtb growth at acidic pH, I discovered a need to analyze or re-analyze transcriptional profiling data (RNA sequencing; RNA-seq). Current workflows available for bacterial RNA-seq analysis are limited and the tools for each step in the process are numerous. Thus, I developed the *Simple Program for Automated reference-based bacterial RNA-seq Transcriptome Analysis* (SPARTA) as a turn-key software package that can analyze raw Illumina sequencing reads and produce relevant plots and differential gene expression tables.

ACKNOWLEDGEMENTS

I would like to acknowledge and thank R.B. Abramovitch for providing mentorship and guidance. I would also like to thank R.A. Britton, S.Y. He, S.D. Manning, M.H. Mulks, M.B. Scholz, and T.K. Teal for their guidance. I thank C.J. Colvin and the members of the New England Regional Center of Excellence for providing support and data collection for the high throughput screening endeavors (Chapter 2). I would like to acknowledge G.B. Coulson for providing additional mentorship and data collection and analysis (Chapter 2). I am grateful to P.A.D. Champion, F. Mba Medie, and D.B. Needle for data collection and analysis (Chapter 3). I would like to thank T.K. Teal, M.B. Scholz, C.T. Brown, and P. Viswanathan for their guidance in software development (Chapter 4) and professional development opportunities to expand my teaching repertoire. I would like to thank N.M. Johnson for help in proofreading and formatting this dissertation. Finally, I would like to thank the MMG department and the Rudolph Hugh Fellowship.

TABLE OF CONTENTS

LIST OF TABLES	ix
LIST OF FIGURES.....	x
KEY TO ABBREVIATIONS	xiii
CHAPTER 1 – Taking aim at bacterial antibiotic resistance with antivirulence therapies	1
Abstract	1
Introduction	1
Molecular mechanisms bacteria use to cause disease and antivirulence compounds that inhibit them	5
Two-component regulatory systems	5
1. LED209	6
2. Ethoxzolamide.....	9
3. NSC inhibitors.....	12
Bacterial adherence mechanisms	15
1. Pilicides	16
2. Curlicides	19
Toxins and Specialized Secretion Mechanisms	22
1. Toxtazins	23
2. Ebselen	27
3. 7086, 7812, 7832	30
4. BPT15 and BBH7.....	33
Metabolic requirements during infection	38
1. D155931	39
2. V-13-009920, V-13-0110503 and V-13-012725	44
Conclusion.....	50
REFERENCES.....	52
CHAPTER 2 – High-throughput screening for inhibitors of <i>Mycobacterium tuberculosis</i> pathogenesis and growth.....	69
Preface	69
Introduction	71
Materials and Methods	73
High-throughput screening assay and data analysis.....	73
Primary hit reconfirmation assay	74
GFP quenching assay	74
Eukaryotic cytotoxicity assay.....	75
Inhibition of Mtb growth in macrophages assay	75
EC ₅₀ determination.....	76
Results	76
DosRST primary hits.....	76

PhoPR primary hits	80
Secondary assay results	86
REFERENCES	90

CHAPTER 3 – The carbonic anhydrase inhibitor ethoxzolamide inhibits the *Mycobacterium tuberculosis* PhoPR-regulon and Esx-1 secretion and attenuates virulence

Preface	93
Abstract	94
Introduction	95
Materials and Methods	96
Bacterial strains and growth conditions	96
High-throughput screening assay and data analysis	97
Transcriptional profiling and data analysis	98
Cell culture	98
Carbonic anhydrase activity assay	99
Cytoplasmic pH and phagosome acidification measurement	99
Analysis of mycobacterial lipids	100
Analysis of Esx-1 protein export	101
Macrophage infections	102
Quantitative single-cell imaging of Mtb exposure to ETZ in mice	102
Results	103
Identification of ethoxzolamide as an inhibitor of the PhoPR regulon	103
Lipid synthesis and Esx-1 protein secretion are modulated by ethoxzolamide.	108
Ethoxzolamide inhibits Mtb PhoPR regulon expression and growth in infected macrophages and mice	112
Discussion	118
Acknowledgements	122
APPENDIX	124
REFERENCES	133

CHAPTER 4 – Linking carbonic anhydrase activity and environmental pH sensing through PhoPR

Introduction	140
Materials and methods	142
Bacterial strains and growth conditions	142
Carbon dioxide modulation of PhoPR-dependent fluorescent reporter expression	142
“Knockout” ethoxzolamide analog experiment for off target effects	143
Carbonic anhydrase overexpression	143
Site directed mutagenesis of PhoR conserved histidine residues	145
Results	145
Expression of the PhoPR regulon is modulated by changes in carbon dioxide concentrations	145
Carbonic anhydrase inhibition deficient analog of ETZ does not affect PhoPR-mediated gene expression	149
Overexpression of Mtb carbonic anhydrase enzymes leads to additive inhibitory effects in combination with ETZ	151

Conserved histidine residues in the PhoR sensing loop suggest a putative mechanism of sensing proton concentrations	153
Discussion	157
REFERENCES.....	162
CHAPTER 5 – The small molecule PH036 depletes intracellular thiol pools and sensitizes <i>Mycobacterium tuberculosis</i> and <i>Staphylococcus aureus</i> to killing at acidic pH.....	165
Abstract	165
Introduction	166
Materials and Methods	167
Bacterial strains and growth conditions	167
EC ₅₀ determination and spectrum of activity in non-mycobacteria	167
Bactericidal Activity of PH036	168
Measuring intracellular redox state	169
Transcriptional profiling and data analysis	169
Structure activity relationship (SAR) and eukaryotic cytotoxicity of PH036.....	170
Fractional killing and potentiation of antimicrobials	171
Measurement of intracellular reactive oxygen species	171
Measurement of free thiol pools.....	172
Results	172
Identification of PH036 as an inhibitor of Mtb growth in a pH-dependent manner	172
PH036 exhibits a narrow spectrum of activity against non-mycobacterial species	175
Structure activity relationship analysis reveals the sulfone group is required for activity .	177
PH036 causes a thiol-associated stress response.....	179
PH036 causes accumulation of intracellular reactive oxygen species	185
Sensitivity to PH036 can be reversed through addition of low molecular weight thiols	188
PH036 depletes intracellular thiol pools	192
Discussion	194
APPENDIX	202
REFERENCES.....	206
CHAPTER 6 – Development of the computational analysis programs SPARTA and HAARP for evaluation of RNA-sequencing and high-throughput screening data	212
Preface.....	212
SPARTA: Simple Program for Automated reference-based bacterial RNA-seq Transcriptome Analysis	214
Abstract	214
Background	215
Implementation.....	216
Results and Discussion.....	223
Future Directions and Functionality.....	227
Conclusions	227
HAARP: High-throughput screening Automated Analysis and Retrieval of Putative hits.....	228
Abstract	228
Background	229
Implementation.....	230

Workflow procedure	230
Data normalization	233
Positive hit filtering.....	234
Results and Discussion.....	235
REFERENCES.....	236
CHAPTER 7 – Conclusions.....	240
REFERENCES.....	246

LIST OF TABLES

Table 1.1. 2-D structures of antivirulence compounds	49
Table 2.1. Table depicting compounds hand selected for follow-up studies	83
Table 5.1. Spectrum of activity for PH036	176
Table 5.2. Structure activity relationship of PH036 and its derivatives against Mtb growth and eukaryotic cytotoxicity	178

LIST OF FIGURES

Figure 1.1. Two-component regulatory sensor transduction systems	14
Figure 1.2. Bacterial adherence mechanisms through Type I, P pili, and curli biogenesis	21
Figure 1.3. Proposed mechanisms for toxtazins A and B inhibition of cholera toxin and toxin co-regulated pilus production	26
Figure 1.4. <i>C. difficile</i> toxin processing in host cells	29
Figure 1.5. Type III secretion system for delivery of bacterial effectors directly into the host cytoplasm	32
Figure 1.6. <i>Mycobacterium tuberculosis</i> type VII secretion of EsxA/EsxB	37
Figure 1.7. Screening scheme for inhibitors of DltA	43
Figure 1.8. Proposed reaction mechanism of cholesterol catabolism in <i>Mycobacterium tuberculosis</i>	48
Figure 2.1. High-throughput screening workflow	78
Figure 2.2. Scatter plot of primary screening hits for the DosRST screen	79
Figure 2.3. Scatter plot of primary screening hits for the PhoPR screen	82
Figure 2.4. Semi-quantitative real-time PCR of E548-0040 on PhoPR regulated genes	84
Figure 2.5. Inhibition of intracellular Mtb growth in infected macrophages	85
Figure 2.6. Reconfirmed compounds exhibiting pH-dependent activity	89
Figure 3.1. Ethoxzolamide inhibits <i>M. tuberculosis</i> CDC1551(<i>aprA'</i> ::GFP) fluorescence and <i>M. tuberculosis</i> carbonic anhydrase activity but does not alter cytoplasmic pH	105
Figure 3.2. ETZ inhibits the induction of the core PhoPR regulon at acidic pH	107
Figure 3.3. ETZ reduces the accumulation of sulfolipid and enhances accumulation of triacylglycerol and phthiocerol dimycocerosate	109
Figure 3.4. ETZ inhibits Esx-1 protein export	111
Figure 3.5. ETZ reduces PhoPR-regulated gene expression and survival in macrophages	113

Figure 3.6. ETZ treatment reduces PhoPR-regulated gene expression and survival <i>in vivo</i>	117
Figure 3.7. Model linking ETZ, CA, and regulation of the PhoPR pathway	121
Figure S3.1 ETZ inhibits the <i>phoPR</i> regulated <i>aprA</i> ::GFP in a dose dependent manner, but does not alter the pH of the medium or phagosome acidification	128
Figure S3.2 ETZ down-regulates the core PhoPR regulon, but not <i>phoP</i>	129
Figure S3.3 ETZ treatment alters lipid species production	130
Figure S3.4 Comparison of percent lung area affected of the section examined for each CMC and ETZ treated animal	131
Figure S3.5 Representative histopathological images from mock treated and ETZ treated mice	132
Figure 4.1. Relative concentration of carbon dioxide (CO ₂), bicarbonate (HCO ₃ ⁻), and carbonate (CO ₃ ²⁻) as a function of pH in aqueous solution	147
Figure 4.2. PhoPR-regulated gene expression is modulated in response to alterations in environmental carbon dioxide levels.....	148
Figure 4.3. “Knockout” analog of ETZ (N-methyl-ETZ) does not inhibit PhoPR-regulated reporter fluorescence	150
Figure 4.4. Mtb carbonic anhydrase overexpression in combination with ETZ treatment leads to enhanced inhibition of PhoPR regulated gene expression	152
Figure 4.5. Multiple alignment of <i>Mycobacterium sp.</i> PhoR sensor loop	155
Figure 4.6. PhoR His72Pro substitution leads to reduced <i>aprA</i> expression at acidic pH	156
Figure 5.1. PH036 inhibits M. tuberculosis growth in a pH-dependent manner and is bactericidal while promoting a reduced intracellular environment	174
Figure 5.2. Transcriptional profiling of Mtb treated with PH036	181
Figure 5.3. PH036 sensitizes Mtb to treatment by oxidizing agents and isoniazid.....	184
Figure 5.4. PH036 treatment leads to accumulation of reactive oxygen species	187
Figure 5.5. Exogenous addition of glutathione rescues PH036-mediated growth inhibition....	190
Figure 5.6. Thioredoxin (Trx) or glutathione synthesis (GSH) pathway <i>E. coli</i> mutants do not exhibit enhanced sensitivity to PH036	191

Figure 5.7. PH036 depletes intracellular free thiols.....	193
Figure 5.8. Speculative reaction mechanism of PH036 with a general disulfide.....	196
Figure 5.9. Speculative model for the mechanism of PH036.....	201
Figure S5.1. PH036 does not affect the cytoplasmic pH of Mtb at pH 5.7.....	203
Figure S5.2. The J analog of PH036 represents the core chemical scaffold required for pH-dependent activity	204
Figure S5.3. Superoxide dismutase deficient <i>S. aureus</i> exhibit enhanced sensitivity to PH036	205
Figure 6.1. SPARTA workflow diagram	217
Figure 6.2. Data analysis execution time comparison between SPARTA and Rockhopper2.....	226
Figure 6.3. HAARP workflow diagram	231
Figure 6.4. Examples of HTS screen-wide diagnostic scatter plots produced by HAARP	232

KEY TO ABBREVIATIONS

BBH.....	Benzyloxybenzylidene-hydrazine
BEI	Biodefense and Emerging Infections research resources repository
BMDM	Bone marrow-derived macrophages
BT.....	Bicarbonate transporter
BTP.....	Benzothiophene
CA	Carbonic anhydrase
cAMP	3'-5'-cyclic adenosine monophosphate
CcA.....	Concanamycin A
CDI.....	<i>Clostridium difficile</i> infection
CFU	Colony forming units
ChIP-seq.....	Chromatin immunoprecipitation sequencing
CMC	Carboxymethyl cellulose
CPD	Cysteine protease domain
CPM	Counts per minute
CT.....	Cholera toxin
CUP	Chaperone usher pathway
DMSO	Dimethyl sulfoxide
DTNB.....	Dithionitrobenzene
DTT	Dithiothreitol
EAEC	Enteroaggregative <i>E. coli</i>
EDTA	Ethylenediaminetetraacetic acid

EHEC	Enterohaemorrhagic <i>E. coli</i>
EtBr	Ethidium bromide
ETZ.....	Ethoxzolamide
EV.....	Empty vector
FDA.....	Food and Drug Administration
GSH.....	Glutathione
GTD.....	Glucosyltransferase domain
HAARP	High-throughput screening automated analysis and retrieval of putative hits
HK	Histidine kinase
HTS	High-throughput screening
IBC	Intracellular bacterial communities
INH.....	Isoniazid
IP ₆	1D-myo-inositol hexakisphosphate
LB.....	Luria-Bertani media
LEE.....	Locus of enterocyte effacement
MCC	Methyl citrate cycle
MDR-TB	Multi-drug resistant tuberculosis
MES.....	2-(N-morpholino)ethanesulfonic acid
MOI	Multiplicity of infection
MOPS	3-(N-morpholino)propanesulfonic acid
Msm.....	<i>Mycobacterium smegmatis</i>
Mtb	<i>Mycobacterium tuberculosis</i>
Mtb luc	<i>Mycobacterium tuberculosis</i> luciferase reporter strain

NCI..... National Cancer Institute

NIAD..... National Institute of Allergy and Infectious Disease

NIH..... National Institutes of Health

NMR..... Nuclear magnetic resonance

NSRB ICCBL..... Institute of Chemistry and Cell Biology

NTZ..... Nitazoxanide

OADC..... Oleic acid, albumin, dextrose, catalase supplement

OD..... Optical density

OE..... Over-expression

PBS..... Phosphate buffered saline

PDH..... Pyruvate dehydrogenase

PDIM..... Phthiocerol dimycocerosate

qRT-PCR..... Semi-quantitative real-time polymerase chain reaction

RNA-seq..... RNA sequencing

RNI..... Reactive nitrogen intermediates

ROS..... Reactive oxygen species

RPM..... Revolutions per minute

RR..... Response regulator

SAR..... Structure activity relationship

SL..... Sulfolipid

SPARTA..... Simple program for automated reference-based bacterial RNA-seq transcriptome analysis

SPR..... Surface plasmon resonance

T7SS	Type 7 secretion system
TAG.....	Triacylglycerol
TAT	Twin arginine translocation
TB.....	Tuberculosis
TCA.....	Tricarboxylic acid cycle
TCP.....	Toxin co-regulated pilus
TCS.....	Two-component regulatory system
TLC	Thin layer chromatography
UPEC.....	Uropathogenic <i>E. coli</i>
UTI	Urinary tract infection
WT.....	Wild-type
YOP	<i>Yersinia</i> outer protein
ZINC.....	ZINC is not commercial

CHAPTER 1 – Taking aim at bacterial antibiotic resistance with antivirulence therapies

Abstract

The continued rise of antibiotic resistant bacterial infections has motivated alternative strategies for target discovery and treatment of microbial infections. Antivirulence therapies represent one such approach. Through inhibition of *in vivo* required virulence factors these compounds disarm the pathogen rather than directly target viability or growth. This approach to treating bacterial-mediated disease has significant advantages over traditional antibiotics as they target factors specific for pathogenesis, potentially reducing selection for resistance and limiting collateral damage to the resident microbiota. Despite the theoretical potential for reducing selective pressure for resistance, recent studies have shown resistance mechanisms for several antivirulence drugs *in vitro*. However, the future of antivirulence therapies remains bright though additional considerations should be given to the environments the pathogen encounters the inhibitor and whether resistance may arise under these conditions. In this review, we present recently described antivirulence compounds, their relevant targets and mechanisms of action.

Introduction

It is no secret that our current practices for treating infectious diseases are not sustainable due to the misuse of antibiotics (1, 2). As a result, resistant bacterial strains have evolved for every known antibiotic (2). Antibiotic resistant infections are associated with increased mortality and are estimated to cause at least 2,000,000 illnesses annually in the United States and approximately 23,000 deaths (3). Additionally, drug resistant illnesses are expensive to treat and often require extended time in the hospital and thus pose additional risks for acquiring secondary infections (4). Confounding the issue further is the lack of new antibiotics entering the clinic that

have novel targets or modes of action. Pharmaceutical discovery and development of novel antimicrobials often requires billions of dollars and longer than a decade before being launched as a commercial drug (5). Together, the net result is a diminishing arsenal of antibiotics that can be used to treat microbial infections, prompting efforts to devise alternative strategies to treat these diseases.

Conventional drug discovery campaigns often seek to identify compounds with bactericidal or bacteriostatic activity by inhibiting targets essential for growth such as protein synthesis and DNA replication (6, 7). The approaches to identify these inhibitors can be classified into two general categories of drug discovery: target-based or phenotypic drug discovery (8). Target-based drug discovery typically uses a purified enzyme in a cell free system to discover inhibitors of a specific protein. Whole cell phenotypic drug discovery seeks to find inhibitors of live cells, usually without any particular target bias (8). Each method has potential drawbacks in further development of positive hits. Compounds isolated through target-based approaches often fail to translate to live cells due to a variety of factors including permeability through the cell envelope into the cytoplasm or efflux of the compound out of the cytoplasm. These shortcomings often require modification of the parent molecule to overcome these obstacles. Phenotypic drug discovery approaches also suffer from several issues, including difficulties in identifying targets of the inhibitors as this method is fundamentally an untargeted approach (8). Although these phenotypic drug discovery approaches were highly effective at finding microbial inhibitors that comprise many of our current antibiotics, treatment with these compounds exerts significant selective pressure for evolution of drug resistant bacteria (9). Antibiotic treatment can eliminate the susceptible bacterial population and leave behind resistant organisms that can rapidly grow to become the dominant proportion of the infecting population.

Further, intrinsic resistance mechanisms exist that predate antibiotic chemotherapy, such as efflux pumps, that can also yield resistance to antibiotic treatment (10, 11). Thus, we need new tactics and inhibitors to combat bacterial disease.

During the course of pathogenesis, invading bacteria need to overcome a variety of obstacles raised by the host immune system and the presence of the resident microbiota. Establishing a productive infection requires that the pathogen is able to sense and adapt to the changing environment within the host, including: pH changes, secretions from the host (e.g. mucus), physical barriers, reduced oxygen tension, as well as the active immune response functioning to prevent the pathogen from colonizing. Further, the ability of displacing or exploiting the resident microbiota is often required for establishing an infection. However, bacterial pathogens are equipped with a diverse array of strategies to subvert the host and cause disease (12). Therefore, disrupting the pathogen's mechanisms to thwart host defenses may serve as a therapeutic approach to combat bacterial infections.

Antivirulence compounds, sometimes referred to as anti-infective compounds, are an alternative approach to traditional therapeutic intervention of bacterial infections that have been actively investigated (13-16). The fundamental paradigm is that these molecules disarm the pathogen by targeting *in vivo* required virulence factors as opposed to growth cycle or viability mechanisms. By inhibiting the function of virulence-associated factors during infection, the invading bacteria are potentially left in a susceptible state to immune clearance and antibiotic-mediated killing (17-19). An additional advantage antivirulence compounds possess is that by not directly targeting growth or viability, the inhibitor will not exert as much selective pressure as traditional antimicrobials, slowing the emergence of resistance to the compound depending on the target and site of infection (18, 19). During broad-spectrum antibiotic therapy, there is no

discrimination between pathogen-associated targets and beneficial microbes, leading to a state of dysbiosis in the host microbiota. This can make the host susceptible to acute and chronic secondary infections (20, 21). Anti-infective compounds can limit off-target effects against the resident microbial community by directly targeting a pathogen-specific virulence factor. Together the increasing understanding of bacterial pathogenesis and sequencing-based approaches have yielded significant insights into the virulence requirements necessary during infection, revealing many potential targets to develop new treatments (13, 22-29).

High-throughput screening (HTS) approaches typically screen thousands of molecules to identify candidate antivirulence compounds. The positive hits derived from these HTS programs can serve a dual purpose: discovery of novel therapeutics and identification of chemical probes to study pathogenic processes. Development of an assay amenable to large-scale screening for inhibitors of *in vivo*-required virulence factors requires careful consideration as to how a positive hit will be distinguished from a negative hit (8). One common approach is to use reporter strains in whole cell phenotypic screens due to the large dynamic range between positive and negative controls to identify potential hits. Since many virulence factors are only required *in vivo*, coupling a fluorescent protein (e.g. GFP) or bioluminescence (e.g. luciferase) to virulence factor gene expression can provide an *in vitro* phenotype to measure whether its expression is modulated in response to a screening molecule. Additionally, HTS of a reporter strain infected model system (e.g. macrophage monolayers) can mimic the *in vivo* system while selecting for cell permeable molecules (30). Leveraging small molecules as probes to dissect the mechanisms of microbial disease through selective inhibition of a virulence factor can provide several advantages over conventional genetic approaches. Exogenous addition of a compound can lead to rapid and potentially reversible inhibition of a specific process during pathogenesis that can be

fine-tuned through dosing. Further, several small molecules may be combined to inhibit multiple steps during infection, similar to a multi-genic knockout strain. Chemical biology approaches bridge basic and translational research as they can aid in defining targets and regulation of virulence factors essential for pathogenesis and provide therapeutic leads for additional drug development (13).

This review provides a brief overview of selected mechanisms that bacteria use to cause disease and recently described antivirulence compounds that inhibit them. The discoveries reviewed here are of several newly identified antivirulence molecules and is not an exhaustive list; therefore we would direct the reader to other reviews for additional examples (14, 16, 31-33). Additional considerations are discussed regarding resistance mechanisms to anti-infective molecules and potential implications for future efforts to discover virulence inhibitors.

Molecular mechanisms bacteria use to cause disease and antivirulence compounds that inhibit them

Two-component regulatory systems

Bacteria must be able to sense environmental cues and co-ordinate adaptive responses to changes in the environment in order to survive and persist. A common sensing and response mechanism in bacteria is the two-component regulatory system (TCS) (34). Prototypical TCS are composed of a sensor histidine kinase (HK) and a response regulator (RR). The HK is usually located within the bacterial membrane and is responsible for sensing the environmental signal. Once the signal has been sensed, the HK will proceed to undergo an activating conformation leading to autophosphorylation activity through the ATPase domain. Phosphotransfer occurs through transfer of the phosphate from the HK at a conserved histidine residue to a conserved

aspartic acid on the response regulator receiver domain. The response regulator will typically dimerize after phosphorylation and act as a transcription factor to induce the regulatory cascade of genes involved in responding to the environmental cue (Figure 1.1.) (34). TCS represent a family of targets that are of particular interest to develop antivirulence therapies as they are not found in mammalian cells, limiting potential off target effects against host-associated factors (34). Further, deletion of TCS have been shown to significantly attenuate pathogenesis, though many TCS are dispensable for *in vitro* growth suggesting that screening for inhibitors of TCS *in vitro* requires a method alternative to growth inhibition, such as using a reporter system coupled to a gene regulated by the TCS (35, 36). Inhibiting virulence-associated TCS “blinds” the pathogen from sensing and coordinating an adaptive response to host cues, potentially sensitizing it to antibiotic treatment and immune clearance.

1. LED209

Many HKs are conserved throughout bacteria and respond to similar environmental cues suggesting potential for broad-spectrum antivirulence inhibitors. For example, the HK QseC contributes to virulence in at least 25 animal and plant pathogens including: *Salmonella enterica* serovar Typhimurium, enterohemorrhagic *E. coli* (EHEC), uropathogenic *E. coli* (UPEC), *Haemophilus influenzae*, and *Francisella tularensis* (37-45). As a bacterial receptor of epinephrine, norepinephrine, and the quorum sensing autoinducer-3 (AI-3), QseC contributes to transducing both host-derived stress signals and interkingdom signaling (Figure 1.1.) (46). In response to these cues, QseC controls the regulation of several virulence-associated genes by undergoing autophosphorylation and transfer of the phosphate to three RR: QseB, QseF, and KdpE. In EHEC, KdpE and QseF regulate induction of the locus of enterocyte effacement (LEE) and *stxAB* genes encoding Shiga toxin production, respectively. QseB regulates genes involved

in flagella and motility (47). Thus, QseC represents a conserved sensory transduction system that controls induction of virulence factors in many pathogens that could be targeted for development of broad-spectrum anti-infective therapeutics.

HTS of approximately 150,000 small organic compounds using a *LEE1::lacZ* reporter in EHEC identified the lead compound LED209 as an inhibitor of QseC-mediated signaling in response to AI-3 (Figure 1.1.) (44). LED209 [N-phenyl-4-(3-phenylthioureido)benzenesulfonamide] (Table 1.1. A) was discovered to be a pro-drug that allosterically modifies QseC lysine residues, impairing the function of the HK and inhibiting QseC-mediated induction of virulence factors *in vitro* and *in vivo* (44, 47). Extensive structure activity relationship (SAR) studies revealed that upon interaction of LED209 and QseC, the loss of an aniline group leads to the release of the active component of the molecule: isothiocyanate. Notably, this reaction was found to occur only inside the bacterium. Treatment of EHEC and *Salmonella* Typhimurium with isothiocyanate *in vitro* and in *ex vivo* infected macrophage models was able to mimic treatment by LED209. Mass spectrometry studies of labeled isothiocyanate revealed direct binding to two conserved QseC lysine residues (K256 and K427). Site-directed mutagenesis of each of these residues to arginine lead to a loss of function of QseC, suggesting that isothiocyanate binding these amino acids is the direct mechanism leading to inactivation of the HK.

To assess *in vivo* potency of LED209 against *Salmonella* Typhimurium, mice were orally administered LED209 or a vehicle control 30 minutes prior to bacterial challenge. At 3 and 6 days post-infection, pre-treatment with LED209 led to at least 50% survival against *S.* Typhimurium. To examine whether repeated dosing at the same concentration could lead to greater protective effects of the compound, mice were treated 3 hours prior, at the time of

bacterial challenge with *S. Typhimurium* and at 3, 6, 9, and 12 hours post-infection. Mock treated mice did not survive past 72 hours post-infection while 43% of LED209 treated mice survived up to 8 days (47).

F. tularensis encodes a QseC homolog that is the sole HK in the genome. Previous work on LED209 demonstrated reduced *F. tularensis* survival in macrophages, suggesting that *F. tularensis* may also be attenuated *in vivo* (44). Mice were infected with a lethal dose of *F. tularensis* via the intranasal route and LED209 was administered in two treatment regimens: 1, 3, 6, 9, 24 hours pre-infection or 1, 3, 6, 9, 24 hours post-infection. Remarkably, mice treated either pre- or post-infection had at least 50% survival after 8 days post-infection. Treatment of *F. tularensis* infected mice at 3 and 6 hours post-infection exhibited the greatest protection with 80% and 50% survival after 12 days (47).

Toxicological studies of LED209 revealed that the compound exhibits low toxicity in mice up to the maximal dose tested of 80 mg/kg. An important target that should not be inhibited by a compound is the human hERG. Inhibition of the normal function of hERG by a drug can cause an irregular heartbeat and may lead to death (48). LED209 exhibited little inhibitory activity against the hERG (4%) at 10 μ M LED209. Pharmacokinetic studies showed LED209 exhibited a short plasma half-life when administered via the intravenous route (5-20 mg/kg LED209). Oral dosing of LED209 ranging from 5-80 mg/kg led to non-proportional increases in plasma levels of the drug. Possible explanations for the non-linear dynamics include possible inhibition of drug efflux pumps in the gut or drug metabolism enzymes in the liver at high concentrations of LED209. Ultimately, it was concluded that the compound possessed good oral bioavailability (44, 47).

LED209 represents a first-in-class broad-spectrum antivirulence therapy that is currently in pre-clinical trials. However, owing to the fact that the compound does not directly inhibit bacterial growth, traditional regulatory measures of how to evaluate a new drug are insufficient for antivirulence therapies. Thus, additional molecular and chemical techniques are required to provide evidence that the compound in question is indeed inhibiting virulence and not directly targeting growth. Interestingly, it was noted that antivirulence therapies might provide a protective effect against repeated infections by the same pathogen as the immune system has been exposed to a pathogen that has been disarmed from its traditional mechanisms to subvert the host and establish an infection (47).

2. Ethoxzolamide

Mycobacterium tuberculosis (Mtb) remains a threat to global health. In 2014, approximately 9.4 million individuals became infected with Mtb and an estimated 1.5 million deaths were a result of this pathogen. The treatment course of antibiotic susceptible Mtb consists of a multi-drug regimen that must be taken for at least 6 months. In areas where public health infrastructure is lacking, patients that do not complete the full treatment course may develop a multi-drug resistant Mtb (MDR-TB) infection. However, patient non-compliance is not the only driver in the rise of MDR-TB. Mtb has a reasonably high mutation rate *in vivo* ($\sim 2\text{-}3 \times 10^{-10}$ mutations/bp/generation) and naturally drug resistant strains can exist in susceptible populations (49). MDR-TB infections were estimated to have caused approximately 190,000 deaths in 2014. Thus, faster acting antibiotics and alternative treatment options are needed.

Mtb contains at least 11 complete TCS and several orphaned HK and RR (50). pH is used as a cue for Mtb to modulate its physiology and these adaptations play a significant role in pathogenesis (51). The PhoPR TCS and its associated regulon have been studied extensively in

Mtb. It has been implicated in sensing and responding to variety of signals including acidic pH and chloride, though the precise signal(s) remain unknown (52-55). Further, a *phoPR* mutant is highly attenuated in animal models of infection (56-58). Therefore, it follows that inhibitors of PhoPR-dependent pH-driven adaptation may function to attenuate Mtb pathogenesis.

Ethoxzolamide (ETZ) was recently identified as an inhibitor of PhoPR signaling in Mtb, presumably through inhibition of carbonic anhydrase activity (59). ETZ (6-ethoxy-1,3-benzothiazole-2-sulfonamide) (Table 1.1. A) was discovered through an HTS of approximately 220,000 compounds using an *in vitro* whole cell phenotypic screen, employing a fluorescent reporter (Mtb CDC1551(*aprA*::GFP)) that is inducible at acidic pH in a PhoPR-dependent manner (54). In this screen, compounds that inhibited the production of GFP fluorescence while leaving growth of Mtb relatively unaffected were hypothesized to be putative inhibitors of PhoPR-signaling. Though PhoPR is required for replication and growth *in vivo*, it is dispensable for *in vitro* growth in rich medium. By taking an unbiased approach to identify Mtb PhoPR inhibitors, previously unrecognized regulators of the TCS at acidic pH could also be identified.

ETZ was classified as a candidate inhibitor of the PhoPR regulon through its ability to inhibit reporter fluorescence in a dose dependent manner while not impacting growth. It was noted that ETZ did not quench GFP fluorescence and did not significantly alter the pH of the media or the pH of Mtb's cytoplasm, suggesting an alternative mechanism leading to reduction of reporter fluorescence. ETZ is an FDA approved drug that was originally used to treat glaucoma, reduce the seizure threshold, and as a general diuretic through its carbonic anhydrase (CA) inhibitory activity. ETZ was shown to be able to inhibit Mtb carbonic anhydrase activity using purified recombinant enzymes (60-70). CA activity was assessed initially to define whether ETZ could act to inhibit Mtb carbonic anhydrases in whole cells and not just under cell

free conditions. Indeed, a complete inhibition of CA activity was observed by ETZ treatment relative to mock treated (DMSO) cultures following 6 days incubation (59). Together, these data established a previously unrecognized link between CA and PhoPR signaling in Mtb (Figure 1.1.). However, it is possible that additional unknown targets of ETZ exist in Mtb that may lead to inhibition of PhoPR-dependent reporter fluorescence.

To investigate the possibility of additional targets of ETZ in Mtb, transcriptional profiling of ETZ treated cultures and a *phoP* transposon mutant (*phoP*::Tn) was performed using RNA-seq. The results revealed a complete overlap of genes downregulated greater than two-fold in ETZ treated Mtb compared to *phoP*::Tn. This set of genes comprises the known core PhoPR regulon that are normally upregulated at acidic pH. Additionally, a few genes were upregulated by ETZ treatment that did not overlap with the *phoP*::Tn. Additional studies are needed to define whether these genes are regulated in a CA-dependent manner.

Phenotypes associated with attenuation of a *phoPR* mutant *in vivo* include altered virulence lipid production and the inability to secrete Esx-1 associated antigens ESAT-6 and CFP-10. Based on the transcriptional profiling data, it was hypothesized that ETZ could recapitulate these PhoPR-dependent defects *in vitro*. Indeed, treatment with ETZ leads to a reduction in the virulence-associated sulfolipid and a concomitant increase in long-chain fatty acids like triacylglycerol and phthiocerol dimycocerosate similar to a knockout of *phoPR* (54, 71, 72). Additionally, under Esx-1 export inducing conditions, ETZ treated Mtb inhibited secretion of the antigens ESAT-6 and CFP-10, similar to a *phoPR* or Esx-1 export system deficient mutant (73, 74). Taken together, Mtb treated with ETZ exhibits defects similar to a *phoPR* mutant, suggesting that during infection, the compound will lead to an attenuated phenotype.

To assess *in vivo* potency, mice were infected with a fluorescent reporter, similar to the strain used during the original screen. However, in addition to the PhoPR-dependent, acidic pH-inducible GFP expression (*aprA*'::GFP), a constitutive mCherry (*smyc*'::mCherry) is also expressed. Mice were treated orally with either ETZ or vehicle 5 days a week for 4 weeks. ETZ treatment resulted in a 0.75 log reduction in bacterial burden within the lungs and significantly reduced GFP fluorescence relative to the mock treated control.

Until recently, it was unknown whether Mtb PhoPR signaling could be inhibited through small molecules, despite the extensive literature supporting the necessity of the TCS during infection. Thus, this study represents the first proof-of-concept that this system in Mtb could be targeted and manipulated using small molecule inhibitors. Additionally, the use of fluorescent reporters can be leveraged for both antivirulence compound discovery and also for drug exposure *in vivo*. Repurposing compounds already approved for human use can provide a faster route for use in the clinic. Finally, this study has implicated a previously unrecognized link between CA and PhoPR-signaling.

3. NSC inhibitors

The PhoPQ TCS is the major virulence regulator in *Salmonella* Typhimurium and related Gram-negative pathogens (e.g. *Shigella flexneri* and *Neisseria meningitidis*). This TCS belongs to the OmpR/PhoB family, which represents approximately a third of the known TCS. Further, PhoPQ has been shown to sense and respond to a variety of signals in *Salmonella* Typhimurium including acidic pH, magnesium stress, and antimicrobial peptides. Upon transducing an activating signal PhoQ undergoes autophosphorylation and transfers a phosphate to the response regulator, PhoP. PhoP then homodimerizes and binds to specific promoter regions, inducing the expression of virulence-associated genes. Due to the broad conservation of structural homology

of the RR dimerization interface, which consists of an $\alpha 4$ - $\beta 4$ - $\alpha 5$ motif, it was hypothesized that disrupting the formation of the PhoP homodimer would prevent the PhoP-DNA interaction and may be applied as a broad-spectrum antivirulence therapy. Thus, a hybrid screening approach, combining structure-guided *in silico* docking studies and *in vitro* experimental verification was applied to a subset of potential inhibitors from the NCI database (75). Of the 1420 compounds virtually screened, 40 were examined experimentally. Using electrophoretic mobility shift assays, a series of 8 compounds were found to inhibit the *Salmonella* Typhimurium PhoP-DNA complex from forming *in vitro* (Figure 1.1.). Unfortunately, none of the compounds tested showed activity to disrupt the formation of PhoP homodimers though several avenues of experimental approaches were examined. Though the direct mechanism remains to be determined, these compounds represent a proof-of-concept study that the broadly conserved RR PhoP can be inhibited through small molecules.

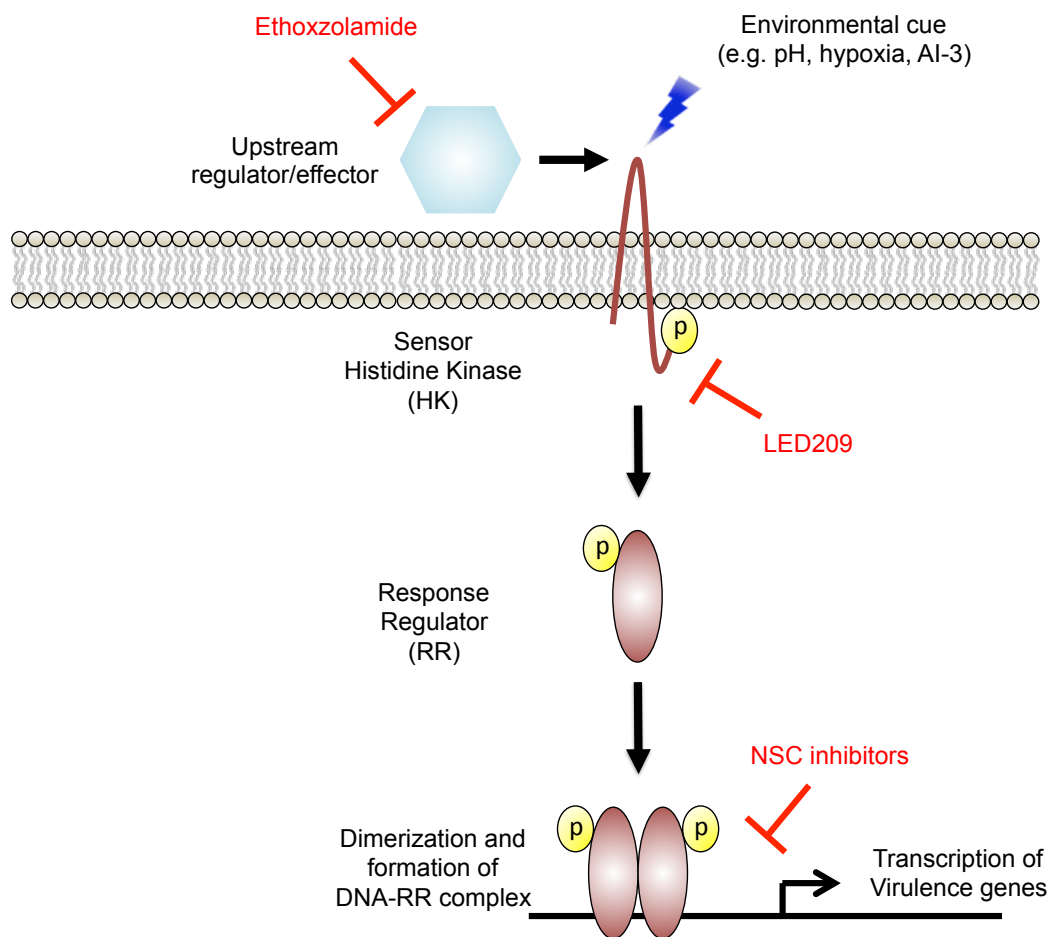


Figure 1.1. Two-component regulatory sensor transduction systems. A prototypical two-component sensor system (TCS) is composed of a histidine kinase (HK) and a response regulator (RR). Upon sensing the environmental signal, the HK undergoes autophosphorylation at a conserved histidine residue. The phosphate is transferred to the response regulator, which typically dimerizes and acts as a transcription factor to alter expression of virulence genes. All inhibitors are shown in red and associated steps at which they function to inhibit TCS signaling. Ethoxzolamide inhibits carbonic anhydrase activity in *Mycobacterium tuberculosis*, leading to downregulation of the virulence associated PhoPR regulon. LED209 directly binds to conserved lysine residues on the HK QseC and allosterically inhibits activation of virulence genes in multiple pathogens. A collection of inhibitors from the NSC inhibit the formation of the *Salmonella enterica* PhoP-DNA complex *in vitro*. Figure inspired by Rasko *et al.* (44).

Bacterial adherence mechanisms

Attachment of bacteria to a host surface is often the first step in initiating and establishing an infection. However, the host possesses several mechanisms to prevent and remove bacteria that do not have specialized apparatuses to facilitate attachment, including the coordinated beating of cilia in the nasopharynx; peristaltic motion in the gastrointestinal tract; and, the presence of the resident microbiota blocking access to invading bacteria (76). Further, pathogenic organisms will only attach and interact with a specific subset of cells that express the appropriate receptor for attachment (77-79). Additional steps beyond attachment by bacterial adhesins are often required for infection to proceed including internalization (e.g. phagocytosis), deeper tissue penetration, biofilm formation, and for some pathogens, systemic distribution (77-79). Pili are arguably the most commonly recognized structures for their role in attachment and virulence in several pathogens including uropathogenic *E. coli* (UPEC) – the leading causative agent of urinary tract infections (79-83). A pilus is a long multi-subunit appendage that is associated with having binding specificity at the terminal subunits, typically through FimH or PapG, for a specific receptor on the host cell surface (78, 79, 82, 83). Many pili and pili-like structures have been identified for several bacterial pathogens (77). However, for the purposes of this review, we will focus on two common and well-studied types associated with UPEC infections: 1) type I and P pilus and 2) curli. Assembly of the type I and P pilus is accomplished through a chaperone in the periplasmic domain and an outer membrane usher protein (82, 83). The chaperone facilitates the folding and transport of the pilin subunits and the usher aids in incorporation of each subunit into the growing appendage (Figure 1.2. A) (82, 83). Another appendage involved in attachment and virulence is termed curli. Curli are synthesized and secreted by an alternative mechanism relative to pili and appear as hair-like structures coating the

cell surface (84, 85). UPEC strains can use curli to form biofilms in the urinary tract to prevent washing out by the normal flow of urine (86, 87). Curli are composed of the major and minor subunits CsgA and CsgB. Interestingly, CsgB acts as an extracellular nucleation factor for the amyloid-like deposit of CsgA leading to the growth of the curli structure. Two soluble accessory chaperone-like proteins called CsgE and CsgF, are implicated in the transport of the curli subunits (CsgA and CsgB) from the Sec system to the outer membrane assembly protein CsgG (Figure 1.2. B) (84, 85).

1. *Pilicides*

The type I and P pili are assembled through what is known as the chaperone-usheer pathway (CUP) and are encoded on the *fim* and *pap* operons, respectively (82). The pilus appendage itself is composed of two parts: 1) the structural major subunit and 2) the flexible N-terminal tip required for receptor specificity and binding. For type I pili the major subunits are composed of FimA, while the minor subunits are made up of FimF, FimG, and the lectin containing terminal subunit FimH. The structural components of P pili are comprised of PapA, while the flexible tip is composed of PapE, PapF, PapK, and the lectin containing terminal subunit PapG (82). All subunits are first secreted in an unfolded state past the inner membrane into the periplasmic space via the SecYEG machinery. The chaperones FimC and PapD proceed to fold and stabilize each subunit for type I and P pili, respectively. Chaperone-subunit complexes are then transferred to the usher (FimD or PapC) that facilitates subunit assembly and elongation of the pili (Figure 1.2. A) (82).

These systems have been extensively studied and crystal structures exist for each component of the type I and P pili machinery (82). Thus, leveraging the available structural data, a series of compounds known as pilicides were rationally designed to directly inhibit type I and P

pili biogenesis and belong to the bicyclic 2-pyridones class of molecules (Table 1.1. B) (88-90). Pilicides do not inhibit bacterial growth but were shown to interfere with UPEC attachment via a hemagglutination-mediated manner (89). Co-crystallization of pilicide 2c with PapD revealed binding on the surface of the chaperone known to interact with the usher PapC. Additional surface-plasmon resonance (SPR) studies showed that the pilicide prevents FimC-FimH from interacting with the usher (FimD). Together, the proposed mechanism for pilicide inhibition of type I and P pili biogenesis is by preventing the chaperone from transferring the pili subunit to the usher (Figure 1.2. B) (89).

Crystal structure-based rational design of FimH antagonists were synthesized, resulting in the promising group of inhibitors known as biphenyl mannosides (91, 92). These initial compounds were efficacious in treating acute, chronic, and antibiotic-resistant UPEC infections *in vivo* (93-95). However, this first round of FimH antagonists suffered from low bioavailability. Thus, additional co-crystal structures of lead mannosides bound to the FimH lectin domain were obtained. Using a rational design strategy, new FimH antagonists were developed with improved drug-like properties (Figure 1.2. A). This new group of inhibitors are known as biaryl mannosides (96). In particular, isoquinolone 22 (2-methyl-4-(1-oxo-1,2-dihydroisoquinolin-7-yl)phenyl α -D-mannopyranoside) (Table 1.1. B) was shown to exhibit low nanomolar potency against FimH based on a hemagglutination assay, improved oral bioavailability and a 10-fold enhanced reduction of bacterial load in a chronic UTI mouse model of infection. The biaryl mannoside 22 analog is a promising lead molecule for further development as an antivirulence therapeutic to treat UTIs (96).

Recent studies have shown that the antiparasitic drug nitazoxanide (NTZ) (Table 1.1. B) is broadly active against the CUP in both enteroaggregative *E. coli* (EAEC) and UPEC strains

(97, 98). NTZ was shown to not directly target growth in EAEC or UPEC but was capable of inhibiting assembly and biogenesis of aggregative adherence fimbriae, type I and P pili (97). Additionally, NTZ inhibited type I pilus-mediated hemagglutination activity in both EAEC and UPEC strains, leading to a shortened duration of infection in EAEC infected animals due to bacterial wash out (97-99). It was noted that NTZ treatment of UPEC reduced the total amount of both the PapC and FimD usher proteins in the outer membrane fraction in a dose dependent manner. To investigate the mechanism for reducing usher protein localization to the outer membrane by NTZ, a series of PapC truncation mutants were examined to identify the precise component of the usher that was disrupted. It was found that NTZ prevents proper folding of the transmembrane β -barrel pore (Figure 1.2. A) (98).

NTZ is broadly active against strict anaerobic pathogens including *Clostridium difficile*, *Helicobacter pylori*, and *Campylobacter jejuni* through inhibition of pyruvate ferredoxin oxidoreductase (100, 101). However, the *Enterobacteriaceae* lack this target and NTZ is effective as a pilicide below the growth inhibitory concentrations observed for the pathogenic anaerobes (97, 98, 102, 103). Repurposing NTZ as a putative antivirulence therapy may be possible as it is an approved treatment for giardiasis and cryptosporidiosis, potentially expediting the process for entering clinical use.

Pilicide discovery and characterization has provided additional insight into the molecular mechanisms governing pili biogenesis. Further, this group of compounds provides an attractive approach to treating pathogenic *E. coli* by inhibiting the ability to adhere to host surfaces and preventing the establishment of infection.

2. Curlicides

Previous studies of UPEC UTIs have suggested that additional mechanisms beyond type I pili formation are required for colonization and establishing a productive infection. Curli are small, hair-like structures that are produced by UPEC strains and are implicated in biofilm formation (84, 85). These amyloid-aggregative features have also been shown to act synergistically with cellulose to promote biofilm formation, host colonization, and survival in a variety of environments (104). Taken together, identification of inhibitors that target both type I pili formation and curli production may provide a therapeutic approach to effectively disrupt colonization, invasion, and biofilm formation of UPEC.

The thiazolo ring-fused 2-pyridones have been shown to act as type I pilicides by preventing the chaperone-pili subunit complex from transferring the subunit to the usher for polymerization and secretion of the pilus (Table 1.1. B) (89). Through exchange of a cyclopropyl group for a CF₃-phenyl moiety on a lead thiazolo ring-fused 2-pyridone pilicide, the analog gained the ability to inhibit Alzheimer's-associated β -amyloid polymerization *in vitro* (105). Encouraged by the ability of the pilicide analog (FN075) (Table 1.1. B) to inhibit amyloid polymerization, it was hypothesized that this compound may also disrupt curli formation. Indeed, FN075 was able to inhibit formation of curli in the UPEC strain UTI89 and disrupt CsgA polymerization *in vitro* by directly binding to the curli major subunit (Figure 1.2. B) (86). To examine whether FN075 could inhibit biofilm formation, curli-dependent biofilm models were identified in UTI89. Pellicle formation was identified as a method to screen for curli-dependent biofilm inhibitors as a curli deficient mutant (UTI89 Δ csgA) could not form a pellicle and expressing *csgA* in trans could restore the wild-type biofilm. FN075 treated cultures resulted in loss of pellicle formation, similar to the *csgA* mutant, suggesting that the compound can inhibit

curli-dependent biofilms. Further, FN075 was able to completely inhibit type I pili biofilm formation. To assess *in vivo* potency of the curlicide, mice were challenged with either UTI89 cultures pretreated with FN075 or an equivalent volume of DMSO (mock treated control) under type I pili inducing conditions. FN075 pretreated cultures resulted in a 10-fold reduction in bladder bacterial load 6 hours post infection relative to the DMSO control. Additionally, the curlicide significantly reduced the total number of IBCs in murine bladders (86).

Taken together, FN075 represents a unique anti-virulence therapy that also exhibits anti-biofilm activity against two adherence mechanisms of UPEC (Figure 1.2. B). The power of structure-based rational inhibitor design is demonstrated in several examples of pilicide and curlicide discovery and subsequent characterization. This modified targeted screening approach can provide researchers molecular probes to dissect previously unknown molecular dynamics of a pathogenic process like pili or curli biogenesis, and improve inhibitors to possess enhanced drug-like properties.

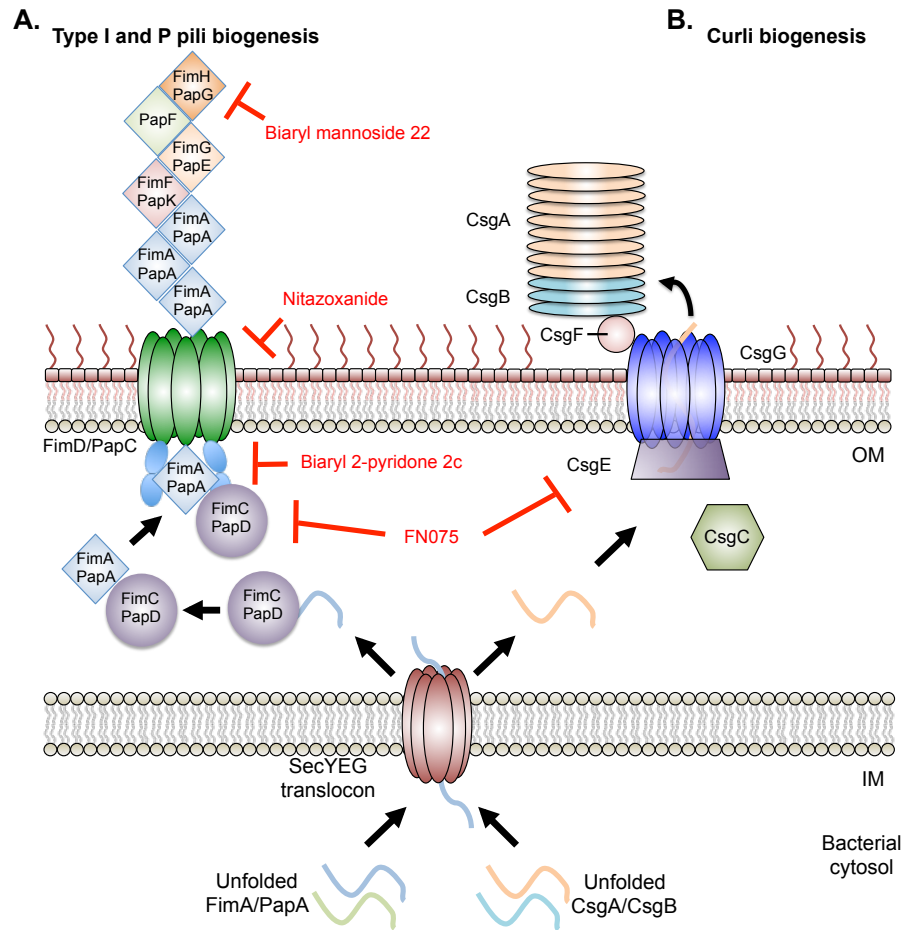


Figure 1.2. Bacterial adherence mechanisms through Type I, P pili, and curli biogenesis. A. Graphical representation of type I and P pili biogenesis in Gram-negative pathogens, such as uropathogenic *E. coli* (UPEC). Unfolded pilin subunits are translocated through the SecYEG translocon into the periplasm. A chaperone (FimC/PapD) folds and stabilizes the subunit, passing it to the secretion machinery for incorporation into the growing appendage. FimD/PapC receives the folded subunit from the chaperone and adds the given subunit to the actively polymerizing pilus. Biaryl mannose 22 inhibits the mannose binding capacity of the terminal subunit (FimH/PapG) in type I and P pili. Nitazoxanide inhibits pore formation of the secretion/polymerization complex (FimD/PapC). Biaryl 2-pyridone 2c binds to the surface of the chaperone (FimC/PapD) and prevents the subunit transfer to the secretion/polymerization complex (FimD/PapC). B. Graphical representation of curli biogenesis in UPEC. Unfolded curli subunits (CsgA/CsgB) are translocated into the periplasm by the SecYEG secretion machinery. CsgC is proposed to act as a chaperone, preventing premature amyloid formation by the unfolded curli subunits (106). CsgE and CsgF act as soluble chaperones to stabilize CsgA/CsgB and transfer the unfolded subunits to the outer membrane assembly protein CsgG. CsgB acts as a nucleation factor for CsgA amyloid formation and deposition onto the growing appendage. FN075 inhibits CsgA polymerization and due to its parent structure, also acts as an inhibitor similar to the biaryl 2-pyridone 2c. All inhibitors are denoted in red. OM – bacterial outer membrane; IM – bacterial inner membrane. Figure inspired by Costa *et al.* (82).

Toxins and Specialized Secretion Mechanisms

Toxin production and delivery to host tissues is essential for several pathogens to promote infection and dissemination. A variety of mechanisms exist to transport toxins and effectors from within the bacterial cytoplasm to the extracellular environment, or in some cases, directly injected through host membranes. Secreted toxins can actively disrupt host intracellular signaling cascades, lead to rearrangements of cytoskeletal architecture, loosen tight junctions, and promote rapid efflux of electrolytes in addition to numerous other effects toxins can have on the host (107). Ultimately, the toxins enhance pathogen survival, invasion or attachment during infection by hijacking or disrupting host processes (Figure 1.3. and Figure 1.4.) (108, 109). Inhibitors of toxin production or function are attractive approaches for the development of antivirulence compounds.

Several microbial pathogens possess specialized secretion machinery to deliver toxins directly into the host cytoplasm. Specifically, the type III, IV, and VI secretion systems (T3SS, T4SS, and T6SS, respectively) are implicated with the ability of direct bacterial toxin injection (82). Particular attention has been given to the T3SS which is broadly conserved in Gram-negative pathogens including *Yersinia sp.*, *Salmonella sp.*, *Shigella sp.*, EHEC, and *Pseudomonas aeruginosa* (Figure 1.5.) (107). The T3SS is often required for virulence and inhibitors of this toxin delivery system may attenuate pathogenesis (108, 109). Recent reviews cover the discovery of antivirulence compounds against T3SS (33, 110), and this chapter will focus on a new discovery in *Y. pestis* (111).

Mycobacterium tuberculosis (Mtb) uses type VII secretion system (T7SS) to export several effectors involved in pathogenesis (Figure 1.6.). Mtb possesses five T7SS termed ESX-1 to ESX-5, though active secretion has not yet been demonstrated for ESX-2 and ESX-4 (112).

The ESX-1 locus is required for transport of two mycobacterial effectors known as EsxA and EsxB (ESAT-6 and CFP-10, respectively). Importantly, the inability to secrete these proteins is associated with the attenuation of the live-vaccine strain *Mycobacterium bovis* BCG (112). Thus, small molecules that target ESX-1 through either inhibiting the secretion machinery directly or its regulation will likely lead to decreased survival of Mtb *in vivo*.

1. Toxtazins

The human pathogen *Vibrio cholerae* causes severe dehydration, vomiting and watery diarrhea. Once in the gut, *V. cholerae* secretes cholera toxin (CT) that causes increased intracellular levels of cyclic AMP (cAMP) in epithelial cells (113). As a result, sodium uptake is decreased, leading to a concomitant extrusion of chloride in the lumen of the gut, producing the characteristic symptoms of watery diarrhea and dehydration (114). The virulence regulator ToxT regulates expression of two of the major virulence factors in *V. cholerae*: CT and the toxin co-regulated pilus (TCP) (Figure 1.3.) (115, 116). ToxT-mediated expression of CT and the TCP has been shown to be inversely regulated by environmental signals relevant to the human gut including bicarbonate (inducing) and bile (repressive) (117). Thus, it follows that identification of compounds that inhibit ToxT will attenuate *V. cholerae*. Indeed, as reviewed elsewhere (13, 14, 16), the antivirulence compound virstatin was discovered as an inhibitor of ToxT dimerization, leading to reduced colonization in an infant mouse model of cholera infection (118, 119). However, resistance to virstatin has been demonstrated, suggesting that additional inhibitors with alternative targets are necessary (119).

Recently, toxtazins A, B and B' were identified in a whole cell screen for inhibitors of ToxT expression (Table 1.1. C) (31). Using a fluorescent reporter (*toxT'*::GFP), approximately 63,000 small molecules were screened for compounds capable of reducing GFP fluorescence but

not significantly affecting growth. The advantage of this screen was that by probing the *toxT* pathway directly, the identified inhibitors would be restricted to those that disrupt expression of the regulator and not general phenotypes associated with reducing virulence.

Toxtazins were able to reduce the production of both CT and the TCP under multiple growth conditions and across tested biotypes (classical and *El Tor*), suggesting that the compounds were affecting *toxT* expression and thus, validating the screen. Toxtazin B was shown to be the most potent in an infant mouse model of *V. cholerae* infection. The compound was able to reduce the bacterial burden approximately 100-fold relative to the DMSO control. Interestingly, toxtazin A had no appreciable effect on bacterial burden *in vivo* and it was hypothesized that this apparent lack of activity may be due to poor bioavailability at the concentrations tested. To verify that *in vivo* toxtazin activity was a result of inhibiting *toxT* expression, at the time of infection, the same inoculum was added to Luria-Bertani (LB) broth treated the same as the mice. Neither toxtazin A or B inhibited *V. cholerae* growth at the tested concentrations. These data suggest that toxtazin B may have therapeutic potential against *V. cholerae*.

To identify the targets of toxtazins A and B, a systematic examination of the *toxT* regulatory cascade was performed. *toxT* expression is regulated by ToxR and TcpP. Additionally, *tcpP* expression is regulated by AphA and AphB. Toxtazin A was shown to not alter expression of *toxR* or *tcpP*, while toxtazin B exhibited reduced TcpP protein and transcript levels (Figure 1.3.). Toxtazin B did not modulate expression of *aphA* or *aphB* and neither compound affected AphA or AphB protein levels. Restoration of ToxT in toxtazin treated cultures by ectopic expression of the regulator resulted in restoration of CT, suggesting that both compounds act upstream of ToxT.

The precise mechanisms for toxtazin A and B remain to be determined, though initial proteomic evidence suggests that *V. cholerae* treated with toxtazin A mounts a general stress response. However, additional data are needed to investigate this observation. The proposed model suggests that toxtazin A inhibits *toxT* transcription and that toxtazin B leads to reduced expression of *tcpP* (Figure 1.3.). This study identified toxtazin B as a candidate for additional development as an alternative therapeutic intervention strategy for cholera infections. Further, these compounds can act as chemical probes to inhibit ToxT-mediated virulence at separate points in the regulatory cascade, potentially enabling additional characterization of the pathway.

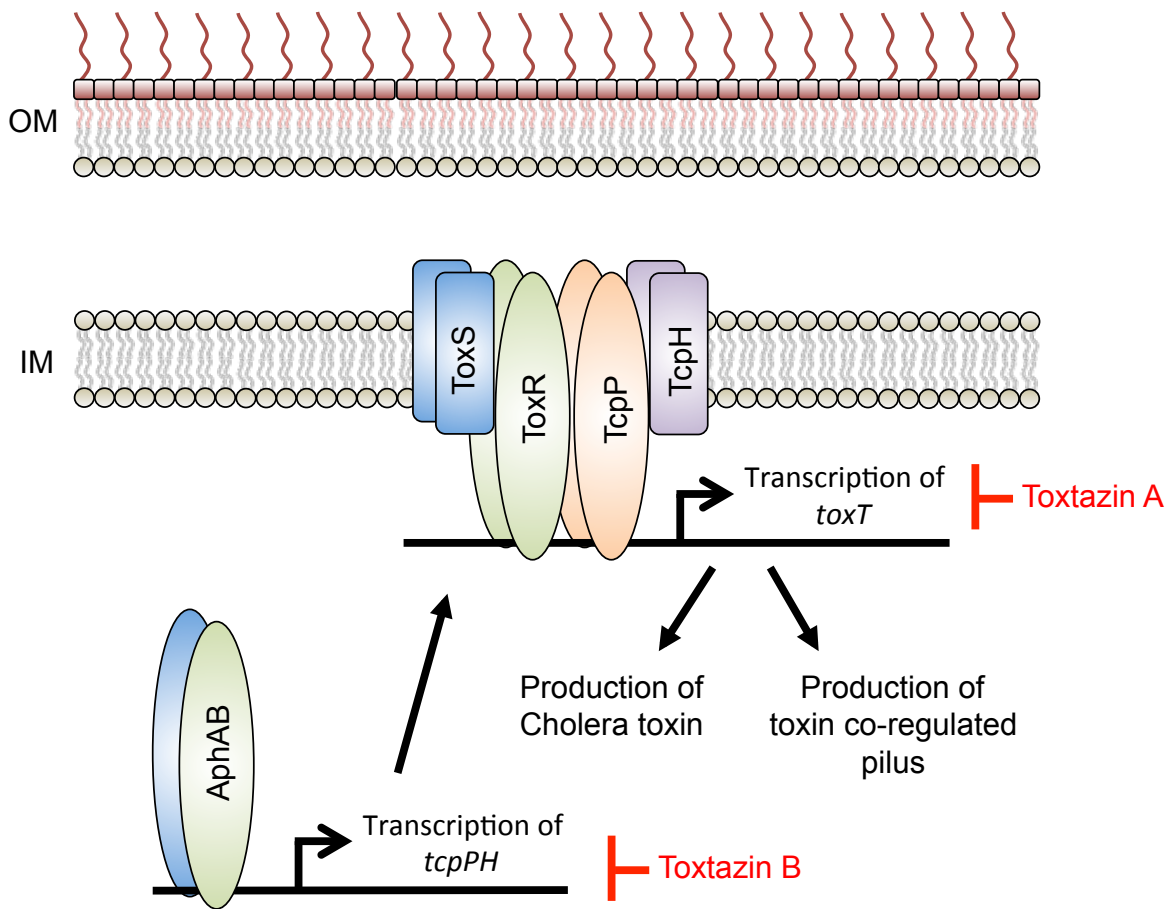


Figure 1.3. Proposed mechanisms for toxtazins A and B inhibition of cholera toxin and toxin co-regulated pilus production. ToxT regulates transcription of genes responsible for producing cholera toxin (CT) and the toxin co-regulated pilus (TCP), which are two virulence factors involved in cholera infections. Toxtazin A inhibits *toxT* transcription and is proposed to act by causing a bacterial general stress response, feeding back to shut down transcription of *toxT*. Toxtazin B inhibits transcription of *tcpPH* and is proposed to act by reducing intracellular levels of TcpP, leading to reduced transcription of *toxT*. Both mechanisms remain to be fully defined. Inhibitors are in red. OM – bacterial outer membrane; IM – bacterial inner membrane. Figure inspired by Anthouard *et al.* (31).

2. Ebselen

Clostridium difficile infections (CDI) are the leading cause of hospital-acquired diarrhea and the etiological agent of pseudomembranous colitis (120). Treatments for CDI include antibiotic therapy and fecal bacteriotherapy. However, recurrent infections are as high as 25% and are often associated with antibiotic resistant strains (121, 122). Fecal bacteriotherapy remains controversial despite its success rate, as the long-term effects are not well understood (123, 124). Only toxigenic strains of *C. difficile* are implicated in CDI (125, 126). Disease causing *C. difficile* strains encode either one or both toxins: TcdA and TcdB (125-127). The toxins are composed of a putative receptor-binding domain, a transmembrane domain, a cysteine protease domain (CPD), and a glucosyltransferase domain (GTD) (128). Upon endocytosis and exposure to acidic pH, the toxin undergoes membrane translocation and exposure to the host sugar 1D-myo-inositol hexakisphosphate (IP₆). IP₆ allosterically activates the CPD allowing cleavage and release of the GTD. The GTD glucosylates the Rho/Rac GTPases leading to cytoskeletal rearrangement, inflammation, and fluid loss associated with CDI (Figure 1.4.) (129). Thus, inhibitors of activating steps in the process of releasing GTD may lead to reduced toxicity and better patient outcomes from CDI.

A targeted HTS using a fluorescent reporter of CPD activity identified 44 potential inhibitors of the protease (130). To refine this pool, cell rounding assays were performed to identify the cytoprotective effects of each inhibitor against full-length toxin. Ebselen (2-phenyl-1,2-benzoselenazol-3-one) (Table 1.1. C) was discovered as a potent inhibitor of toxin-mediated cell death and as an immediate candidate for further development as it is in phase II clinical trials for unrelated diseases (131). Notably, ebselen exhibits glutathione peroxidase-like activity and has been identified as an inhibitor of additional bacterial virulence factors including: thioredoxin

reductase, antigen85, and diguanylate-cyclase enzymes (132-135). Together, this suggests that ebselen may be applied as a broad-spectrum antivirulence therapy.

Ebselen inhibited recombinant CPD and full-length toxin in a dose-dependent manner, exhibiting an IC_{50} of 17.2 nM against TcdB (Figure 1.4.). Mass spectrometry analysis confirmed covalent modification of the active-site cysteine and, unexpectedly, an additional cysteine on the opposing CPD surface. To investigate whether ebselen inhibited release of the GTD, western blot analysis revealed a dose-dependent reduction in glucosylation of Rac1, a Rho/Rac GTPase, consistent with CPD-mediated cleavage being inhibited. A non-cleavable mutant of TcdB (TcdB L543A) exhibited similarly delayed kinetics of toxin-induced cell death as ebselen treated wild type toxin, underscoring the proposed mechanism of ebselen inhibition of TcdB. To assess the *in vivo* effects of ebselen treatment, mice pre-treated with a lethal dose of TcdB were injected with either ebselen or DMSO. After 12 hours, DMSO treated mice exhibited significant signs of toxicity while ebselen treated mice had no observable changes in vital signs after 3 days. Next, mice were treated with antibiotics to disrupt the resident microbiota and then challenged with a toxigenic multi-drug resistant strain of *C. difficile*. Animals were treated with either vehicle or ebselen for 5 days via oral gavage. Ebselen reduced CDI associated tissue pathology in a dose-dependent manner, however, bacterial burden between DMSO and ebselen treated animals were similar. If ebselen concludes clinical trials for its alternative uses, repurposing this compound as an alternative, non-antibiotic therapy to neutralize the toxicity of TcdA and TcdB in CDI may be expedited. Additionally, due to inhibitory effects against virulence factors in other pathogens, ebselen is another promising candidate for exploration as a broad-spectrum antivirulence therapy.

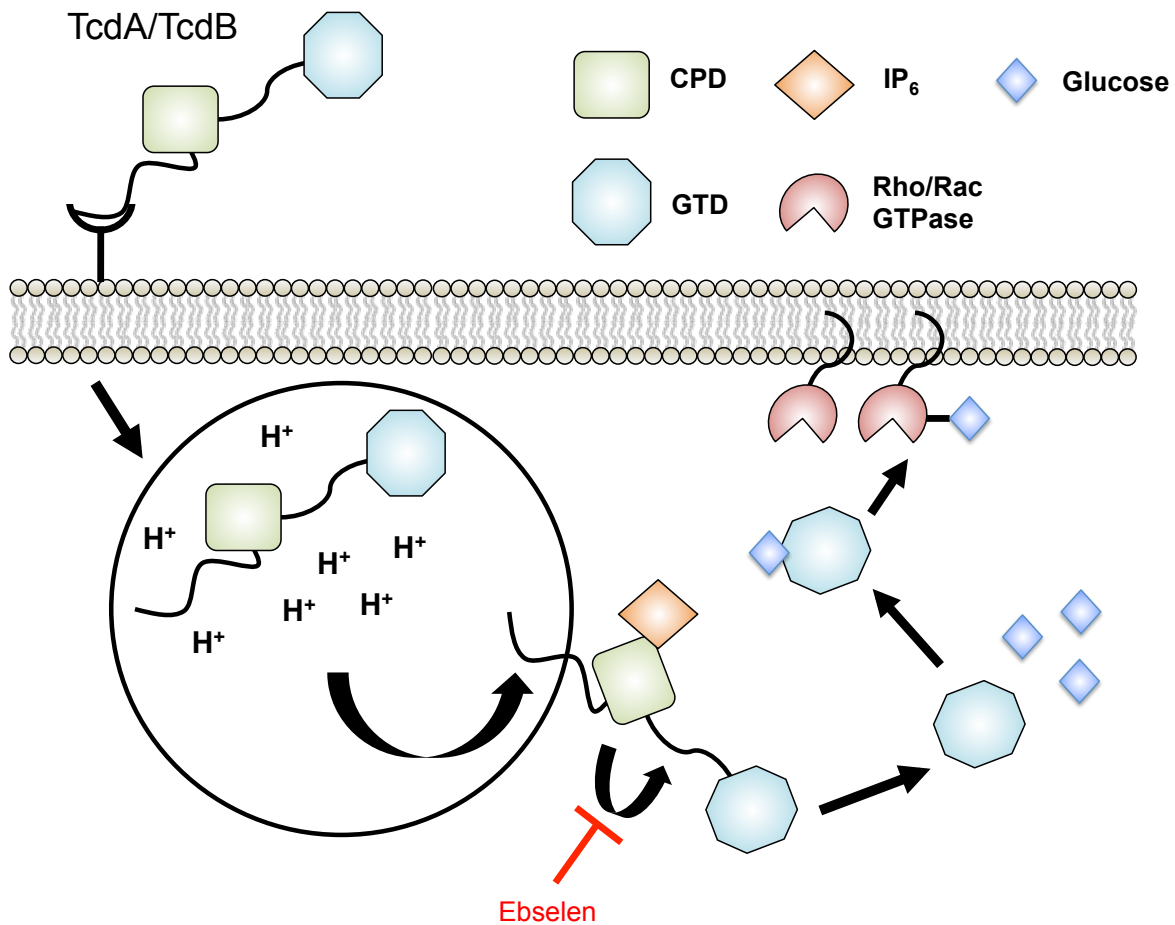


Figure 1.4. *C. difficile* toxin processing in host cells. TcdA and TcdB are the two toxins produced by disease-associated *C. difficile*. Host processing of the toxins are mediated by endocytosis of the full-length toxin into an acidified compartment, leading to surface exposure of the cysteine protease domain (CPD) and glucosyltransferase domain (GTD). Interaction of the CPD with 1D-myo-inositol hexakisphosphate (IP₆) leads to activation and autocatalysis of the linker region between the CPD and GTD. GTD is released into the host cytoplasm and alters intracellular signaling through glucosylation of Rho/Rac GTPase activity. Ebselen inhibits the protease activity of CPD, preventing the release of GTD into the host cytoplasm. The Ebselen inhibitor is in red. Figure inspired by Bender *et al.* (130).

3. 7086, 7812, 7832

Yersinia pestis is the causative agent of plague in humans (136). The Gram-negative zoonotic pathogen is spread through aerosols or via fleabites leading to pneumonic or bubonic plague, respectively. Currently, there is not a licensed vaccine against *Y. pestis* in the United States and antibiotics must be given within 24-hours if exposed to the aerosolized form. *Y. pestis* possesses a T3SS that is essential for virulence *in vivo* (Figure 1.5.) (137, 138). A mutant strain lacking the ATPase domain (YscN) is completely attenuated in a mouse model of infection (111). Additionally, a homolog of YscN in EHEC is required for full virulence and secretion of effectors (139). Delivery of the *Yersinia* outer protein (Yop) effectors YopH (phosphatase) and YopE (Rho GTPase activator) via the T3SS, enable intracellular survival through disruption of cellular signaling (140, 141). Within the bacterial cytosol, Yops are maintained in a partially unfolded state by the specific *Yersinia* chaperone (Syc). The partial unfolding of the protein-chaperone complex is necessary for stability and translocation through the T3SS as the pore is not large enough for fully folded proteins (Figure 1.5.) (142, 143). The ATPase YscN is responsible for removal of the chaperone from the complex in preparation for the subsequent secretion of the Yop effectors (Figure 1.5.) (144). Taken together, the T3SS ATPase domain of YscN provides an attractive target for development of small molecule inhibitors.

The ZINC database of commercially available compounds was screened computationally using a structure-guided rational design scheme against the active site of YscN (111). Initially, 36 compounds were examined for inhibition of catalytic activity in an expression optimized YscN and the related ATPase from *Burkholderia mallei*. The compounds that showed appreciable ATPase inhibitory activity were tested for their ability to inhibit YopE secretion in *Y. pestis* infected macrophages. Notably, compounds 7086, 7812, and 7832 (Table 1.1. C) exhibited

at least 50% inhibition of the YscN catalytic domain and >90% inhibition of YopE secretion in an *ex vivo* model of infection, but did not affect *Y. pestis* growth *in vitro*. All three compounds exhibited minor or no cytotoxic effects against eukaryotic cells .

This study identified a group of small molecule inhibitors of the essential *Y. pestis* ATPase required for the secretion of Yop effectors via the T3SS. These novel scaffolds represent potential foundations to build on and undergo structure activity relationship studies to identify related compounds with enhanced drug-like properties against YscN.

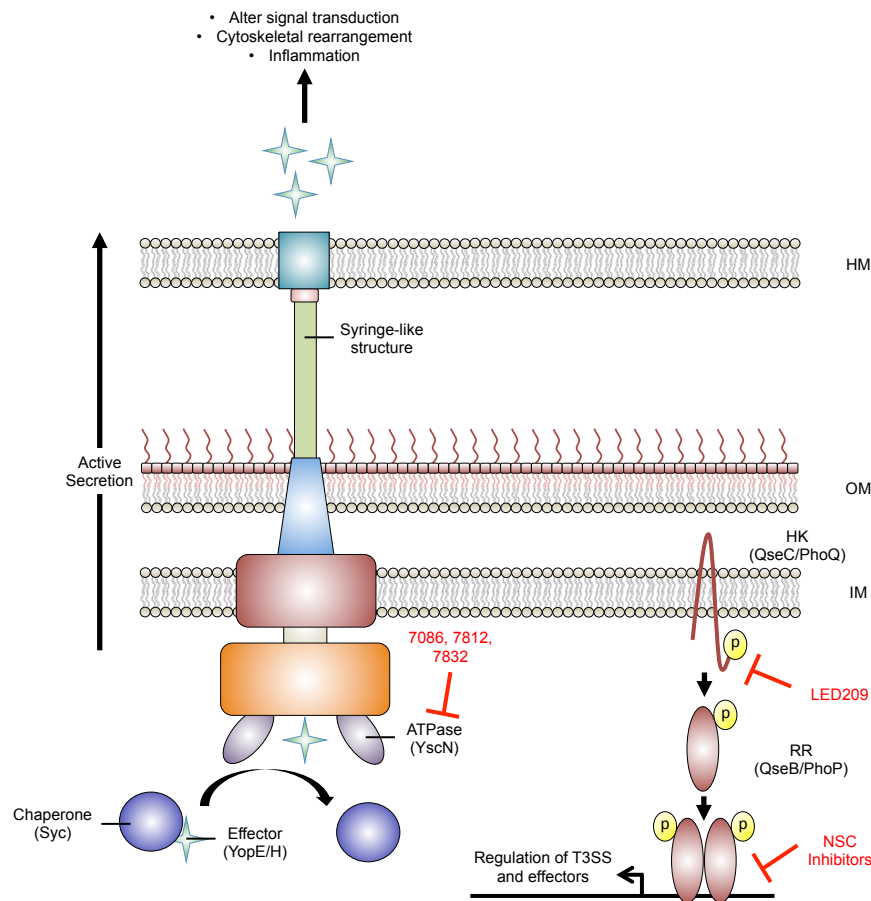


Figure 1.5. Type III secretion system for delivery of bacterial effectors directly into the host cytoplasm. The type III secretion system (T3SS) resembles a syringe-like structure that bacterial pathogens use to inject effectors directly into the host cytoplasm. The terminal tip of the T3SS interacts with the host cell, creating a pore for active (ATP-dependent) delivery of substrates that disrupt host signaling, lead to cytoskeletal rearrangements, and inflammation as a few examples. *Yersinia pestis* uses effector proteins known as *Yersinia* outer proteins (Yops) to cause disease. Within the bacterial cytoplasm the chaperone known as specific *Yersinia* chaperone (Syc) stabilizes and partially folds Yops for delivery to the T3SS. The ATPase YscN is responsible for dissociating the chaperone-effector complex and failure to do so results in bacterial attenuation. The compounds 7086, 7812, and 7832 inhibit kinase activity of YscN *in vitro*, potentially attenuating *Yersinia pestis* *in vivo*. The HK QseC is a global virulence regulator in several Gram-negative pathogens including *S. Typhimurium*. QseC has been shown to globally regulate the pathogenicity island associated with T3SS production and the effector *sifA* (39). LED209 is a potent regulator of QseC and attenuates *S. Typhimurium* during infection through inhibiting virulence gene induction, including the T3SS. Additionally, the *S. Typhimurium* PhoPQ two-component regulatory system is implicated in regulating several virulence-associated genes including the T3SS secreted effector SrfJ (145). The NSC inhibitors have been shown to inhibit the PhoP-DNA complex formation *in vitro*, potentially disrupting virulence gene expression, including *srfJ*, in *S. Typhimurium*. Inhibitors are shown in red. HM – host membrane; OM – bacterial outer membrane; IM – bacterial inner membrane; HK – histidine kinase; RR – response regulator. Figure inspired by Rasko *et al.*, and Costa *et al.* (14, 82).

4. **BPT15 and BBH7**

Mycobacterium tuberculosis (Mtb) is an intracellular pathogen that inhabits macrophage phagosomes during the course of pathogenesis. Mtb is able to arrest phagosome maturation and prevent lysosomal fusion through a variety of mechanisms (146). Protein secretion systems like ESX-1 and the associated substrate EsxA, have been proposed to enable Mtb to lyse cell membranes allowing for cytosolic escape, resulting in tissue damage that can promote spread of the pathogen (147). Deletion of the ESX-1 locus leads to an attenuated phenotype during infection (148). However, ESX-1 is not required for growth *in vitro* and it has proven difficult to identify conditions amenable to HTS to discover inhibitors of ESX-1 secretion.

A recent study developed a novel approach to identify small molecules that disrupt Mtb's ability to secrete EsxA (149). Previous work has implicated cytolytic activity of Mtb at high multiplicities of infection (MOIs) as the result of EsxA intoxication in eukaryotic cells (150, 151). HTS of a proprietary library of ~11,000 compounds was carried out to identify EsxA secretion inhibitors by infecting MRC-5 lung fibroblasts at a high MOI with Mtb and measuring cell survival. Additionally, to distinguish potential ESX-1 inhibitors from compounds generally toxic to bacterial growth, Mtb cultures were counter-screened for inhibition of growth *in vitro*. Compounds that promoted cell survival and did not affect growth were predicted to be small molecules that target ESX-1 dependent secretion of EsxA (Figure 1.6.).

A total of 55 hits were identified as potential antivirulence inhibitors of EsxA secretion. Following cheminformatic analysis, several analogs belonging to the benzyloxybenzylidene-hydrazine (BBH) and benzothiophene (BTP) classes of molecules were identified from the screen suggesting some specificity against mycobacterial secretion by these scaffolds. Two particularly potent inhibitors, BBH7 and BTP15, were chosen for additional characterization

(Table 1.1. C). Interestingly, BBH7 inhibited intracellular growth to a degree similar to the antibiotic rifampicin, while BTP15 had no effect on Mtb survival in infected fibroblasts, suggesting divergent mechanisms of action for each compound. To assess the inhibitory effects of protein secretion by BBH7 and BTP15, treated culture filtrates were collected and EsxA secretion was analyzed by immunoblotting. BBH7 generally inhibited Mtb protein secretion in a dose-dependent manner, whereas increasing levels of BTP15 exhibited specificity for decreasing EsxA secretory activity.

To characterize the targets of BBH7 and BTP15, traditional routes of identifying mutants was not possible since these compounds do not directly target growth *in vitro*. Global transcriptional profiling by RNA-seq revealed unique signatures for each inhibitor. BTP15 treatment led to differential expression of genes almost exclusively associated with the DosR (DevR) regulon – a group of genes shown to promote a state of nonreplicating persistence, enhancing long-term intracellular survival. The two-component systems PhoPR and MprAB have been implicated in linking the DosR regulon and regulation of ESX-1 secretion through the *espACD* locus (56, 152, 153). Loss of *mprAB* leads to upregulation of *espA* and reduced secretion of EsxA (153). Quantitative real-time PCR (qRT-PCR) revealed greater than two-fold upregulation of *espA* in BTP15 treated cultures, suggesting BTP15 may be inhibiting MprAB activity. RNA-seq analysis of BBH7 exhibited large changes in genes involved in cell wall processes and heavy metal detoxification. Notably, the ESX transmembrane ATPases were significantly upregulated in addition to the P-type ATPase genes *ctpC* and *ctpG*, indicating disrupted cell-wall/membrane transport for both secreted proteins and heavy metals. Other genes involved in heavy metal detoxification like the multi-copper oxidase (*mmcO*), copper-dependent regulator *ricR*, and zinc stress-responsive genes (e.g. *cadI*, *esxG*, *esxH*) were also upregulated by

BBH7 treatment. Thus, BBH7 inhibition of Mtb protein secretion may be a result of permeability defects in the cell wall and zinc/copper intoxication.

BPT15 was determined to be a potent inhibitor of kinase activity of the HK MprB (Figure 1.6.). To test whether BBH7 treatment leads to altered membrane permeability, Mtb cultures were treated with the inhibitor and tested for the accumulation of the DNA binding dye ethidium bromide (EtBr). If membrane permeability is enhanced by BBH7, it is predicted that an increased concentration of the dye will be able to pass through the membrane and bind DNA leading to higher fluorescence relative to the untreated control. Indeed, BBH7 treatment led to higher intracellular fluorescence, substantiating the transcriptional data suggesting altered membrane permeability. Next, to examine whether BBH7 leads to zinc or copper intoxication, Mtb cultures were treated with physiological levels of each ion. Notably, ZnSO₄ enhanced EsxA secretion in a dose dependent manner. In contrast, no effect on EsxA protein transport was observed when treated with copper. Together, these data suggest that BBH7 does not lead to zinc or copper intoxication as a mechanism for decreased secretion of EsxA. It was also shown that known inhibitors of intracellular ATP concentrations and the Mtb cell wall had no observable effect on EsxA secretion. Finally, both BBH7 and BPT15 hamper Mtb's ability to arrest phagosome maturation in infected THP-1 macrophages as shown by the enhanced colocalization of Mtb in acidified compartments relative to mock treated controls.

Though the direct mechanism of action remains to be determined for BBH7 (Figure 1.6.), it is clear that treatment with this inhibitor leads to membrane permeability defects in Mtb. Further, each compound is capable of inhibiting Mtb survival in infected macrophages through decreased EsxA secretion via distinct mechanisms, suggesting that these scaffolds may be used as chemical probes to refine ESX-1 dependent secretion mechanisms in addition to potential

development as antivirulence molecules. Additionally, BPT15 represents a first-in-class inhibitor of MprAB-regulated ESX-1 secretion (Figure 1.6.).

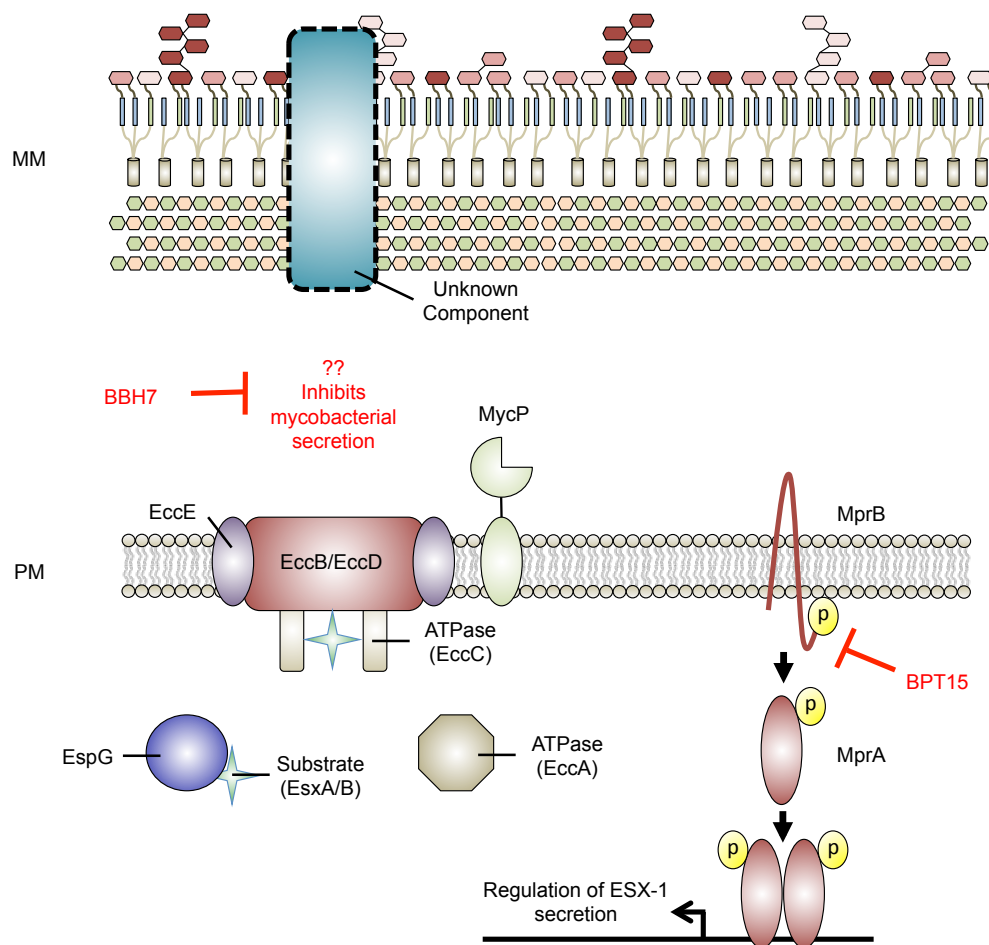


Figure 1.6. *Mycobacterium tuberculosis* type VII secretion of EsxA/EsxB. *Mycobacterium tuberculosis* (Mtb) possesses a type VII secretion system (T7SS) (ESX-1) for export of host effector proteins EsxA and EsxB. Little is known about the exact mechanism and structure of the secretion machinery. However, the current working mechanism is that T7SS substrates are targeted for secretion by an unstructured C-terminal signal sequence (similar to type IV secretion systems). The substrates EsxA and EsxB form a dimer for secretion and stabilized by the soluble chaperone EspG and potentially exported in an ATP-dependent manner. Further, the protease MycP is required for secretion, though the exact role it plays in secretion is unclear. Regulation of ESX-1 secretion is accomplished by several cellular systems including the two-component regulator MprAB through the *espACD* operon. BPT15 inhibits the kinase activity of the sensor kinase MprB, leading to reduced secretion of EsxA, attenuating Mtb-mediated phagosome maturation arrest. BBH7 inhibits an unknown factor leading to reduced general secretion of Mtb and survival in fibroblasts. Inhibitors are in red. MM – mycobacterial membrane; PM – plasma membrane. Figure inspired by Rasko *et al.*, and Costa *et al.* (14, 82).

Metabolic requirements during infection

The outcome of a bacterial infection is determined either by the host's ability to control the infection through immune effectors meant to clear the pathogen or countermeasures produced by the invading microbe to subvert them (154). However, the interplay between the host and bacterial pathogen's metabolic requirements is often overlooked. Indeed, minor perturbations to metabolism of either system during infection can have a significant impact on the outcome in favor of either the host or pathogen (155).

Intracellular pathogens have a unique challenge during the course of infection as they often occupy host membrane-encapsulated compartments, limiting access to amino acids and carbon sources for growth. Further, intracellular pathogens directly compete with the host cell for metabolic requirements with each attempting to tip the balance in favor of themselves. Several successful human pathogens, including *Mycobacterium tuberculosis*, *Salmonella enterica*, *Chlamydia trachomatis*, and *Listeria monocytogenes*, have been recently reviewed with unique metabolic plasticity during pathogenesis in intracellular environments and specialized approaches to effectively acquire necessary metabolites to promote disease (155).

Mycobacterium tuberculosis (Mtb) inhabits a variety of environmental niches during infection. One common site is within the macrophage phagosome that resembles early endosomes. Many of these compartments include the transferrin receptor allowing Mtb access to the endosomal recycling pathway to acquire nutrients (156). However, upon macrophage activation, the compartment is removed from the recycling pathway and phagosome maturation is initiated, resulting in a significantly more hostile and nutrient restricted environment (157-159). The metabolic requirements of Mtb in each of these settings are illustrated by the differential requirement for cholesterol. Mtb encodes an extensive suite of genes for degradation

of sterols and has the ability to completely metabolize cholesterol for growth (Figure 1.7.) (160). Further, it has been shown that Mtb requires cholesterol for growth in *in vitro* studies with activated macrophages and at sites of infection that correlate with the presence of interferon-gamma producing T-cells in mice (161, 162). These data suggest that interferon-gamma-mediated activation results in a shift of metabolites available to Mtb leading to the requirement of cholesterol metabolism for growth. Further, the ability of Mtb to sense the chemical environment of the host and adapt its own metabolism to persist provides potential to identify inhibitors that disrupt *in vivo* growth requirements through modulation of bacterial or host factors.

1. D155931

Upon interferon-gamma activation, Mtb residing within the macrophage phagosome are exposed to a variety of antibacterial stresses, including acidic pH, reactive oxygen and nitrogen species, and reduced oxygen tension (52, 163-165). The capacity of Mtb to resist these antimicrobial insults is crucial for establishing a persistent infection. Persistent, non-replicating Mtb are one of the main reasons for the extended duration of treatment (166). Therefore, identification of compounds that target factors Mtb uses to resist immune pressures and persist within the host, may function to reduce the duration of treatment.

Mtb resistance to reactive nitrogen intermediates (RNI) generated from nitric oxide is the result of several bacterial countermeasure systems including the peroxynitrite reductase and peroxidase. This system is composed of four parts: a peroxiredoxin – alkylhydroperoxide reductase subunit C (AhpC), a thioredoxin-related oxidoreductase – AhpD, dihydrolipamide acyltransferase (DlaT), and lipamide dehydrogenase (Lpd) (167-169). The latter two components are named for their function as a part of the Mtb pyruvate dehydrogenase complex

(PDH) (167). Based on a study showing that a DlaT-deficient strain of Mtb (*ΔdlaT*) failed to cause disease in mice (170), Nathan and colleagues sought to identify small molecule inhibitors of DlaT. To verify the previous results and assess the impact of *ΔdlaT* in an animal model that more closely mimics human infection, guinea pigs (171) were infected with wild-type, *ΔdlaT*, and *ΔdlaT* expressing a wild-type copy of *dlaT*. Indeed, the *ΔdlaT* strain was unable to cause disease and exhibited little tissue pathology relative to the wild-type and complemented strains (172). With this result in hand, a medium-throughput target-based screen was devised to screen for inhibitors of DlaT. The assay leverages the sequential electron transfer reactions from NADH by Lpd to DlaT to AhpD and finally to the compound dithionitrobenzene (DTNB), which when reduced turns yellow (Figure 1.7.). A library of ~15,000 compounds with drug-like characteristics was screened and identified 34 compounds exhibiting >50% inhibition of the electron transfer reaction. The most potent scaffolds were rhodanine-based (2-thioxo-thiazolidi-4-ones) molecules. However, many of the candidate compounds also exhibited inhibitory activity against the related porcine PDH. To develop Mtb specific inhibitors, an additional 1000 rhodanine-based compounds were synthesized and tested against the Mtb enzymes (Lpd, DlaT, and AhpD reaction complex; and Mtb PDH) as well as bovine thioredoxin reductase and porcine PDH. One compound, D155931, exhibited Mtb specific inhibitory activity was selected for additional follow-up studies (Table 1.1. D) (172).

To assess the target and kinetics of D155931, the compound was incubated in the presence of reduced recombinant DlaT and was found to be an irreversible competitive inhibitor of the enzyme. *In vitro* non-replicating conditions for Mtb were generated using rich medium buffered to pH 5.5 and supplemented with sub lethal fluxes of nitric oxide via nitrite (172). D155931 was shown to reduce Mtb growth synergistically with nitrite by approximately 100-

fold relative to bacteria treated with the compound in the absence of nitrite. Further, D155931 had no observable effects on Mtb growth under replicating conditions. Notably, D155931 was unable to modulate mycobacterial growth in murine-derived macrophages. Therefore, the authors reasoned that by masking the anionic character of the compound and increasing its lipophilicity, it may result in increased entry into macrophages. Thus, a propanolic ester of D155931 was selected for all further studies and was denoted D157070 (Table 1.1. D) (172). This compound also exhibited potentiation of nitrite against Mtb growth under non-replication conditions *in vitro*. In an effort to validate the efficacy of D157070 against non-replicating Mtb, several *in vitro* persistence models were tested. Across all systems tested, the compound was able to reduce the total number of recoverable bacteria by at least two logs relative to the negative control.

To test whether D157070 was reducing Mtb viability under non-replicating conditions in a DlaT-dependent manner, the *AdlaT* and its complemented strain were treated with the compound for four days using the *in vitro* model of non-replicating persistence described above (172). Importantly, the *AdlaT* mutant was resistant to D157070 treatment in the presence or absence of nitrite, while the complemented strain regained sensitivity to the compound in combination with nitrite. Further, metabolic intermediates of pyruvate metabolism were measured to assess whether D157070 inhibits the Mtb PDH. Mtb was grown on glycolytic carbon sources under non-replicating conditions and the relative levels of amino acids produced in the wild-type, *AdlaT*, and the complemented strain were measured. Notably, the pyruvate-derived amino acid valine accumulated at higher levels in response to D157070 treatment in the wild-type and complement relative to *AdlaT*. In contrast, the basal levels of alanine were higher in *AdlaT* relative to the wild-type and complemented strain. These data support that the reduction

in survival of non-replicating Mtb is due to the compound targeting DlaT and in the absence of the DlaT, Mtb remodels its intermediary metabolism.

Finally, to assess the efficacy of D157070 in an *ex vivo* model of infection, Mtb infected murine-derived macrophages were treated with the compound for 48 hours. Macrophages treated with D157070 exhibited an approximately 2.5 log reduction in bacterial load. Notably, these cells were not stimulated with interferon-gamma, suggesting that D157070 is capable of killing Mtb in non-activated macrophages. Further, D157070 was shown to exhibit low cytotoxicity against eukaryotic cells. Taken together, this study represents the first report of a small molecule capable of targeting the *in vivo* required target DlaT. Importantly, non-replicating mycobacteria were sensitized to killing through inhibition of a key component of Mtb defense against host-derived RNI and bacterial central metabolism, potentially shortening the duration of treatment (172).

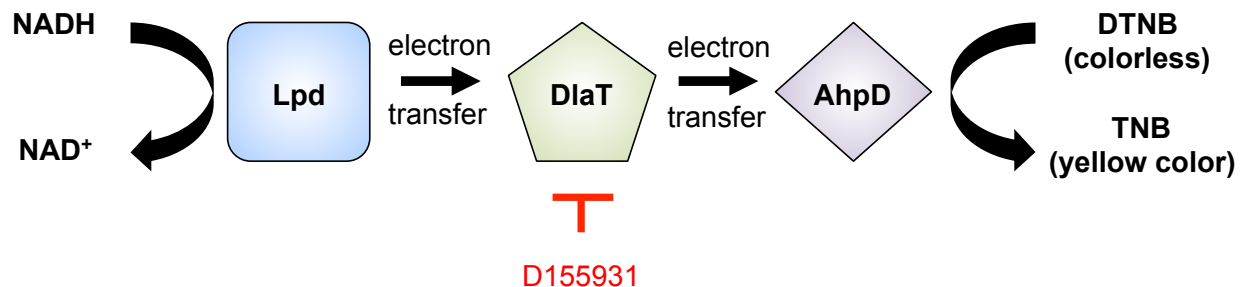


Figure 1.7. Screening scheme for inhibitors of DltA. Mtb RNI resistance and pyruvate metabolism is mediated by AhpCD, DltA, and Lpd. Using the sequential electron transfer reaction initiated by Lpd oxidizing NADH, inhibitors were screened for the ability to inhibit the reduction of the DTNB by AhpD. D155931 was identified as an inhibitor exhibiting competitive kinetics against DltA. Inhibitor is shown in red.

2. V-13-009920, V-13-0110503 and V-13-012725

Whole cell phenotypic screens for inhibitors of metabolic requirements necessary *in vivo* often suffer from an inability to adequately recapitulate the environment that the pathogen encounters within the host. Thus, there is a significant attrition rate associated with *in vitro* identification of potential inhibitors and activity in subsequent assays to validate the compound during infection. Intracellular pathogens such as Mtb, inhabit macrophages during pathogenesis *in vivo* and infecting macrophage cell lines can be adapted to HTS. HTS of a proprietary library of ~340,000 compounds using J774 macrophages infected with an Mtb fluorescent reporter identified ~1,356 validated hits with an IC₅₀ value <50 μ M (30). These hits were then subjected to a counterscreen to discover inhibitors of cholesterol catabolism. Mtb isocitrate lyase (Icl1) is a bifunctional enzyme acting in both the glyoxylate shunt of the TCA cycle and as a methylisocitrate lyase in the methylcitrate cycle (MCC) (173, 174). The MCC is used by Mtb to integrate propionyl-CoA into central carbon metabolism by producing pyruvate and succinate (173, 175). Notably, propionyl-CoA is generated during cholesterol catabolism and if steps in the MCC are disrupted, such as an Mtb Icl1 mutant (*Δicl1*), it is hypothesized that toxic intermediates accumulate leading to an inability to grow. Thus, a novel chemical rescue assay was used to select for potential inhibitors of cholesterol catabolism by growing *Δicl1* in rich medium supplemented with cholesterol. If enzymatic steps were inhibited during cholesterol degradation, toxic intermediates of the MCC would not accumulate and consequently allow for growth of *Δicl1*. Indeed, three candidate compounds were identified, V-13-009920, V-13-012725, and V-13-011503 (Table 1.1. D). To distinguish between which compounds inhibit processes in the MCC versus cholesterol catabolism, each candidate inhibitor was subjected to the same chemical rescue assay described above but was supplemented with propionate as

opposed to cholesterol. V-13-012725 and V-13-011503 were confirmed to rescue growth in the presence of cholesterol but not propionate, suggesting that these molecules were acting by disrupting cholesterol degradation. In contrast, V-13-00920 was capable of rescuing growth of *ΔiclI* in both cholesterol and propionate, suggesting that this compound may be targeting an enzyme in the MCC.

Detoxification of the propionyl-CoA produced during cholesterol degradation requires the MCC (173, 175). The first step in the MCC is the condensation of oxaloacetate with propionyl-CoA by the enzyme PrpC (175). Thus, to identify whether V-13-009920 inhibits PrpC, recombinant enzyme was incubated in the presence of the compound. Indeed, V-13-009920 inhibited purified PrpC with an IC₅₀ of approximately 4.0 μM (30). Notably, this compound exhibited an IC₅₀ of 3.0 μM in Mtb infected macrophages and a 10-fold more potent IC₅₀ in minimal medium containing cholesterol (0.3 μM). Additionally, growth in minimal medium containing cholesterol revealed that V-13-009920 is bacteriostatic against Mtb. Disruption of Mtb intracellular growth by inhibiting PrpC supports a previous report that has established a *prpCD* double mutant exhibits an attenuated phenotype in macrophages (175). Recent studies have shown that the growth defect of *ΔiclI* grown solely on propionate is the result of a defective MCC and siphoning carbon away from the TCA cycle, leading to accumulation of potentially toxic intermediates (176). Additionally, vitamin B12 has been shown to rescue growth of *ΔiclI* grown on propionate through redirecting carbon to the TCA cycle via the methyl-malonyl pathway (176, 177). However, it is unlikely that TCA intermediates are limiting due to V-13-009920 chemical rescue assays being performed in rich medium supplemented with cholesterol and chemical inhibition of PrpC is unlikely to reroute carbon through the vitamin B12-dependent

methyl-malonyl pathway. Therefore, the intracellular Mtb growth defects by V-13-009920 are likely the result of toxic intermediates accumulating in the MCC.

To refine whether V-13-012725 and V-13-011503 inhibit cholesterol degradation, Mtb was grown in the presence of radiolabeled cholesterol and the evolution of $^{14}\text{CO}_2$ was monitored via radiorespirometry. Both compounds reduced the total amount of $^{14}\text{CO}_2$ produced, suggesting inhibition of catabolic steps in the degradation of cholesterol. Mass spectrometry analysis of treated culture lysates revealed a single peak not observed in mock treated controls that corresponded to 3-hydroxy-9,10-seconandrost-1,3,5(10)-triene-9,17-dione (3-HSA), which is a known metabolite of A/B ring degradation of cholesterol (Figure 1.8.) (178). *In vitro* enzymatic assays of the key enzymes HsaA-HsaD required during degradation of A/B rings of cholesterol, it was shown that V-13-012725 and V-13-011503 inhibit HsaAB. HsaAB is a two-component, flavin-dependent hydroxylase that catalyzes the 4-hydroxylation of ring A to a catechol (Figure 1.7.). *In vitro* killing kinetics assays of Mtb grown in minimal medium containing cholesterol as the sole carbon source revealed that both compounds were bacteriostatic.

Though the precise biochemical mechanisms of action for V-13-009920, V-13-012725 and V-13-011503 remain to be determined, this study identified three compounds that potently inhibit the MCC and cholesterol catabolism during infection, respectively (Figure 1.8.). Additional animal studies are needed to verify whether these compounds function during an *in vivo* model of infection. However, medicinal chemistry and structure activity relationship approaches can provide moieties required for activity and enhanced drug-like properties if the inhibitors prove to be inactive or toxic *in vivo*. Further, deletion or disruption of HsaAB and its impact on mycobacterial survival are currently unknown, though chemical inhibition predicts that this enzyme complex is likely required during infection. An additional advantage of

inhibiting cholesterol degradation or the MCC is that systemic treatment may be desirable as Mtb potentially relies on cholesterol as a carbon source for extracellular growth in caseating granulomas. Taken together, V-13-009920, V-13-012725 and V-13-011503 represent the first known inhibitors of PrpC and cholesterol catabolism in Mtb and can be leveraged as chemical probes to further define the mechanisms underlying the requirement for cholesterol during Mtb pathogenesis.

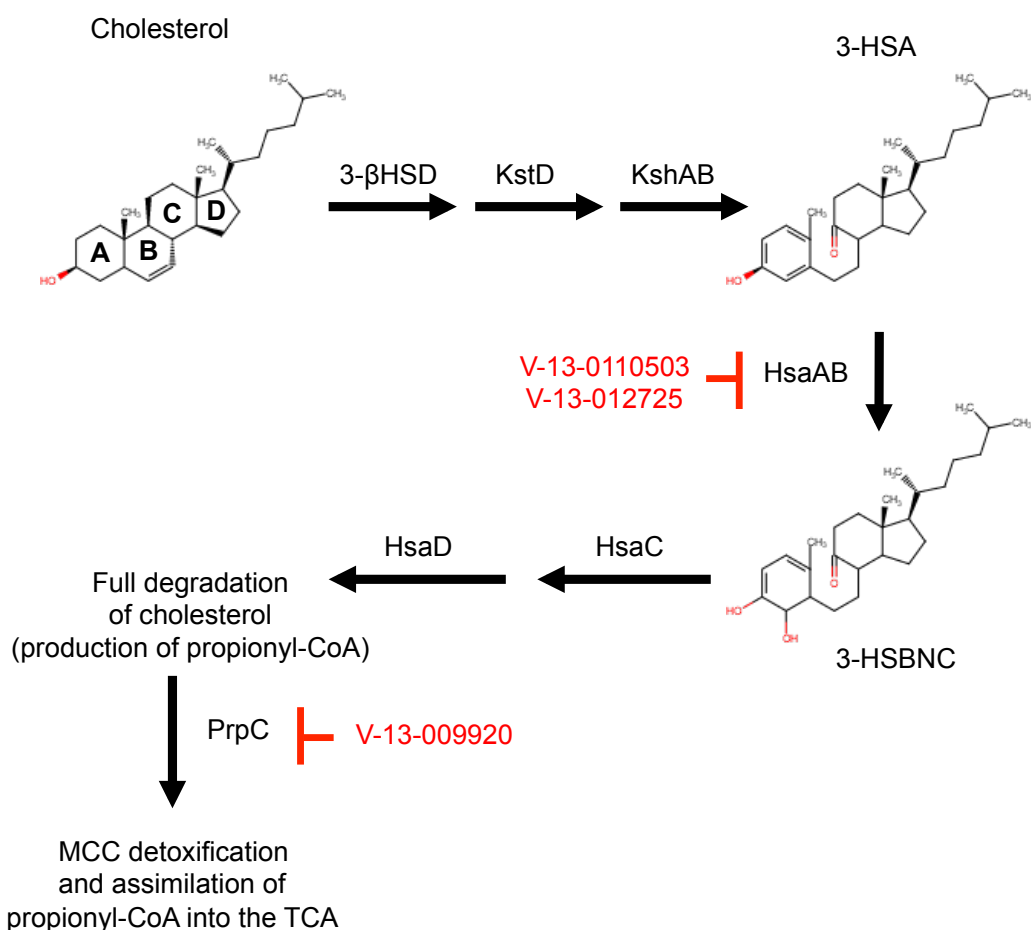


Figure 1.8. Proposed reaction mechanism of cholesterol catabolism in *Mycobacterium tuberculosis*. During the course of infection, *Mycobacterium tuberculosis* (Mtb) requires cholesterol as a carbon source for persistence and growth. Remarkably, Mtb is capable of fully catabolizing cholesterol through the proposed mechanism above. A/B ring catabolism is accomplished through a series of enzymatic and non-enzymatic steps. HsaAB likely catalyzes the hydroxylation of 3-HAS to 3-HSBNC and is inhibited by V-13-0110503 and V-13-012725. Propionyl-CoA is produced during cholesterol catabolism and is detoxified and assimilated into the TCA cycle via the methyl-citrate cycle (MCC). The small molecule V-13-009920 inhibits the first enzyme, PrpC, in the MCC. This inhibition results in attenuated survival in Mtb infected macrophages. Inhibitors are seen in red. Model is based on (179).

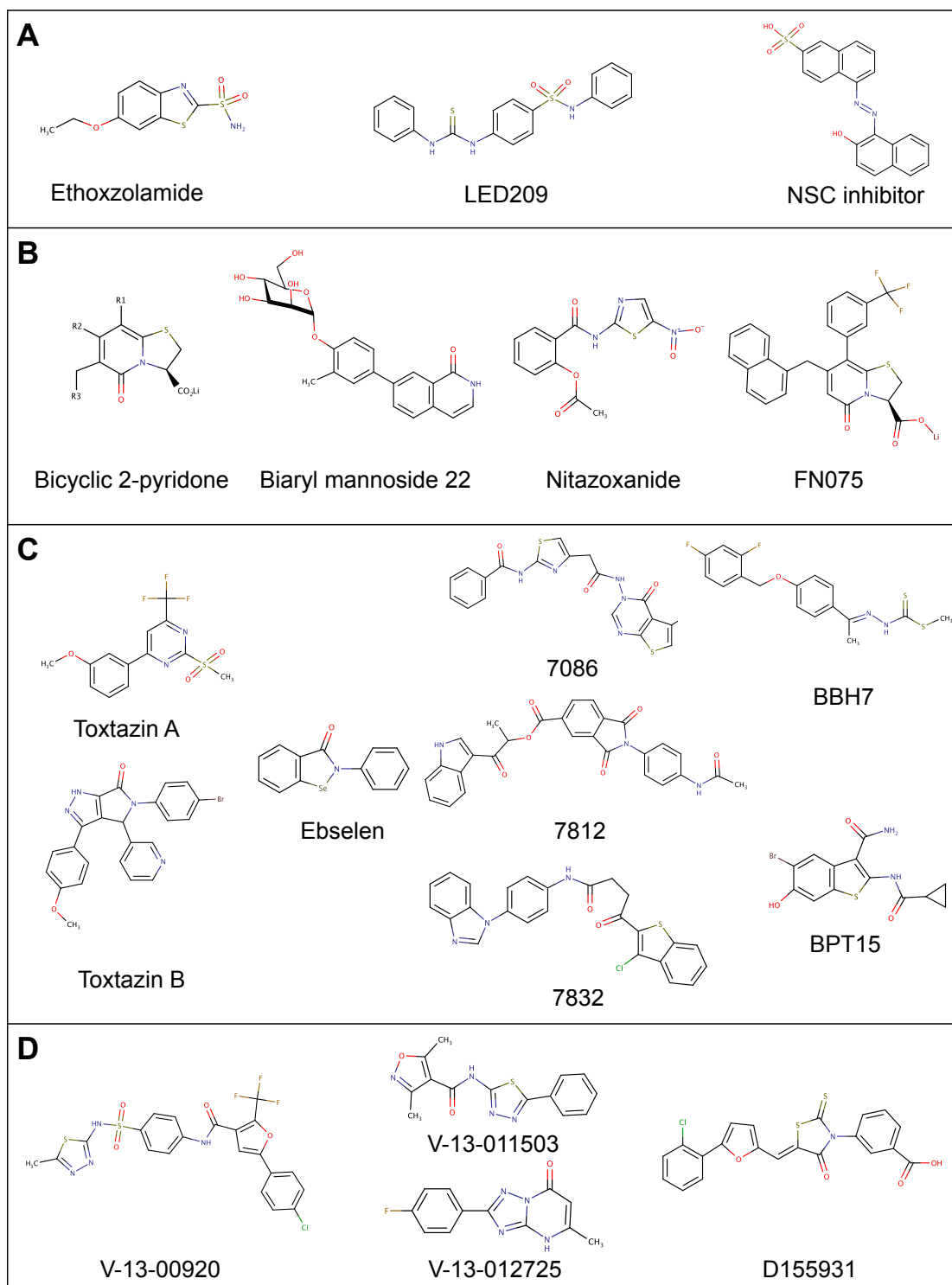


Table 1.1. 2-D structures of antivirulence compounds. A. Two-component regulator system inhibitors. B. Pilicide and curlicide structures. C. Toxin production and delivery system inhibitors. D. Metabolic requirement inhibitors.

Conclusion

The recently discovered antivirulence compounds are evidence for the increasing understanding of the intricate processes of host-pathogen interactions. The knowledge we have acquired studying the *in vivo* requirements for pathogenesis have enabled more sophisticated screening approaches that better approximate environments encountered during infection to identify inhibitors that disrupt bacterial virulence. Further, we can leverage these inhibitors as chemical scalpels to refine our understanding of host-pathogen dynamics. Additionally, to develop antivirulence therapeutics robust to the effects of selection for resistance, consideration must be given regarding the impact on pathogen fitness from inhibiting virulence factors in relevant environmental niches.

One of the theoretical advantages of antivirulence approaches is that by targeting virulence factors and not directly inhibiting growth, these compounds will exert reduced selective pressure for resistance. However, recent studies have shown potential mechanisms for resistance to antivirulence compounds *in vitro* (47, 118). Further, careful consideration should be given to whether the pathogen inhabits additional environmental niches where the virulence factor is either not expressed or is required for non-pathogenic processes (e.g. UPEC attachment in the intestines) potentially leading to resistance during systemic treatment (19). Therefore, to develop more evolutionarily robust therapeutics, it will be useful to consider pathogen fitness in multiple environments and the subsequent impact of inhibiting specific virulence factors in those niches.

Conventional antibiotic discovery approaches require significant investment in both time and money before they can be used in a clinical setting. Repurposing unrelated inhibitors approved for human use as antivirulence compounds can potentially expedite the time frame for

clinical use and revitalize currently used antibiotics. The future for antivirulence approaches to treat bacterial-mediated disease remains bright with several compounds in pre-clinical and clinical trials.

REFERENCES

REFERENCES

1. **Davies J, Davies D.** 2010. Origins and evolution of antibiotic resistance. *Microbiol Mol Biol Rev* **74**:417-433.
2. **D'Costa VM, McGrann KM, Hughes DW, Wright GD.** 2006. Sampling the antibiotic resistome. *Science* **311**:374-377.
3. **CDC.** 2013. Antibiotic Resistance Threats in the United States, 2013. Centers for Disease Control and Prevention, Atlanta, GA., <http://www.cdc.gov/drugresistance/threat-report-2013/>.
4. **CDC.** 2011. Antimicrobial Resistance Posing Growing Health Threat. Center for Disease Control and Prevention, Atlanta, GA., http://www.cdc.gov/media/releases/2011/p0407_antimicrobialresistance.html.
5. **Payne DJ, Gwynn MN, Holmes DJ, Pompliano DL.** 2007. Drugs for bad bugs: confronting the challenges of antibacterial discovery. *Nat Rev Drug Discov* **6**:29-40.
6. **Silver LL.** 2011. Challenges of antibacterial discovery. *Clin Microbiol Rev* **24**:71-109.
7. **Aminov RI.** 2010. A brief history of the antibiotic era: lessons learned and challenges for the future. *Front Microbiol* **1**:134.
8. **Farha MA, Brown ED.** 2015. Unconventional screening approaches for antibiotic discovery. *Ann N Y Acad Sci* **1354**:54-66.
9. **Holmes AH, Moore LS, Sundsfjord A, Steinbakk M, Regmi S, Karkey A, Guerin PJ, Piddock LJ.** 2016. Understanding the mechanisms and drivers of antimicrobial resistance. *Lancet* **387**:176-187.
10. **Cox G, Wright GD.** 2013. Intrinsic antibiotic resistance: mechanisms, origins, challenges and solutions. *Int J Med Microbiol* **303**:287-292.
11. **D'Costa VM, King CE, Kalan L, Morar M, Sung WW, Schwarz C, Froese D, Zazula G, Calmels F, Debruyne R, Golding GB, Poinar HN, Wright GD.** 2011. Antibiotic resistance is ancient. *Nature* **477**:457-461.
12. **Staskawicz BJ, Mudgett MB, Dangl JL, Galan JE.** 2001. Common and contrasting themes of plant and animal diseases. *Science* **292**:2285-2289.

13. **Anthouard R, DiRita VJ.** 2015. Chemical biology applied to the study of bacterial pathogens. *Infect Immun* **83**:456-469.
14. **Rasko DA, Sperandio V.** 2010. Anti-virulence strategies to combat bacteria-mediated disease. *Nat Rev Drug Discov* **9**:117-128.
15. **Lee YM, Almqvist F, Hultgren SJ.** 2003. Targeting virulence for antimicrobial chemotherapy. *Curr Opin Pharmacol* **3**:513-519.
16. **Cegelski L, Marshall GR, Eldridge GR, Hultgren SJ.** 2008. The biology and future prospects of antivirulence therapies. *Nat Rev Microbiol* **6**:17-27.
17. **Then RL, Sahl HG.** 2010. Anti-infective strategies of the future: is there room for species-specific antibacterial agents? *Curr Pharm Des* **16**:555-566.
18. **Ternent L, Dyson RJ, Krachler AM, Jabbari S.** 2015. Bacterial fitness shapes the population dynamics of antibiotic-resistant and -susceptible bacteria in a model of combined antibiotic and anti-virulence treatment. *J Theor Biol* **372**:1-11.
19. **Allen RC, Popat R, Diggle SP, Brown SP.** 2014. Targeting virulence: can we make evolution-proof drugs? *Nat Rev Microbiol* **12**:300-308.
20. **Sekirov I, Russell SL, Antunes LC, Finlay BB.** 2010. Gut microbiota in health and disease. *Physiol Rev* **90**:859-904.
21. **McFarland LV.** 2008. Antibiotic-associated diarrhea: epidemiology, trends and treatment. *Future Microbiol* **3**:563-578.
22. **Schnappinger D.** 2007. Genomics of host-pathogen interactions. *Prog Drug Res* **64**:311, 313-343.
23. **Rosamond J, Allsop A.** 2000. Harnessing the power of the genome in the search for new antibiotics. *Science* **287**:1973-1976.
24. **Nagaraj NS, Singh OV.** 2010. Using genomics to develop novel antibacterial therapeutics. *Crit Rev Microbiol* **36**:340-348.
25. **Haney SA, Alksne LE, Dunman PM, Murphy E, Projan SJ.** 2002. Genomics in anti-infective drug discovery--getting to endgame. *Curr Pharm Des* **8**:1099-1118.
26. **Wilson DJ.** 2012. Insights from genomics into bacterial pathogen populations. *PLoS Pathog* **8**:e1002874.

27. **Roemer T, Davies J, Giaever G, Nislow C.** 2012. Bugs, drugs and chemical genomics. *Nat Chem Biol* **8**:46-56.
28. **Pucci MJ.** 2007. Novel genetic techniques and approaches in the microbial genomics era: identification and/or validation of targets for the discovery of new antibacterial agents. *Drugs R D* **8**:201-212.
29. **Amini S, Tavazoie S.** 2011. Antibiotics and the post-genome revolution. *Curr Opin Microbiol* **14**:513-518.
30. **VanderVen BC, Fahey RJ, Lee W, Liu Y, Abramovitch RB, Memmott C, Crowe AM, Eltis LD, Perola E, Deininger DD, Wang T, Locher CP, Russell DG.** 2015. Novel inhibitors of cholesterol degradation in *Mycobacterium tuberculosis* reveal how the bacterium's metabolism is constrained by the intracellular environment. *PLoS Pathog* **11**:e1004679.
31. **Anthouard R, DiRita VJ.** 2013. Small-molecule inhibitors of toxT expression in *Vibrio cholerae*. *MBio* **4**.
32. **LaSarre B, Federle MJ.** 2013. Exploiting quorum sensing to confuse bacterial pathogens. *Microbiol Mol Biol Rev* **77**:73-111.
33. **Charro N, Mota LJ.** 2015. Approaches targeting the type III secretion system to treat or prevent bacterial infections. *Expert Opin Drug Discov* **10**:373-387.
34. **Gao R, Stock AM.** 2009. Biological insights from structures of two-component proteins. *Annu Rev Microbiol* **63**:133-154.
35. **Shestov M, Ontanon S, Tozeren A.** 2015. Encyclopedia of bacterial gene circuits whose presence or absence correlate with pathogenicity--a large-scale system analysis of decoded bacterial genomes. *BMC Genomics* **16**:773.
36. **Beier D, Gross R.** 2006. Regulation of bacterial virulence by two-component systems. *Curr Opin Microbiol* **9**:143-152.
37. **Weiss DS, Brotcke A, Henry T, Margolis JJ, Chan K, Monack DM.** 2007. In vivo negative selection screen identifies genes required for *Francisella* virulence. *Proc Natl Acad Sci U S A* **104**:6037-6042.
38. **Unal CM, Singh B, Fleury C, Singh K, Chavez de Paz L, Svensater G, Riesbeck K.** 2012. QseC controls biofilm formation of non-typeable *Haemophilus influenzae* in addition to an AI-2-dependent mechanism. *Int J Med Microbiol* **302**:261-269.

39. **Moreira CG, Weinshenker D, Sperandio V.** 2010. QseC mediates *Salmonella enterica* serovar typhimurium virulence in vitro and in vivo. *Infect Immun* **78**:914-926.
40. **Moreira CG, Sperandio V.** 2012. Interplay between the QseC and QseE bacterial adrenergic sensor kinases in *Salmonella enterica* serovar Typhimurium pathogenesis. *Infect Immun* **80**:4344-4353.
41. **Mokrievich AN, Kondakova AN, Valade E, Platonov ME, Vakhrameeva GM, Shaikhutdinova RZ, Mironova RI, Blaha D, Bakhteeva IV, Titareva GM, Kravchenko TB, Kombarova TI, Vidal D, Pavlov VM, Lindner B, Dyatlov IA, Knirel YA.** 2010. Biological properties and structure of the lipopolysaccharide of a vaccine strain of *Francisella tularensis* generated by inactivation of a quorum sensing system gene qseC. *Biochemistry (Mosc)* **75**:443-451.
42. **Kostakioti M, Hadjifrangiskou M, Pinkner JS, Hultgren SJ.** 2009. QseC-mediated dephosphorylation of QseB is required for expression of genes associated with virulence in uropathogenic *Escherichia coli*. *Mol Microbiol* **73**:1020-1031.
43. **Kostakioti M, Hadjifrangiskou M, Cusumano CK, Hannan TJ, Janetka JW, Hultgren SJ.** 2012. Distinguishing the contribution of type 1 pili from that of other QseB-misregulated factors when QseC is absent during urinary tract infection. *Infect Immun* **80**:2826-2834.
44. **Rasko DA, Moreira CG, Li de R, Reading NC, Ritchie JM, Waldor MK, Williams N, Taussig R, Wei S, Roth M, Hughes DT, Huntley JF, Fina MW, Falck JR, Sperandio V.** 2008. Targeting QseC signaling and virulence for antibiotic development. *Science* **321**:1078-1080.
45. **Hadjifrangiskou M, Kostakioti M, Chen SL, Henderson JP, Greene SE, Hultgren SJ.** 2011. A central metabolic circuit controlled by QseC in pathogenic *Escherichia coli*. *Mol Microbiol* **80**:1516-1529.
46. **Clarke MB, Hughes DT, Zhu C, Boedeker EC, Sperandio V.** 2006. The QseC sensor kinase: a bacterial adrenergic receptor. *Proc Natl Acad Sci U S A* **103**:10420-10425.
47. **Curtis MM, Russell R, Moreira CG, Adebesein AM, Wang C, Williams NS, Taussig R, Stewart D, Zimmermann P, Lu B, Prasad RN, Zhu C, Rasko DA, Huntley JF, Falck JR, Sperandio V.** 2014. QseC inhibitors as an antivirulence approach for Gram-negative pathogens. *MBio* **5**:e02165.
48. **Sanguinetti MC, Tristani-Firouzi M.** 2006. hERG potassium channels and cardiac arrhythmia. *Nature* **440**:463-469.

49. **Ford CB, Lin PL, Chase MR, Shah RR, Iartchouk O, Galagan J, Mohaideen N, Ioerger TR, Sacchettini JC, Lipsitch M, Flynn JL, Fortune SM.** 2011. Use of whole genome sequencing to estimate the mutation rate of *Mycobacterium tuberculosis* during latent infection. *Nat Genet* **43**:482-486.
50. **Bretl DJ, Demetriadou C, Zahrt TC.** 2011. Adaptation to environmental stimuli within the host: two-component signal transduction systems of *Mycobacterium tuberculosis*. *Microbiol Mol Biol Rev* **75**:566-582.
51. **Vandal OH, Roberts JA, Odaira T, Schnappinger D, Nathan CF, Ehrt S.** 2009. Acid-Susceptible Mutants of *Mycobacterium tuberculosis* Share Hypersusceptibility to Cell Wall and Oxidative Stress and to the Host Environment. *Journal of Bacteriology* **191**:625-631.
52. **Rohde KH, Abramovitch RB, Russell DG.** 2007. *Mycobacterium tuberculosis* invasion of macrophages: linking bacterial gene expression to environmental cues. *Cell Host Microbe* **2**:352-364.
53. **Walters SB, Dubnau E, Kolesnikova I, Laval F, Daffe M, Smith I.** 2006. The *Mycobacterium tuberculosis* PhoPR two-component system regulates genes essential for virulence and complex lipid biosynthesis. *Molecular Microbiology* **60**:312-330.
54. **Abramovitch RB, Rohde KH, Hsu FF, Russell DG.** 2011. *aprABC*: a *Mycobacterium tuberculosis* complex-specific locus that modulates pH-driven adaptation to the macrophage phagosome. *Mol Microbiol* **80**:678-694.
55. **Tan S, Sukumar N, Abramovitch RB, Parish T, Russell DG.** 2013. *Mycobacterium tuberculosis* Responds to Chloride and pH as Synergistic Cues to the Immune Status of its Host Cell. *PLoS Pathog* **9**:e1003282.
56. **Gonzalo-Asensio J, Mostowy S, Harders-Westerveen J, Huygen K, Hernandez-Pando R, Thole J, Behr M, Gicquel B, Martin C.** 2008. PhoP: A Missing Piece in the Intricate Puzzle of *Mycobacterium tuberculosis* Virulence. *Plos One* **3**:e3496.
57. **Martin C, Williams A, Hernandez-Pando R, Cardona PJ, Gormley E, Bordat Y, Soto CY, Clark SO, Hatch GJ, Aguilar D, Ausina V, Gicquel B.** 2006. The live *Mycobacterium tuberculosis* *phoP* mutant strain is more attenuated than BCG and confers protective immunity against tuberculosis in mice and guinea pigs. *Vaccine* **24**:3408-3419.
58. **Perez E, Samper S, Bordas Y, Guilhot C, Gicquel B, Martin C.** 2001. An essential role for *phoP* in *Mycobacterium tuberculosis* virulence. *Molecular Microbiology* **41**:179-187.

59. **Johnson BK, Colvin CJ, Needle DB, Mba Medie F, Champion PA, Abramovitch RB.** 2015. The Carbonic Anhydrase Inhibitor Ethoxzolamide Inhibits the Mycobacterium tuberculosis PhoPR Regulon and Esx-1 Secretion and Attenuates Virulence. *Antimicrob Agents Chemother* **59**:4436-4445.
60. **Carta F, Maresca A, Covarrubias AS, Mowbray SL, Jones TA, Supuran CT.** 2009. Carbonic anhydrase inhibitors. Characterization and inhibition studies of the most active beta-carbonic anhydrase from Mycobacterium tuberculosis, Rv3588c. *Bioorg Med Chem Lett* **19**:6649-6654.
61. **Nishimori I, Minakuchi T, Vullo D, Scozzafava A, Innocenti A, Supuran CT.** 2009. Carbonic anhydrase inhibitors. Cloning, characterization, and inhibition studies of a new beta-carbonic anhydrase from Mycobacterium tuberculosis. *J Med Chem* **52**:3116-3120.
62. **Maresca A, Carta F, Vullo D, Scozzafava A, Supuran CT.** 2009. Carbonic anhydrase inhibitors. Inhibition of the Rv1284 and Rv3273 beta-carbonic anhydrases from Mycobacterium tuberculosis with diazenylbenzenesulfonamides. *Bioorg Med Chem Lett* **19**:4929-4932.
63. **Maresca A, Scozzafava A, Vullo D, Supuran CT.** 2013. Dihalogenated sulfanilamides and benzolamides are effective inhibitors of the three beta-class carbonic anhydrases from Mycobacterium tuberculosis. *J Enzyme Inhib Med Chem* **28**:384-387.
64. **Guzel O, Maresca A, Scozzafava A, Salman A, Balaban AT, Supuran CT.** 2009. Discovery of low nanomolar and subnanomolar inhibitors of the mycobacterial beta-carbonic anhydrases Rv1284 and Rv3273. *J Med Chem* **52**:4063-4067.
65. **Pacchiano F, Carta F, Vullo D, Scozzafava A, Supuran CT.** 2011. Inhibition of beta-carbonic anhydrases with ureido-substituted benzenesulfonamides. *Bioorg Med Chem Lett* **21**:102-105.
66. **Buchieri MV, Riafrecha LE, Rodriguez OM, Vullo D, Morbidoni HR, Supuran CT, Colinas PA.** 2013. Inhibition of the beta-carbonic anhydrases from Mycobacterium tuberculosis with C-cinnamoyl glycosides: identification of the first inhibitor with anti-mycobacterial activity. *Bioorg Med Chem Lett* **23**:740-743.
67. **Maresca A, Vullo D, Scozzafava A, Manole G, Supuran CT.** 2013. Inhibition of the beta-class carbonic anhydrases from Mycobacterium tuberculosis with carboxylic acids. *J Enzyme Inhib Med Chem* **28**:392-396.
68. **Minakuchi T, Nishimori I, Vullo D, Scozzafava A, Supuran CT.** 2009. Molecular cloning, characterization, and inhibition studies of the Rv1284 beta-carbonic anhydrase from Mycobacterium tuberculosis with sulfonamides and a sulfamate. *J Med Chem* **52**:2226-2232.

69. **von Gnielinski N, Nienaber L, Mason L, Ellis S, Triccas JA, Davis RA, Hofmann A.** 2014. Non-classical β -carbonic anhydrase inhibitors-towards novel anti-mycobacterials. *Med Chem Commun* **5**:1563-1566.
70. **Ceruso M, Vullo D, Scozzafava A, Supuran CT.** 2014. Sulfonamides incorporating fluorine and 1,3,5-triazine moieties are effective inhibitors of three beta-class carbonic anhydrases from *Mycobacterium tuberculosis*. *J Enzyme Inhib Med Chem* **29**:686-689.
71. **Jain M, Petzold CJ, Schelle MW, Leavell MD, Mougous JD, Bertozzi CR, Leary JA, Cox JS.** 2007. Lipidomics reveals control of *Mycobacterium tuberculosis* virulence lipids via metabolic coupling. *Proc Natl Acad Sci U S A* **104**:5133-5138.
72. **Baker JJ, Johnson BK, Abramovitch RB.** 2014. Slow growth of *Mycobacterium tuberculosis* at acidic pH is regulated by *phoPR* and host-associated carbon sources. *Mol Microbiol* **94**:56-59.
73. **Frigui W, Bottai D, Majlessi L, Monot M, Josselin E, Brodin P, Garnier T, Gicquel B, Martin C, Leclerc C, Cole ST, Brosch R.** 2008. Control of *M. tuberculosis* ESAT-6 secretion and specific T cell recognition by *PhoP*. *PLoS Pathog* **4**:e33.
74. **Stanley SA, Raghavan S, Hwang WW, Cox JS.** 2003. Acute infection and macrophage subversion by *Mycobacterium tuberculosis* require a specialized secretion system. *Proc Natl Acad Sci U S A* **100**:13001-13006.
75. **Tang YT, Gao R, Havranek JJ, Groisman EA, Stock AM, Marshall GR.** 2012. Inhibition of bacterial virulence: drug-like molecules targeting the *Salmonella enterica* *PhoP* response regulator. *Chem Biol Drug Des* **79**:1007-1017.
76. **Ofek I, Hasty DL, Doyle RJ, Ofek I.** 2003. Bacterial adhesion to animal cells and tissues. ASM Press, Washington, D.C.
77. **Proft T, Baker EN.** 2009. Pili in Gram-negative and Gram-positive bacteria - structure, assembly and their role in disease. *Cell Mol Life Sci* **66**:613-635.
78. **Pizarro-Cerda J, Cossart P.** 2006. Bacterial adhesion and entry into host cells. *Cell* **124**:715-727.
79. **Kline KA, Falker S, Dahlberg S, Normark S, Henriques-Normark B.** 2009. Bacterial adhesins in host-microbe interactions. *Cell Host Microbe* **5**:580-592.
80. **Thanassi DG, Bliska JB, Christie PJ.** 2012. Surface organelles assembled by secretion systems of Gram-negative bacteria: diversity in structure and function. *FEMS Microbiol Rev* **36**:1046-1082.

81. **Sauer FG, Mulvey MA, Schilling JD, Martinez JJ, Hultgren SJ.** 2000. Bacterial pili: molecular mechanisms of pathogenesis. *Curr Opin Microbiol* **3**:65-72.
82. **Costa TR, Felisberto-Rodrigues C, Meir A, Prevost MS, Redzej A, Trokter M, Waksman G.** 2015. Secretion systems in Gram-negative bacteria: structural and mechanistic insights. *Nat Rev Microbiol* **13**:343-359.
83. **Lillington J, Geibel S, Waksman G.** 2015. Reprint of "Biogenesis and adhesion of type 1 and P pili". *Biochim Biophys Acta* **1850**:554-564.
84. **Evans ML, Chapman MR.** 2014. Curli biogenesis: order out of disorder. *Biochim Biophys Acta* **1843**:1551-1558.
85. **Van Gerven N, Klein RD, Hultgren SJ, Remaut H.** 2015. Bacterial amyloid formation: structural insights into curli biogenesis. *Trends Microbiol* **23**:693-706.
86. **Cegelski L, Pinkner JS, Hammer ND, Cusumano CK, Hung CS, Chorell E, Aberg V, Walker JN, Seed PC, Almqvist F, Chapman MR, Hultgren SJ.** 2009. Small-molecule inhibitors target Escherichia coli amyloid biogenesis and biofilm formation. *Nat Chem Biol* **5**:913-919.
87. **Hung C, Zhou Y, Pinkner JS, Dodson KW, Crowley JR, Heuser J, Chapman MR, Hadjifrangiskou M, Henderson JP, Hultgren SJ.** 2013. Escherichia coli biofilms have an organized and complex extracellular matrix structure. *MBio* **4**:e00645-00613.
88. **Svensson A, Larsson A, Emtenas H, Hedenstrom M, Fex T, Hultgren SJ, Pinkner JS, Almqvist F, Kihlberg J.** 2001. Design and evaluation of pilicides: potential novel antibacterial agents directed against uropathogenic Escherichia coli. *Chembiochem* **2**:915-918.
89. **Pinkner JS, Remaut H, Buelens F, Miller E, Aberg V, Pemberton N, Hedenstrom M, Larsson A, Seed P, Waksman G, Hultgren SJ, Almqvist F.** 2006. Rationally designed small compounds inhibit pilus biogenesis in uropathogenic bacteria. *Proc Natl Acad Sci U S A* **103**:17897-17902.
90. **Berg V, Sellstedt M, Hedenstrom M, Pinkner JS, Hultgren SJ, Almqvist F.** 2006. Design, synthesis and evaluation of peptidomimetics based on substituted bicyclic 2-pyridones-targeting virulence of uropathogenic E. coli. *Bioorg Med Chem* **14**:7563-7581.
91. **Han Z, Pinkner JS, Ford B, Obermann R, Nolan W, Wildman SA, Hobbs D, Ellenberger T, Cusumano CK, Hultgren SJ, Janetka JW.** 2010. Structure-based drug design and optimization of mannoside bacterial FimH antagonists. *J Med Chem* **53**:4779-4792.

92. **Han Z, Pinkner JS, Ford B, Chorell E, Crowley JM, Cusumano CK, Campbell S, Henderson JP, Hultgren SJ, Janetka JW.** 2012. Lead optimization studies on FimH antagonists: discovery of potent and orally bioavailable ortho-substituted biphenyl mannosides. *J Med Chem* **55**:3945-3959.
93. **Totsika M, Kostakioti M, Hannan TJ, Upton M, Beatson SA, Janetka JW, Hultgren SJ, Schembri MA.** 2013. A FimH inhibitor prevents acute bladder infection and treats chronic cystitis caused by multidrug-resistant uropathogenic *Escherichia coli* ST131. *J Infect Dis* **208**:921-928.
94. **Cusumano CK, Pinkner JS, Han Z, Greene SE, Ford BA, Crowley JR, Henderson JP, Janetka JW, Hultgren SJ.** 2011. Treatment and prevention of urinary tract infection with orally active FimH inhibitors. *Sci Transl Med* **3**:109ra115.
95. **Guiton PS, Cusumano CK, Kline KA, Dodson KW, Han Z, Janetka JW, Henderson JP, Caparon MG, Hultgren SJ.** 2012. Combinatorial small-molecule therapy prevents uropathogenic *Escherichia coli* catheter-associated urinary tract infections in mice. *Antimicrob Agents Chemother* **56**:4738-4745.
96. **Jarvis C, Han Z, Kalas V, Klein R, Pinkner JS, Ford B, Binkley J, Cusumano CK, Cusumano Z, Mydock-McGrane L, Hultgren SJ, Janetka JW.** 2016. Antivirulence Isoquinolone Mannosides: Optimization of the Biaryl Aglycone for FimH Lectin Binding Affinity and Efficacy in the Treatment of Chronic UTI. *ChemMedChem* **11**:367-373.
97. **Shamir ER, Warthan M, Brown SP, Nataro JP, Guerrant RL, Hoffman PS.** 2010. Nitazoxanide inhibits biofilm production and hemagglutination by enteroaggregative *Escherichia coli* strains by blocking assembly of AafA fimbriae. *Antimicrob Agents Chemother* **54**:1526-1533.
98. **Chahales P, Hoffman PS, Thanassi DG.** 2016. Nitazoxanide Inhibits Pilus Biogenesis by Interfering with Folding of the Usher Protein in the Outer Membrane. *Antimicrob Agents Chemother* **60**:2028-2038.
99. **Bolick DT, Roche JK, Hontecillas R, Bassaganya-Riera J, Nataro JP, Guerrant RL.** 2013. Enteroaggregative *Escherichia coli* strain in a novel weaned mouse model: exacerbation by malnutrition, biofilm as a virulence factor and treatment by nitazoxanide. *J Med Microbiol* **62**:896-905.
100. **Warren CA, van Opstal E, Ballard TE, Kennedy A, Wang X, Riggins M, Olekhnovich I, Warthan M, Kolling GL, Guerrant RL, Macdonald TL, Hoffman PS.** 2012. Amixicile, a novel inhibitor of pyruvate: ferredoxin oxidoreductase, shows efficacy against *Clostridium difficile* in a mouse infection model. *Antimicrob Agents Chemother* **56**:4103-4111.

101. **Hoffman PS, Sisson G, Croxen MA, Welch K, Harman WD, Cremades N, Morash MG.** 2007. Antiparasitic drug nitazoxanide inhibits the pyruvate oxidoreductases of *Helicobacter pylori*, selected anaerobic bacteria and parasites, and *Campylobacter jejuni*. *Antimicrob Agents Chemother* **51**:868-876.
102. **Sisson G, Goodwin A, Raudonikienė A, Hughes NJ, Mukhopadhyay AK, Berg DE, Hoffman PS.** 2002. Enzymes associated with reductive activation and action of nitazoxanide, nitrofurans, and metronidazole in *Helicobacter pylori*. *Antimicrob Agents Chemother* **46**:2116-2123.
103. **Dubreuil L, Houcke I, Mouton Y, Rossignol JF.** 1996. In vitro evaluation of activities of nitazoxanide and tizoxanide against anaerobes and aerobic organisms. *Antimicrob Agents Chemother* **40**:2266-2270.
104. **Saldana Z, Xicohtencatl-Cortes J, Avelino F, Phillips AD, Kaper JB, Puente JL, Giron JA.** 2009. Synergistic role of curli and cellulose in cell adherence and biofilm formation of attaching and effacing *Escherichia coli* and identification of Fis as a negative regulator of curli. *Environ Microbiol* **11**:992-1006.
105. **Aberg V, Norman F, Chorell E, Westermarck A, Olofsson A, Sauer-Eriksson AE, Almqvist F.** 2005. Microwave-assisted decarboxylation of bicyclic 2-pyridone scaffolds and identification of Abeta-peptide aggregation inhibitors. *Org Biomol Chem* **3**:2817-2823.
106. **Evans ML, Chorell E, Taylor JD, Aden J, Gotheson A, Li F, Koch M, Sefer L, Matthews SJ, Wittung-Stafshede P, Almqvist F, Chapman MR.** 2015. The bacterial curli system possesses a potent and selective inhibitor of amyloid formation. *Mol Cell* **57**:445-455.
107. **Cornelis GR, Van Gijsegem F.** 2000. Assembly and function of type III secretory systems. *Annu Rev Microbiol* **54**:735-774.
108. **Stavrinides J, McCann HC, Guttman DS.** 2008. Host-pathogen interplay and the evolution of bacterial effectors. *Cell Microbiol* **10**:285-292.
109. **Keyser P, Elofsson M, Rosell S, Wolf-Watz H.** 2008. Virulence blockers as alternatives to antibiotics: type III secretion inhibitors against Gram-negative bacteria. *J Intern Med* **264**:17-29.
110. **Duncan MC, Linington RG, Auerbuch V.** 2012. Chemical inhibitors of the type three secretion system: disarming bacterial pathogens. *Antimicrob Agents Chemother* **56**:5433-5441.

111. **Swietnicki W, Carmany D, Retford M, Guelta M, Dorsey R, Bozue J, Lee MS, Olson MA.** 2011. Identification of small-molecule inhibitors of *Yersinia pestis* Type III secretion system YscN ATPase. *PLoS One* **6**:e19716.
112. **Houben EN, Korotkov KV, Bitter W.** 2014. Take five - Type VII secretion systems of *Mycobacteria*. *Biochim Biophys Acta* **1843**:1707-1716.
113. **Angelichio MJ, Spector J, Waldor MK, Camilli A.** 1999. *Vibrio cholerae* intestinal population dynamics in the suckling mouse model of infection. *Infect Immun* **67**:3733-3739.
114. **Sanchez J, Holmgren J.** 2011. Cholera toxin - a foe & a friend. *Indian J Med Res* **133**:153-163.
115. **Taylor RK, Miller VL, Furlong DB, Mekalanos JJ.** 1987. Use of *phoA* gene fusions to identify a pilus colonization factor coordinately regulated with cholera toxin. *Proc Natl Acad Sci U S A* **84**:2833-2837.
116. **DiRita VJ, Parsot C, Jander G, Mekalanos JJ.** 1991. Regulatory cascade controls virulence in *Vibrio cholerae*. *Proc Natl Acad Sci U S A* **88**:5403-5407.
117. **Almagro-Moreno S, Pruss K, Taylor RK.** 2015. Intestinal Colonization Dynamics of *Vibrio cholerae*. *PLoS Pathog* **11**:e1004787.
118. **Shakhnovich EA, Hung DT, Pierson E, Lee K, Mekalanos JJ.** 2007. Virstatin inhibits dimerization of the transcriptional activator ToxT. *Proc Natl Acad Sci U S A* **104**:2372-2377.
119. **Hung DT, Shakhnovich EA, Pierson E, Mekalanos JJ.** 2005. Small-molecule inhibitor of *Vibrio cholerae* virulence and intestinal colonization. *Science* **310**:670-674.
120. **Surawicz CM, Brandt LJ, Binion DG, Ananthakrishnan AN, Curry SR, Gilligan PH, McFarland LV, Mellow M, Zuckerbraun BS.** 2013. Guidelines for diagnosis, treatment, and prevention of *Clostridium difficile* infections. *Am J Gastroenterol* **108**:478-498; quiz 499.
121. **Kelly CP.** 2012. Can we identify patients at high risk of recurrent *Clostridium difficile* infection? *Clin Microbiol Infect* **18 Suppl 6**:21-27.
122. **Hu MY, Katchar K, Kyne L, Maroo S, Tummala S, Dreisbach V, Xu H, Leffler DA, Kelly CP.** 2009. Prospective derivation and validation of a clinical prediction rule for recurrent *Clostridium difficile* infection. *Gastroenterology* **136**:1206-1214.

123. **van Nood E, Vrieze A, Nieuwdorp M, Fuentes S, Zoetendal EG, de Vos WM, Visser CE, Kuijper EJ, Bartelsman JF, Tijssen JG, Speelman P, Dijkgraaf MG, Keller JJ.** 2013. Duodenal infusion of donor feces for recurrent *Clostridium difficile*. *N Engl J Med* **368**:407-415.
124. **Pamer EG.** 2014. Fecal microbiota transplantation: effectiveness, complexities, and lingering concerns. *Mucosal Immunol* **7**:210-214.
125. **Shim JK, Johnson S, Samore MH, Bliss DZ, Gerding DN.** 1998. Primary symptomless colonisation by *Clostridium difficile* and decreased risk of subsequent diarrhoea. *Lancet* **351**:633-636.
126. **Kyne L, Warny M, Qamar A, Kelly CP.** 2000. Asymptomatic carriage of *Clostridium difficile* and serum levels of IgG antibody against toxin A. *N Engl J Med* **342**:390-397.
127. **Drudy D, Harnedy N, Fanning S, Hannan M, Kyne L.** 2007. Emergence and control of fluoroquinolone-resistant, toxin A-negative, toxin B-positive *Clostridium difficile*. *Infect Control Hosp Epidemiol* **28**:932-940.
128. **Pruitt RN, Lacy DB.** 2012. Toward a structural understanding of *Clostridium difficile* toxins A and B. *Front Cell Infect Microbiol* **2**:28.
129. **Shen A, Lupardus PJ, Gersch MM, Puri AW, Albrow VE, Garcia KC, Bogyo M.** 2011. Defining an allosteric circuit in the cysteine protease domain of *Clostridium difficile* toxins. *Nat Struct Mol Biol* **18**:364-371.
130. **Bender KO, Garland M, Ferreyra JA, Hryckowian AJ, Child MA, Puri AW, Solow-Cordero DE, Higginbottom SK, Segal E, Banaei N, Shen A, Sonnenburg JL, Bogyo M.** 2015. A small-molecule antivirulence agent for treating *Clostridium difficile* infection. *Sci Transl Med* **7**:306ra148.
131. **trials Nc.** <https://clinicaltrials.gov/ct2/results?term=ebselen&Search=Search>. Accessed
132. **Lu J, Vlamis-Gardikas A, Kandasamy K, Zhao R, Gustafsson TN, Engstrand L, Hoffner S, Engman L, Holmgren A.** 2013. Inhibition of bacterial thioredoxin reductase: an antibiotic mechanism targeting bacteria lacking glutathione. *FASEB J* **27**:1394-1403.
133. **Lieberman OJ, Orr MW, Wang Y, Lee VT.** 2014. High-throughput screening using the differential radial capillary action of ligand assay identifies ebselen as an inhibitor of diguanylate cyclases. *ACS Chem Biol* **9**:183-192.

134. **Favrot L, Grzegorzewicz AE, Lajiness DH, Marvin RK, Boucau J, Isailovic D, Jackson M, Ronning DR.** 2013. Mechanism of inhibition of Mycobacterium tuberculosis antigen 85 by ebselen. *Nat Commun* **4**:2748.
135. **Bhabak KP, Mugesh G.** 2010. Functional mimics of glutathione peroxidase: bioinspired synthetic antioxidants. *Acc Chem Res* **43**:1408-1419.
136. **Butler T.** 2009. Plague into the 21st century. *Clin Infect Dis* **49**:736-742.
137. **Pan NJ, Brady MJ, Leong JM, Goguen JD.** 2009. Targeting type III secretion in *Yersinia pestis*. *Antimicrob Agents Chemother* **53**:385-392.
138. **Cornelis GR, Boland A, Boyd AP, Geuijen C, Iriarte M, Neyt C, Sory MP, Stainier I.** 1998. The virulence plasmid of *Yersinia*, an antihost genome. *Microbiol Mol Biol Rev* **62**:1315-1352.
139. **Ritchie JM, Waldor MK.** 2005. The locus of enterocyte effacement-encoded effector proteins all promote enterohemorrhagic *Escherichia coli* pathogenicity in infant rabbits. *Infect Immun* **73**:1466-1474.
140. **Pujol C, Bliska JB.** 2005. Turning *Yersinia* pathogenesis outside in: subversion of macrophage function by intracellular yersiniae. *Clin Immunol* **114**:216-226.
141. **Pujol C, Bliska JB.** 2003. The ability to replicate in macrophages is conserved between *Yersinia pestis* and *Yersinia pseudotuberculosis*. *Infect Immun* **71**:5892-5899.
142. **Neyt C, Cornelis GR.** 1999. Insertion of a Yop translocation pore into the macrophage plasma membrane by *Yersinia enterocolitica*: requirement for translocators YopB and YopD, but not LcrG. *Mol Microbiol* **33**:971-981.
143. **Dacheux D, Goure J, Chabert J, Usson Y, Attree I.** 2001. Pore-forming activity of type III system-secreted proteins leads to oncosis of *Pseudomonas aeruginosa*-infected macrophages. *Mol Microbiol* **40**:76-85.
144. **Akeda Y, Galan JE.** 2005. Chaperone release and unfolding of substrates in type III secretion. *Nature* **437**:911-915.
145. **Cordero-Alba M, Bernal-Bayard J, Ramos-Morales F.** 2012. SrfJ, a *Salmonella* type III secretion system effector regulated by PhoP, RcsB, and IolR. *J Bacteriol* **194**:4226-4236.
146. **Kinchen JM, Ravichandran KS.** 2008. Phagosome maturation: going through the acid test. *Nat Rev Mol Cell Biol* **9**:781-795.

147. **De Leon J, Jiang G, Ma Y, Rubin E, Fortune S, Sun J.** 2012. Mycobacterium tuberculosis ESAT-6 exhibits a unique membrane-interacting activity that is not found in its ortholog from non-pathogenic Mycobacterium smegmatis. *J Biol Chem* **287**:44184-44191.
148. **Pym AS, Brodin P, Brosch R, Huerre M, Cole ST.** 2002. Loss of RD1 contributed to the attenuation of the live tuberculosis vaccines Mycobacterium bovis BCG and Mycobacterium microti. *Mol Microbiol* **46**:709-717.
149. **Rybniker J, Chen JM, Sala C, Hartkoorn RC, Vocat A, Benjak A, Boy-Rottger S, Zhang M, Szekely R, Greff Z, Orfi L, Szabadkai I, Pato J, Keri G, Cole ST.** 2014. Anticytolytic screen identifies inhibitors of mycobacterial virulence protein secretion. *Cell Host Microbe* **16**:538-548.
150. **Takii T, Yamamoto Y, Chiba T, Abe C, Belisle JT, Brennan PJ, Onozaki K.** 2002. Simple fibroblast-based assay for screening of new antimicrobial drugs against Mycobacterium tuberculosis. *Antimicrob Agents Chemother* **46**:2533-2539.
151. **Hsu T, Hingley-Wilson SM, Chen B, Chen M, Dai AZ, Morin PM, Marks CB, Padiyar J, Goulding C, Gingery M, Eisenberg D, Russell RG, Derrick SC, Collins FM, Morris SL, King CH, Jacobs WR, Jr.** 2003. The primary mechanism of attenuation of bacillus Calmette-Guerin is a loss of secreted lytic function required for invasion of lung interstitial tissue. *Proc Natl Acad Sci U S A* **100**:12420-12425.
152. **Pang X, Vu P, Byrd TF, Ghanny S, Soteropoulos P, Mukamolova GV, Wu S, Samten B, Howard ST.** 2007. Evidence for complex interactions of stress-associated regulons in an mprAB deletion mutant of Mycobacterium tuberculosis. *Microbiology* **153**:1229-1242.
153. **Pang X, Samten B, Cao G, Wang X, Tvinnereim AR, Chen XL, Howard ST.** 2013. MprAB regulates the espA operon in Mycobacterium tuberculosis and modulates ESX-1 function and host cytokine response. *J Bacteriol* **195**:66-75.
154. **Rohmer L, Hocquet D, Miller SI.** 2011. Are pathogenic bacteria just looking for food? Metabolism and microbial pathogenesis. *Trends Microbiol* **19**:341-348.
155. **Olive AJ, Sassetti CM.** 2016. Metabolic crosstalk between host and pathogen: sensing, adapting and competing. *Nat Rev Microbiol* **14**:221-234.
156. **Clemens DL, Horwitz MA.** 1996. The Mycobacterium tuberculosis phagosome interacts with early endosomes and is accessible to exogenously administered transferrin. *J Exp Med* **184**:1349-1355.

157. **Tan S, Russell DG.** 2015. Trans-species communication in the *Mycobacterium tuberculosis*-infected macrophage. *Immunol Rev* **264**:233-248.
158. **Fratti RA, Vergne I, Chua J, Skidmore J, Deretic V.** 2000. Regulators of membrane trafficking and *Mycobacterium tuberculosis* phagosome maturation block. *Electrophoresis* **21**:3378-3385.
159. **Schaible UE, Sturgill-Koszycki S, Schlesinger PH, Russell DG.** 1998. Cytokine activation leads to acidification and increases maturation of *Mycobacterium avium*-containing phagosomes in murine macrophages. *J Immunol* **160**:1290-1296.
160. **Pandey AK, Sasseti CM.** 2008. Mycobacterial persistence requires the utilization of host cholesterol. *Proc Natl Acad Sci U S A* **105**:4376-4380.
161. **Rothchild AC, Jayaraman P, Nunes-Alves C, Behar SM.** 2014. iNKT cell production of GM-CSF controls *Mycobacterium tuberculosis*. *PLoS Pathog* **10**:e1003805.
162. **Griffin JE, Gawronski JD, Dejesus MA, Ioerger TR, Akerley BJ, Sasseti CM.** 2011. High-resolution phenotypic profiling defines genes essential for mycobacterial growth and cholesterol catabolism. *PLoS Pathog* **7**:e1002251.
163. **Lancaster JR, Jr.** 2006. Nitroxidative, nitrosative, and nitrative stress: kinetic predictions of reactive nitrogen species chemistry under biological conditions. *Chem Res Toxicol* **19**:1160-1174.
164. **Voskuil MI, Schnappinger D, Visconti KC, Harrell MI, Dolganov GM, Sherman DR, Schoolnik GK.** 2003. Inhibition of respiration by nitric oxide induces a *Mycobacterium tuberculosis* dormancy program. *J Exp Med* **198**:705-713.
165. **Rohde K, Yates RM, Purdy GE, Russell DG.** 2007. *Mycobacterium tuberculosis* and the environment within the phagosome. *Immunol Rev* **219**:37-54.
166. **McCune RM, Feldmann FM, Lambert HP, McDermott W.** 1966. Microbial persistence. I. The capacity of tubercle bacilli to survive sterilization in mouse tissues. *J Exp Med* **123**:445-468.
167. **Tian J, Bryk R, Itoh M, Suematsu M, Nathan C.** 2005. Variant tricarboxylic acid cycle in *Mycobacterium tuberculosis*: identification of alpha-ketoglutarate decarboxylase. *Proc Natl Acad Sci U S A* **102**:10670-10675.
168. **Bryk R, Lima CD, Erdjument-Bromage H, Tempst P, Nathan C.** 2002. Metabolic enzymes of mycobacteria linked to antioxidant defense by a thioredoxin-like protein. *Science* **295**:1073-1077.

169. **Bryk R, Griffin P, Nathan C.** 2000. Peroxynitrite reductase activity of bacterial peroxiredoxins. *Nature* **407**:211-215.
170. **Shi S, Ehrt S.** 2006. Dihydrolipoamide acyltransferase is critical for *Mycobacterium tuberculosis* pathogenesis. *Infect Immun* **74**:56-63.
171. **McMurray DN.** 2001. Disease model: pulmonary tuberculosis. *Trends Mol Med* **7**:135-137.
172. **Bryk R, Gold B, Venugopal A, Singh J, Samy R, Pupek K, Cao H, Popescu C, Gurney M, Hotha S, Cherian J, Rhee K, Ly L, Converse PJ, Ehrt S, Vandal O, Jiang X, Schneider J, Lin G, Nathan C.** 2008. Selective killing of nonreplicating mycobacteria. *Cell Host Microbe* **3**:137-145.
173. **Griffin JE, Pandey AK, Gilmore SA, Mizrahi V, McKinney JD, Bertozzi CR, Sassetti CM.** 2012. Cholesterol catabolism by *Mycobacterium tuberculosis* requires transcriptional and metabolic adaptations. *Chem Biol* **19**:218-227.
174. **Gould TA, van de Langemheen H, Munoz-Elias EJ, McKinney JD, Sacchettini JC.** 2006. Dual role of isocitrate lyase 1 in the glyoxylate and methylcitrate cycles in *Mycobacterium tuberculosis*. *Mol Microbiol* **61**:940-947.
175. **Munoz-Elias EJ, Upton AM, Cherian J, McKinney JD.** 2006. Role of the methylcitrate cycle in *Mycobacterium tuberculosis* metabolism, intracellular growth, and virulence. *Mol Microbiol* **60**:1109-1122.
176. **Eoh H, Rhee KY.** 2014. Methylcitrate cycle defines the bactericidal essentiality of isocitrate lyase for survival of *Mycobacterium tuberculosis* on fatty acids. *Proc Natl Acad Sci U S A* **111**:4976-4981.
177. **Savvi S, Warner DF, Kana BD, McKinney JD, Mizrahi V, Dawes SS.** 2008. Functional characterization of a vitamin B-12-dependent methylmalonyl pathway in *Mycobacterium tuberculosis*: Implications for propionate metabolism during growth on fatty acids. *Journal of Bacteriology* **190**:3886-3895.
178. **Dresen C, Lin LY, D'Angelo I, Tocheva EI, Strynadka N, Eltis LD.** 2010. A flavin-dependent monooxygenase from *Mycobacterium tuberculosis* involved in cholesterol catabolism. *J Biol Chem* **285**:22264-22275.
179. **Capyk JK, Casabon I, Gruninger R, Strynadka NC, Eltis LD.** 2011. Activity of 3-ketosteroid 9 α -hydroxylase (KshAB) indicates cholesterol side chain and ring degradation occur simultaneously in *Mycobacterium tuberculosis*. *J Biol Chem* **286**:40717-40724.

CHAPTER 2 – High-throughput screening for inhibitors of *Mycobacterium tuberculosis* pathogenesis and growth

Preface

Treatment of *Mycobacterium tuberculosis* (Mtb) requires a multi-drug regimen to be taken for at least six months. The front-line antibiotics used to combat a drug-susceptible infection include: isoniazid, rifampicin, ethambutol, and pyrazinamide. These drugs were discovered during the mid-twentieth century and although they have had a profound impact on reducing the morbidity and mortality of Mtb infections, resistance to these treatments is on the rise. Thus, new treatments and targets are needed to treat Mtb infections.

A contributing factor to the increase in drug-resistant strains of Mtb is patient non-compliance in completing the duration of treatment, a difficult task in areas where public health infrastructure is lacking. Therapeutic strategies that reduce the length of treatment could dramatically alter the control of tuberculosis disease and reduce the incidence of recurrent drug-resistant infections. The extended treatment length of Mtb is associated with the bacterium entering a persistent state during pathogenesis making it recalcitrant to antibiotic therapy. Notably, the front-line therapeutic pyrazinamide is implicated in significantly contributing to eradication of these persistent bacteria due to its ability to penetrate Mtb containing lung lesions (1). Pyrazinamide is only active at acidic pH, suggesting that many of these persisters are localized in acidic environments (2). Therefore it follows that disrupting Mtb's ability to enter a persistent state or resist acidic pH may shorten the course of therapy.

Mtb is able to sense host cues and modulate its physiology to adapt to the changing environment. The Mtb two-component regulatory systems (TCSs) DosRST and PhoPR are

implicated in sensing and responding to the host immune pressures hypoxia/nitric oxide/carbon monoxide and pH, respectively (3-9). Both systems are required for pathogenesis and loss of either TCS leads to significant attenuation in animal models of infection (7, 10-14). The DosRST TCS plays a significant role in Mtb's ability to establish a persistent infection. Further, Mtb frequently encounters acidic environments during the course of infection ranging from the macrophage phagosome to necrotic, caseating granulomas. Previous work has shown that the PhoPR TCS responds to acidic pH, suggesting that PhoPR-mediated, pH-driven adaptation is required for Mtb virulence. Taken together, the DosRST and PhoPR TCS represent attractive therapeutic targets that may function to shorten the course of therapy. However, despite the requirements *in vivo*, both systems are dispensable for Mtb growth *in vitro* making it difficult to screen for DosRST or PhoPR inhibitors by conventional high-throughput screening (HTS) methods.

Fluorescent reporter strains are powerful tools for discovery and characterization of antimicrobials. They can function as synthetic phenotypes for pathways not directly required for *in vitro* growth. Indeed, we constructed two GFP expressing reporter strains that are induced in a DosRST or PhoPR dependent manner during hypoxia/nitric oxide or acidic pH, respectively (6, 15). Leveraging these fluorescent reporter strains, we conducted two whole-cell phenotypic high-throughput screens of the same compound library for inhibitors of hypoxia- and pH-driven adaptation. We identified many candidate inhibitors of the environmental sensing pathways and general inhibitors of Mtb growth. Secondary assays authenticated several lead compounds for subsequent validation, exhibiting activity in Mtb infected macrophages and low eukaryotic cytotoxicity. Ethoxzolamide was successfully identified as a PhoPR-regulon inhibitor, likely through its carbonic anhydrase inhibitory activity, establishing a previously unrecognized link

between Mtb carbonic anhydrases, carbon dioxide, pH-sensing, and PhoPR-signaling (Chapter 3).

The pH-dependent activity of pyrazinamide suggests that a conditionally active compound against Mtb at acidic pH is a viable and relatively untapped therapeutic approach to controlling the pathogen. An additional advantage to performing both screens against the same compound library is the ability to resolve inhibitors of Mtb growth that are only active at acidic pH. This capability is possible as the DosRST screen was performed at neutral pH and the PhoPR screen was executed at acidic pH. By comparing positive hits against Mtb growth in both screens, those that were only identified in the PhoPR screen suggest pH-dependent activity. Indeed, we identified compounds that exhibited pH-dependent growth inhibition against Mtb (Figure 2.6.). As a proof-of-concept study, we followed up a compound termed PH036 that exhibits enhanced anti-mycobacterial activity against Mtb growth at acidic pH relative to neutral pH (Chapter 5). Taken together, the high-throughput screens successfully identified inhibitors of virulence-associated environmental sensing pathways and compounds with pH-dependent activity, providing potentially new therapeutic leads against the ongoing battle against Mtb.

Introduction

We employed whole-cell phenotypic screening methods to identify inhibitors of PhoPR- and DosRST-mediated adaptation in *Mycobacterium tuberculosis* (9). Previously, we constructed fluorescent reporter strains in the clinical isolate Mtb CDC1551 to monitor activity of each TCS under a relevant environmental signal (e.g. hypoxia or acidic pH). The CDC1551(*hspX*::GFP) reporter exhibits hypoxia and nitric oxide inducible fluorescence in a DosRST-dependent manner and was used to screen for inhibitors of the DosRST regulon (15). Additionally, the

CDC1551(*aprA*'::GFP) reporter exhibits pH-inducible fluorescence in a PhoPR-dependent manner and was implemented in the high-throughput screen to discover inhibitors of the PhoPR regulon (6, 9). Both reporter strains exhibit large dynamic ranges between positive (rifampicin) and negative controls during hypoxia or under acidic conditions, making both biosensors amenable to high-throughput screening.

Despite the requirement of DosRST and PhoPR *in vivo*, both TCSs are dispensable for growth *in vitro*. Thus, using the fluorescent reporter strains as synthetic phenotypes, we screened ~273,000 compounds for inhibitors of the DosRST- or PhoPR-dependent GFP fluorescence. The compound libraries were provided by the Institute of Chemistry and Cell Biology (ICCB) at Harvard University and represent broad chemical diversity. The compounds screened consisted of small molecules, natural products, and known bioactives. Reporter strains were grown in 384-well plates containing the screening compounds (~10 μ M) in rich medium buffered to either pH 7.0 or pH 5.7 for the DosRST and PhoPR screens, respectively. Following six days incubations, plates were examined for fluorescence and growth. Data were analyzed using the HAARP custom software suite (Chapter 6).

Potential inhibitors of the DosRST or PhoPR regulon are expected to exhibit reduced GFP fluorescence while growth is relatively unaffected, due to their dispensability *in vitro*. These hits were categorized as Class I inhibitors that have at least 1.5-fold fluorescence to growth inhibition ratio with greater than 35% fluorescence inhibition. In addition to the Class I hits, we expected to find general inhibitors of Mtb growth. These compounds were categorized as Class II molecules that inhibit greater than 50% fluorescence and growth. Class III compounds were classified in the CDC1551(*aprA*'::GFP) screen as inhibitors of bacterial growth while fluorescence is relatively unaffected. We expected these inhibitors to be compounds that

likely target pathways not associated with affecting transcription/translation of the reporter but slow Mtb growth (e.g. cell wall processes). Finally, by comparing Class II inhibitors from both screens, we were able to resolve compounds that inhibit Mtb growth in a pH-dependent manner.

Materials and Methods

High-throughput screening assay and data analysis

A 272,358 compound library arrayed in 384-well optical microtiter plates was provided by the NSRB ICCBL at Harvard University. Two columns of each plate were left blank for positive and negative controls of 0.3 μ M rifampicin and dimethyl sulfoxide (DMSO), respectively. Mtb CDC1551(*aprA*'::GFP) was grown in Middlebrook 7H9 medium, buffered at pH 7.0 with 100 mM 3-(N-morpholino)propanesulfonic acid (MOPS), to mid- to late-log phase. The cultures were then pelleted, re-suspended in 7H9 buffered at pH 5.7 with 100 mM 2-(N-morpholino)ethanesulfonic acid (MES) and dispensed into the 384-well assay plates at an optical density (OD) of 0.2. Mtb CDC1551(*hspX*'::GFP) was grown in Middlebrook 7H9 medium, buffered at pH 7.0 with 100 mM MOPS, to mid- to late-log phase. The cultures were then pelleted, re-suspended in fresh 7H9 buffered at pH 7.0 and dispensed into the 384-well assay plates at an optical density (OD) of 0.05. The plates were incubated for 6 days at 37°C and both fluorescence and OD were measured on a plate reader. For analysis of hits, the HAARP custom software suite was used. Potential PhoPR or DosRST regulon inhibitors (Class I) were flagged as compounds that had: i) greater than 35% fluorescence inhibition, and ii) at least a 1.5-fold greater fluorescence inhibition as compared to growth inhibition. Inhibitors of Mtb growth (Class II) were binned as hits that had greater than 50% fluorescence and growth inhibition. Class III inhibitors of Mtb CDC1551(*aprA*'::GFP) were defined as compounds that had: i) greater than

50% growth inhibition, ii) less than 50% fluorescence inhibition, and iii) at least 1.5-fold greater growth inhibition as compared to fluorescence inhibition. Primary hits were manually curated for removal of known antibiotics. Raw data set submission and cherry pick preparation were also analyzed using HAARP.

Primary hit reconfirmation assay

The fluorescent reporter strains were grown and arrayed into 384-well microtiter assay plates as described above. Two columns of each plate were left blank for positive and negative controls of 0.3 μ M rifampicin and dimethyl sulfoxide (DMSO), respectively. Cherry pick compounds were added at a final concentration of 10 μ M to each well. The plates were incubated for 6 days at 37°C and both fluorescence and OD were measured on a plate reader. For analysis of hits, the HAARP custom software suite was used. Re-confirmed hits were determined if the same inhibition profile was observed in both the primary and secondary screen.

GFP quenching assay

The fluorescent reporter strains were grown and arrayed into 384-well microtiter assay plates as described in the primary screen methods. Two columns of each plate were left blank for positive and negative controls of 0.3 μ M rifampicin and dimethyl sulfoxide (DMSO), respectively. Mtb reporter strains were incubated for 6 days to induce GFP fluorescence in the absence of the cherry picks. Following 6 days of incubation, cherry pick compounds were added to each well and read for fluorescence quenching activity. For analysis of hits, the HAARP custom software suite was used.

Eukaryotic cytotoxicity assay

Primary murine bone marrow-derived macrophages (BMDMs) were isolated and cultured as previously described (17). Briefly, BMDMs were isolated from wild type (WT) C57Bl/6 mice (Charles River) and grown at 37°C (5% CO₂) in DMEM (Corning CellGro) containing 10% fetal bovine serum (Thermo Scientific), 20% L-cell conditioned medium, 1 mM pyruvate, 2 mM L-glutamine, and 1 mM penicillin/streptomycin (Corning CellGro). Cells were grown until confluent, scraped, and plated in white 384-well microtiter plates in medium lacking antibiotics at 2×10^5 cells/mL. Cells were allowed to adhere overnight before addition of experimental treatments. The positive and negative controls for cytotoxicity were 1% Triton X-100 and DMSO in medium lacking antibiotics, respectively. Cells were incubated for 6 days at 37°C (5% CO₂) and analyzed for viability using the CellTiter-Glo (Promega) luminescence kit. For analysis, the HAARP custom software suite was used. Hits were binned as non-cytotoxic if they exhibited less than 10% cytotoxicity.

Inhibition of Mtb growth in macrophages assay

BMDMs were prepared as described above. BMDMs were infected with Mtb expressing luciferase (Mtb luc) as previously described. Briefly, Mtb luc was cultured in Middlebrook 7H9 medium and grown to mid- to late-log phase. The culture optical density was determined, pelleted, and re-suspended in basal uptake buffer (17). Mtb luc aggregates are dispersed into individual bacilli by syringing the culture 6-8 times with a tuberculin syringe. BMDMs are infected with Mtb luc at an OD of 0.05. Two columns of each plate were left blank for positive and negative controls of 0.3 μ M rifampicin and dimethyl sulfoxide (DMSO), respectively. Cells were incubated for 6 days at 37°C (5% CO₂) and analyzed for viability using the BacTiter-Glo

(Promega) luminescence kit. For analysis, the HAARP custom software suite was used. Hits were binned as active in macrophages if greater than 25% growth inhibition was observed relative to the positive control rifampicin.

EC₅₀ determination

Cherry pick compounds were arrayed in 6 individual 384-well microtiter plates in 2.5-fold decreasing dilutions (1 mM – 10 μ M). The fluorescent reporter strains were grown and arrayed into 384-well microtiter assay plates as described in the primary screen methods. Two columns of each plate were left blank for positive and negative controls of 0.3 μ M rifampicin and dimethyl sulfoxide (DMSO), respectively. Cherry pick compounds were added at a final concentration of 10 μ M – 0.1 μ M (e.g. a 100-fold dilution from the stock plate). The plates were incubated for 6 days at 37°C and both fluorescence and OD were measured on a plate reader. For analysis of hits, the HAARP custom software suite was used. Positive hits were defined as compounds that exhibited greater than 50% growth inhibition at a concentration \sim 1 μ M.

Results

DosRST primary hits

A measure of the quality of a high-throughput screen is known as a Z' factor and represents the degree to which the assay has a sufficient dynamic range to resolve positive hits (16). The value ranges from 0 to 1 and a value greater than 0.5 represents an excellent screen with a sufficient dynamic range capable of identifying putative hits (16). The exact calculation of this value is elaborated upon in Chapter 4. The DosRST screen yielded a total Z' of 0.9, suggesting that there was a sufficient dynamic range to discover potential inhibitors of the

DosRST regulon and general inhibitors of Mtb growth. Following screening of the initial 272,358 compound library, 1087 inhibitors were identified as either Class I or Class II compounds, resulting in a 0.4% total hit rate after removing known antibiotics (Figure 2.1. A). The Class I hits comprised 252 of the 1087 primary hits, while 835 compounds were identified as potential general inhibitors of Mtb growth (Figure 2.2.). Further, the Class I compounds had 143 small molecules and 109 natural products. The Class II hits were composed of 383 small molecules and 452 natural products. Notably, a distinct cluster of scaffolds matching to Artemisinin and its analogs were discovered as potent inhibitors of DosRST-dependent fluorescence while growth was relatively unaffected (Figure 2.2.).

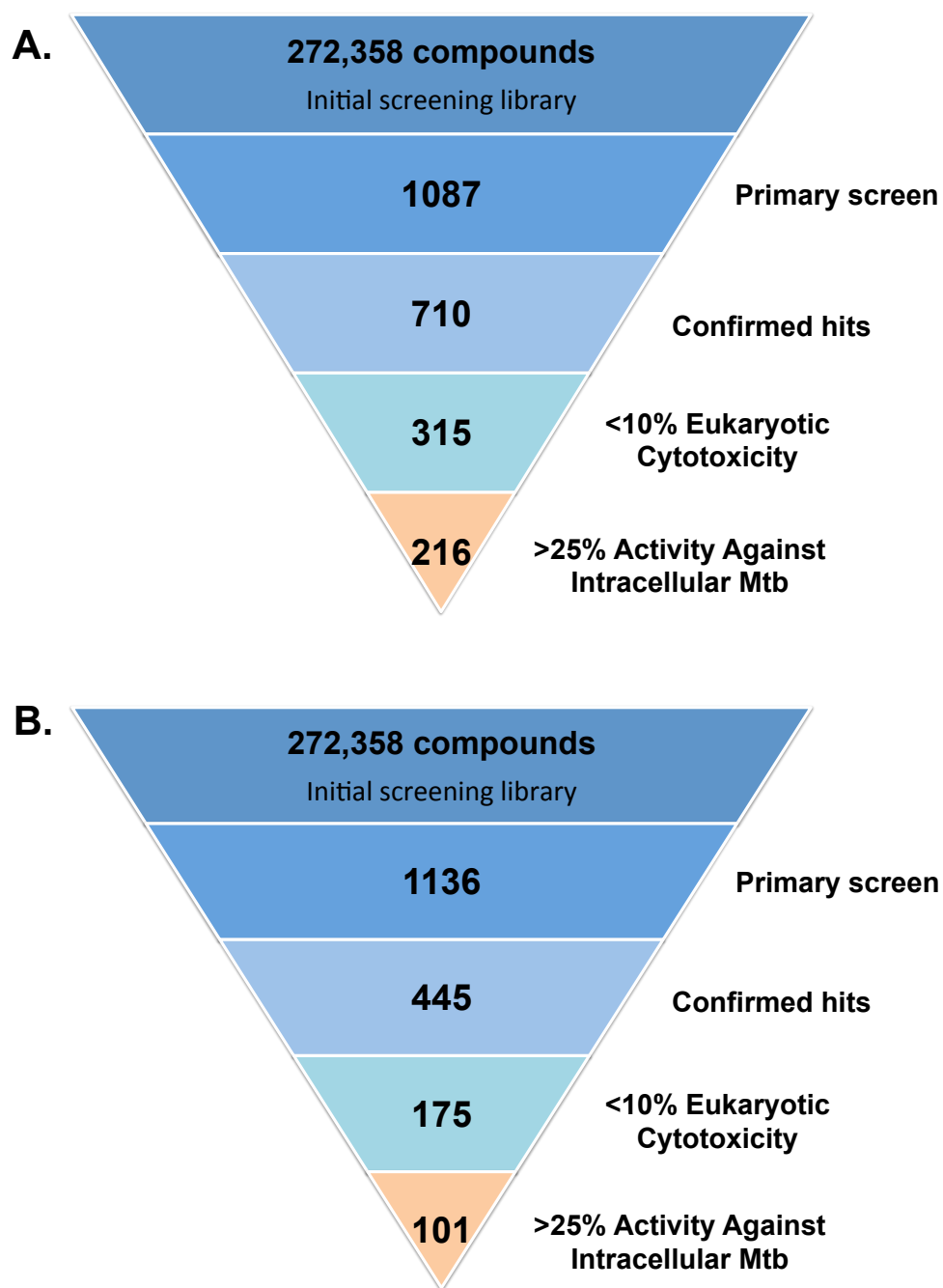


Figure 2.1. High-throughput screening workflow. Inverted pyramids describing the general workflow and attrition rate associated with the high-throughput screens for inhibitors of the A) DosRST regulon and B) the PhoPR regulon.

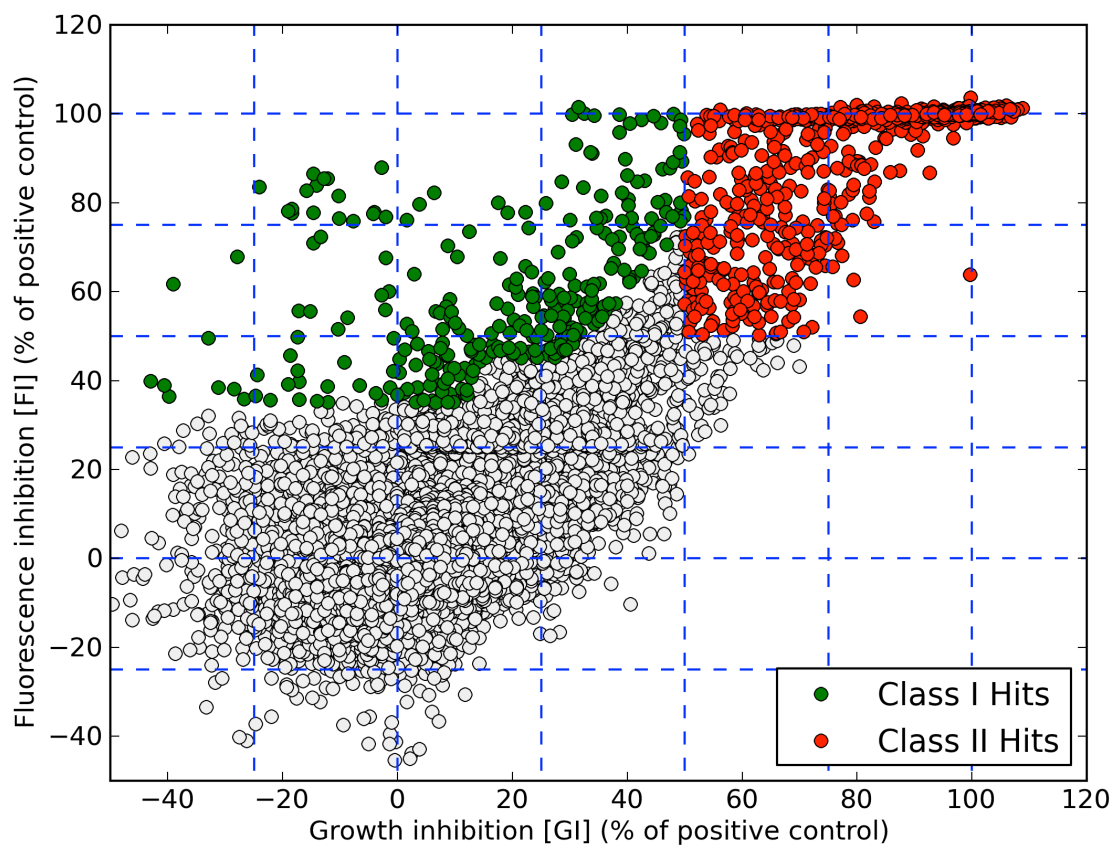


Figure 2.2. Scatter plot of primary screening hits for the DosRST screen. Potential inhibitors of the DosRST regulon are highlighted in green (Class I Hits) and inhibitors that are likely targeting Mtb growth are shown in red (Class II Hits). Output is from HAARP.

PhoPR primary hits

Following screening of the initial 272,358 compound library, 1136 inhibitors were identified as either Class I, II, or III compounds, resulting in a 0.42% total hit rate after removing known antibiotics (Figure 2.1. B). Further, the screen itself had a high Z' factor of 0.82, indicating a dynamic range large enough to adequately resolve hits. The Class I hits comprised 259 of the 1136 primary hits, while 877 compounds were identified as potential inhibitors of Mtb growth (Class II and III) (Figure 2.3.). Further, the Class I compounds had 111 small molecules and 148 natural products. The Class II hits were composed of 308 small molecules and 377 natural products. The Class III hits had 105 small molecules and 87 natural products. During the course of the HTS, several compounds were hand selected for proof-of-concept follow-up including the potential PhoPR regulon inhibitor ethoxzolamide (ETZ) (Chapter 3).

Seven fresh powders were purchased for follow-up studies (Table 2.1.). These compounds were identified as candidate PhoPR-regulon inhibitors. Compounds were subjected to dose-response curves ranging from 80 – 0.13 μ M at pH 7.0 and 5.7. Two compounds (5352227 and 1505426 [ETZ]) reconfirmed as inhibitors of PhoPR-mediated fluorescence at acidic pH (Table 2.1.). Further, the EC₅₀ of 5352227 is high (~40 μ M), though additional studies are needed to verify whether its chemical properties can be enhanced to inhibit the PhoPR regulon. Two of the compounds (E548-0073 and E548-0040) also initially reconfirmed as Class I inhibitors. However, during additional follow-up studies, it was noted that addition of the compound to pH 5.7 medium alone results in a time dependent chemical reaction leading pink medium. Further, during RNA preparation, Mtb incubated in the presence of either of these compounds retained the color, suggesting that E548-0073 and E548-0040 were likely acting as GFP quenchers. Interestingly, neither of these compounds significantly inhibits PhoPR-regulated

gene expression (Figure 2.4.), but treatment of infected macrophages results in strong inhibition of Mtb growth (Figure 2.5.). Additional studies are needed to identify whether the observed attenuation in macrophages is the result of the compound targeting a bacterial or host factor. RNA-seq transcriptional profiling is currently underway to test whether these compounds target a bacterial factor.

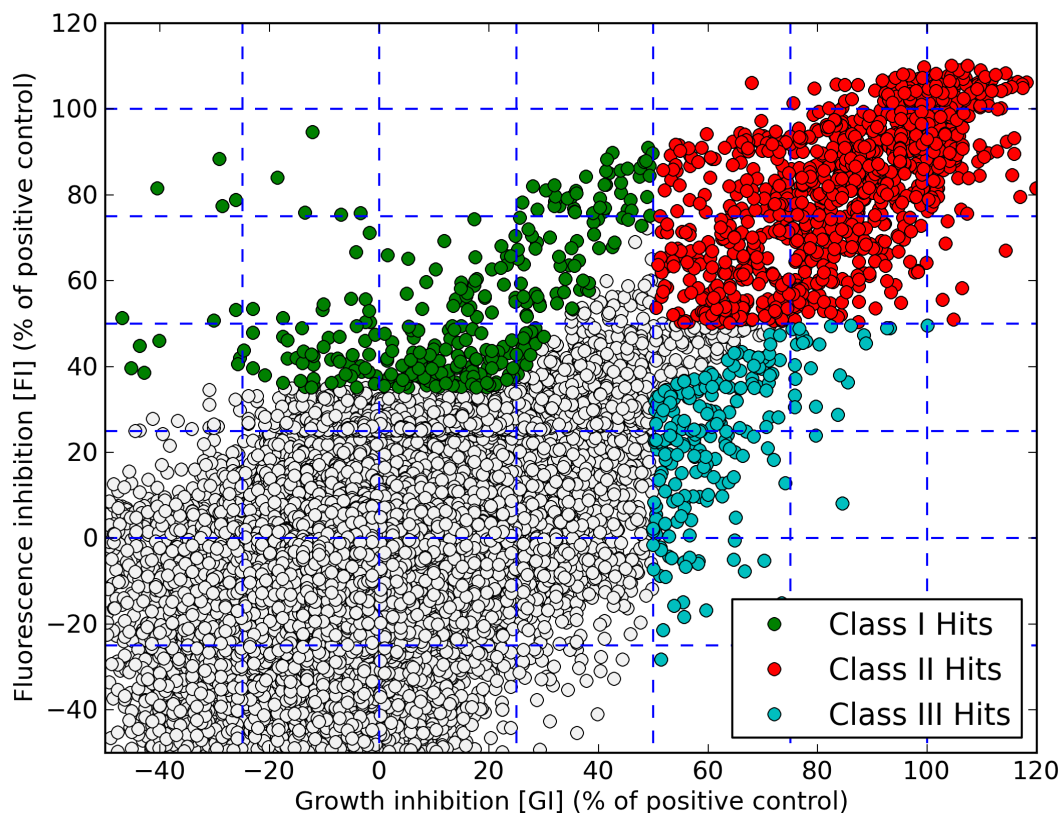


Figure 2.3. Scatter plot of primary screening hits for the PhoPR screen. Potential inhibitors of the PhoPR regulon are highlighted in green (Class I Hits). Inhibitors that are likely targeting Mtb growth are shown in red (Class II Hits). Compounds that slow Mtb growth while not significantly inhibiting transcription/translation of the PhoPR-dependent reporter fluorescence (*aprA*::GFP) are shown in blue (Class III Hits). Output is from HAARP.

Manufacturer	Catalog number	Reconfirmed as a Class I inhibitor?
ChemDiv	E548-0073	Yes*
ChemDiv	E548-0040	Yes*
AKSci	MFCD00276170	No
ChemBridge	5352227	Yes
ChemDiv	6264-0020	No
ChemDiv	K087-0176	No
Microsource	1505426	Yes

Table 2.1. Table depicting compounds hand selected for follow-up studies. Compounds shown were identified as candidate inhibitors of the PhoPR regulon and 2 (5352227 and 1505426 [Ethoxzolamide]) reconfirmed with Class I like properties. * indicates that it was later determined that these compounds act as time-dependent quenchers at pH 5.7.

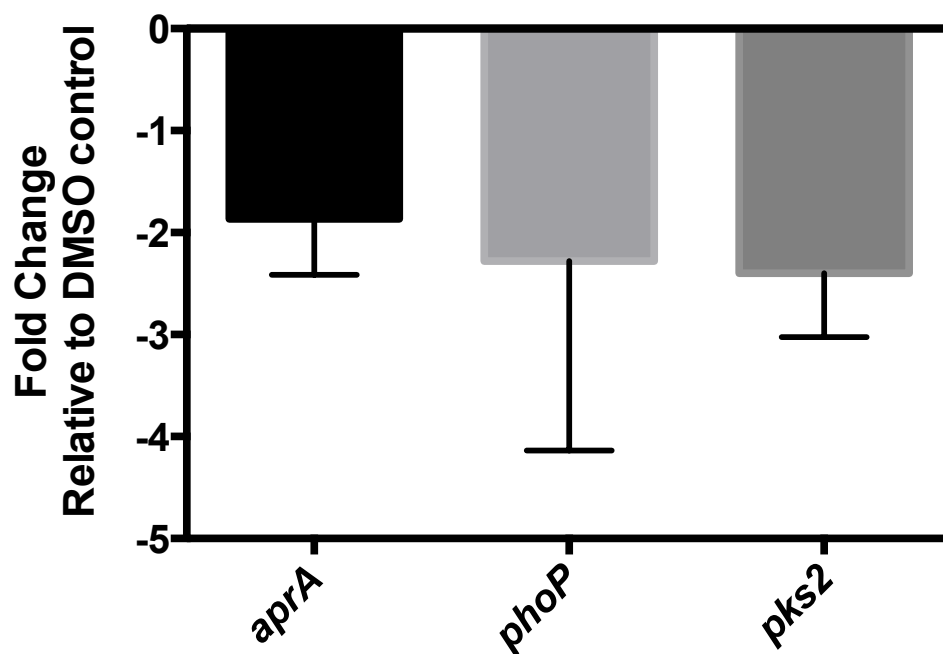


Figure 2.4. Semi-quantitative real-time PCR of E548-0040 on PhoPR regulated genes. The relative transcript abundances of PhoPR-regulated genes when treated with 15 μ M E548-0040 at pH 5.7 for 6 days do not change significantly relative to the wild-type control. In my hands, approximately two-fold change is the limit of detection. Error bars represent the standard deviation of three technical replicates.

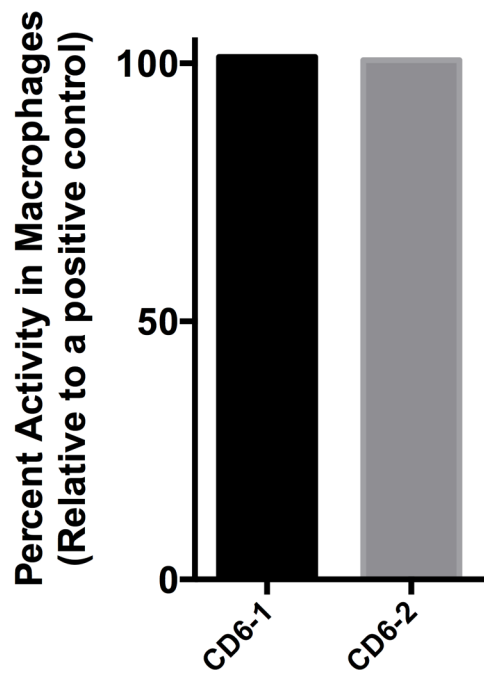


Figure 2.5. Inhibition of intracellular Mtb growth in infected macrophages. CD6-1 (E548-0073) and CD6-2 (E548-0040) inhibit Mtb growth in bone marrow-derived macrophages. Data are from activity against intracellular Mtb during the cherry pick secondary assays.

Secondary assay results

For secondary follow-up assays, cherry picks were arrayed into three groups of hits: i) DosRST specific compounds, ii) common inhibitors, and iii) PhoPR specific compounds. Initially, the cherry picks were brought up to a volume sufficient for completing all secondary assays (12 μ L) at a final concentration of 1 mM. The follow-up assays followed a general workflow of: i) hit re-confirmation, ii) eukaryotic cytotoxicity assay, iii) activity against Mtb in infected macrophages, and iv) EC₅₀ analysis (Figure 2.1.). Each counter-screen was developed and validated prior to assaying cherry pick compounds.

Reconfirmation of primary hits was performed in a similar manner as the initial screens. Briefly, Mtb reporter strains were grown in rich 7H9 Middlebrook medium buffered at pH 7.0 until mid- to late-log phase. Fluorescent biosensors were then pelleted, re-suspended in their respective media, and plated in 384-well microtiter plates in the presence of cherry pick compounds (~10 μ M). Following 6 days incubation, plates were analyzed for fluorescence and Mtb growth. Based on the observed fluorescence and growth inhibition profiles from the re-confirmation assay compared to the primary hit profile, 710 hits reconfirmed for the DosRST screen (Figure 2.1. A) and 445 hits reconfirmed for the PhoPR screen (Figure 2.1. B). The final reconfirmation rate for the DosRST screen was 65% and 40% for the PhoPR screen. Of the 710 reconfirmed hits from the DosRST screen, 80 compounds exhibited a validated Class I profile and 630 compounds reconfirmed as Class II compounds. The 445 reconfirmed PhoPR screen hits are composed of 32 Class I compounds, 399 Class II inhibitors, and 14 Class III compounds.

To identify whether compounds were acting as quenchers of GFP and not inhibiting adaptation processes or growth, cherry pick compounds were added following 6 days incubation and read immediately on the plate reader. Compounds that had greater than 25% fluorescence

inhibition were considered quenchers. Of the total cherry pick compounds assayed for reconfirmation, 63 were called as quenchers of GFP fluorescence and deemed false positives from the primary screen.

To assess whether the validated compounds from both screens are cytotoxic to eukaryotic cells, primary bone marrow-derived macrophages (BMDMs) were incubated in the presence of each cherry pick compound ($\sim 10 \mu\text{M}$). Cytotoxicity was assessed by measuring cell viability (available ATP) using a commercial luciferase-based assay following 6 days incubation with cherry pick compounds. Compounds that exhibited less than 10% cytotoxicity relative to the negative control, were deemed as inhibitors that are likely not generally cytotoxic to mammalian cells. Approximately 315 compounds (Class I – 44; Class II – 270) from the DosRST screen were deemed as not cytotoxic, while 175 compounds (Class I – 17; Class II – 148; Class III – 10) from the PhoPR screen exhibited less than 10% cytotoxicity (Figure 2.1.).

The ability to modulate Mtb viability in an infected macrophage is essential for further development of potential therapeutic leads. Primary BMDMs were infected at an MOI of 1:1 with Mtb expressing luciferase (Mtb luc) and allowed to infect for 1 hour. Infected macrophages were incubated for 6 days in the presence of reconfirmed compounds that exhibited low cytotoxicity. Mtb viability was assessed by measuring bacterial ATP using a commercial luciferase kit. Two-hundred and sixteen compounds from the DosRST screen and 101 inhibitors from the PhoPR screen exhibited greater than 25% growth inhibition relative to the rifampicin positive control (Figure 2.1.).

Finally, to identify compounds that exhibit less than $\sim 1 \mu\text{M}$ activity against Mtb growth *in vitro*, approximate EC_{50} curves were generated for all validated hits. Mtb reporter strains were grown under non-inducing conditions (buffered pH 7.0 Middlebrook 7H9 medium) to mid- to

late-log phase, pelleted and re-suspended under inducing conditions: buffered pH 5.7 Middlebrook 7H9 medium for the Mtb CDC1551(*aprA*::GFP) reporter and fresh pH 7.0 7H9 medium for the Mtb CDC1551(*hspX*::GFP) reporter. Fluorescent biosensors were then incubated in the presence of a 6-point dilution series (2.5-fold) for each validated cherry pick at a final concentration ranging from ~10 μ M – 0.1 μ M. Following 6 days incubation, fluorescence and Mtb growth were measured. Data were analyzed using the HAARP custom software suite (Chapter 6), revealing 33 inhibitors from the PhoPR screen and 54 compounds from the DosRST screen with greater than 50% growth inhibition at ~1 μ M.

Through examination of the common inhibitors of Mtb growth between the DosRST and PhoPR screens, we were able to resolve 214 compounds that were only active at pH 5.7. These compounds were of particular interest to characterize as putative therapeutic leads due to the Mtb front-line drug pyrazinamide that is active at acidic pH and possesses the ability to target persistent Mtb. Of the 214 compounds, 44 fresh powders were purchased for additional validation and characterization. Nineteen of the 44 pH-dependent inhibitors of Mtb growth were reconfirmed as exhibiting enhanced activity at pH 5.7 relative to pH 7.0 (Figure 2.6.). Notably, a compound termed PH036 was selected for subsequent characterization due to the ability to inhibit Mtb growth to a greater degree than the front-line Mtb antibiotic rifampicin (Figure 2.6.).

Taken together, both the DosRST and PhoPR screens were successful in identifying candidate compounds that were validated using a series of secondary assays for subsequent characterization. Additionally, by screening the same library of compounds at both neutral and acidic pH, inhibitors that are active in a pH-dependent manner as well as a pH-independent manner could be identified.

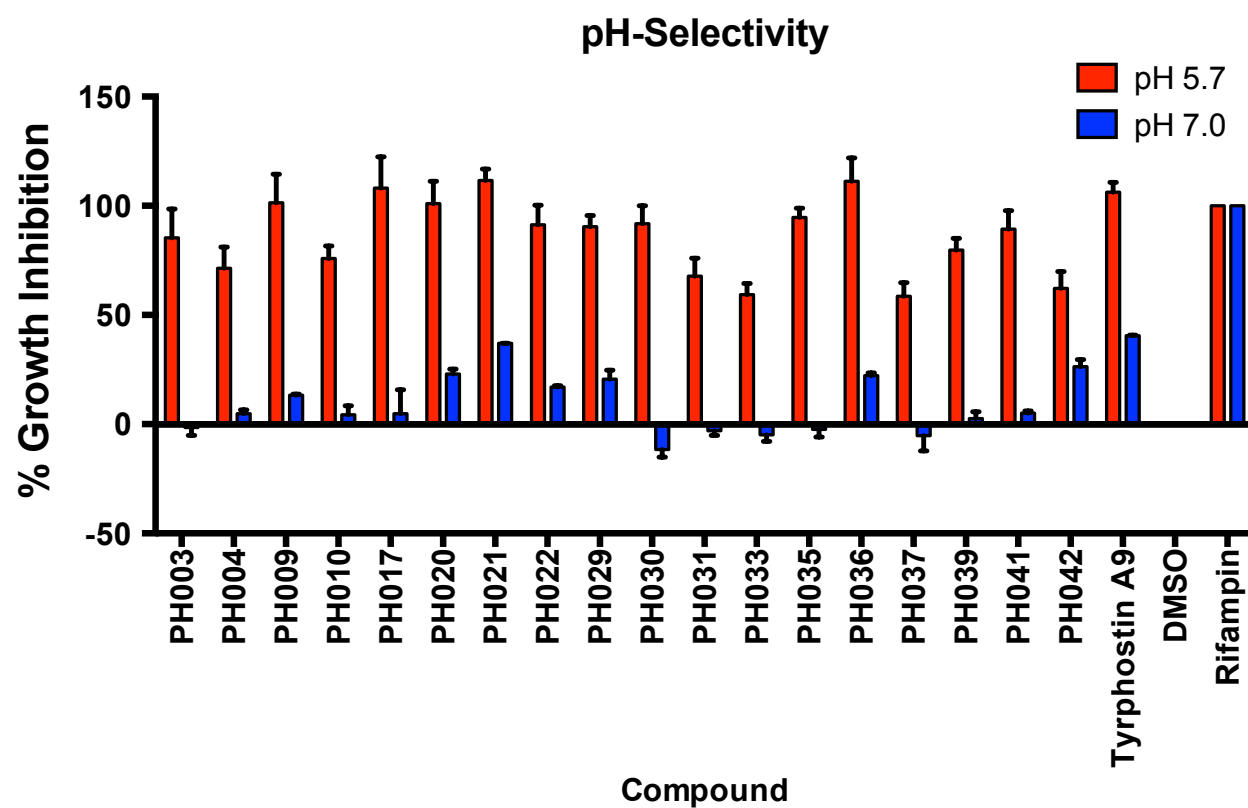


Figure 2.6. Reconfirmed compounds exhibiting pH-dependent activity. 19 of the 44 purchased fresh powders that reconfirmed as having enhanced inhibitory activity against Mtb growth at acidic pH relative to pH 7.0. Figure was generated by Garry Coulson.

REFERENCES

REFERENCES

1. **Prideaux B, Via LE, Zimmerman MD, Eum S, Sarathy J, O'Brien P, Chen C, Kaya F, Weiner DM, Chen PY, Song T, Lee M, Shim TS, Cho JS, Kim W, Cho SN, Olivier KN, Barry CE, 3rd, Dartois V.** 2015. The association between sterilizing activity and drug distribution into tuberculosis lesions. *Nat Med* **21**:1223-1227.
2. **Zhang Y, Scorpio A, Nikaido H, Sun Z.** 1999. Role of acid pH and deficient efflux of pyrazinoic acid in unique susceptibility of *Mycobacterium tuberculosis* to pyrazinamide. *J Bacteriol* **181**:2044-2049.
3. **Park HD, Guinn KM, Harrell MI, Liao R, Voskuil MI, Tompa M, Schoolnik GK, Sherman DR.** 2003. Rv3133c/dosR is a transcription factor that mediates the hypoxic response of *Mycobacterium tuberculosis*. *Mol Microbiol* **48**:833-843.
4. **Kumar A, Toledo JC, Patel RP, Lancaster JR, Jr., Steyn AJ.** 2007. *Mycobacterium tuberculosis* DosS is a redox sensor and DosT is a hypoxia sensor. *Proc Natl Acad Sci U S A* **104**:11568-11573.
5. **Rohde KH, Abramovitch RB, Russell DG.** 2007. *Mycobacterium tuberculosis* invasion of macrophages: linking bacterial gene expression to environmental cues. *Cell Host Microbe* **2**:352-364.
6. **Abramovitch RB, Rohde KH, Hsu FF, Russell DG.** 2011. *aprABC*: a *Mycobacterium tuberculosis* complex-specific locus that modulates pH-driven adaptation to the macrophage phagosome. *Mol Microbiol* **80**:678-694.
7. **Walters SB, Dubnau E, Kolesnikova I, Laval F, Daffe M, Smith I.** 2006. The *Mycobacterium tuberculosis* PhoPR two-component system regulates genes essential for virulence and complex lipid biosynthesis. *Molecular Microbiology* **60**:312-330.
8. **Baker JJ, Johnson BK, Abramovitch RB.** 2014. Slow growth of *Mycobacterium tuberculosis* at acidic pH is regulated by phoPR and host-associated carbon sources. *Mol Microbiol* **94**:56-59.
9. **Johnson BK, Colvin CJ, Needle DB, Mba Medie F, Champion PA, Abramovitch RB.** 2015. The Carbonic Anhydrase Inhibitor Ethoxzolamide Inhibits the *Mycobacterium tuberculosis* PhoPR Regulon and Esx-1 Secretion and Attenuates Virulence. *Antimicrob Agents Chemother* **59**:4436-4445.
10. **Converse PJ, Karakousis PC, Klinkenberg LG, Kesavan AK, Ly LH, Allen SS, Grosset JH, Jain SK, Lamichhane G, Manabe YC, McMurray DN, Nuermberger**

- EL, Bishai WR.** 2009. Role of the dosR-dosS two-component regulatory system in *Mycobacterium tuberculosis* virulence in three animal models. *Infect Immun* **77**:1230-1237.
11. **Martin C, Williams A, Hernandez-Pando R, Cardona PJ, Gormley E, Bordat Y, Soto CY, Clark SO, Hatch GJ, Aguilar D, Ausina V, Gicquel B.** 2006. The live *Mycobacterium tuberculosis* *phoP* mutant strain is more attenuated than BCG and confers protective immunity against tuberculosis in mice and guinea pigs. *Vaccine* **24**:3408-3419.
 12. **Perez E, Samper S, Bordas Y, Guilhot C, Gicquel B, Martin C.** 2001. An essential role for *phoP* in *Mycobacterium tuberculosis* virulence. *Molecular Microbiology* **41**:179-187.
 13. **Gonzalo-Asensio J, Mostowy S, Harders-Westerveen J, Huygen K, Hernandez-Pando R, Thole J, Behr M, Gicquel B, Martin C.** 2008. PhoP: A Missing Piece in the Intricate Puzzle of *Mycobacterium tuberculosis* Virulence. *Plos One* **3**:e3496.
 14. **Arbues A, Aguilo JI, Gonzalo-Asensio J, Marinova D, Uranga S, Puentes E, Fernandez C, Parra A, Cardona PJ, Vilaplana C, Ausina V, Williams A, Clark S, Malaga W, Guilhot C, Gicquel B, Martin C.** 2013. Construction, characterization and preclinical evaluation of MTBVAC, the first live-attenuated *M. tuberculosis*-based vaccine to enter clinical trials. *Vaccine* **31**:4867-4873.
 15. **Tan S, Sukumar N, Abramovitch RB, Parish T, Russell DG.** 2013. *Mycobacterium tuberculosis* Responds to Chloride and pH as Synergistic Cues to the Immune Status of its Host Cell. *PLoS Pathog* **9**:e1003282.
 16. **Johnson BK, Abramovitch RB.** 2015. Macrophage Infection Models for *Mycobacterium tuberculosis*. *Methods Mol Biol* **1285**:329-341.
 17. **Zhang JH, Chung TD, Oldenburg KR.** 1999. A Simple Statistical Parameter for Use in Evaluation and Validation of High Throughput Screening Assays. *J Biomol Screen* **4**:67-73.

CHAPTER 3 – The carbonic anhydrase inhibitor ethoxzolamide inhibits the *Mycobacterium tuberculosis* PhoPR-regulon and Esx-1 secretion and attenuates virulence

The discovery and initial characterization of ethoxzolamide presented in this chapter has been previously published:

Johnson B.K., Colvin C.J., Needle D.B., Mba Medie F., Champion P.A.D., and Abramovitch R.B. (2015) The carbonic anhydrase inhibitor ethoxzolamide inhibits the *Mycobacterium tuberculosis* PhoPR-regulon and Esx-1 secretion and attenuates virulence. *Antimicrobial Agents and Chemotherapy*, 59:4436–4445

Preface

Following the high throughput screen and subsequent secondary assays ethoxzolamide (ETZ) was identified as an inhibitor meeting the profile of a PhoPR regulon inhibitor. Ethoxzolamide is an FDA approved medication that was originally used to treat glaucoma, reduce seizure threshold, and as a general diuretic through its carbonic anhydrase inhibitory activity. Currently, ETZ is not often prescribed in the clinic due to the development of more potent analogs possessing fewer undesirable side effects (e.g. dizziness, nausea, etc.) (1-5). Interestingly, many of these analogs were not identified as putative inhibitors of PhoPR signaling despite being present in the screening library. However, ETZ provides a desirable platform for subsequent characterization and development as it is no longer patented, is inexpensive to manufacture, and is already FDA approved for use in humans suggesting potential in being repurposed.

Carbonic anhydrase activity is associated with a variety of cellular processes including maintenance of pH and CO₂ homeostasis, gluconeogenesis, lipogenesis, and growth and virulence in several pathogens. Specifically, Mtb encodes three carbonic anhydrase enzymes that can be inhibited by ETZ. Further, two of the three enzymes (*Rv1284* and *Rv3588c*) are required for growth in an *in vivo* mouse model of infection (6). I hypothesized that ETZ inhibition of Mtb carbonic anhydrase activity would disrupt PhoPR-mediated, pH-driven adaptation. To investigate this hypothesis I compared the ability of ETZ to chemocopy defects associated with a *phoPR* mutant *in vitro* and *in vivo*. Indeed, phenotypes associated with a *phoPR* mutant could be mimicked with ETZ treatment including impaired Esx-1 protein secretion, altered production of virulence lipids, and attenuated virulence in *ex vivo* and *in vivo* models of infection. Inhibition of Mtb carbonic anhydrase activity in whole cells does not lead to disrupted pH homeostasis under acidic conditions *in vitro*. Further, the target of ETZ is likely Mtb carbonic anhydrase as a modified molecule that does not bind to the carbonic anhydrase active site does not lead to inhibition of PhoPR signaling (Chapter 4). The observed attenuation *in vivo* is likely due to ETZ targeting Mtb carbonic anhydrase, as high concentrations of the compound do not affect phagosome acidification. I propose a model suggesting a direct link between carbonic anhydrase and Mtb's ability to sense and respond to acidic pH in a PhoPR-dependent manner.

Abstract

Mycobacterium tuberculosis (Mtb) must sense and adapt to host environmental cues to establish and maintain an infection. The two-component regulatory system PhoPR plays a central role in sensing and responding to acidic pH within the macrophage and is required for Mtb intracellular replication and growth *in vivo*. Therefore, isolation of compounds that inhibit PhoPR-dependent

adaptation may identify new anti-virulence therapies to treat tuberculosis. Here we report that the carbonic anhydrase inhibitor ethoxzolamide inhibits the PhoPR regulon and reduces pathogen virulence. We show that treatment of Mtb with ethoxzolamide recapitulates *phoPR* mutant phenotypes, including: downregulation of the core PhoPR regulon, altered accumulation of virulence-associated lipids, and inhibition of Esx-1 protein secretion. Quantitative single-cell imaging of a PhoPR-dependent fluorescent reporter strain demonstrates that ethoxzolamide inhibits PhoPR-regulated genes in infected macrophages and mouse lungs. Moreover, ethoxzolamide reduces Mtb growth in both macrophages and infected mice. Ethoxzolamide inhibits Mtb carbonic anhydrase activity supporting a previously unrecognized link between carbonic anhydrase activity and PhoPR signaling. We propose that ethoxzolamide may be pursued as a new class of anti-virulence therapy that functions by modulating expression of the PhoPR regulon and Esx-1-dependent virulence.

Introduction

Mycobacterium tuberculosis (Mtb) is a successful pathogen because it overcomes a variety of obstacles raised by the host immune response. The ability of Mtb to sense host immune pressures and orchestrate adaptive responses to these cues is essential for pathogen virulence. It follows that identification of chemical compounds that disrupt the ability of Mtb to sense and respond to host cues may function to attenuate pathogen virulence.

Mtb uses environmental pH as a cue to modulate its physiology. These pH-dependent adaptations play a central role in Mtb pathogenesis (7). Transcriptional profiling of Mtb infected macrophages identified an Mtb regulon induced at acidic pH (8) that significantly overlaps the PhoPR two-component regulatory system regulon (9-11), suggesting a role for PhoPR in pH-

driven adaptation. *phoPR*-inactivated Mtb mutant strains are highly attenuated during mouse and guinea pig infections, supporting that this pathway is a suitable target for new drug development (12, 13).

Conventional antimicrobial discovery campaigns seeking to identify bactericidal or – static compounds are often performed *in vitro*. However, many targets required for Mtb pathogenesis, including environmental sensing pathways, are only essential *in vivo* and would be missed using standard approaches. Compounds that target *in vivo* essential bacterial virulence factors are known as anti-virulence therapies (14). Anti-virulence therapies are advantageous over traditional antibiotics because they preserve endogenous microbiota by targeting pathogen-specific pathways and may reduce selective pressure for the development of resistance since bacterial growth is not directly targeted. Several anti-virulence compounds have been discovered that target bacterial virulence regulators, quorum sensing, toxin production and delivery, and adhesion and colonization within the host (14-19). The goal of this study was to identify compounds that inhibit the Mtb PhoPR regulon and may thus function as anti-virulence therapies.

Materials and Methods

Bacterial strains and growth conditions

Mtb experiments, unless otherwise stated, were performed with Mtb strain CDC1551. The CDC1551(*aprA*'::GFP) fluorescent reporter strain was generated by fusing the promoter region of *aprA* (*mcr7*, Rv2395a) upstream of GFP in the pSE100 replicating plasmid and transforming the plasmid into CDC1551 (11). The *phoP*::Tn and Δ *phoPR* mutants have been previously described (11, 20). Cultures were maintained in standing tissue culture flasks in 7H9

Middlebrook medium supplemented with 10% oleic acid, albumin, dextrose, catalase (OADC) and 0.05% Tween-80 and incubated at 37°C with 5% CO₂.

High-throughput screening assay and data analysis

A ~220,000 compound library arrayed in 384-well optical microtiter plates was provided by the NSRB ICCBL at Harvard University. Two columns of each plate were left blank for positive and negative controls of 0.3 µM rifampicin and dimethyl sulfoxide (DMSO), respectively. Mtb CDC1551(*aprA*'::GFP) was grown in Middlebrook 7H9 medium, buffered at pH 7.0 with 100 mM 3-(N-morpholino)propanesulfonic acid (MOPS), to mid- to late-log phase. The cultures were then pelleted, re-suspended in 7H9 buffered at pH 5.7 with 100 mM 2-(N-morpholino)ethanesulfonic acid (MES) and dispensed into the 384-well assay plates at an optical density (OD) of 0.2. The plates were incubated for 6 days at 37°C and both fluorescence and OD were measured on a plate reader. For analysis of hits, fluorescence and growth inhibition were normalized based on the rifampicin (100%) and DMSO (0%) controls. Potential PhoPR regulon inhibitors were flagged as compounds that had: i) greater than 35% fluorescence inhibition, and ii) at least a 1.5-fold greater fluorescence inhibition as compared to growth inhibition.

For EC₅₀ determinations, Mtb CDC1551(*aprA*'::GFP) was grown to mid- to late-log phase in non-inducing medium (7H9, pH 7.0), pelleted, and re-suspended in GFP inducing medium (7H9, pH 5.7) in the presence of a 14-point dilution series (2.5-fold) of ethoxzolamide (ETZ) at a final concentration ranging from 3 nM to 500 µM. Fluorescence and growth inhibition were normalized based on the rifampicin (100%) and DMSO (0%) controls. EC₅₀ values were calculated based on a variable slope, four-parameter non-linear least squares regression model in the GraphPad Prism software package (ver. 6).

Transcriptional profiling and data analysis

For RNA-seq experiments, Mtb cultures were grown at 37°C in T-25 vented, standing tissue culture flasks in 8 mL of buffered 7H9 medium seeded at an initial OD of 0.2. Three conditions were examined with two biological replicates: 1) DMSO treated, pH 7.0, 2) DMSO treated, pH 5.7, and 3) 40 µM ETZ treated, pH 5.7. The *phoP::Tn* mutant was grown in a similar manner and treated with DMSO at pH 5.7. Following six days incubation, total bacterial RNA was extracted as previously described (8). RNA-sequencing, data analysis and qPCR were performed as described by Baker *et al.* (21) with minor modifications (Appendix). Differentially expressed genes were determined to be statistically significant based on a false discovery rate adjusted p-value of $p < 0.05$. The transcriptional profiling data have been submitted to the NCBI GEO database (accession number: GSE63917).

Cell culture

Primary murine bone marrow derived macrophages (BMDMs) were isolated and grown as previously described (22). Briefly, BMDMs were isolated from wild type (WT) C57Bl/6 mice (Charles River) and grown at 37°C (5% CO₂) in DMEM (Corning CellGro) containing 10% fetal bovine serum (Thermo Scientific), 20% L-cell conditioned medium, 1 mM pyruvate, 2 mM L-glutamine, and 1 mM penicillin/streptomycin (Corning CellGro). Cells were grown until confluent, scraped, and plated in medium lacking antibiotics at either 1×10^5 cells/mL for macrophage infections or 2×10^5 cells/mL for measuring phagosome acidification. Cells were allowed to adhere overnight before addition of Mtb or experimental treatments.

Carbonic anhydrase activity assay

Carbonic anhydrase (CA) activity was measured using a modified Maren endpoint method (23) based on acidification of the media by CA conversion of CO₂. WT Mtb CDC1551 cultures were grown for six days at 37°C in T-150 vented, standing tissue culture flasks in 50 mL of 7H9 medium seeded at an initial OD of 0.2. Two conditions were examined: 1) DMSO treated, pH 5.7, and 2) ETZ treated (80 µM), pH 5.7. Cells were then pelleted, washed once in cold assay buffer (20 mM Tris, 20 mM NaCl, pH 8.3), re-suspended in 500 µL cold assay buffer and transferred to 2 mL screw cap tubes containing 200 µL of 0.1mm glass beads. Cell lysis was achieved by bead beating at max speed for 2 minutes. Lysates were clarified by centrifugation at 21,000 x g for 1 minute. Clarified lysates were transferred to new tubes and kept on ice. The CA assay apparatus utilized: 15x88 mm Pyrex glass tubes, 14 mm serum stoppers, 18 gauge 1.5 inch needles, 1 mL syringes, 1 mm tubing, sample evaporator needles, and 0.22 µm syringe filters (to prevent aerosol escape). All assay components were kept on ice before and during the assay. 450 µL of ddH₂O was added to the tube with 50 µL cell lysate. CO₂ was bubbled in at a constant rate and 500 µL of cold color indicator buffer (20 mM imidazole, 5 mM Tris, 0.2 mM 4-nitrophenol) was added, and timing was initiated. The color is monitored until clearing, comparing it to a previously cleared sample. Data are representative of at least two biological replicates with similar findings in each experiment.

Cytoplasmic pH and phagosome acidification measurement

Cytoplasmic pH was measured as previously described by Purdy *et al.* (24). WT Mtb CDC1551 was grown in a similar manner as the transcriptional profiling experiments. Four conditions were examined: 1) DMSO treated, pH 7.0, 2) DMSO treated, pH 5.7, 3) 80 µM ETZ, pH 7.0, and 4)

80 μ M ETZ, pH 5.7. Cytoplasmic pH was measured following 6 days incubation. Phagosome acidification was measured using pHrodo labeled beads (Life Technologies) fed to BMDMs in a 96-well black assay plate. One column did not contain any cells for a media and beads only control. Five conditions were examined: 1) 100 μ M ETZ, 2) 80 μ M ETZ, 3) 40 μ M ETZ, 4) 100 nM Concanamycin A (CcA), and 5) an equivalent volume of DMSO. Cells were pre-treated for 4 hours with ETZ and DMSO before addition of particles. CcA was added 30 minutes prior to assay initiation. pHrodo green labeled particles (ex. 509 nm, em. 533 nm) were added to each well in pre-warmed live cell imaging solution (Life Technologies) at 1 mg/mL. The assay was carried out in a Perkin Elmer plate reader at 37°C for 100 minutes taking readings at 5-minute intervals.

Analysis of mycobacterial lipids

Lipid analysis was conducted as previously described (21). Briefly, Mtb cultures were grown at 37°C in standing, vented T-75 tissue culture flasks in 40 ml of minimal medium supplemented with 10 mM pyruvate and seeded at an initial OD of 0.1. Four conditions were examined: 1) DMSO treated, pH 7.0, 2) DMSO treated, pH 5.7, 3) 80 μ M ETZ, pH 7.0, and 4) 80 μ M ETZ, pH 5.7. Following 3 days incubation, lipids were radiolabeled by adding 8 mCi of [1,2- 14 C] sodium acetate to each culture. Following 6 days of labeling, the lipids were extracted and analyzed by thin layer chromatography (TLC). Total extractable lipid 14 C incorporation was determined using a scintillation counter. To analyze lipid species, 20,000 counts per minute (CPM) were loaded at the origin of a 100 cm² high performance TLC silica gel 60 aluminum sheet. To separate sulfolipid (SL) and triacylglycerol (TAG), TLCs were developed with the chloroform:methanol:water (90:10:1 v/v/v) and hexane:diethyl ether:acetic acid (80:20:1, v/v/v)

solvent systems, respectively (21). To examine phthiocerol dimycocerosate (PDIM) accumulation the 2D TLC was developed with 1) petroleum ether:ethyl acetate (98:2, v/v) and 2) petroleum ether:acetone (98:2, v/v) (11). Radiolabeled lipids were detected with a phosphor screen and Typhoon Imager and quantified using ImageJ software (25). Radiolabeling experiments, lipid extractions and analyses were repeated in two independent biological replicates with similar findings in both replicates. TAG and PDIM species were previously identified using these solvent systems and mass spectroscopy(11). SL identity was confirmed using a SL standard (provided by BEI resources) that was visualized by staining with phosphomolybdic acid followed by charring (Figure. S3.3. C).

Analysis of Esx-1 protein export

Mycobacterium tuberculosis Erdman and Δ esat-6 strains were a gift from Jeffery S. Cox (26). Mtb was cultured in 7H9 medium, collected by centrifugation, washed once with 5 mL of Sauton's broth and re-suspended in 50 mL of Sauton's broth in the presence or absence of 80 μ M ETZ. After 5 days of growth at 37°C, the cells were diluted, washed and treated as above. The cultures were grown at 37°C with gentle shaking for 4 days. Lysates were prepared as described previously (26). The secreted protein fraction was concentrated using Amicon filter systems with a 3 kDa molecular weight cut-off and total protein concentrations were determined by the MicroBCA assay (Promega). 13.5 mg of cell lysates and culture filtrates were separated on a 4-20% pre-cast gel (Bio-Rad) and transferred to nitrocellulose. Nitrocellulose membranes were incubated with antibodies against ESAT-6 (Abcam, ab26246), CFP-10, MPT32, or RNAP β (Abcam, 8RB13) and detected using chemiluminescence (LumiGLO[®])(27). The following reagents were obtained through BEI Resources, NIAID, NIH: Polyclonal Anti-

Mycobacterium tuberculosis CFP-10 (Gene *Rv3874*) (antiserum, Rabbit), NR-13801, Polyclonal Anti-*Mycobacterium tuberculosis* Mpt32 (Gene *Rv1860*) (antiserum, Rabbit), NR-13807.

Macrophage infections

Macrophage infections were performed as described (22). Briefly, BMDMs were infected at an multiplicity of infection (MOI) of 1:1 with Mtb CDC1551 in 24-well tissue culture treated plates. Infected BMDMs were treated with 80 μ M ETZ or an equivalent volume of DMSO every two days for 9 days total. At days 3, 6 and 9, intracellular bacteria were quantified by lysing macrophage monolayers and performing serial dilution plating of lysates on 7H10 agar. Each treatment was added to three separate wells per plate to provide three biological replicates per time point. Survival assays were repeated in three independent experiments with similar findings in each experiment. For fluorescence microscopy experiments, macrophages were seeded on glass coverslips before infection with Mtb CDC1551(*aprA*'::GFP *smyc*'::mCherry). Samples were treated every two days with 100 μ M ETZ or an equal volume of DMSO for 9 days. Monolayers were then fixed in 4% paraformaldehyde and imaged by confocal microscopy. Imaging experiments were repeated with three biological replicates with similar results.

Quantitative single-cell imaging of Mtb exposure to ETZ in mice

C57BL/6 mice were infected via the intranasal route with 1000 colony forming units (CFU) of the Erdman (*aprA*'::GFP *smyc*'::mCherry) dual fluorescent reporter. Mice were treated with 100 mg/kg of ETZ or an equal volume of 0.25% carboxymethyl cellulose (CMC) 5 days per week for 4 weeks via oral gavage. After 4 weeks, the right lung was homogenized and plated for enumeration of the bacterial load and the left lung was fixed in 4% paraformaldehyde before

being transferred to 30% sucrose for confocal microscopy imaging and evaluation for histopathological hallmarks of TB disease (Appendix). This experiment was repeated and the data from the two independent biological replicates were similar and therefore combined. Mice were euthanized by carbon dioxide asphyxiation followed by cervical dislocation. Animal experiments were conducted following protocols approved by the Michigan State University Institutional Animal Care and Use Committee.

Results

Identification of ethoxzolamide as an inhibitor of the PhoPR regulon

We employed a whole-cell phenotypic screen to identify inhibitors of the PhoPR regulon. The CDC1551(*aprA*'::GFP) fluorescent reporter exhibits pH-inducible fluorescence that is fully dependent on PhoPR (11). Although PhoPR is required for growth *in vivo*, a PhoPR mutant grows well in rich medium at acidic pH; therefore, compounds that inhibit pH-inducible reporter fluorescence, but not growth, are anticipated to be inhibitors of the PhoPR pathway. To discover inhibitors of the PhoPR regulon we conducted a high throughput screen (HTS) of a ~220,000 compound library composed of small molecules representing broad chemical diversity. The reporter strain was grown in 384 well plates containing the compound library (at a concentration of ~10 μ M) in rich medium buffered at pH 5.7. Following 6 days of incubation, plates were examined for GFP fluorescence and growth. Ethoxzolamide (ETZ, Figure 3.1. A) was identified as a compound that inhibits Mtb reporter fluorescence but that does not reduce growth. ETZ inhibits CDC1551(*aprA*'::GFP) reporter fluorescence with a half-maximal effective concentration (EC_{50}) of 5.6 μ M at pH 5.7, (Figure 3.1. B). Growth was mostly unaffected at pH 5.7 across the range of ETZ concentrations tested (Figure 3.1. B). Basal *aprA* expression is also

dependent on PhoPR at neutral pH and we observed inhibition of reporter fluorescence at pH 7.0 with a similar EC_{50} of 4.7 μ M (Fig. S3.1. A). ETZ is a carbonic anhydrase (CA) inhibitor that has previously been shown to inhibit recombinant Mtb CA proteins (28). We examined if ETZ inhibits Mtb CA activity and observed full inhibition of CA activity in Mtb whole cells treated with ETZ for 6 days (Figure 3.1. C). ETZ does not quench GFP fluorescence, alter the pH of the culture medium (Figure S3.1. B) and only caused a slight acidification of cytoplasmic pH (Figure 3.1. D). These data support two novel findings: 1) ETZ inhibits the PhoPR regulon, and 2) a previously unrecognized link may exist between Mtb CA activity and PhoPR signaling.

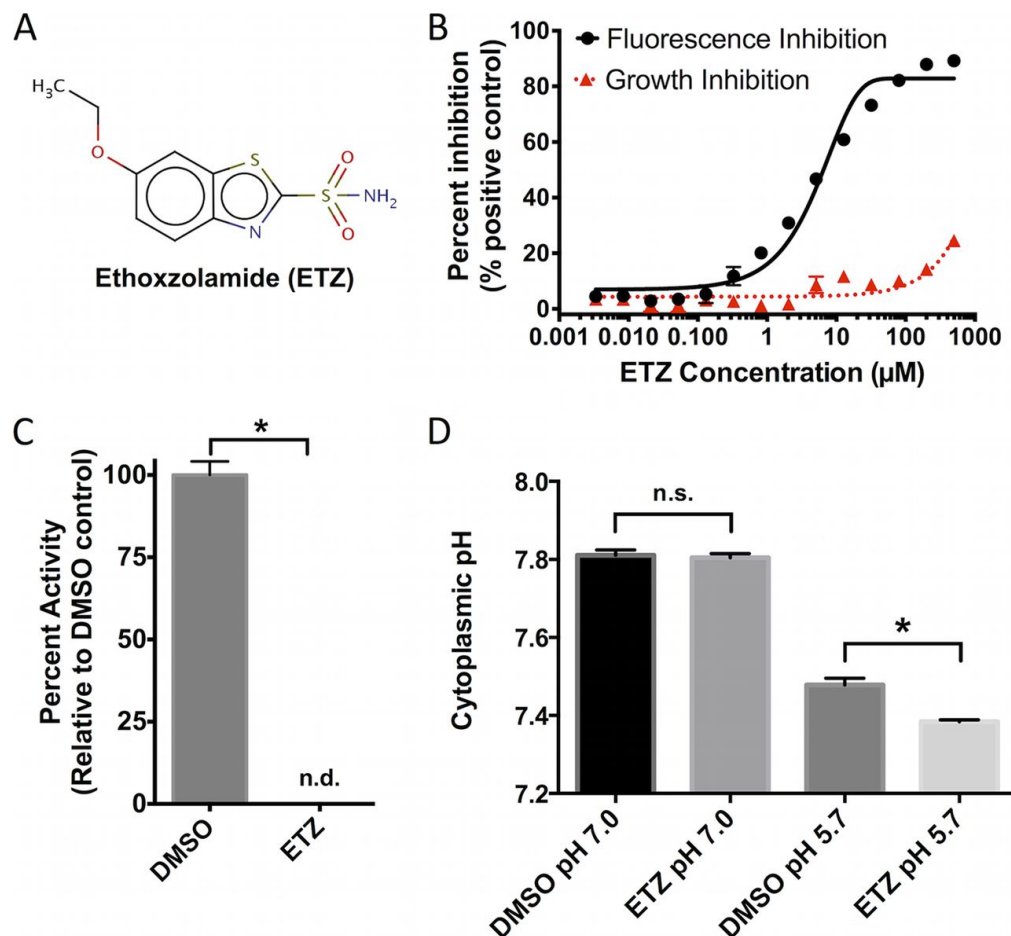


Figure 3.1. Ethoxzolamide inhibits *M. tuberculosis* CDC1551(*aprA'*::GFP) fluorescence and *M. tuberculosis* carbonic anhydrase activity but does not alter cytoplasmic pH. (A) Chemical structure of ethoxzolamide (ETZ) (6-ethoxy-1,3-benzothiazole-2-sulfonamide). (B) ETZ inhibits PhoPR-dependent CDC1551(*aprA'*::GFP) fluorescence in a concentration-dependent manner at pH 5.7, with an EC_{50} of 5.6 μM and little effect on growth. (C) *M. tuberculosis* carbonic anhydrase activity is not detectable (n.d.) in whole cells when treated with ETZ (80 μM) compared to a DMSO control. (D) *M. tuberculosis* treated with ETZ (80 μM) for 6 days exhibits no change in cytoplasmic pH at pH 7.0 and only slightly acidified cytoplasm (<0.1 pH units) at pH 5.7. The data are representative of at least two biological replicates, and the error bars are the standard deviations from at least three technical replicates. *, $P < 0.05$, calculated based on a two-tailed t test.

Prior transcriptional profiling and ChIP-seq studies have defined a core regulon that is directly regulated by PhoP and induced by acidic pH (8-11, 29, 30). To determine if ETZ inhibits the PhoPR regulon we performed RNA-seq transcriptional profiling. Mtb CDC1551 was inoculated into rich medium buffered at pH 5.7 in the presence of either 40 μ M ETZ or an equivalent volume of DMSO. As a positive control for PhoPR-regulated genes, a DMSO treated *phoP* transposon mutant strain (*phoP*::Tn) was cultured using the above described conditions. To identify genes regulated by acidic pH, we also examined the transcriptional profile of DMSO treated Mtb at pH 5.7 as compared to pH 7.0. After 6 days incubation, total RNA was isolated and subjected to RNA sequencing. ETZ treatment of Mtb caused the downregulation (>2 -fold, $p<0.05$) of 45 genes (Figure 3.2.). Remarkably, all 45 of these genes were also downregulated in the *phoP*::Tn mutant and 40 were induced by acidic pH (Figure 3.2. BC). ETZ downregulated genes include many genes previously shown to be directly controlled by PhoP and are involved in lipid synthesis, carbon metabolism, and virulence (Figure 3.2. C) (29, 30). Many of the remaining 137 genes downregulated in the *phoP*::Tn mutant but not by ETZ (>2 -fold, $p<0.05$), are significantly downregulated by ETZ but less than 2-fold (e.g. *espR*, *espA*, *esxA*, Figure 3.2. A). To confirm the RNA-seq results, we conducted semi-quantitative real-time PCR on the *phoP* gene and two well-characterized PhoP-regulated genes, *aprA* and *pks2*. In ETZ treated Mtb, we observed that *aprA* and *pks2* were downregulated >5 fold at both pH 7.0 and 5.7 (Figure S3.2.). *phoP* did not exhibit substantial differential regulation by ETZ, demonstrating that ETZ is not acting by modulating *phoP* gene expression. These findings validate ETZ as an inhibitor of the core PhoPR regulon.

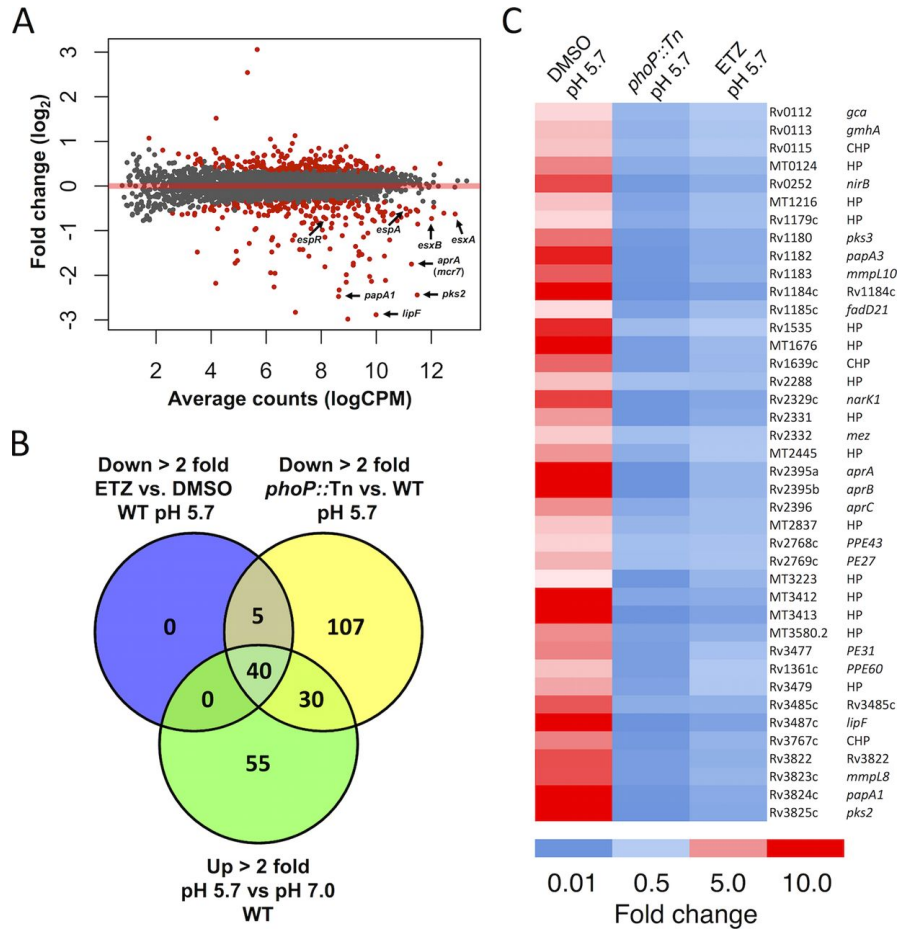


Figure 3.2. ETZ inhibits the induction of the core PhoPR regulon at acidic pH. (A) RNA-seq transcriptional profiling shows that PhoPR-regulated genes are significantly downregulated when treated with ETZ at pH 5.7 compared to the DMSO control at pH 5.7. Red dots are significantly differentially expressed genes compared to the control ($P < 0.05$). Black dots are not significantly differentially expressed genes compared to the control. (B) A complete overlap is observed between genes downregulated (Down) (>2-fold, $P < 0.05$) by ETZ treatment and the mock-treated *phoP*::Tn mutant strain. Forty of these genes are also induced at pH 5.7 compared to pH 7.0 (>2-fold, $P < 0.05$). Up, upregulated; vs., versus. (C) A heat map of the 40 acidic-pH-induced and PhoPR- and ETZ-repressed (>2-fold, $P < 0.05$) genes. CHP, conserved hypothetical protein; HP, hypothetical protein.

Lipid synthesis and Esx-1 protein secretion are modulated by ethoxzolamide.

PhoPR controls cell envelope lipids and Esx-1 dependent secretion of ESAT-6 (EsxA) (31, 32). Therefore, we examined if ETZ modulates these virulence factors. The PhoPR-dependent *mmpL8-pks2* operon (Rv3823c-Rv3825c) is responsible for the production of sulfolipid (SL) and is strongly induced at acidic pH (9, 21, 33, 34). Transcriptional profiling data demonstrated a ~5-fold downregulation of this operon when treated with ETZ at acidic pH (Figure 3.2. C), suggesting that similar to a *phoPR* knockout mutant ($\Delta phoPR$), ETZ may downregulate the accumulation of SL. To test this hypothesis, ^{14}C radiolabeled lipids were isolated from wild type (WT) and $\Delta phoPR$ mutant strains grown at pH 7.0 and pH 5.7 treated with either ETZ or an equal volume of DMSO. A lipid migrating with a position consistent with SL was induced ~2.5 fold at pH 5.7 as compared to pH 7.0 in DMSO, whereas, this lipid was not detected in ETZ treated cells and the $\Delta phoPR$ mutant (Figure 3.3. A, Fig. S3.3. AC). It has been shown previously that mutant strains with reduced accumulation of PhoPR-regulated lipids compensate by over-accumulating other long chain fatty acids, such as triacylglycerol (TAG) and phthiocerol dimycoserate (PDIM) (11, 21, 35). At pH 5.7, as compared to the DMSO control, TAG was induced 5.5-fold and 6.5-fold in ETZ treated Mtb and the $\Delta phoPR$ mutant strain, respectively (Figure 3.3. B, Figure S3.3. A). Similarly, at pH 5.7, we observed a 2-fold increase in the accumulation of PDIM species in the ETZ treated samples as compared to the DMSO treated cells (Figure 3.3. C). Therefore, ETZ treatment phenocopies the $\Delta phoPR$ mutant strain for alteration of lipid species production.

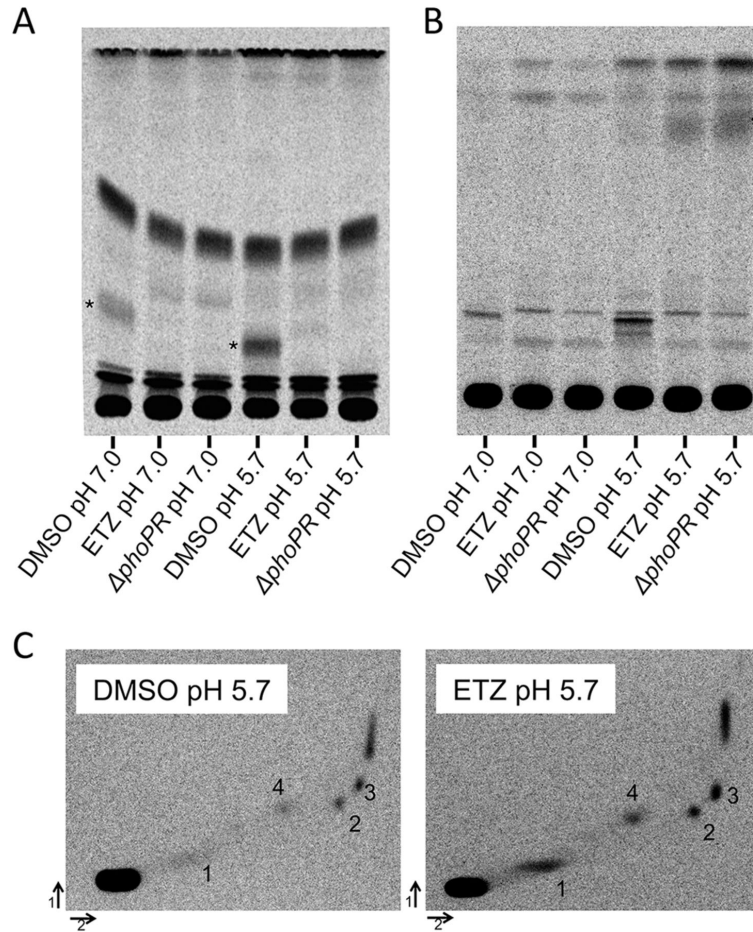


Figure 3.3. ETZ reduces the accumulation of sulfolipid and enhances accumulation of triacylglycerol and phthiocerol dimycocerosate. Radio-TLC showing that *M. tuberculosis* treated with 80 μ M ETZ and the $\Delta phoPR$ mutant strain exhibit a lack of accumulation of sulfolipid (SL) (denoted by *) (A) and enhanced accumulation of triacylglycerol (TAG) (denoted by *) (B). (C) 2D radio-TLC demonstrating that ETZ treatment increases the accumulation of TAG (spot 1), phthiocerol dimycocerosate (PDIM) species (spots 2 and 3), and an unidentified lipid species (spot 4) at pH 5.7 compared to a DMSO control. The data are representative of two biological replicates, with similar findings in the two experiments.

ESAT-6 protein is expressed in a *phoP* mutant strain but it is not exported from the bacterial cell (31). Therefore, we tested if ETZ treatment altered the secretion of Esx-1-exported proteins. Mtb Erdman was grown in rich medium and passaged twice in Sauton's minimal medium to measure Esx-1 export. During growth in Sauton's medium the cells were untreated, treated with ETZ during both passages (WT++, Figure 3.4.), or only treated with ETZ in the final passage (WT-+, Figure 3.4.). ETZ did not affect ESAT-6 and CFP-10 expression, but strongly and selectively reduced their secretion, as it did not alter that of Sec-secreted protein, Mpt-32 (Figure 3.4.). Moreover, transcriptional profiling revealed that *espR* and the *espACD* operon were significantly downregulated (>1.5-fold, $p < 0.05$) in ETZ treated cultures. Recently, Cao and colleagues have shown that PhoPR directly regulates EspR-dependent expression of *espACD* (32). EspA and ESAT-6 secretion are mutually dependent and loss of *espR* and *espA* expression leads to reduced Esx-1 function, loss of ESAT-6 secretion, and attenuated virulence (29, 36). Therefore, both transcriptional profiling in Mtb CDC1551 and biochemical approaches in Mtb Erdman support that ETZ inhibits Esx-1 secretion. Selective inhibition of PhoPR-dependent physiologies, such as SL synthesis and Esx-1 export, is predicted to reduce Mtb virulence (37).

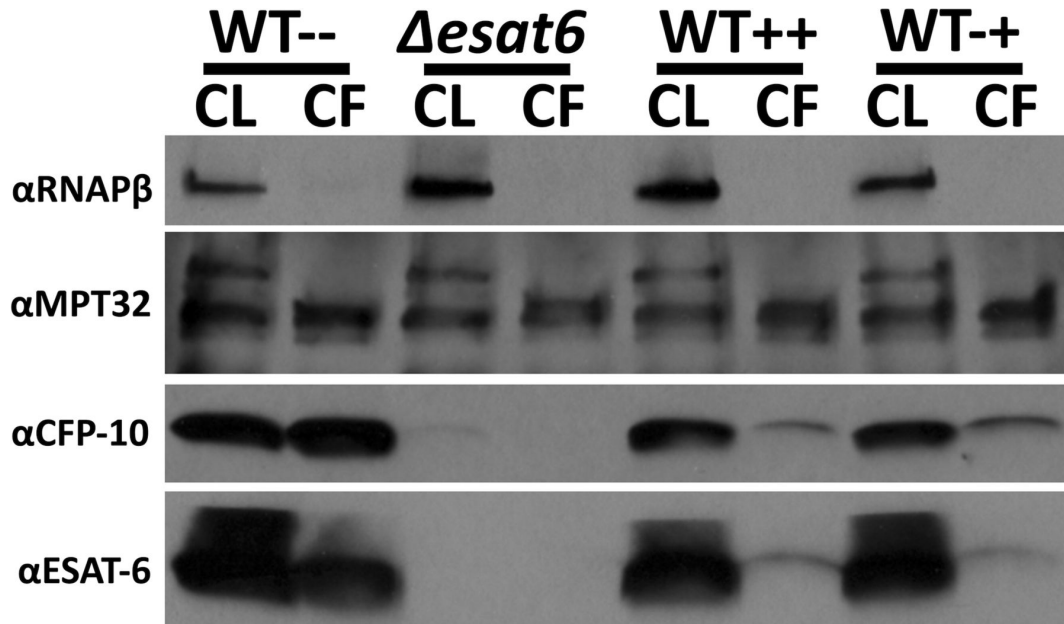


Figure 3.4. ETZ inhibits Esx-1 protein export. Western blot analysis of cell lysates (CL) and culture filtrates (CF) of wild-type (WT) *M. tuberculosis* Erdman and Δ esat-6 strains grown in Sauton's medium with or without addition of ETZ (80 μ M). The RNAP- β subunit served as a control for lysis and as a loading control for CL, and Mpt32 served as loading control for CF and as a measure of Sec secretion. The CFP-10 and ESAT-6 antibodies detected the EsxB and EsxA proteins, respectively, from the WT *M. tuberculosis* Erdman strain. ETZ treatment inhibits the secretion of ESAT-6 and CFP-10. —, no ETZ added; ++, ETZ added in both passages; +, ETZ added in second passage only. The data are representative of three biological replicates.

Ethoxzolamide inhibits Mtb PhoPR regulon expression and growth in infected macrophages and mice

The PhoPR regulon is induced within 20 minutes of Mtb phagocytosis by macrophages and remains induced over a period of at least 14 days (38). To determine if ETZ modulates the PhoPR regulon in macrophages, we infected murine bone marrow derived macrophages (BMDMs) with the CDC1551 (*aprA*::GFP, *smyc*::mCherry) reporter strain. This strain exhibits PhoPR-inducible expression of GFP and constitutive expression of mCherry (11). The infected macrophages were treated with ETZ or DMSO and single-cell reporter fluorescence was quantified 6 days post-infection. ETZ treatment caused >90% inhibition of reporter GFP fluorescence in infected macrophages (Figure 3.5. AB). Moreover, in a 9-day macrophage survival assay, ETZ treatment significantly inhibited the ability of Mtb to grow intracellularly (Figure 3.5. C). Notably, both ETZ treated and untreated bacteria exhibited a similar initial decrease in growth during the first 3 days of infection. However, the untreated Mtb successfully adapted to the macrophage environment and grew ~0.5 logs over the next six days while the ETZ treated cells could not transition into a growth phase. This phenotype is similar to that observed with a PhoPR mutant strain (12) and consistent with ETZ functioning as an anti-virulence agent targeting PhoPR-dependent macrophage adaptation.

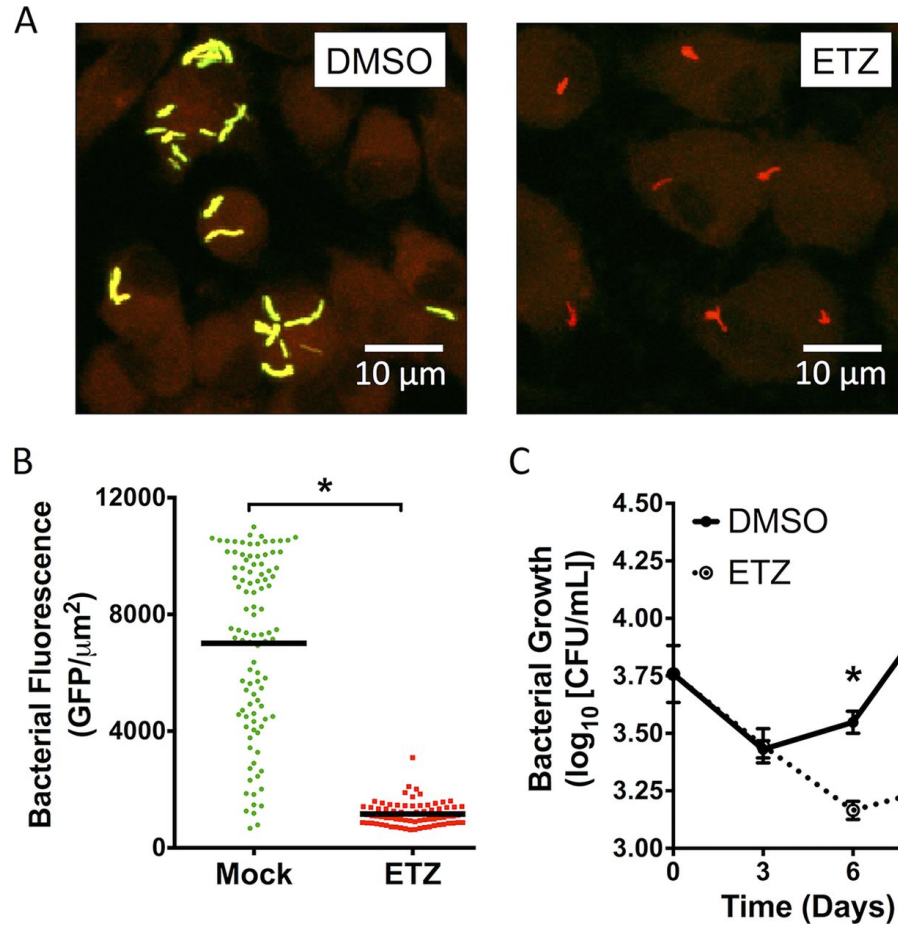


Figure 3.5. ETZ reduces PhoPR-regulated gene expression and survival in macrophages. Primary murine BMDMs were infected with the *M. tuberculosis* CDC1551(*aprA'*::GFP *smyc'*::mCherry) reporter at an MOI of 1:1 and treated with DMSO or ETZ (100 μ M) every 2 days for 9 days. (A) Confocal microscopy images demonstrate that ETZ treatment inhibits the PhoPR regulon in infected macrophages. The merged images show GFP (PhoPR-inducible signal) and mCherry (constitutive signal) fluorescence. (B) Single-cell quantification of reporter fluorescence shows that ETZ significantly downregulates PhoPR-dependent GFP fluorescence compared to a DMSO control. Statistical significance was calculated based on the Mann-Whitney rank test (*, $P < 0.001$). (C) Treatment of infected BMDMs with 80 μ M ETZ reduces growth ~ 1 log compared to the DMSO control. The data shown are three biological replicates and representative of three independent experiments. Statistical significance was calculated based on a two-tailed t test (*, $P < 0.001$). The error bars are the standard deviations from three biological replicates.

ETZ is also a eukaryotic CA inhibitor. Therefore, it is possible that the observed intracellular Mtb phenotypes may, in part, be driven by ETZ targeting macrophage CA activity. Because PhoPR is induced by acidic pH in macrophages, we examined if ETZ inhibits phagosome acidification. BMDMs were treated with DMSO, ETZ or concanamycin A (an inhibitor of the vacuolar ATPase) four hours prior to being fed with beads coated with the pH-sensitive dye pHrodo. Phagosome acidification was monitored for one hundred minutes using a plate reader. Even at concentrations as high as 100 mM, ETZ did not alter phagosome acidification (Figure S3.1. C), supporting the idea that ETZ-induced inhibition of Mtb growth is mediated by PhoPR regulon inhibition, rather than by altering the environment within the macrophage phagosome.

We next examined if ETZ can modulate the PhoPR regulon *in vivo*. C57Bl/6 mice were infected with the Erdman (*aprA*::GFP *smc*::mCherry) dual fluorescent reporter strain and the mice were treated orally with either 100 mg/kg of ETZ or an equal volume of 0.25% carboxymethyl cellulose (as a mock treatment) 5 days per week for 4 weeks. In animals, ETZ is previously reported to have a half-life of 2.5-5.5 hours, is rapidly absorbed with 65% bioavailability, and has an LD₅₀ of ~1000 mg/kg with no observable drug-related organ lesions at 100 mg/kg (1-4, 39, 40). Quantitative single-cell imaging was used to measure the induction of reporter fluorescence in lung tissues. For this approach, lung tissue was sectioned, imaged by confocal microscopy and bacterial fluorescence quantified using Volocity image analysis software (20, 41). Individual bacterial cells were identified using the constitutive mCherry signal and then GFP fluorescence was measured for ~3000 bacterial cells across multiple fields of view from lungs of mice in the same treatment group. Two independent experiments were conducted with similar results; therefore, the data from both experiments were combined for

analysis. The Erdman (*aprA*'::GFP *smyc*'::mCherry) reporter exhibited a strong induction of GFP fluorescence in infected mice in mock-treated mouse lungs (Figure 3.6. A). Notably, single cells in the mock treated samples exhibited substantial heterogeneity of GFP fluorescence providing additional evidence that Mtb experiences a variety of microenvironments during the course of infection (Figure 3.6. B). In contrast, ETZ strongly downregulated GFP reporter fluorescence in mouse lungs with 3-fold inhibition of GFP signal as compared to the mock treated control (Figure 3.6. B). Importantly, the distribution of reporter fluorescence was dramatically altered by ETZ treatment, with a more homogeneous population of cells expressing low levels of GFP. For example, 49% of Mtb cells in ETZ treated lungs quantified for GFP fluorescence are in the bottom decile of fluorescence ($<1000 \text{ GFP/mm}^2$) as compared to 5% of cells in the mock-treated mice (Figure 3.6. B). This approach demonstrates that quantitative analysis of fluorescent Mtb reporter strains in host tissues can be applied as a biomarker for pathway-specific drug exposure *in vivo*. ETZ treated mouse lungs did not have a significant reduction in the area of the lung showing Mtb-associated granulomatous pneumonia (Figure S3.4.). The lesions in both mock and ETZ treated mice consisted of multifocal infiltrates of epithelioid to multinucleated macrophages, obliterating and expanding alveolar lumina, often with cuffs of lymphocytic infiltrate surrounding adjacent arterioles (Figure S3.5.). There were occasional instances of lymphohistiocytic pleuritis in both groups. The effect of ETZ treatment on bacterial survival *in vivo* was also examined. We observed a significant 0.72 log reduction of bacterial survival in the lungs of ETZ treated mice as compared to the mock-treated control (Figure 3.6. C). Therefore, adequate ETZ exposure was achieved in mouse lungs to repress the PhoPR regulon and attenuate virulence. Together, these data support that ETZ functions by an anti-virulence mechanism and attenuates Mtb virulence *in vivo* by i) targeting Mtb inside

macrophages and the mouse lung, ii) downregulating the PhoPR regulon, and iii) reducing the expression of virulence pathways such as lipid metabolism and Esx-1 secretion.

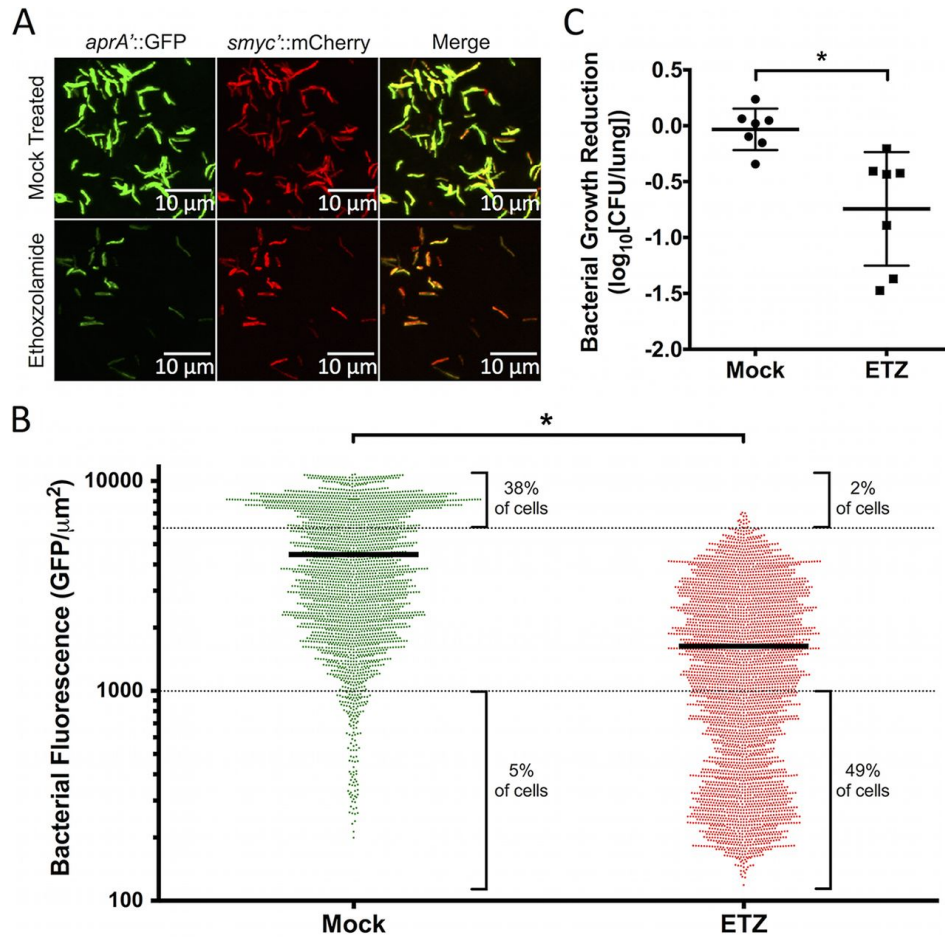


Figure 3.6. ETZ treatment reduces PhoPR-regulated gene expression and survival *in vivo*. C57BL/6 mice were infected with 1,000 CFU of the *M. tuberculosis* Erdman (*aprA'::GFP smyc'::mCherry*) fluorescent reporter strain and treated with ETZ for 4 weeks. (A) ETZ downregulates PhoPR-dependent GFP fluorescence *in vivo*. The images show reporter fluorescence in mouse lung tissue. (B) Single-cell quantification of reporter fluorescence in infected mouse lungs shows that ETZ significantly downregulates PhoPR-dependent GFP fluorescence compared to the level in mock-treated mice. GFP fluorescence was quantified for ~3,000 bacteria. Statistical significance was calculated based on the Mann-Whitney rank test (*, $P < 0.0001$). (C) *M. tuberculosis* survival is attenuated in ETZ-treated lungs. The data presented are from seven animals per treatment group, and statistical significance was calculated using a two-tailed *t* test (*, $P < 0.01$). The data are combined from two independent experiments.

Discussion

We identified ETZ as an inhibitor of the PhoPR regulon by conducting a whole-cell HTS using an acidic-pH inducible, PhoPR-dependent reporter strain. This HTS is particularly unique in that it was performed *in vitro*, but identified an inhibitor of a target, the PhoPR regulon, that is only required for growth in macrophages and *in vivo*. To our knowledge, there are no known chemical inhibitors of the PhoPR regulon. Recently, Cole and colleagues identified an anti-virulence inhibitor of Esx-1 secretion using an anti-cytolytic screen (37), although the mechanism of this compound appears to be PhoPR-independent. ETZ does not alter Mtb cytoplasmic pH-homeostasis (Figure 3.1. D) and is thus acting by a mechanism that is distinct from compounds found to modulate cytoplasmic pH homeostasis (42-44). ETZ, therefore, represents a first-in-class agent and strategy to inhibit Mtb pH-dependent adaptation and virulence. Inhibiting an adaptation pathway required for pathogen virulence *in vivo* exemplifies an anti-virulence strategy, a new approach to drug development that is proposed to slow the evolution of drug resistance (14-18).

ETZ is an FDA approved drug prescribed for the treatment of glaucoma, seizure threshold reduction, and utilized as a general diuretic through the CA inhibitory properties of the compound (45). Because ETZ is already proven to be safe in humans, it may be possible to repurpose ETZ for the treatment of Mtb. The PhoPR mutant strain is highly attenuated in animal infections and is currently being developed as a potential attenuated Mtb vaccine (46). Thus, it will be of considerable interest to continue the development of ETZ for the treatment of TB, possibly as an adjunct therapy with current drug regimens. Given the incomplete inhibition of the PhoPR regulon *in vivo* (Figure 3.6. B), improvements to compound potency or lung distribution may improve ETZ efficacy *in vivo*.

The mechanism by which ETZ modulates the PhoPR regulon remains to be determined. It is possible that ETZ functions by directly targeting PhoPR or targeting a PhoPR-associated regulator (such as WhiB3 (47)); however, given that ETZ has been shown to inhibit Mtb CA activity in whole cells (Fig. 1C), we hypothesize that ETZ may indirectly inhibit the PhoPR regulon by interfering with CA activity (Fig. 7). Mtb carries 3 CA genes, Rv3273, Rv1284 and Rv3588c of which the latter two are required for survival in mice (48). Because CA catalyzes the reaction of CO₂ to bicarbonate and a proton, CA may function to modulate local pH (49, 50). We did not, however, observe any change in the pH of the culture medium and only a slight change of <0.1 pH units in the Mtb cytoplasm, suggesting that if the mechanism is pH dependent it may be localized to the cell envelope. Depending on the cellular localization of CAs (predicted to be extra-cytoplasmic, (51)), and anion/cation homeostasis (*e.g.* protons, bicarbonate, ammonium, and chloride), CA activity could potentially promote an acidified or alkalinized cell envelope (52). Given that ETZ inhibits PhoPR signaling and PhoPR is induced by acidic pH, we predict that CA may promote an acidified pseudoperiplasm. In this model (Figure 3.7.), CA is generating extracellular proton and bicarbonate ions. The bicarbonate can be transported by a bicarbonate transporter (BT, Mtb has several predicted BT genes) to maintain the cytoplasmic pH. CA will cause protons to accumulate in the pseudoperiplasm causing the activation of the PhoR kinase and the PhoPR pathway. ETZ would inhibit this process by inhibiting CA and reducing the accumulation of protons in the pseudoperiplasm (Figure 3.7.). This model is supported by studies of the acid-adapted stomach pathogen *Helicobacter pylori*, which maintains periplasmic pH through a CA-dependent mechanism (53, 54). Alternatively, CA may be impacting central carbon metabolism enzymes that rely on bicarbonate/CO₂, such as PckA and other carboxylases, and modulate PhoPR through feedback associated with altered redox homeostasis or carbon

metabolism. pH and the equilibrium of carbonic acid/bicarbonate/ CO_2 in water are physically linked and in many biological systems CO_2 is indirectly sensed by monitoring pH (55). Notably, the PhoPR regulon is induced at a threshold of $\sim\text{pH } 6.3$ (11), the same pH at which the dissolved inorganic carbon equilibrium favors CO_2 to dissolve in water. Therefore, it is tempting to speculate that PhoPR may function as a CO_2 sensor that uses pH as a proxy for dissolved CO_2 .

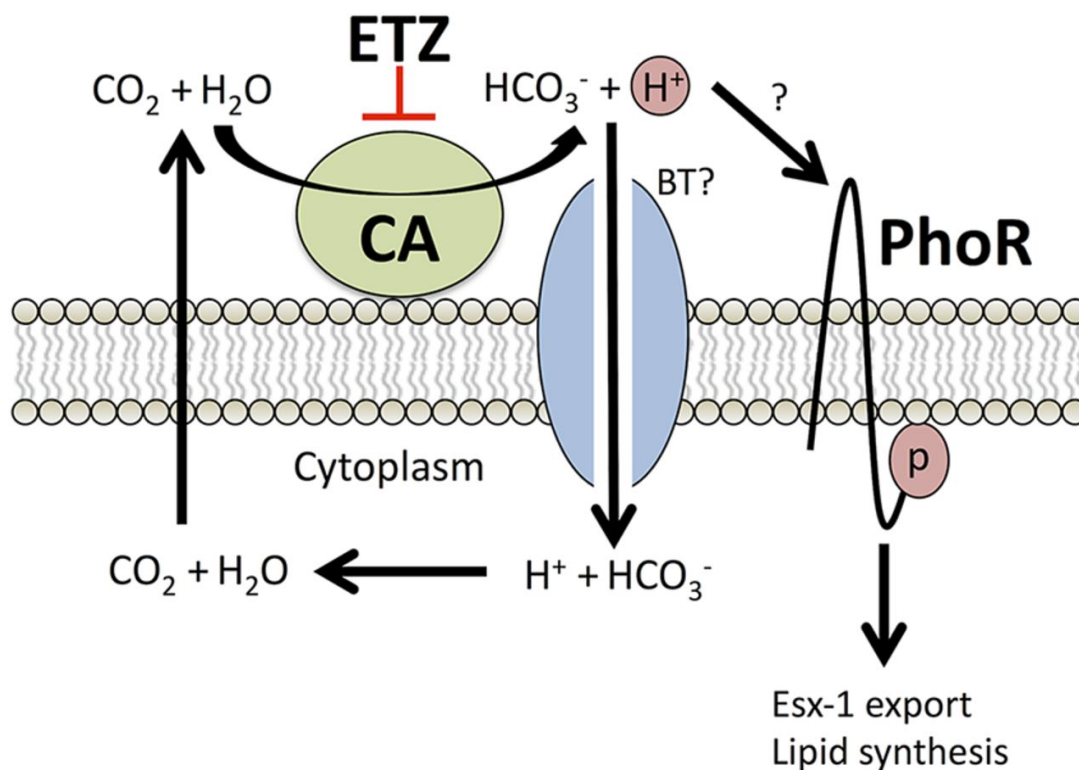


Figure 3.7. Model linking ETZ, CA, and regulation of the PhoPR pathway. PhoPR is activated at a similar pH (~6.3) as the dissolved inorganic carbon equilibrium that favors CO_2 to dissolve in water. CA will interconvert $\text{CO}_2 + \text{H}_2\text{O}$ to $\text{HCO}_3^- + \text{H}^+$. Bicarbonate may be shuttled into the cytoplasm by a bicarbonate transporter (BT) to act in maintaining pH homeostasis or metabolism, while the proton produced in the reaction may promote the acidification of the extracellular environment surrounding PhoR, leading to induction of the PhoPR regulon. ETZ would inhibit this process by inhibiting CA and limiting the accumulation of protons in the pseudoperiplasm. This model is inspired by models from Sedlakova et al. (54) and Rasko and Sperandio (8).

Reporter strains are powerful tools for both the discovery and characterization of new antimicrobials. These strains are synthetic phenotypes and enable whole cell screens to discover inhibitors of pathways that are otherwise inaccessible for high throughput assays. Importantly, we show with the reporter strain used here, that these strains can also be used as biomarkers to determine *in vivo* exposure of the bacterium to a newly discovered compound. In this manner, the reporter strain enables a rapid determination of whether the compound is targeting the pathway of interest in host tissues. Our study demonstrates the proof-of-concept that Mtb fluorescent reporter strains can be used for the discovery and *in vivo* characterization of inhibitors of Mtb two-component regulatory pathways. Many two-component signal transduction systems are required for Mtb pathogenesis (56); therefore, this approach may be applied to the discovery of other inhibitors that blind Mtb to environmental stimuli and attenuate virulence.

Acknowledgements

We thank the New England Regional Center of Excellence (U54 AI057159) for providing the screening libraries and Su Chiang and Doug Flood for assistance in preparing the compound libraries for screening. The High Performance Computing Cluster and iCER at Michigan State University provided computational support. The MSU RTSF provided technical support for the RNA-seq library preparation and sequencing. The MSU Center for Advanced Microscopy provided confocal microscopy support. We thank Kyle Rohde, Garry Coulson, Kathy Meek, Martha Mulks and members of the Abramovitch lab for critical reading of the manuscript. Research reported in this study from the Champion lab was supported by funding from the Great Lakes Regional Center of Excellence (GLRCE, U54AI057153) and by the National Institute of Allergies and Infectious Diseases of the National Institutes of Health (NIH-NIAID) under award

numbers R01AI106872 to P.A.C. F.M. is supported by a postdoctoral fellowship from the Eck Institute for Global Health at the University of Notre Dame. Research reported in this study from the Abramovitch lab was supported by start-up funding from Michigan State University and AgBioResearch, and grants from the NIH-NIAID (R21AI105867), the GLRCE (U54AI057153), the Michigan Economic Development Corporation (AGR2014-00199) and the Jean P. Schultz Endowed Biomedical Research Fund at the MSU College of Human Medicine.

APPENDIX

APPENDIX

Supplemental materials and methods

pH of medium determination

To examine whether ETZ alters the pH of the medium, WT Mtb CDC1551 was grown in a similar manner as the transcriptional profiling experiments. Two conditions were examined: 1) DMSO treated, pH 5.7 or 2) 80 μ M ETZ treated, pH 5.7. After 6 days incubation, cells were pelleted and supernatants were collected and filtered twice through 0.22 μ m filters. The pH of the supernatants was then measured on a pH meter.

Data analysis of RNA-seq transcriptional profiling experiments

Differential gene expression was calculated by normalizing data utilizing the trimmed mean of M-values normalization method (57) and filtering genes that had >2 average normalized counts per million (CPM) within the edgeR package (58). Statistical analysis was performed in RStudio (ver. 0.97.551) by fitting an additive generalized linear model (59) or exact test (60) with the negative binomial distribution for each set of conditions and testing for differential gene expression utilizing the edgeR package. Differentially expressed genes were determined to be statistically significant based on >2-fold differentially regulated and an adjusted $p < 0.05$.

Confocal microscopy and pathology of ETZ treated lungs

PFA fixed mouse lungs were frozen in a 30% sucrose PBS pH 7.4 solution, frozen in a dry ice, ethanol bath, and stored at -80°C until imaging. At the time of imaging, lungs were thawed and hand-sectioned using a sterile scalpel. Sections were transferred to a microscope slide and 10 μ L of ProLong® Gold antifade reagent (Invitrogen) was added. Samples were then mounted on a

glass coverslip and imaged immediately. Images were obtained using an Olympus FV1000 confocal microscope. Settings for GFP and mCherry fluorescence were held constant through the image acquisition to allow for comparison between samples. For quantification of Mtb reporter fluorescence, bacilli were identified in the mCherry channel and the corresponding sum of GFP fluorescence was measured using the Volocity software package (Perkin Elmer). At least 1500 bacilli were counted across multiple fields of view and lungs.

For histopathology, transverse sections of each lung specimen was fixed in 4% paraformaldehyde for 48 hours, transferred to 50% ethanol for 4 hours, processed routinely, embedded in paraffin, and sectioned at 4 μ m, followed by routine hematoxylin and eosin staining. Photomicrographs were acquired, and using Image-J the total area of each lung section was measured, as was the area of each lesion and a percentage of lung affected was calculated from this data.

Supporting gene expression information

Tables can be found in the GEO database using the accession number: GSE63917.

Gene expression tables of DMSO treated Mtb genes differentially expressed (>2 fold, $p < 0.05$) at pH 5.7 as compared to pH 7.0 .

Gene expression tables of ETZ treated Mtb genes differentially expressed (>2 fold, $p < 0.05$) at pH 5.7 as compared to DMSO treated Mtb at pH 5.7.

Gene expression tables of the *phoP*::Tn Mtb genes differentially expressed (>2 fold, $p < 0.05$) at pH 5.7 as compared to DMSO treated Mtb at pH 5.7.

Gene expression tables of DMSO treated Mtb at pH 5.7 as compared to pH 7.0.

Gene expression tables of ETZ treated Mtb at pH 5.7 as compared to DMSO treated Mtb at pH 5.7.

Gene expression tables of DMSO treated *phoP*::Tn Mtb at pH 5.7 as compared to DMSO treated Mtb at pH 5.7.

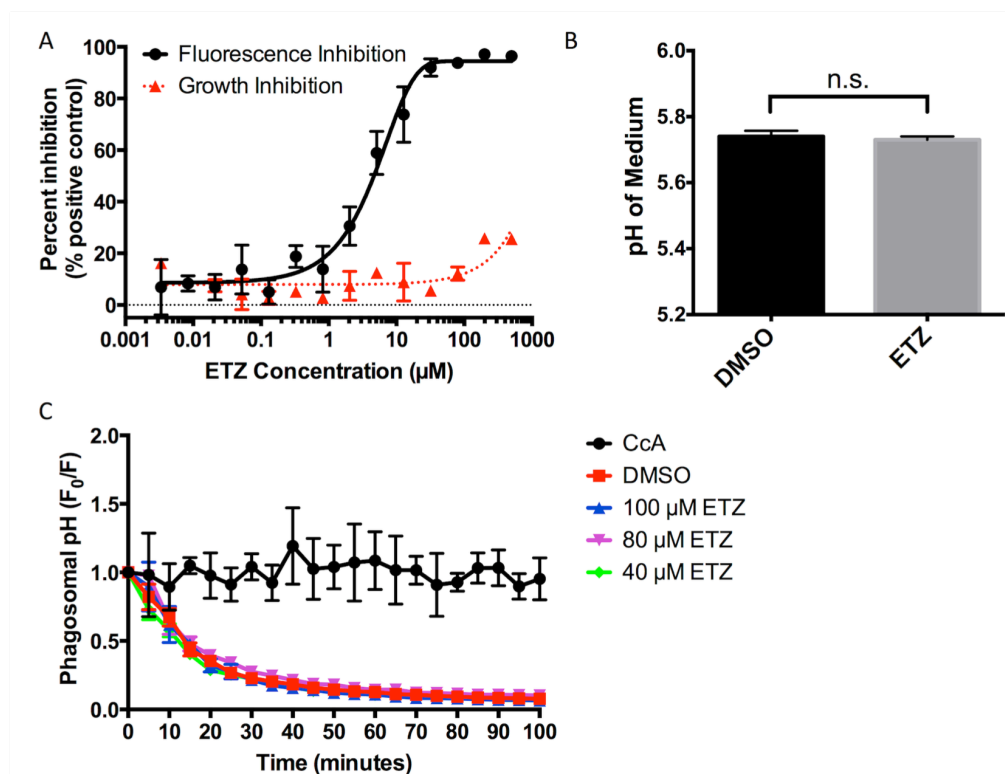


Figure S3.1.: ETZ inhibits the *phoPR* regulated *aprA'*::GFP in a dose dependent manner, but does not alter the pH of the medium or phagosome acidification. (A) ETZ inhibits PhoPR-dependent *aprA'*::GFP fluorescence in a concentration dependent manner at pH 7.0 with an EC₅₀ of 4.7 μ M and little effect on growth. (B) The pH of the culture medium is not altered when Mtb is treated with ETZ (80 μ M) compared to a DMSO control after 6 days incubation at pH 5.7. (C) pHrodo labeled particles (Life Technologies) were fed to BMDMs pre-treated for 4 hours with: ETZ (100, 80, or 40 μ M) or an equivalent volume of DMSO. Concanamycin A (CcA, 100 nM) inhibits phagosome acidification through inhibition of the vacuolar ATPase and added 30 minutes before feeding of labeled particles. pHrodo fluorescence increases as pH decreases and was monitored every 5 minutes for 100 minutes. Treatments were present throughout the assay. F_0 : fluorescence at time 0. F : fluorescence at each time point. Error bars represent the standard deviation from at least three technical replicates. Data are representative of at least two biological replicates. Error bars are the standard deviation of at least 3 technical replicates.

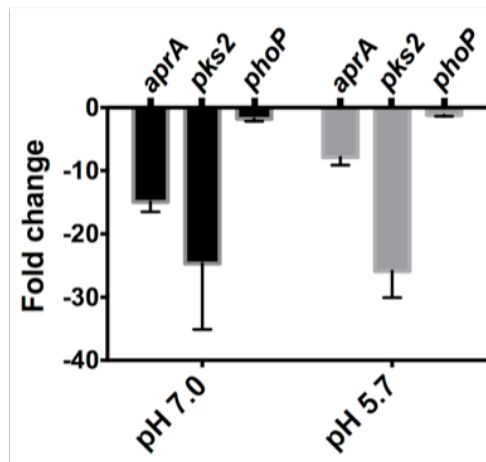


Figure S3.2.: ETZ down-regulates the core PhoPR regulon, but not *phoP*. (A) Semi-quantitative RT-PCR validation of RNA-seq transcriptional profiling reveals that ETZ down-regulates PhoPR-regulated genes (*aprA* and *pks2*), but not *phoP*. Error bars are the standard deviation of three technical replicates. Data are representative of three biological replicates. (B) ETZ is chemically capable of down-regulating the core PhoPR regulon at acidic pH, similar to the *phoP*::Tn mutant ($p < 0.05$). Some of the discrepancy between ETZ treatment and the *phoP*::Tn mutant can be reconciled with the notion that gene disruption of a high level regulator like PhoPR will lead to a more robust gene misregulation phenotype compared to that of chemically disrupting PhoPR signaling through ETZ treatment.

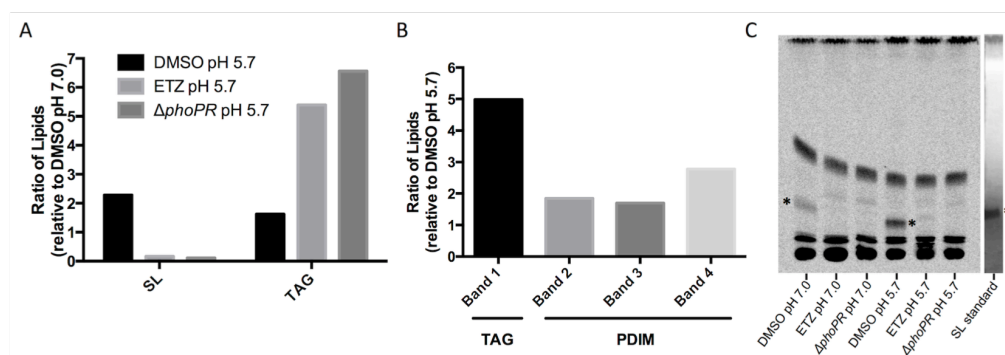


Figure S3.3.: ETZ treatment alters lipid species production. (A and B) Quantitation of lipid analysis as summarized in **Figure 3**. (C) Radio-TLC showing Mtb treated with 80 μ M ETZ and the $\Delta phoPR$ mutant strain exhibit a lack of accumulation of sulfolipid (SL) (*), consistent with that of a SL standard. The unlabeled SL standard was resolved on the same TLC plate as radio-labeled lipids and charred with phosphomolybdic acid for visualization. Data are representative of two biological replicates with similar findings in each experiment.

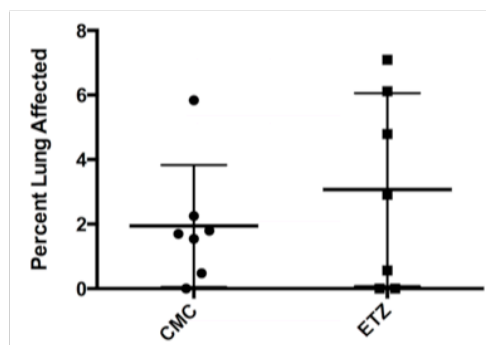


Figure S3.4.: Comparison of percent lung area affected of the section examined for each CMC and ETZ treated animal. There is no significant difference between the two groups.

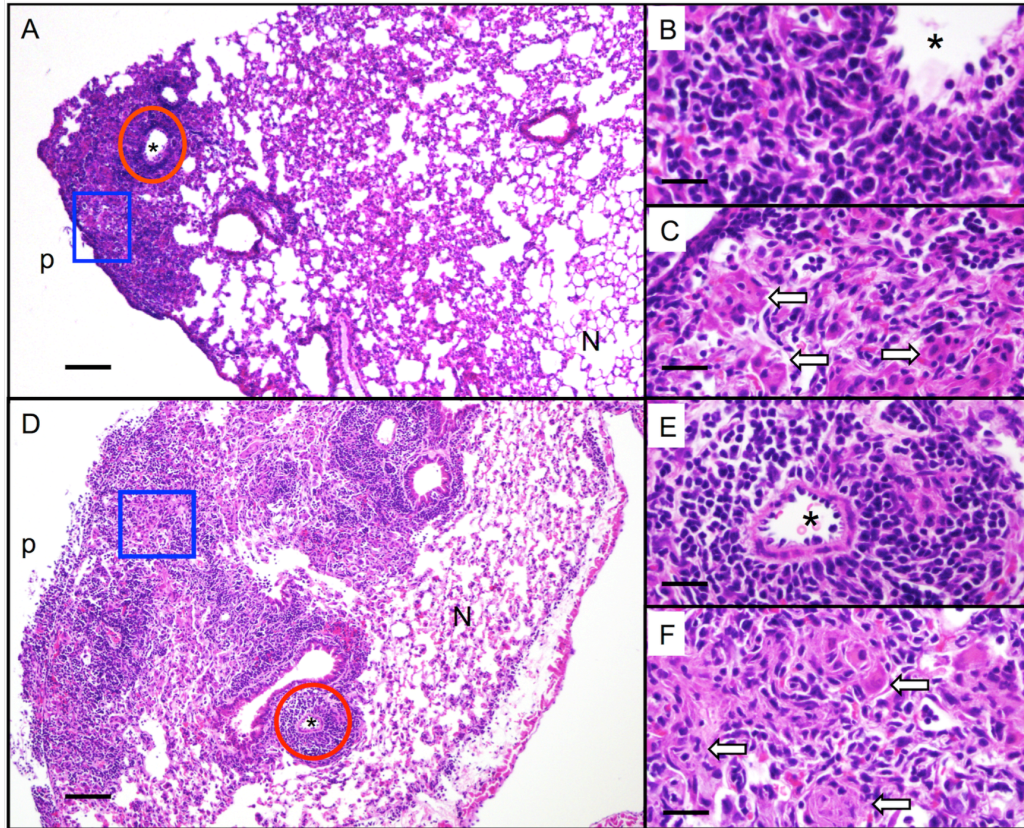


Figure S3.5.: Representative histopathological images from mock treated and ETZ treated mice. Lung tissue from ETZ (A,B,C) and CMC (D,E,F) treated mice, hematoxylin and eosin. Panels A and D: 40x, bar = 140 μ m; panels B, C, E, and F: 200x, bar = 45 μ m. Panel B is the area encircled in red in Panel A; Panel C is the area boxed in blue in Panel A; Panel E is the area encircled in red in Panel D; and Panel F is the area boxed in blue in Panel D. Histopathologic lesions of granulomatous pneumonia were similar between both treatment groups. Lesions consisted of multifocal infiltrates of epithelioid to multinucleated macrophages (boxed in blue) obliterating and expanding alveolar lumina, often with cuffs of lymphocytic infiltrate (encircled in red) surrounding adjacent arterioles. There were also occasional instances of lymphohistiocytic pleuritic (p) in both groups. Panels B and E show tight cuffs of lymphoplasmacytic infiltrate surrounding arterioles (lumina denoted by *). Panels C and F show epithelioid to multinucleated macrophages (arrows) filling and expanding the alveolar lumina. Note the similarity of the lesions between the two groups. N denotes normal pulmonary parenchyma, * denotes arteriolar lumina.

REFERENCES

REFERENCES

1. **Maren TH, Brechue WF, Bar-Ilan A.** 1992. Relations among IOP reduction, ocular disposition and pharmacology of the carbonic anhydrase inhibitor ethoxzolamide. *Exp Eye Res* **55**:73-79.
2. **Drance SM.** 1960. Ethoxzolamide (cardrase) in the management of chronic simple glaucoma. *Arch Ophthalmol* **64**:433-437.
3. **Drance SM.** 1959. The effects of ethoxzolamide (cardrase) on intraocular pressure. *Arch Ophthalmol* **62**:679-684.
4. **Moyer JH, Ford RV.** 1958. Laboratory and clinical observations on ethoxzolamide (cardrase) as a diuretic agent. *Am J Cardiol* **1**:497-504.
5. **Mincione F, Scozzafava A, Supuran CT.** 2007. The development of topically acting carbonic anhydrase inhibitors as anti-glaucoma agents. *Curr Top Med Chem* **7**:849-854.
6. **Sassetti CM, Rubin EJ.** 2003. Genetic requirements for mycobacterial survival during infection. *Proc Natl Acad Sci U S A* **100**:12989-12994.
7. **Vandal OH, Nathan CF, Ehrt S.** 2009. Acid Resistance in *Mycobacterium tuberculosis*. *Journal of Bacteriology* **191**:4714-4721.
8. **Rohde KH, Abramovitch RB, Russell DG.** 2007. *Mycobacterium tuberculosis* invasion of macrophages: linking bacterial gene expression to environmental cues. *Cell Host Microbe* **2**:352-364.
9. **Walters SB, Dubnau E, Kolesnikova I, Laval F, Daffe M, Smith I.** 2006. The *Mycobacterium tuberculosis* PhoPR two-component system regulates genes essential for virulence and complex lipid biosynthesis. *Molecular Microbiology* **60**:312-330.
10. **Gonzalo-Asensio J, Mostowy S, Harders-Westerveen J, Huygen K, Hernandez-Pando R, Thole J, Behr M, Gicquel B, Martin C.** 2008. PhoP: A Missing Piece in the Intricate Puzzle of *Mycobacterium tuberculosis* Virulence. *Plos One* **3**:e3496.
11. **Abramovitch RB, Rohde KH, Hsu FF, Russell DG.** 2011. *aprABC*: a *Mycobacterium tuberculosis* complex-specific locus that modulates pH-driven adaptation to the macrophage phagosome. *Mol Microbiol* **80**:678-694.

12. **Perez E, Samper S, Bordas Y, Guilhot C, Gicquel B, Martin C.** 2001. An essential role for *phoP* in *Mycobacterium tuberculosis* virulence. *Molecular Microbiology* **41**:179-187.
13. **Martin C, Williams A, Hernandez-Pando R, Cardona PJ, Gormley E, Bordat Y, Soto CY, Clark SO, Hatch GJ, Aguilar D, Ausina V, Gicquel B.** 2006. The live *Mycobacterium tuberculosis phoP* mutant strain is more attenuated than BCG and confers protective immunity against tuberculosis in mice and guinea pigs. *Vaccine* **24**:3408-3419.
14. **Rasko DA, Sperandio V.** 2010. Anti-virulence strategies to combat bacteria-mediated disease. *Nat Rev Drug Discov* **9**:117-128.
15. **Hu MY, Katchar K, Kyne L, Maroo S, Tummala S, Dreisbach V, Xu H, Leffler DA, Kelly CP.** 2009. Prospective derivation and validation of a clinical prediction rule for recurrent *Clostridium difficile* infection. *Gastroenterology* **136**:1206-1214.
16. **Shim JK, Johnson S, Samore MH, Bliss DZ, Gerding DN.** 1998. Primary symptomless colonisation by *Clostridium difficile* and decreased risk of subsequent diarrhoea. *Lancet* **351**:633-636.
17. **Kyne L, Warny M, Qamar A, Kelly CP.** 2000. Asymptomatic carriage of *Clostridium difficile* and serum levels of IgG antibody against toxin A. *N Engl J Med* **342**:390-397.
18. **Ternent L, Dyson RJ, Krachler AM, Jabbari S.** 2015. Bacterial fitness shapes the population dynamics of antibiotic-resistant and -susceptible bacteria in a model of combined antibiotic and anti-virulence treatment. *J Theor Biol* **372**:1-11.
19. **Drudy D, Harnedy N, Fanning S, Hannan M, Kyne L.** 2007. Emergence and control of fluoroquinolone-resistant, toxin A-negative, toxin B-positive *Clostridium difficile*. *Infect Control Hosp Epidemiol* **28**:932-940.
20. **Tan S, Sukumar N, Abramovitch RB, Parish T, Russell DG.** 2013. *Mycobacterium tuberculosis* Responds to Chloride and pH as Synergistic Cues to the Immune Status of its Host Cell. *PLoS Pathog* **9**:e1003282.
21. **Baker JJ, Johnson BK, Abramovitch RB.** 2014. Slow growth of *Mycobacterium tuberculosis* at acidic pH is regulated by *phoPR* and host-associated carbon sources. *Mol Microbiol* **94**:56-59.
22. **Johnson BK, Abramovitch RB.** 2015. Macrophage Infection Models for *Mycobacterium tuberculosis*. *Methods Mol Biol* **1285**:329-341.

23. **Brion LP, Schwartz JH, Zavilowitz BJ, Schwartz GJ.** 1988. Micro-method for the measurement of carbonic anhydrase activity in cellular homogenates. *Anal Biochem* **175**:289-297.
24. **Purdy GE, Niederweis M, Russell DG.** 2009. Decreased outer membrane permeability protects mycobacteria from killing by ubiquitin-derived peptides. *Mol Microbiol* **73**:844-857.
25. **Schneider CA, Rasband WS, Eliceiri KW.** 2012. NIH Image to ImageJ: 25 years of image analysis. *Nat Methods* **9**:671-675.
26. **Hung DT, Shakhnovich EA, Pierson E, Mekalanos JJ.** 2005. Small-molecule inhibitor of *Vibrio cholerae* virulence and intestinal colonization. *Science* **310**:670-674.
27. **DiRita VJ, Parsot C, Jander G, Mekalanos JJ.** 1991. Regulatory cascade controls virulence in *Vibrio cholerae*. *Proc Natl Acad Sci U S A* **88**:5403-5407.
28. **Carta F, Maresca A, Covarrubias AS, Mowbray SL, Jones TA, Supuran CT.** 2009. Carbonic anhydrase inhibitors. Characterization and inhibition studies of the most active beta-carbonic anhydrase from *Mycobacterium tuberculosis*, Rv3588c. *Bioorg Med Chem Lett* **19**:6649-6654.
29. **Raghavan S, Manzanillo P, Chan K, Dovey C, Cox JS.** 2008. Secreted transcription factor controls *Mycobacterium tuberculosis* virulence. *Nature* **454**:717-721.
30. **Solans L, Gonzalo-Asensio J, Sala C, Benjak A, Uplekar S, Rougemont J, Guilhot C, Malaga W, Martin C, Cole ST.** 2014. The PhoP-dependent ncRNA Mcr7 modulates the TAT secretion system in *Mycobacterium tuberculosis*. *PLoS Pathog* **10**:e1004183.
31. **Frigui W, Bottai D, Majlessi L, Monot M, Josselin E, Brodin P, Garnier T, Gicquel B, Martin C, Leclerc C, Cole ST, Brosch R.** 2008. Control of *M. tuberculosis* ESAT-6 secretion and specific T cell recognition by PhoP. *PLoS Pathog* **4**:e33.
32. **Cao G, Howard ST, Zhang P, Wang X, Chen XL, Samten B, Pang X.** 2014. EspR, a regulator of the ESX-1 secretion system in *Mycobacterium tuberculosis*, is directly regulated by the two-component systems MprAB and PhoPR. *Microbiology* doi:10.1099/mic.0.000023.
33. **Staskawicz BJ, Mudgett MB, Dangel JL, Galan JE.** 2001. Common and contrasting themes of plant and animal diseases. *Science* **292**:2285-2289.
34. **Asensio JG, Maia C, Ferrer NL, Barilone N, Laval F, Soto CY, Winter N, Daffe M, Gicquel B, Martin C, Jackson M.** 2006. The virulence-associated two component

- PhoP-PhoR system controls the biosynthesis of polyketide-derived lipids in *Mycobacterium tuberculosis*. *Journal of Biological Chemistry* **281**:1313-1316.
35. **Jain M, Petzold CJ, Schelle MW, Leavell MD, Mougous JD, Bertozzi CR, Leary JA, Cox JS.** 2007. Lipidomics reveals control of *Mycobacterium tuberculosis* virulence lipids via metabolic coupling. *Proc Natl Acad Sci U S A* **104**:5133-5138.
 36. **Fortune SM, Jaeger A, Sarracino DA, Chase MR, Sassetti CM, Sherman DR, Bloom BR, Rubin EJ.** 2005. Mutually dependent secretion of proteins required for mycobacterial virulence. *Proc Natl Acad Sci U S A* **102**:10676-10681.
 37. **Piovan L, Alves MFM, Juliano L, Brömme D, Cunha RLOR, Andrade LH.** 2010. Chemoenzymatic synthesis of organoselenium(IV) compounds and their evaluation as cysteine protease inhibitors. *Journal of the Brazilian Chemical Society* **21**:2108-2118.
 38. **Pucci MJ.** 2007. Novel genetic techniques and approaches in the microbial genomics era: identification and/or validation of targets for the discovery of new antibacterial agents. *Drugs R D* **8**:201-212.
 39. **Eller MG, Schoenwald RD.** 1984. Determination of ethoxzolamide in the iris/ciliary body of the rabbit eye by high-performance liquid chromatography: comparison of tissue levels following intravenous and topical administrations. *J Pharm Sci* **73**:1261-1264.
 40. **Maren TH.** 1967. Carbonic anhydrase: chemistry, physiology, and inhibition. *Physiol Rev* **47**:595-781.
 41. **Evans ML, Chorell E, Taylor JD, Aden J, Gotheson A, Li F, Koch M, Sefer L, Matthews SJ, Wittung-Stafshede P, Almquist F, Chapman MR.** 2015. The bacterial curli system possesses a potent and selective inhibitor of amyloid formation. *Mol Cell* **57**:445-455.
 42. **Weiss DS, Brotcke A, Henry T, Margolis JJ, Chan K, Monack DM.** 2007. In vivo negative selection screen identifies genes required for *Francisella* virulence. *Proc Natl Acad Sci U S A* **104**:6037-6042.
 43. **Butler T.** 2009. Plague into the 21st century. *Clin Infect Dis* **49**:736-742.
 44. **Pan NJ, Brady MJ, Leong JM, Goguen JD.** 2009. Targeting type III secretion in *Yersinia pestis*. *Antimicrob Agents Chemother* **53**:385-392.
 45. **Cornelis GR, Van Gijsegem F.** 2000. Assembly and function of type III secretory systems. *Annu Rev Microbiol* **54**:735-774.

46. **Sanchez J, Holmgren J.** 2011. Cholera toxin - a foe & a friend. *Indian J Med Res* **133**:153-163.
47. **Singh A, Crossman DK, Mai D, Guidry L, Voskuil MI, Renfrow MB, Steyn AJC.** 2009. *Mycobacterium tuberculosis* WhiB3 Maintains Redox Homeostasis by Regulating Virulence Lipid Anabolism to Modulate Macrophage Response. *Plos Pathogens* **5**:e1000545.
48. **Rengarajan J, Bloom BR, Rubin EJ.** 2005. Genome-wide requirements for *Mycobacterium tuberculosis* adaptation and survival in macrophages. *Proc Natl Acad Sci U S A* **102**:8327-8332.
49. **Rasko DA, Moreira CG, Li de R, Reading NC, Ritchie JM, Waldor MK, Williams N, Taussig R, Wei S, Roth M, Hughes DT, Huntley JF, Fina MW, Falck JR, Sperandio V.** 2008. Targeting QseC signaling and virulence for antibiotic development. *Science* **321**:1078-1080.
50. **Khajanchi BK, Kozlova EV, Sha J, Popov VL, Chopra AK.** 2012. The two-component QseBC signalling system regulates in vitro and in vivo virulence of *Aeromonas hydrophila*. *Microbiology* **158**:259-271.
51. **Lu J, Vlamis-Gardikas A, Kandasamy K, Zhao R, Gustafsson TN, Engstrand L, Hoffner S, Engman L, Holmgren A.** 2013. Inhibition of bacterial thioredoxin reductase: an antibiotic mechanism targeting bacteria lacking glutathione. *FASEB J* **27**:1394-1403.
52. **Swietnicki W, Carmany D, Retford M, Guelta M, Dorsey R, Bozue J, Lee MS, Olson MA.** 2011. Identification of small-molecule inhibitors of *Yersinia pestis* Type III secretion system YscN ATPase. *PLoS One* **6**:e19716.
53. **Dacheux D, Goure J, Chabert J, Usson Y, Attree I.** 2001. Pore-forming activity of type III system-secreted proteins leads to oncosis of *Pseudomonas aeruginosa*-infected macrophages. *Mol Microbiol* **40**:76-85.
54. **Akeda Y, Galan JE.** 2005. Chaperone release and unfolding of substrates in type III secretion. *Nature* **437**:911-915.
55. **Anthouard R, DiRita VJ.** 2013. Small-molecule inhibitors of toxT expression in *Vibrio cholerae*. *MBio* **4**.
56. **Surawicz CM, Brandt LJ, Binion DG, Ananthakrishnan AN, Curry SR, Gilligan PH, McFarland LV, Mellow M, Zuckerbraun BS.** 2013. Guidelines for diagnosis, treatment, and prevention of *Clostridium difficile* infections. *Am J Gastroenterol* **108**:478-498; quiz 499.

57. **Robinson MD, Oshlack A.** 2010. A scaling normalization method for differential expression analysis of RNA-seq data. *Genome Biol*:R25.
58. **Robinson MD, McCarthy DJ, Smyth GK.** 2010. edgeR: a Bioconductor package for differential expression analysis of digital gene expression data. *Bioinformatics* **26**:139-140.
59. **McCarthy DJ, Chen Y, Smyth GK.** 2012. Differential expression analysis of multifactor RNA-seq experiments with respect to biological variation. *Nucleic Acids Res* **40**:4288-4297.
60. **Robinson MD, Smyth GK.** 2008. Small sample estimation of negative binomial dispersion, with applications to SAGE data. *Biostatistics* **9**:321-332.

CHAPTER 4 – Linking carbonic anhydrase activity and environmental pH sensing through PhoPR

Introduction

The ability for bacteria to sense and respond to signals from the environment is crucial for survival. Microbes are frequently exposed to fluctuations in external or internal pH and if left unaccounted for these changes can lead to impaired survival. As a result, a variety of homeostatic maintenance systems have evolved to sense and respond to acidic or alkali pH challenges. A wide-range of approaches to maintain pH homeostasis exist, ranging from constitutive expression of counter measure mechanisms to finely tuned inducible systems (1-3). Though the mechanisms are diverse, a common thread is the preservation of the proton motive force (PMF) through modification of the transmembrane pH and electrical gradient.

As an intracellular pathogen, Mtb is exposed to a variety of environmental stresses including acidic pH within the macrophage phagosome (4). The biochemical mechanism of how Mtb detects acidification of the external environment remains to be definitively shown. However, the work described above is consistent with studies from other groups implicating the two-component regulator PhoPR as a crucial signal transduction system in sensing and responding to acidification of the external milieu (5-9). Inhibition of the core PhoPR regulon by ethoxzolamide, a known carbonic anhydrase inhibitor, provides evidence supporting that carbon dioxide (CO₂) may play a role in signaling a decrease in environmental pH.

Carbon dioxide levels play key regulatory roles across all of life. CO₂ is produced by the citric acid cycle during aerobic respiration. In mammals, altered levels of tissue CO₂ due to disrupted homeostatic mechanisms can cause systemic acidosis or alkalosis, potentially leading to death. Fungal and bacterial systems often use carbon dioxide levels to modulate virulence

gene expression. Regulation of a pathogen's virulence suite is necessary from a metabolic perspective, but also from an environmental perspective as well. For example, *Vibrio cholerae* exists in a motile, non-pathogenic state within the aquatic environment. However, upon exposure to high levels of CO₂ within a mammalian host, *V. cholerae* will induce its virulence cascade, begin to aggregate and produce cholera toxin. Specifically, it was shown that it was a carbonic anhydrase dependent mechanism as introduction of ethoxzolamide could ameliorate the induction of CO₂ dependent virulence (10, 11). Several examples of bacterial sensing carbon dioxide as a proxy for alterations in pH through carbonic anhydrase dependent mechanisms have been characterized (1, 2).

Carbonic anhydrases (CAs) are zinc-containing metalloenzymes that catalyze the interconversion between CO₂ and water to bicarbonate and a proton. Though this reversible reaction can occur spontaneously, CA enzymes can catalyze the reaction near the rate of substrate diffusion. CAs are implicated in diffusing pH gradients to maintain pH homeostasis and as a mechanism to retain bicarbonate/CO₂ inside the cell for metabolism. Mtb possesses three carbonic anhydrases: Rv1284 (*canA*), Rv3273, and Rv3588c (*canB*). With three copies of CA, two of which are required for virulence *in vivo*, it suggests these enzymes provide a necessary function during pathogenesis (12). Within the phagosome, Mtb is exposed to decreasing pH via the proton pumping vacuolar ATPase, necessitating a mechanism to initiate production of factors to arrest phagosome maturation and maintain the PMF to persist within this hostile environment. The following preliminary data provides a foundation for future work to define the biochemical mechanism linking carbonic anhydrase and PhoPR as a system for sensing and responding to acidic pH through changes in CO₂.

Materials and methods

Bacterial strains and growth conditions

Mtb experiments, unless otherwise stated, were performed with Mtb strain CDC1551. The CDC1551(*aprA*'::GFP) fluorescent reporter strain was generated by fusing the promoter region of *aprA* (*mcr7*, Rv2395a) upstream of GFP in the pSE100 replicating plasmid and transforming the plasmid into CDC1551 (8). The *ΔphoPR* mutant and its complemented strain have been previously described (7, 8). Cultures were maintained in standing tissue culture flasks in 7H9 Middlebrook medium supplemented with 10% oleic acid, albumin, dextrose, catalase (OADC) and 0.05% Tween-80 and incubated at 37°C with 5% CO₂ unless indicated otherwise.

Carbon dioxide modulation of PhoPR-dependent fluorescent reporter expression

Mtb CDC1551(*aprA*'::GFP) was grown in Middlebrook 7H9 medium, buffered at pH 7.0 with 100 mM MOPS, to mid- to late-log phase. The cultures were then pelleted, re-suspended in 7H9 buffered at either pH 7.0 or pH 5.7 (100 mM MES as the buffer for pH 7H9 pH 5.7) and dispensed into T-25 flasks, seeded at an initial OD of 0.2 in 8 mL of broth. Four conditions were examined at either 5% or ambient CO₂: 1) DMSO pH 7.0, 2) 40 μM ETZ pH 7.0, 3) DMSO pH 5.7, and 4) 40 μM ETZ pH 5.7. Cultures were incubated for three and six days and transferred to a 96-well assay plate. Samples were analyzed for fluorescence using a Perkin Elmer EnSpire plate reader. Growth was measured by removing a 1 mL aliquot from each culture and analyzed using a spectrophotometer. CDC1551(*aprA*'::GFP) reporter fluorescence was normalized per bacteria by taking the ratio of fluorescence and optical density.

“Knockout” ethoxzolamide analog experiment for off target effects

Synthesis of N-methyl-ethoxzolamide was performed by Dr. Marc Iles of Temple University. Mtb CDC1551(*aprA*'::GFP) was grown in Middlebrook 7H9 medium, buffered at pH 7.0 with 100 mM MOPS, to mid- to late-log phase. The cultures were then pelleted, re-suspended in 7H9 buffered at either pH 7.0 or pH 5.7 (100 mM MES as the buffer for pH 7H9 pH 5.7) and dispensed into 96-well assay plates, seeded at an initial OD of 0.2. EC₅₀ analysis was performed as previously described (13). Briefly, N-methyl-ethoxzolamide and ethoxzolamide were added to Mtb CDC1551(*aprA*'::GFP) cultures in 2.5-fold dilutions ranging from 80-0.13 μ M. Cultures were incubated for six days and analyzed for fluorescence and optical density on Perkin Elmer EnSpire plate reader. Fluorescence and growth inhibition were normalized based on rifampicin (100%) and DMSO (0%) controls. EC₅₀ values were calculated based on a variable slope, four-parameter non-linear least squares regression model in the GraphPad Prism software package (ver. 6).

Carbonic anhydrase overexpression

Mtb CDC1551 carbonic anhydrases (*Rv1284*, *Rv3273*, *Rv3588c*) were PCR amplified using Phusion (Thermo Scientific) polymerase. Amplification products were gel extracted (Qiagen) and cloned into a Topo vector (pCR IV-TOPO Zero Blunt, Thermo Scientific). Topo vectors containing the carbonic anhydrase insert were transformed into *E. coli* (One-Shot TOP10, Thermo Scientific) and selected using kanamycin (25 μ g/mL) on LB agar overnight at 37 °C. Resistant clones were picked and grown in LB broth containing kanamycin (25 μ g/mL) shaking at 200 RPM, overnight at 37 °C. Topo vectors containing the desired Mtb carbonic anhydrase insert were extracted using a mini-prep kit (Qiagen). Inserts were sequence confirmed using M13

forward (-20) and reverse primers (Thermo Scientific). Sequence confirmed inserts were digested using *NdeI* and *HinDIII* (NEB), gel extracted (Qiagen), and ligated (T4 DNA ligase; NEB) into the replicating plasmid pVV16 (hsp60 constitutive promoter) that had been previously digested with the same two enzymes and dephosphorylated with calf intestinal phosphatase (NEB). Ligation reactions were transformed into *E. coli* (One-Shot TOP10, Thermo Scientific) and selected on LB agar containing hygromycin (100 µg/mL) overnight at 37 °C. Resistant clones were picked and grown in LB broth containing kanamycin (25 µg/mL) shaking at 200 RPM, overnight at 37 °C. pVV16 vectors containing the desired Mtb CA insert were extracted using a mini-prep kit (Qiagen). Completed overexpression constructs were electroporated into Mtb CDC1551. Transformants were selected on 7H10 agar containing OADC and hygromycin (50 µg/mL). Resistant clones were picked and grown in 7H9 supplemented with OADC and hygromycin (50 µg/mL). Transcription levels of *Rv3588c* overexpression in Mtb CDC1551 were measured using semi-quantitative real-time PCR. The increased relative transcription was determined to be >30-fold higher at both pH 7.0 and 5.7 compared to the empty vector control in Mtb CDC1551 after six days incubation. Mtb CDC1551 cultures either overexpressing Mtb CA or the empty vector control were grown to mid- to late-log phase in 7H9 Middlebrook broth supplemented with OADC and hygromycin (50 µg/mL). Cultures were pelleted and re-suspended in either pH 7.0 or 5.7 buffered 7H9 + OADC containing hygromycin (50 µg/mL) and seeded at an initial OD of 0.2. Cultures were exposed to two treatments at pH 7.0 and 5.7: 1) DMSO or 2) 40 µM ethoxzolamide. Following six days incubation, total bacterial RNA was extracted as previously described (9). Bacterial growth was assessed by removing a 1 mL aliquot prior to RNA processing and optical density was measured using a spectrophotometer. Semi-

quantitative real-time PCR was performed as previously described to assess *aprA*, *pks2*, and *phoP* transcript abundance (8).

Site directed mutagenesis of PhoR conserved histidine residues

Mutagenesis studies of Mtb CDC1551 *phoR* used the complementation construct previously described on the integrative vector pMV306 (7). Site-directed mutagenesis was performed using the QuikChange™ kit protocol (Agilent) with minor modifications for the extension time to amplify pMV306. Mutations were sequence confirmed prior to transformation into Mtb CDC1551 Δ *phoPR* background. Transformants were selected on 7H10 agar supplemented with OADC and kanamycin (25 µg/mL). Clones were picked and grown in 7H9 broth supplemented with OADC and kanamycin (25 µg/mL). The following strains were grown to mid- to late-log in 8 mL of 7H9 + OADC: Δ *phoPR*, Δ *phoPR* complemented with wild-type copy of *phoPR*, Δ *phoPR* complemented with the following individual *phoR* substitutions: His40Ala, His72Pro, His114Val, or His114Asp. Cultures were pelleted, re-suspended in either pH 7.0 or 5.7 buffered 7H9 + OADC and seeded in 8 mL at an OD of 0.2. Following six days incubation, total bacterial RNA was extracted as previously described (9). Semi-quantitative real-time PCR was performed as previously described to assess *aprA*, *pks2*, and *phoP* transcript abundance and compared relative to the wild-type copy of *phoPR* (8).

Results

Expression of the PhoPR regulon is modulated by changes in carbon dioxide concentrations

The discovery of the carbonic anhydrase inhibitor ethoxzolamide as an antagonist of PhoPR mediated signaling prompted additional experiments to define the role Mtb carbonic

anhydrase activity plays in pH sensing. At neutral pH, the inorganic carbon equilibrium favors bicarbonate to dissolve in water. However, as pH decreases, equilibrium shifts towards increasing levels of dissolved carbon dioxide (Figure 4.1.). Notably, the pH at which carbon dioxide is favored to dissolve in water is ~6.3, similar to the pH at which PhoPR regulated genes are induced and is similar to the pH of a resting macrophage phagosome (9, 14). Based on the proposed model (Figure 3.7.), we hypothesized that under ambient concentrations of carbon dioxide, PhoPR regulated genes will not be strongly induced due to the reduced concentrations of dissolved carbon dioxide that can be converted to bicarbonate and a proton by carbonic anhydrase. To investigate whether PhoPR regulated genes were responsive to alterations in carbon dioxide concentrations, the CDC1551(*aprA*'::GFP) fluorescent reporter strain was inoculated into buffered rich medium (Middlebrook 7H9 + OADC) at pH 7.0 and 5.7, and grown in the presence of high (5%) or low (ambient) levels of carbon dioxide. Each flask was treated with either 40 μ M ETZ or an equivalent volume of DMSO. After 6 days incubation, PhoPR-regulated GFP fluorescence normalized to optical density (OD) was 1.5-fold lower in ambient CO₂ relative to high CO₂ conditions at acidic pH (Figure 4.2.). ETZ treatment reduced fluorescence per bacteria to that of DMSO treated cultures at pH 7.0 and 5.7. There is a statistically significant difference between carbon dioxide levels in DMSO treated bacteria at pH 7.0, the difference is small (0.75-fold) and each condition has comparable levels of basal GFP expression. ETZ treatment of cultures at neutral pH further reduced GFP fluorescence relative to DMSO treated cultures. These data suggest that carbon dioxide concentrations modulate PhoPR-regulated gene expression at neutral and acidic pH in a carbonic anhydrase-dependent manner.

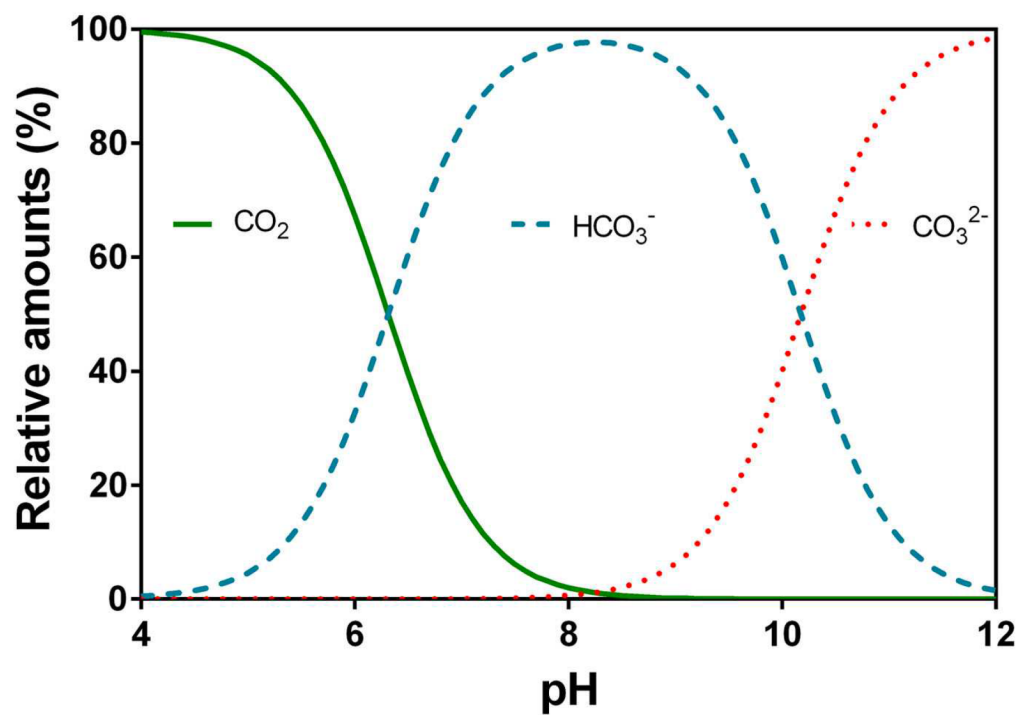


Figure 4.1. Relative concentration of carbon dioxide (CO₂), bicarbonate (HCO₃⁻), and carbonate (CO₃²⁻) as a function of pH in aqueous solution. The relative species of inorganic carbon equilibrium as a function of pH. Figure and data were derived from (15).

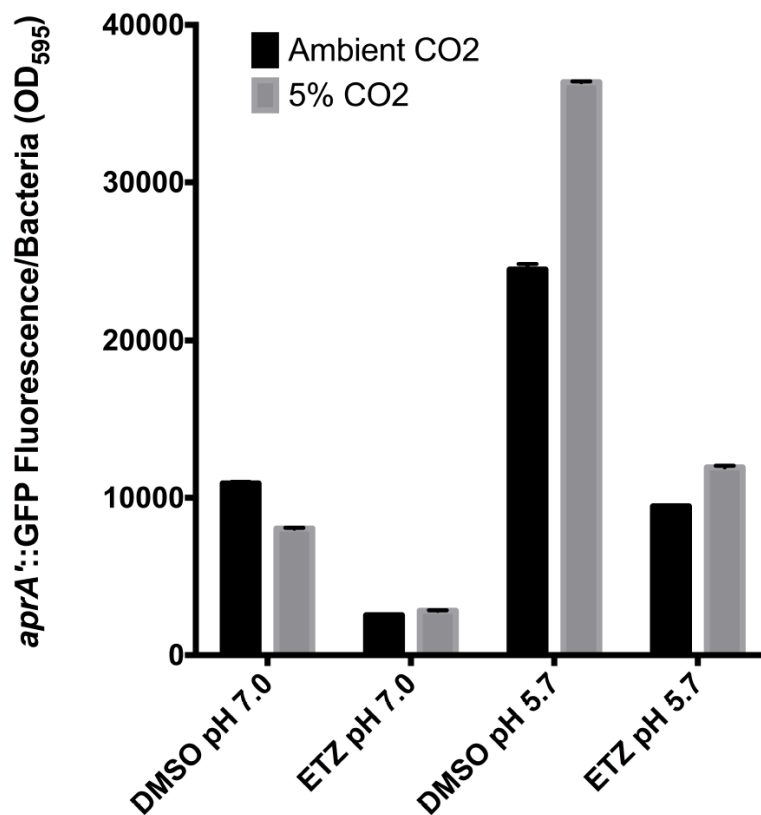


Figure 4.2. PhoPR-regulated gene expression is modulated in response to alterations in environmental carbon dioxide levels. The CDC1551(*aprA'::GFP*) fluorescent reporter was incubated for six days in buffered 7H9 adjusted to either pH 7.0 or pH 5.7 under high (5%) or low (ambient) carbon dioxide levels. PhoPR regulated reporter fluorescence per bacterium is responsive to changes in environmental carbon dioxide. Fluorescence and optical density were quantified with three technical replicates and data shown are representative of two biological replicates. All differences are statistically significant (t-test, $p < 0.05$) except for ETZ treatment at pH 7.0.

Carbonic anhydrase inhibition deficient analog of ETZ does not affect PhoPR-mediated gene expression

The structurally related carbonic anhydrase inhibitor acetazolamide is often preferentially given over ethoxzolamide to treat altitude sickness due to reduced side effects from the drug. However, previous work has shown that the traditional understanding of inhibiting CA activity by acetazolamide is not the dominant mechanism that leads to alleviation of altitude sickness (16). This result was achieved by structurally modifying the sulfonamide moiety of the molecule, which is required for binding in the active site of carbonic anhydrase for acetazolamide and any of the derived CA inhibitors, including ethoxzolamide. By converting the sulfonamide to a methyl-sulfonyl group, CA inhibitory activity is lost. To test whether additional targets beyond carbonic anhydrase are involved in the inhibitory effects of ethoxzolamide on the PhoPR regulon, a methyl-sulfonyl moiety-containing analog of ETZ (N-methyl-ETZ) was synthesized by a collaborator, Dr. Marc Iles (Figure 4.3.). The CDC1551(*aprA*'::GFP) fluorescent reporter was grown to mid- to late-log phase at neutral pH in buffered rich medium (Middlebrook 7H9 + OADC). Cultures were re-suspended at an OD₆₀₀ of 0.2 in buffered rich medium at pH 5.7 and incubated for 6 days in the presence of ETZ, N-methyl-ETZ, or an equivalent volume of DMSO. ETZ inhibits PhoPR-mediated GFP fluorescence in a dose dependent manner, while N-methyl-ETZ exhibits little inhibition across all concentrations tested (Figure 4.3.). These data suggest that inhibition of Mtb carbonic anhydrase is likely the dominant mechanism leading to inhibition of the core PhoPR regulon. However, we cannot rule out that an alternative enzyme with a similar active site is targeted by the intact molecule.

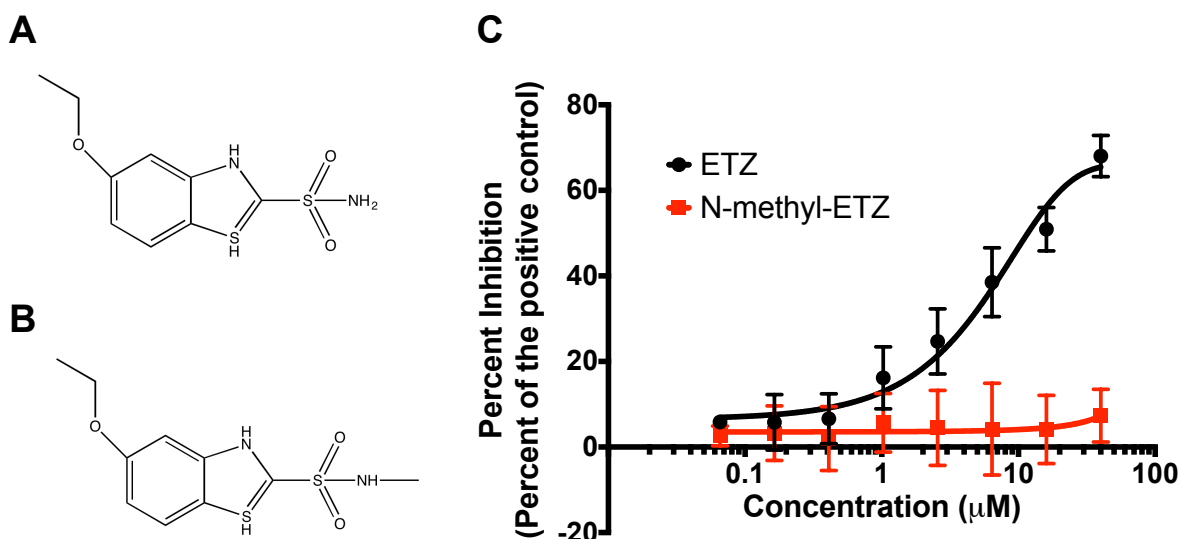


Figure 4.3. “Knockout” analog of ETZ (N-methyl-ETZ) does not inhibit PhoPR-regulated reporter fluorescence. N-methyl-ETZ does not inhibit carbonic anhydrase activity, allowing the ability to probe for additional targets independent of carbonic anhydrase inhibition. A) Chemical structure of ethoxzolamide (ETZ) B) Chemical structure of N-methylethoxzolamide (N-methyl-ETZ). C) N-methyl-ETZ does not affect Mtb CDC1551(*aprA*’::GFP) reporter fluorescence after six days incubation at pH 5.7. Data are representative of two biological replicates.

Overexpression of Mtb carbonic anhydrase enzymes leads to additive inhibitory effects in combination with ETZ

The *Mycobacterium tuberculosis* genome encodes three carbonic anhydrase enzymes: *Rv1284*, *Rv3273*, and *Rv3588c*. All three enzymes have been shown to exhibit carbonic anhydrase activity. Further, *Rv1284* and *Rv3588c* are required for Mtb survival in a murine model of infection and are predicted to be extracytoplasmic (12). We hypothesized that if CA is the dominant target of ETZ, overexpression of each of the Mtb carbonic anhydrase enzymes would ameliorate the effects of ETZ inhibiting the PhoPR regulon. Each Mtb CA coding sequence was cloned into the replicating overexpression plasmid pVV16 under the constitutive hsp60 promoter and transformed into Mtb CDC1551. Mtb CA overexpression strains and an empty vector (EV) containing strain were cultured for 6 days in buffered rich medium at pH 7.0 and 5.7. Cultures were treated with either 40 μ M ETZ or an equivalent volume of DMSO. Gene expression responses to each of the treatments per strain were quantified using semi-quantitative real-time PCR relative to the DMSO treated EV control. ETZ treatment of the EV control exhibited reduced transcript abundance of *aprA* and *pks2* approximately 7- and 13-fold, respectively (Figure 4.4.). Surprisingly, ETZ treatment of Mtb overexpressing each CA enzyme led to enhanced inhibition of *aprA* and *pks2* expression (at least 3-fold and 10-fold, respectively relative to the DMSO control) (Figure 4.4.). This result was puzzling and counter to the proposed hypothesis of ameliorating the effects of ETZ treatment.

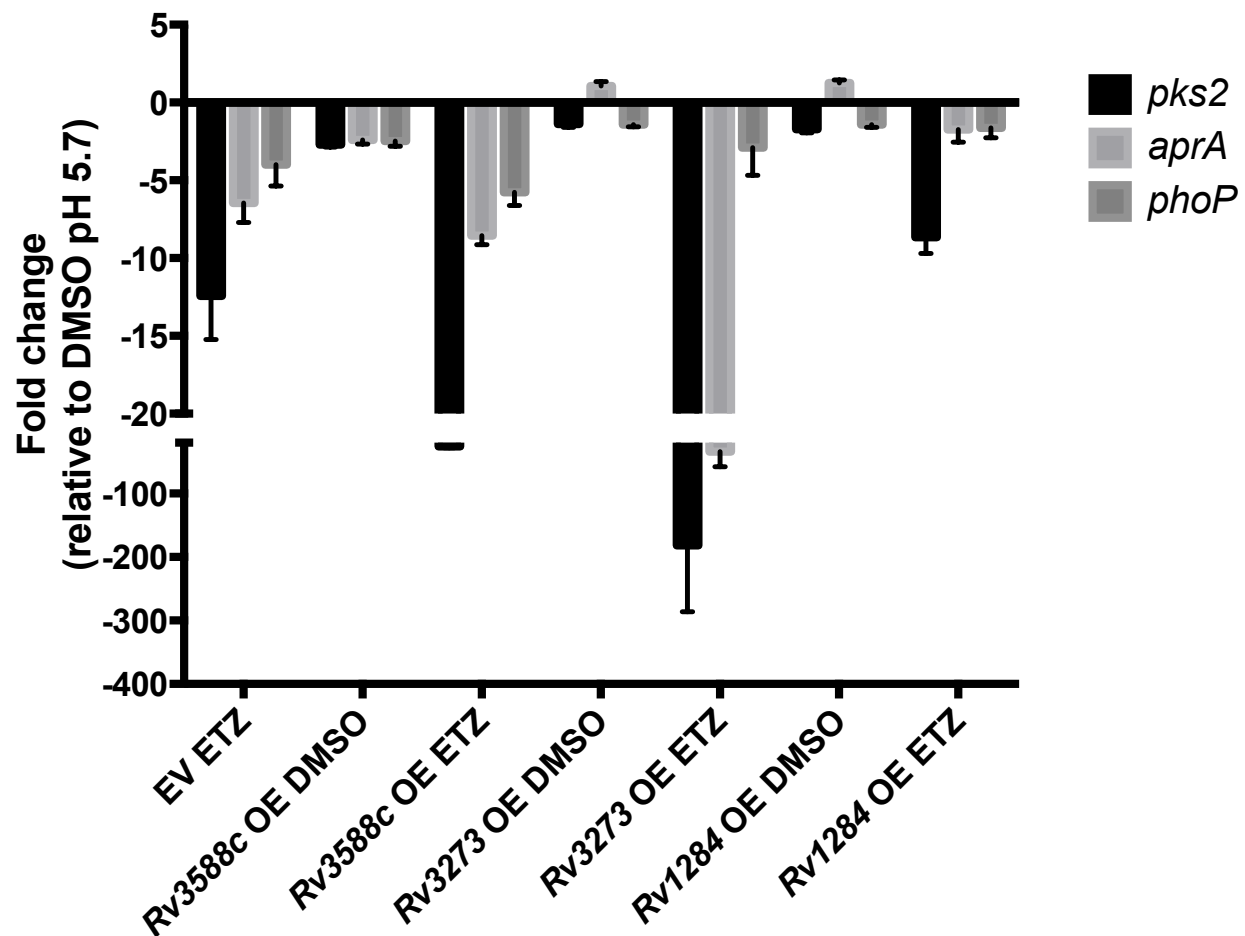


Figure 4.4. Mtb carbonic anhydrase overexpression in combination with ETZ treatment leads to enhanced inhibition of PhoPR regulated gene expression. Overexpression of all three Mtb carbonic anhydrases (*Rv3588c*, *Rv3273*, *Rv1284*) in Mtb CDC1551 wild-type leads to enhanced or comparable inhibition of PhoPR-regulated gene expression. qRT-PCR comparing *pks2*, *aprA*, and *phoP* gene expression in the empty vector (EV) and overexpression (OE) Mtb CDC1551 strains after six days incubation at pH 5.7. Error bars represent the standard deviation of three technical replicates.

Conserved histidine residues in the PhoR sensing loop suggest a putative mechanism of sensing proton concentrations

The Mtb PhoR homolog PhoQ in *Salmonella* Typhimurium has been shown to directly respond to increased proton concentrations leading to an activating conformational change mediated by protonation of a conserved histidine residue (17). Performing a multiple alignment of the PhoR sensing loop domain across *Mycobacteria* sp. reveals a series of three conserved histidine residues (Figure 4.5.). Notably, within the slow growing, pathogenic *Mycobacterium* spp. (Mtb complex), two residues (His72 and His114) are conserved, suggesting putative functional conservation for mammalian pathogenesis as these amino acids are substituted to introduce either structural differences or alterations in charge within the environmental *Mycobacteria* sp. The pKa at which histidine residues are predicted to be protonated is approximately pH 6.2-6.5 (18). Previous transcriptional studies have observed induction of the PhoPR regulon in a similar pH range, suggesting a potential role of histidine protonation directly sensing environmental changes in proton concentrations similar to the *Salmonella* Typhimurium PhoQ (9). To investigate this hypothesis, we conducted site-directed mutagenesis studies to test putative pH responsive histidine residues. The histidine located at the amino acid position 72 was substituted to proline (His72Pro) and the histidine residue at position 114 was substituted to either valine (His114Val) or aspartic acid (His114Asp). The completely conserved histidine (His40) was substituted to alanine (His40Ala) as there was no alternative residue suggested based on the multiple alignment. Site-directed mutant constructs were transformed into the *M. tuberculosis* CDC1551 Δ phoPR background. Cultures were incubated for 6 days under either neutral (pH 7.0) or acidic (pH 5.7) conditions in rich medium. The ability for each construct to effectively complement the mutant was assessed by semi-quantitative real-time PCR.

Specifically, *aprA* transcript abundance was quantified relative to *M. tuberculosis* CDC1551 Δ *phoPR* complemented with a wild-type copy of *phoPR*. Substitution of His40 to alanine resulted in at least a 3-fold down regulation of *aprA* at both neutral and acidic pH, suggesting that this residue is required for full function of the protein (Figure 4.6.). Changes at His114 resulted in modest upregulation of *aprA* expression relative to the empty vector control (Figure 4.6.). The only residue exhibiting pH-dependent alterations in *aprA* expression relative to the control was the His72Pro mutation (~3.5-fold reduction) (Figure 4.6.). Taken together, the pH-dependence and reduction in *aprA* expression in the His72Pro strain suggests that this residue may be playing a role in PhoR sensing of environmental pH. However, due to the incomplete inhibition of *aprA*, it is possible that additional residues are required for sensing pH.

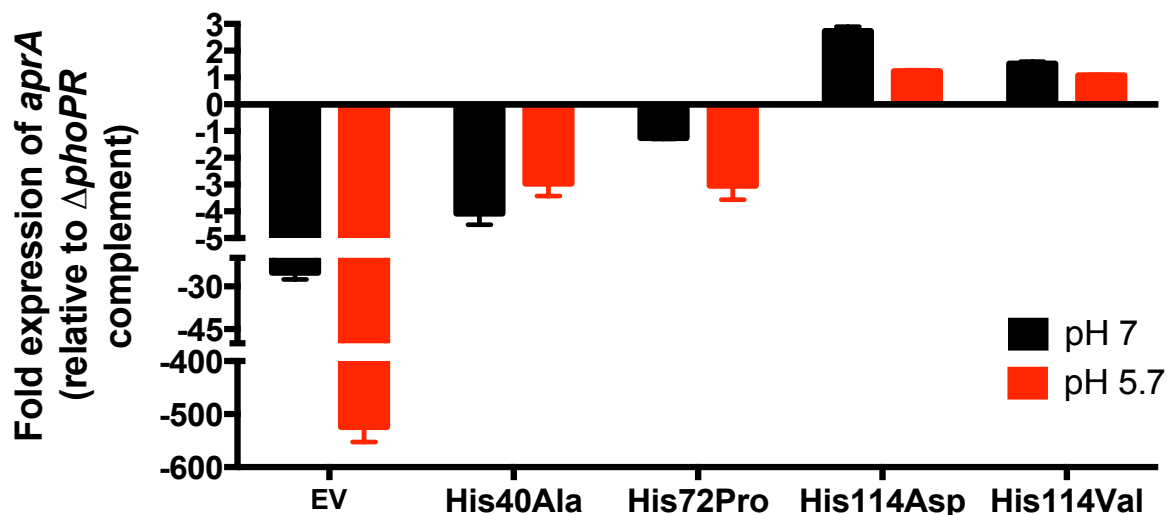


Figure 4.6. PhoR His72Pro substitution leads to reduced *aprA* expression at acidic pH. Site-directed mutagenesis of conserved histidine residues in the PhoR sensing loop reveal His72 as a potential residue required for pH sensing and induction of PhoPR regulated gene expression. qRT-PCR comparing *aprA* expression at pH 7.0 and 5.7 of CDC1551 Δ *phoPR* empty vector (EV) and His substitutions after six days incubation relative to the Δ *phoPR* complemented strain. Error bars represent the standard deviation of three technical replicates.

Discussion

The discovery of ethoxzolamide as an antagonist of PhoPR-mediated, pH-driven adaptation suggests that Mtb carbonic anhydrase activity is both essential for pathogenesis and likely acts upstream of the two-component system. Previous work has implicated *Rv1284* and *Rv3588c* as essential for Mtb growth in an *in vivo* murine model of infection (12). Further, it has been noted that *Rv1284* is significantly upregulated (~14-fold) after 96 hours of starvation, suggesting that enzymatic activity is required during the persistent stage of infection (19). Taken together, ETZ has provided the field a chemical probe to investigate a previously unrecognized link between sensing changes in environmental pH and CO₂, carbonic anhydrase activity, pH-adaptation, and PhoPR-regulated gene expression during pathogenesis.

Bacterial and fungal pathogens have developed sensitive mechanisms to detect and respond to changes in pH and carbon dioxide. This is particularly important for pathogens that possess both environmental and multicellular hosts as reservoirs. The ability to distinguish between both environments is likely to be essential to increase persistence. Once the pathogen is within the host, further dissection of the local niche may be necessary to determine whether the environment is appropriate to initiate virulence factor production based on carbon dioxide levels (e.g. nasopharynx, intestinal tract, lungs, etc.). Carbonic anhydrase-mediated mechanisms of identifying and responding to changes in environmental CO₂ levels as well as changes in pH have been characterized in a variety of bacterial pathogens, including *V. cholerae* and *H. pylori* (10, 20). During pathogenesis, Mtb likely experiences a variety of carbon dioxide concentrations based on its site of infection (e.g. extracellular, within the phagosome, circulating in the blood, etc.). Based on our model and the inorganic carbon equilibrium favoring CO₂ as pH decreases, we observed that PhoPR-regulated genes are more strongly induced at acidic pH under high (5%)

CO₂ conditions relative to ambient levels of carbon dioxide. These data suggest that carbonic anhydrase activity may function to modulate local pH and promote an acidified periplasm during acid stress at high CO₂. An additional method that could be used to identify changes in periplasmic pH is through a TAT-secreted pH-sensitive GFP. Mtb possesses the required machinery for TAT secretion and is a viable approach to secrete a fully folded protein into the periplasm. A potential drawback from this approach may be the requirement of a confocal microscope within the BSL-3 laboratory as the signal may be too diffuse for a plate reader based assay.

Prior work in *Salmonellae* have identified that the two-component system PhoPQ can directly sense and respond to changes in proton concentrations through a conserved histidine residue in the periplasm exposed sensor loop (17). The conservation of three histidine residues within the slow-growing pathogenic *Mycobacterium sp.* PhoR sensor loop suggests a possible function similar to *Salmonellae* in sensing changes in local proton concentrations. Mutation of His72 to proline yielded a minor reduction of *aprA* expression in a pH-dependent manner, while other histidine mutations did not specifically affect transcript abundance at acid pH. It is tempting to speculate that Mtb may have evolved multiple residues that require protonation to induce an activating conformation of PhoR. Thus, additional mutations of His114 in combination with His72 may be necessary to inhibit Mtb's ability to respond to acidic pH. It is also possible that PhoPR responds to a variety of signals similar to PhoPQ in *Salmonellae*. Indeed, recent work from our group and others have shown that PhoPR functions to slow Mtb growth and maintain redox homeostasis at acidic pH and that the two-component system responds to changes in environmental chloride concentrations (6-8). Additionally, it has been postulated that PhoPR responds to divalent cations, such as magnesium (5). Ultimately, to identify whether

PhoPR directly senses and responds to changes in pH, whether through protonation of conserved histidine residues or an alternative mechanism requires additional studies. Specifically, reconstituting PhoR in vesicles whose interior has a lower pH than the exterior, we may be able to identify whether autophosphorylation activity is increased in direct response to low pH, indicating that activation of the kinase is a result of acidic pH. We may further probe the necessity of specific residues required for pH sensing through site-directed mutagenesis studies in the PhoR sensing loop. Another method to identify whether PhoR adopts an activating conformation in response to acidic pH is through NMR spectroscopy at neutral and low pH. These experiments do not exclude additional signals acting on PhoPR during pathogenesis, but would provide a definitive signal to which the two-component system senses and responds.

Ethoxzolamide is a potent inhibitor of Mtb carbonic anhydrase activity in whole cells and purified recombinant enzymes. Despite this evidence, it is necessary to identify whether the observed phenotypes associated with ETZ inhibition of PhoPR-regulated gene expression is a result of carbonic anhydrase inhibition. The RNA-seq transcriptional profiling of ETZ treated cultures at acidic pH did not reveal a clear set of additional targets to investigate. Further, carbonic anhydrase transcripts were not significantly elevated in response to ETZ treatment relative to DMSO at pH 5.7. To address potential off-target effects, I utilized the carbonic anhydrase inhibition deficient analog of ETZ (N-methyl-ETZ). Indeed, N-methyl-ETZ was unable to modulate PhoPR-dependent, acidic pH inducible GFP fluorescence in the CDC1551(*aprA*'::GFP) reporter strain of Mtb. These data suggest that PhoPR regulon inhibition by ETZ treatment is a result of carbonic anhydrase inhibition. To further probe this hypothesis, I overexpressed each carbonic anhydrase in Mtb. Surprisingly, I found that overexpression led to either enhanced or comparable inhibitory effects of PhoPR-regulated gene expression when

treated in combination with ETZ relative to the treated empty vector control. This was contrary to the expected result of reducing the inhibitory effects of ETZ by increasing the total amount of carbonic anhydrase present in the cell. These phenotypes may be a result of a variety of factors, including inappropriate enzymatic localization and limiting cofactor availability. *Rv1284* and *Rv3588c* are predicted to be extracytoplasmic and *Rv3273* is predicted to be membrane bound both by computational prediction based on amino acid content and experimentally by mass spectrometry of Mtb fractions (21). Further, transcriptional profiling by our group and others observed that CA expression remains low at both neutral and acidic pH. Overexpression of non-cytoplasmic enzymes and not the subsequent export machinery could lead to accumulation of active enzymatic activity normally not occurring within the cytoplasm. Consequently, when ETZ is introduced, a large proportion of inactive enzyme is present within the cytoplasm, perhaps acting in a fashion similar to a dominant negative protein in concert with ETZ inhibition. Another possibility includes that CA enzymes require zinc (Zn) as a cofactor for activity. The rich medium 7H9 contains approximately 6.5 μM Zn and may be a limiting factor in the overexpression Mtb strains, leading to non-functional protein acting as a dominant negative to active enzymes. Thus, addition of exogenous Zn may lead to rescue of enzymatic activity. In contrast, if the CA enzymes are unable to incorporate Zn as it is a limiting factor, may be due in part to Zn or other cation transporters not able to transport sufficient intracellular levels of the essential cofactor for CA. As a result, addition of exogenous Zn may be ineffective and potentially lead to confounding effects of Zn toxicity if it is supplemented at high concentrations. Though *Rv1284* and *Rv3588c* have been identified using mass spectrometry in extracytoplasmic regions and membrane fractions of Mtb, additional studies have also suggested the possible export of *Rv1284* and alternative locales for *Rv3588c*. Thus, more precise localization of Mtb

carbonic anhydrase is required to refine models of PhoPR regulon inhibition and perhaps provide evidence for the observed enhanced effects of overexpressing the enzymes. Ultimately, deletions of each carbonic anhydrase in Mtb are required to identify its requirement for induction of PhoPR-regulated gene expression at acidic pH. However, due to the redundancy of enzymatic function, it may be necessary to make double mutant or delete all three genes to provide the desired phenotype mimicking that of a PhoPR mutant. Alternative approaches include titratable overexpression of each enzyme to potentially account for not also overexpressing export machinery. Further, it may be possible to express anti-sense transcripts to “knock down” each carbonic anhydrase. Another approach may be to identify bicarbonate transporter deficient strains or small molecule inhibitors that prevent acidification of the periplasm. However, these strains may have pleiotropic effects as inhibiting such a transporter may also disrupt pH and anion homeostasis. Taken together, additional experiments are needed to define the link between PhoPR sensing/responding to acidic pH and carbonic anhydrase in Mtb.

Chemical probes are useful tools to illuminate new bacterial physiology. Ethoxzolamide is an example of this and has identified a previously unrecognized link between carbonic anhydrase and the virulence associated two-component system PhoPR. Though the biochemical mechanism remains to be determined, the above work provides a foundation to explore the consequences of impairing Mtb’s ability to sense and respond to CO₂/acidic pH. Additionally, ETZ may be repurposed to function as an adjunct therapy in the clinic to treat Mtb due to its historical uses and approval for human use.

REFERENCES

REFERENCES

1. **Krulwich TA, Sachs G, Padan E.** 2011. Molecular aspects of bacterial pH sensing and homeostasis. *Nat Rev Microbiol* **9**:330-343.
2. **Cummins EP, Selfridge AC, Sporn PH, Sznajder JI, Taylor CT.** 2014. Carbon dioxide-sensing in organisms and its implications for human disease. *Cell Mol Life Sci* **71**:831-845.
3. **Tresguerres M, Buck J, Levin LR.** 2010. Physiological carbon dioxide, bicarbonate, and pH sensing. *Pflugers Arch* **460**:953-964.
4. **Vandal OH, Nathan CF, Ehrt S.** 2009. Acid Resistance in *Mycobacterium tuberculosis*. *Journal of Bacteriology* **191**:4714-4721.
5. **Walters SB, Dubnau E, Kolesnikova I, Laval F, Daffe M, Smith I.** 2006. The *Mycobacterium tuberculosis* PhoPR two-component system regulates genes essential for virulence and complex lipid biosynthesis. *Molecular Microbiology* **60**:312-330.
6. **Baker JJ, Johnson BK, Abramovitch RB.** 2014. Slow growth of *Mycobacterium tuberculosis* at acidic pH is regulated by phoPR and host-associated carbon sources. *Mol Microbiol* **94**:56-59.
7. **Tan S, Sukumar N, Abramovitch RB, Parish T, Russell DG.** 2013. *Mycobacterium tuberculosis* Responds to Chloride and pH as Synergistic Cues to the Immune Status of its Host Cell. *PLoS Pathog* **9**:e1003282.
8. **Abramovitch RB, Rohde KH, Hsu FF, Russell DG.** 2011. *aprABC*: a *Mycobacterium tuberculosis* complex-specific locus that modulates pH-driven adaptation to the macrophage phagosome. *Mol Microbiol* **80**:678-694.
9. **Rohde KH, Abramovitch RB, Russell DG.** 2007. *Mycobacterium tuberculosis* invasion of macrophages: linking bacterial gene expression to environmental cues. *Cell Host Microbe* **2**:352-364.
10. **Abuaita BH, Withey JH.** 2009. Bicarbonate Induces *Vibrio cholerae* virulence gene expression by enhancing ToxT activity. *Infect Immun* **77**:4111-4120.
11. **Shimamura T, Watanabe S, Sasaki S.** 1985. Enhancement of enterotoxin production by carbon dioxide in *Vibrio cholerae*. *Infect Immun* **49**:455-456.

12. **Sassetti CM, Rubin EJ.** 2003. Genetic requirements for mycobacterial survival during infection. *Proc Natl Acad Sci U S A* **100**:12989-12994.
13. **Johnson BK, Colvin CJ, Needle DB, Mba Medie F, Champion PA, Abramovitch RB.** 2015. The Carbonic Anhydrase Inhibitor Ethoxzolamide Inhibits the Mycobacterium tuberculosis PhoPR Regulon and Esx-1 Secretion and Attenuates Virulence. *Antimicrob Agents Chemother* **59**:4436-4445.
14. **Rohde K, Yates RM, Purdy GE, Russell DG.** 2007. *Mycobacterium tuberculosis* and the environment within the phagosome. *Immunol Rev* **219**:37-54.
15. **Pedersen O, Colmer TD, Sand-Jensen K.** 2013. Underwater photosynthesis of submerged plants - recent advances and methods. *Front Plant Sci* **4**:140.
16. **Teppema LJ, Swenson ER.** 2015. The noncarbonic anhydrase inhibiting acetazolamide analog N-methylacetazolamide reduces the hypercapnic, but not hypoxic, ventilatory response. *Physiol Rep* **3**.
17. **Prost LR, Daley ME, Le Sage V, Bader MW, Le Moual H, Klevit RE, Miller SI.** 2007. Activation of the bacterial sensor kinase PhoQ by acidic pH. *Mol Cell* **26**:165-174.
18. **Liao SM, Du QS, Meng JZ, Pang ZW, Huang RB.** 2013. The multiple roles of histidine in protein interactions. *Chem Cent J* **7**:44.
19. **Betts JC, Lukey PT, Robb LC, McAdam RA, Duncan K.** 2002. Evaluation of a nutrient starvation model of Mycobacterium tuberculosis persistence by gene and protein expression profiling. *Mol Microbiol* **43**:717-731.
20. **Marcus EA, Moshfegh AP, Sachs G, Scott DR.** 2005. The periplasmic alpha-carbonic anhydrase activity of Helicobacter pylori is essential for acid acclimation. *J Bacteriol* **187**:729-738.
21. **Gu S, Chen J, Dobos KM, Bradbury EM, Belisle JT, Chen X.** 2003. Comprehensive proteomic profiling of the membrane constituents of a Mycobacterium tuberculosis strain. *Mol Cell Proteomics* **2**:1284-1296.

CHAPTER 5 – The small molecule PH036 depletes intracellular thiol pools and sensitizes *Mycobacterium tuberculosis* and *Staphylococcus aureus* to killing at acidic pH

This work is in preparation for journal submission. Contributions and authors for the work described below:

Johnson, B.K. [¶], Coulson, G.B. [¶], Colvin, C.J., Fillinger, R., Ortiz, J., Hammer, N.D., Abramovitch, R.B.

[¶] *Both authors contributed equally to this work*

Text for this chapter is original work by Ben K Johnson.

Abstract

Mycobacterium tuberculosis (Mtb) must sense and adapt to host-mediated environmental stresses such as acidic pH and reactive oxygen species (ROS). pH-driven physiological adaptations are required for Mtb virulence and growth in macrophages and *in vivo*. Mtb mutants unable to resist acid and ROS stresses are highly attenuated during pathogenesis. Therefore, isolation of compounds that inhibit acidic pH-driven Mtb physiology may identify new treatments for tuberculosis. Here we report that the acidic pH-dependent compound PH036 depletes intracellular free thiol pools, sensitizing Mtb to killing by acidic pH and potentiates bactericidal activity of isoniazid and oxidizing agents. Additionally, we found that PH036 exhibits a narrow spectrum of activity against non-mycobacteria species, showing activity against *Staphylococcus aureus* but no activity against Gram-negative pathogens. We show that treatment of PH036 promotes a reduced intracellular environment, is bactericidal against Mtb,

induces a thiol-associated stress response, and enhanced accumulation of intracellular ROS. Exogenous addition of low molecular weight thiols can rescue PH036-mediated bacterial killing. We propose that chemically depleting Mtb free thiol pools at acidic pH leads to an attenuated response to oxidative damage, resulting in bacterial killing and may serve as a therapeutic target for treating Mtb.

Introduction

Mycobacterium tuberculosis (Mtb) is the leading cause of death by an infectious disease (1, 2). Mtb is a highly successful human pathogen due to its ability to sense and adapt its physiology in response to host cues (e.g. acidic pH and hypoxia) and enter a state of non-replicating persistence (3-6). Treatment of Mtb is challenging due to the long course of therapy required to clear persistent bacteria. Due to patient non-compliance and the spread of antibiotic resistant Mtb, new treatments and targets are required to combat Mtb infections. Therefore, compounds that inhibit targets of Mtb persistence could shorten the course of therapy.

Mtb uses environmental pH to modulate its physiology and these pH-dependent adaptations are essential for pathogenesis (7). In a resting macrophage, Mtb is capable of inhibiting phagosome maturation and lysosomal fusion (8-14). Exclusion of the vacuolar ATPase results in a mildly acidic environment (pH 6.1-6.4) (15, 16). However, upon IFN- γ activation, the macrophage phagosome acidifies to pH 4.5-5.7 (16-18). Additionally, Mtb encounters acidified environments during the persistent state of infection within intact granulomas and also in caseating necrotic granulomas (19). Mtb mutants unable to resist acid stress are highly attenuated for growth in macrophages and *in vivo* (20, 21). Further evidence supporting that Mtb encounters acidic pH during infection is the front-line anti-tuberculosis drug pyrazinamide, which is only

active at acidic pH (22, 23). The goal of this work was to identify compounds that are active at acidic pH, target persistence-associated Mtb physiology, and potentiate currently used antibiotics.

Materials and Methods

Bacterial strains and growth conditions

Mycobacterium tuberculosis (Mtb) experiments, unless otherwise stated, were performed with Mtb strain CDC1551 or *Mycobacterium smegmatis* (Msm) strain mc²155. Cultures were maintained in standing tissue culture flasks in 7H9 Middlebrook medium supplemented with 10% oleic acid, albumin, dextrose, catalase (OADC) and 0.05% Tween-80 and incubated at 37°C with 5% CO₂ unless noted otherwise. *Staphylococcus aureus* experiments were performed with *S. aureus* strain Newman and maintained in shaking 15 mL Falcon tubes or Erlenmeyer flasks in Luria-Bertani (LB) broth. Where necessary, 7H9 or LB media were buffered to pH 7.0 with 100 mM MOPS or pH 5.7 with 100 mM MES.

EC₅₀ determination and spectrum of activity in non-mycobacteria

For EC₅₀ determinations, cultures were incubated in 96-well microtiter plates in the presence of an 8-point (2.5-fold) dilution series of PH036 ranging from 80 µM – 0.13 µM. Mtb cultures were grown to mid- to late-log phase and then pelleted, re-suspended in 7H9 buffered at pH 7.0 or 5.7 and dispensed into the 96-well assay plates at an optical density (OD) of 0.1 and incubated for 6 days at 37°C with 5% CO₂. Msm cultures were grown to mid- to late-log phase and then pelleted, re-suspended in 7H9 buffered at pH 7.0 or 5.7 and dispensed into the 96-well assay plates at an optical density (OD) of 0.1 and incubated for 3 days at 37°C.

The activity of PH036 against non-mycobacteria was performed in buffered pH 7.0 or pH 5.7 LB broth, shaking at 200 RPM at 37°C. Cultures were grown overnight and then back diluted to a starting optical density (OD) of 0.05 in 96-well microtiter plates. A range of Gram positive and Gram negative bacteria were tested including: *Staphylococcus aureus* Newman, *Escherichia coli* K12, and *Salmonella enterica* Typhimurium. The assay was allowed to proceed for 6-8 hours and incubated in the presence of an 8-point (2.5-fold) dilution series of PH036 ranging from 80 μ M – 0.13 μ M. Growth (OD) was monitored using a Perkin Elmer EnVision plate reader. Growth inhibition was normalized based on the rifampicin (100%) and DMSO (0%) controls for mycobacterial cultures. Non-mycobacteria cultures were normalized for growth based on the kanamycin (100%) and DMSO (0%) controls. EC₅₀ values were calculated based on a variable slope, four-parameter non-linear least squares regression model in the GraphPad Prism software package (ver. 6).

Bactericidal Activity of PH036

Mtb cultures were prepared at an OD₆₀₀ of 0.1 in buffered 7H9 media (pH 5.7) in 96-well plates as described above. A final concentration of 80 μ M of each drug was added and the treated cultures incubated for a period of 3 days. At the end of the incubation, 10-fold serial dilutions were performed for each condition and viable bacterial CFUs were enumerated by plating on 7H10 agar. Bactericidal activity of each compound was determined by comparing bacterial CFUs after treatment to the initial inoculum. Cultures treated with DMSO and rifampicin were included as negative and positive controls, respectively.

Measuring intracellular redox state

The intracellular redox state of Mtb cultures treated with the compounds of interest was determined using the redox-sensitive Mtb reporter strain CDC1551::roGFP-R12 (5, 24, 25). Briefly, Mtb was cultured in buffered pH 7.0 or 5.7 7H9 media lacking catalase (e.g. OAD) in 96-well plates containing 0.1 – 20 μ M PH036 at a starting OD₆₀₀ of 0.2. For each experimental condition, non-fluorescent wild-type CDC1551 transformed with empty vector was used as a control for background signal subtraction. At 6 h post-treatment, fluorescence emission was read at 510 nm after excitation at 400 nm and 480 nm, and the relative abundance of the oxidized and reduced roGFP species were measured, respectively. The 400/480 nm ratio of drug-treated cultures were normalized to the DMSO control which represented the baseline redox state of the cell. Dithiothreitol (DTT) was used as a control for a reductive environment and diamide was used as a control for oxidizing environments.

Transcriptional profiling and data analysis

For RNA-seq experiments, Mtb cultures were grown at 37°C in T-25 vented, standing tissue culture flasks in 8 mL of buffered 7H9 medium (pH 7.0 or 5.7) lacking catalase to an OD₆₀₀ of 0.5. Cultures were subsequently treated with 10 μ M PH036. As a baseline control, cultures treated with an equal amount of DMSO were used. Each treatment was performed in duplicate flasks (technical replicates) and repeated over two independent (biological) replicates. Following a 4 h incubation period in the presence of drug, total bacterial RNA was extracted, quality controlled and sequenced as previously described (26). RNA-seq data was analyzed using the

SPARTA software package (27). The transcriptional profiling data will be submitted to the NCBI GEO database.

Structure activity relationship (SAR) and eukaryotic cytotoxicity of PH036

Several analogs of PH036 were purchased to determine the active moiety of the compound. Compounds B-J (Table 5.2.) were assessed for growth inhibitory activity in Mtb using an 8-point (2.5-fold) dilution series ranging from 80 – 0.13 μ M at pH 5.7 in a similar manner as EC₅₀ determinations described above. Following 6 days incubation, cultures were analyzed for growth using OD relative to the rifampin (100%) and DMSO (0%), positive and negative controls, respectively.

Eukaryotic cytotoxicity of PH036 and its analogs were assessed as previously described (28). Briefly, J774 macrophages were grown at 37°C (5% CO₂) in DMEM (Corning CellGro) containing 10% fetal bovine serum (Thermo Scientific), 1 mM pyruvate, 2 mM L-glutamine, and 1 mM penicillin/streptomycin (Corning CellGro). Cells were grown until confluent, scraped, and plated in medium lacking antibiotics at either 1 x 10⁵ cells/mL. Cells were allowed to adhere overnight before addition of experimental treatments. Cells were incubated for 3 days at 37°C with 5% CO₂ and assessed for viability using the CellTiter Glo (Promega) luciferase kit. Cytotoxicity was normalized based on the 1% Triton X-100 (100%) and DMSO (0%) controls. EC₅₀ and half-maximal cell cytotoxicity concentration (CC₅₀) values were calculated based on a variable slope, four-parameter non-linear least squares regression model in the GraphPad Prism software package (ver. 6).

Fractional killing and potentiation of antimicrobials

Mtb cultures were grown to mid- to late-log phase, pelleted, and re-suspended in buffered pH 7.0 or 5.7 7H9 lacking catalase at an OD of 0.1. Cells were assessed for viability in the presence or absence of 10 μ M PH036 in combination with: DMSO, 1 mM DTT, 1 mM diamide, 100 μ M clofazimine, 0.3 μ M rifampin, or 10 μ M isoniazid. Following 3 days incubation in 96-well microtiter plates, cells were diluted in a 10-fold serial dilution series for each condition and viable bacterial CFUs were enumerated by plating on 7H10 agar.

Measurement of intracellular reactive oxygen species

Intracellular reactive oxygen species were measured using the CellROX Green reagent (Invitrogen) as previously described by Saini et al., (29). Briefly, Mtb was grown to mid- to late-log in Middlebrook 7H9 and inoculated into 5 mL of buffered 7H9 pH 7.0 or 5.7 lacking catalase at a starting OD of 0.5 and incubated in the presence of indicated concentrations of compounds. Following 4 or 24 hours incubation, a final concentration of 5 μ M CellROX green (Thermo Fisher) was added to cultures for 1 hour at 37 °C. Cells were washed twice in PBS supplemented with 0.05% Tween80 and re-suspended in the wash buffer and analyzed according to the manufacturers instructions. DTT (20 μ M), and diamide (2 and 20 μ M) served as controls. *S. aureus* cultures were grown overnight in LB at 37°C with shaking at 200 RPM. Cultures were pelleted and re-suspended in buffered pH 7.0 or pH 5.7 LB medium at an OD of 0.1. Cells were treated with a 4-point (2-fold) dilution series of PH036, DTT, or menadione ranging from 80 – 10 μ M. An equivalent volume of DMSO was added as a negative control. Following 6 hours of treatment, cultures were incubated with 5 μ M CellROX Green for 30 minutes at 37°C with shaking at 200 RPM. Cells were washed twice with PBS and re-suspended in 0.6 mL of PBS

before being arrayed in a 96-well microtiter plate. Fluorescence and growth were analyzed using a Perkin Elmer plate reader.

Measurement of free thiol pools

Mtb cultures were grown to mid- to late-log phase in 7H9 medium lacking catalase, pelleted, and re-suspended in 8 mL buffered pH 7.0 or 5.7 7H9 at an OD of 0.25. Five treatments were assessed: 1) DMSO, 2) 2 μ M PH036, 3) 20 μ M PH036, 4) 20 μ M auranofin, and 5) isoniazid. Following 24 hours of treatment, bacteria were normalized by OD, pelleted, washed twice in PBS + 0.05% tyloxapol, and re-suspended in 0.75 mL thiol assay buffer (100 mM potassium phosphate pH 7.4, and 1 mM EDTA). Cells were lysed by bead beating for 2 minutes at room temperature. Supernatants were removed and assayed using the Cayman Thiol Detection Assay kit (Cayman Chemical).

Results

Identification of PH036 as an inhibitor of Mtb growth in a pH-dependent manner

We conducted two whole-cell phenotypic high-throughput screens (HTS) at neutral and acidic pH for inhibitors of the DosRST and PhoPR regulons, respectively, using an identical chemical library. The ~220,000 compound screening library was composed of small molecules representing broad chemical diversity. Positive hits that did not target either the DosRST or PhoPR regulon but generally inhibited growth of Mtb were also identified. By examining the overlap among common inhibitors that slow Mtb growth, compounds were found that are active in a pH-dependent manner. Small molecules that exhibited a profile of at least 50% growth reduction and were unique to the HTS at acidic pH were considered for additional follow-up and

characterization as pH-dependent inhibitors of Mtb growth. PH036 (Figure 5.1. A) was identified as a compound that met the profile of slowing Mtb growth at acidic pH while leaving growth at neutral pH relatively unaffected. At acidic pH (pH 5.7), PH036 inhibits Mtb growth with a half-maximal effective concentration (EC_{50}) of 3.2 μ M (Figure 5.1. B). Treatment of Mtb at neutral pH (pH 7.0) with PH036 results in a diminished ability to inhibit bacterial growth relative to acidic pH (Figure 4.1. B). However, at concentrations greater than 30 μ M, Mtb growth is slowed in a dose-dependent manner under neutral pH conditions (Figure 5.1. B), suggesting that the mechanism through which PH036 is acting may not be exclusive to acidic pH. However, Mtb may be more sensitive at low pH due to bacterial pH-driven adaptations that when disrupted by PH036, render Mtb non-viable. PH036 does not affect Mtb cytoplasmic pH, indicating it is not functioning as an ionophore (Figure S5.1.). To assess whether PH036 is acting in a bactericidal or bacteriostatic manner at acidic pH, Mtb was treated with a high dose of the compound (80 μ M) for 3 days at pH 5.7. Bacterial growth is reduced greater than two-logs relative to the initial inoculum and similar to the rifampin positive control, suggesting the PH036 is bactericidal *in vitro* (Figure 5.1. C).

Mtb exhibits a reduced cytoplasm at acidic pH and requires PhoPR to maintain redox poise (5). To test whether the ability of PH036 to kill Mtb at acidic pH is the result of altered redox homeostasis, Mtb expressing a redox active GFP was treated with increasing concentrations of PH036. Indeed, PH036 treatment leads to a reduced cytoplasmic environment in a dose-dependent and pH-independent manner (Figure 5.1. D). These data support several findings: 1) PH036 inhibits Mtb growth in a pH-dependent manner, 2) PH036 is bactericidal, and 3) the compound promotes a reduced cytoplasm establishing a link between Mtb redox homeostasis and viability at acidic pH.

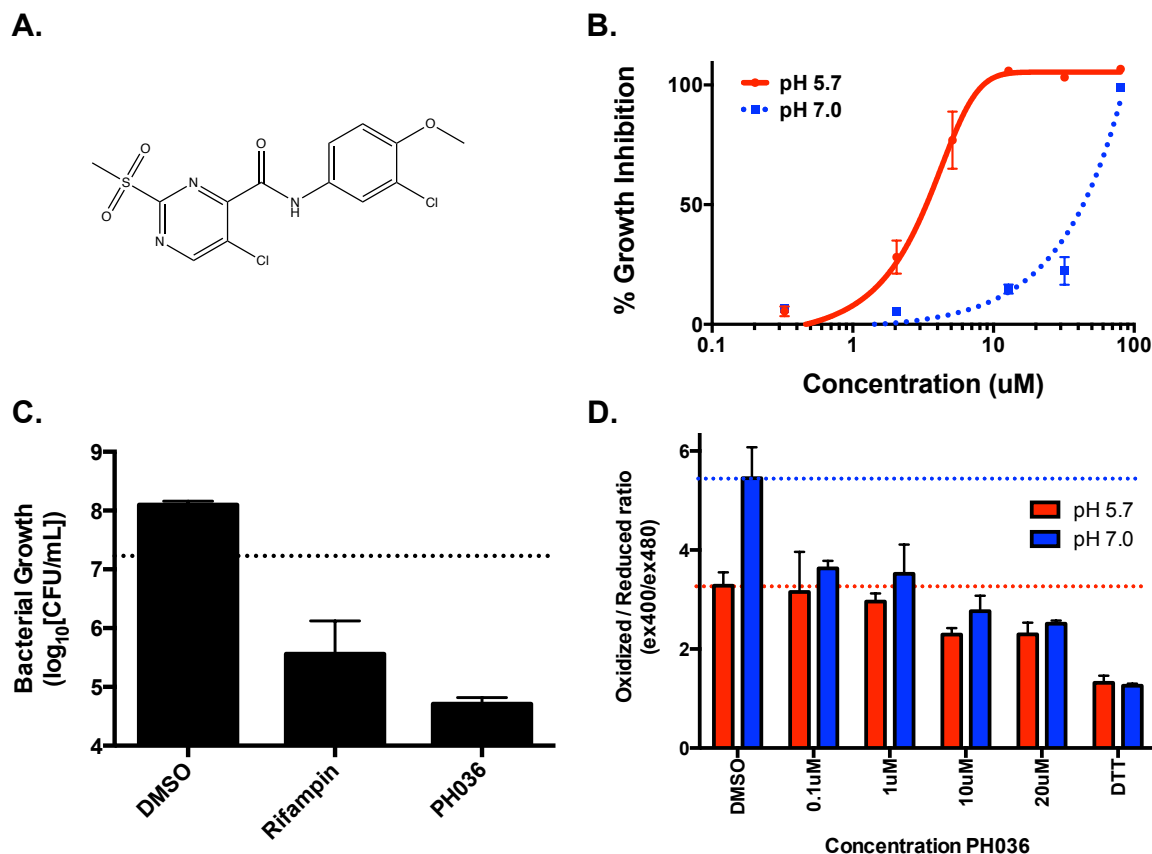


Figure 5.1. PH036 inhibits *M. tuberculosis* growth in a pH-dependent manner and is bactericidal while promoting a reduced intracellular environment. A) Chemical structure of PH036 (5-chloro-N-(3-chloro-4-methoxyphenyl)-2-methylsulfonylpyrimidine-4-carboxamide). B) Treatment with PH036 inhibits Mtb growth in a dose-dependent manner at pH 5.7 with an EC₅₀ of 3.2 μM. Bacterial growth is inhibited at pH 7.0 in a dose-dependent manner at concentrations greater than 30 μM. C) PH036 is bactericidal at pH 5.7 following 3 days of treatment (80 μM). D) PH036 promotes a reduced cytoplasm in a dose-dependent and pH-independent manner. Data shown are representative of at least two independent experiments. Garry Coulson generated the data for this figure and was assembled by Ben K Johnson.

PH036 exhibits a narrow spectrum of activity against non-mycobacterial species

To assess whether PH036 acts as a broad inhibitor of bacterial growth at acidic pH, a non-pathogenic *Mycobacterium* sp. (*M. smegmatis*; Msm) and selected Gram-positive and Gram-negative bacteria were treated with the compound at neutral and acidic pH (Table 5.1.). Msm and non-mycobacterial species of bacteria were grown in 96-well assay plates in medium buffered to pH 7.0 or 5.7. Notably, following 3 days of treatment, Msm exhibited an EC₅₀ of greater than 80 µM, at both neutral and acidic pH, suggesting activity of PH036 is more specific to Mtb pH-adaptation physiology or due to the greater number of efflux pumps present in Msm (30). Of the non-mycobacteria tested, only *Staphylococcus aureus* is susceptible to PH036 (Table 5.1.). However, both the EC₅₀s at acidic and neutral pH are similar in *S. aureus* with mild pH-dependent activity. Taken together, these data suggest a common mechanism with which PH036 is acting to inhibit bacterial growth between Mtb and *S. aureus*.

Organism	EC ₅₀ pH 5.7 (μM)	EC ₅₀ pH 7.0 (μM)
<i>M. tuberculosis</i>	3.2	>80
<i>M. smegmatis</i>	>80	>80
<i>S. aureus</i>	11.64	16.52
<i>E. coli</i>	>80	>80
<i>S. enterica</i>	>80	>80

Table 5.1. Spectrum of activity for PH036. Table depicting half-maximal effective concentrations (EC₅₀) of PH036 against various *Mycobacterium sp.*, Gram-positive, and Gram-negative bacteria. Data were generated for *M. tuberculosis* and *M. smegmatis* by Garry Coulson. *S. aureus*, *E. coli*, and *S. enterica* data were generated by Ben K Johnson.

Structure activity relationship analysis reveals the sulfone group is required for activity

PH036 (compound A; Table 5.2.) exhibits potent cytotoxicity against eukaryotic cells and we sought to define the chemical groups required for activity against Mtb while minimizing cytotoxic effects against mammalian cells. To define the reactive moieties of PH036, the core chemical structure was determined and several analogs of the parent molecule (Table 5.2.; compound A – PH036) were purchased to assess the minimum required scaffold for activity (Table 5.2.). Chemical groups at the R1 and R2 regions of the core structure (Table 5.2.) revealed that the sulfone moiety at the R1 position was indispensable for activity against Mtb at pH 5.7. In the H and I analogs, the methylsulfone group has been replaced with alternative groups, rendering both molecules inactive against Mtb. Notably, the J analog of PH036 revealed that the R2 moiety is not required for activity against Mtb, suggesting that the J scaffold is sufficient for slowing Mtb growth at acidic pH. Further, this PH036 analog also did not exhibit cytotoxicity against macrophages up to the highest concentration tested (80 μ M), suggesting that by removing the 5-chloro-N-(3-chloro-4-methoxyphenyl) (R2) group, the cytotoxic target of the parent PH036 molecule is no longer targeted. However, we cannot rule out whether loss of the R2 moiety leads to an inability of the J analog to enter the macrophage, though this is unlikely as the compound retains activity against Mtb (Figure S5.2.).

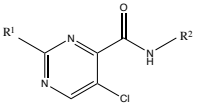
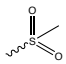
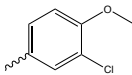
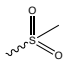
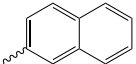
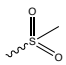
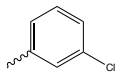
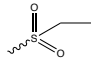
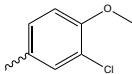
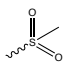
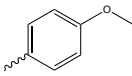
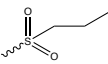
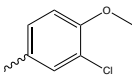
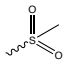
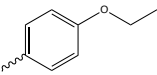
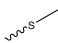
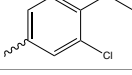
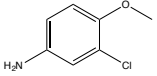
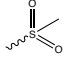
			<i>M. tuberculosis</i>	J774 mΦ
Compound	R ¹	R ²	EC ₅₀ (μM)	CC ₅₀ (μM)
A			1.85	17.07
B			1.81	14.19
C			1.92	10.64
D			2.36	11.89
E			1.97	17.47
F			4.01	10.33
G			1.15	18.38
H			>80	>80
I	-		>80	>80
J		H	8.09	>80

Table 5.2. Structure activity relationship of PH036 and its derivatives against Mtb growth and eukaryotic cytotoxicity. Table depicting the effects of varying chemical moieties at the R1 and R2 positions from the parent compound (A; PH036) on Mtb growth and macrophage cytotoxicity at the half-maximal effective concentration. EC₅₀ data were generated by Garry Coulson. CC₅₀ data were generated by Ben K Johnson. Table made by Ben K Johnson.

PH036 causes a thiol-associated stress response

Global transcriptional profiling was performed to determine whether specific genes or pathways are differentially expressed in response to PH036 treatment. Differential gene expression that is specific to or enhanced at pH 5.7 may provide insights into the increased sensitivity of Mtb to PH036 at acidic pH. Mtb was inoculated into rich medium buffered at pH 7.0 or 5.7 in the presence of either 10 μ M PH036 or an equivalent volume of DMSO. After 4 hours incubation, total RNA was isolated and subjected to RNA sequencing. PH036 treatment of Mtb caused the upregulation of 231 genes (>2-fold, $p < 0.05$) and 264 genes (>2-fold, $p < 0.05$) at pH 7.0, and pH 5.7 (Figure 5.2. A), respectively. Many of the genes upregulated at either pH are also regulated by the alternative sigma factor *sigH* in response to oxidative/thiol stress response (Figure 5.2. B) (31). Indeed, *sigH* was significantly upregulated (>5-fold, $p < 0.05$), including several genes within its regulon such as the thioredoxin reductases (*trxB*, *trxB2*, *trxC*), lipid synthesis genes (*papA4*), cysteine synthesis (*cysM*), and several predicted oxidoreductases (*Rv2454c*, *Rv3463*). Additionally, ferredoxins and additional oxidoreductases were significantly upregulated when treated with PH036. Notably, an oxidative stress response associated with detoxification of superoxide species through superoxide dismutase (*sodA*, *sodC*) or the membrane-associated oxidoreductase (*sodA*, *sseA*, *doxX*) complex was not observed, uncoupling a general oxidative stress response from PH036 treatment (Figure 5.2. C) (32). However, the catalase/peroxidase *katG* was upregulated at least 4-fold at both pH 7.0 and 5.7, suggesting that reactive oxygen species are likely being generated and require detoxification. During reductive stress, Mtb has a variety of mechanisms to counteract increased reducing equivalents and one method is through the uptake of nitrate and reducing it to nitrite, thus consuming intracellular reducing equivalents (33, 34). Indeed, the predicted nitrate uptake/extrusion gene *narK2* and

probable nitrate reductase *narX* were upregulated >2-fold ($p < 0.05$) at pH 5.7, suggesting that PH036 treatment leads to enhanced reductive stress and corroborates the redox-active GFP data (Figure 5.1. D). In contrast, under the conditions tested, Mtb treated with DMSO at pH 5.7 downregulates *narK2* and *narX* despite exhibiting a reduced cytoplasm suggesting alternative routes to balance its redox pool. This underscores the hypothesis that PH036 promotes reductive stress by overcoming these “normal” homeostatic mechanisms causing Mtb to utilize additional systems in an attempt to maintain redox balance. Taken together, these data suggest that PH036 is active against Mtb at both neutral and acidic pH. However, the enhanced sensitivity of Mtb to PH036 treatment at acidic pH is likely through acidic pH-altered physiology.

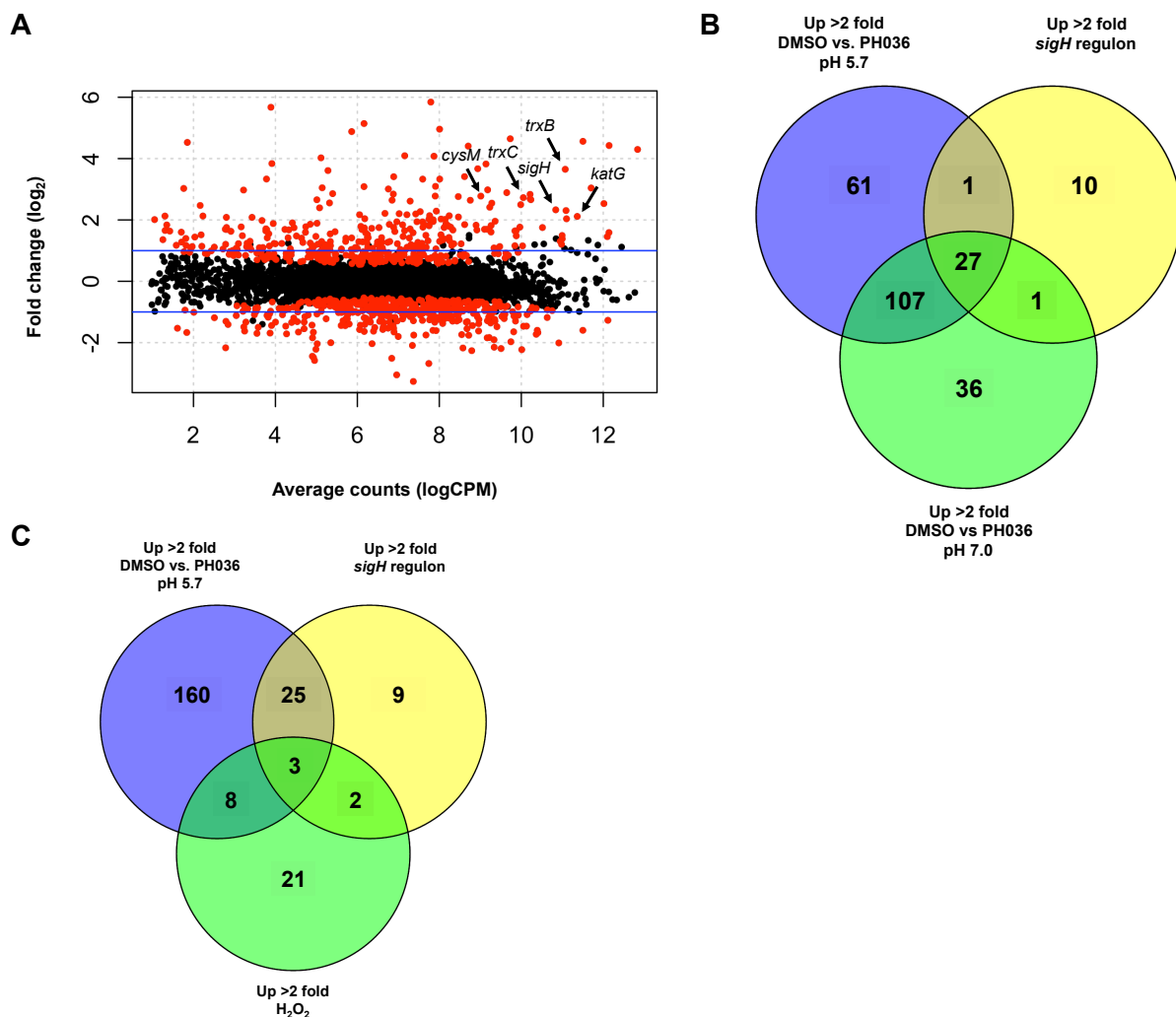


Figure 5.2. Transcriptional profiling of Mtb treated with PH036. A) Representative RNA-seq scatter plot of Mtb treated with 10 μ M PH036 for 4 hours (pH 5.7). Highlighted genes are involved in the alternative sigma factor *sigH* regulon and *katG* is an Mtb catalase/peroxidase. Black dots are not statistically significant and red dots are statistically significant ($p < 0.05$). B) Venn diagram of genes upregulated (>2 -fold, $p < 0.05$) in PH036 treated Mtb at pH 7.0 and 5.7 overlapping with the *sigH* regulon ($\sim 80\%$ overlap) (31). Genes not similar between conditions are the result of either not meeting cutoffs or are hypothetical proteins. Note the significant overlap between both neutral and acidic pH in PH036 treated cultures, suggesting a similar transcriptional profile, though many genes are not common between pHs. C) PH036 treatment at pH 5.7 includes a thiol-stress response through the alternative sigma factor *sigH* and is dissimilar to a hydrogen peroxide oxidative stress response (35). Data are the average of two-biological replicates. Comparisons are within Rv genes only. CDC1551 specific genes are removed. RNA was isolated and submitted for sequencing by Garry Coulson. Data were analyzed and figures were generated by Ben K Johnson.

Based on the transcriptional profiling data suggesting a thiol-associated stress response, we hypothesized that treatment with PH036 may sensitize Mtb to general and thiol-specific oxidation reagents such as diamide, clofazimine, and the *katG* activated prodrug isoniazid (INH) through disrupting the bacterium's redox poise (36). To determine whether PH036 causes enhanced sensitivity to thiol oxidation by diamide, Mtb was inoculated into rich medium buffered at pH 5.7 in the presence or absence of 10 μ M PH036 in combination with either 1 mM diamide, 1 mM dithiothreitol (DTT), or an equivalent volume of DMSO. After 3 days of treatment, cultures were plated onto 7H10 agar plates and bacterial viability was assessed through enumerating colony-forming units (CFU). Treatment with PH036 alone resulted in an approximately 2-fold reduction in bacterial growth relative to the initial inoculum (Figure 5.3.). Diamide treated cultures led to 1.8-fold growth. However, in the presence of diamide, PH036 sensitizes Mtb to thiol oxidation, resulting in greater than 8-fold enhanced killing relative to the initial inoculum, suggesting potentiation interactions between the compounds (Figure 5.3.). To assess whether Mtb is generally sensitive to oxidative stress, 10 μ M PH036 was incubated in combination with clofazimine (100 μ M) for 3 days at pH 5.7. Clofazimine is a redox cycling compound that can directly compete with menaquinone and spontaneously produce reactive oxygen species (37). The concentration of clofazimine was chosen based on monotherapy at 100 μ M not significantly slowing Mtb growth at acidic pH. Indeed, clofazimine alone led to relatively unchanged levels of Mtb growth. However, clofazimine in combination with PH036 resulted in approximately a 24-fold reduction in bacterial growth. These data suggest that treatment with PH036 results in an impaired ability to respond to oxidizing agents.

To test the hypothesis that upregulation of *katG* in PH036 treated Mtb will sensitize the bacteria to isoniazid, Mtb were inoculated into rich medium buffered to pH 5.7 in the presence or

absence of PH036 (10 μ M) in combination with rifampin (0.3 μ M), INH (10 μ M), or an equivalent volume of DMSO for 3 days. PH036 treatment and INH alone resulted in comparable levels of killing, with approximately 2-fold reduction in bacterial growth relative to the initial inoculum (Figure 5.3.). However, in the presence of INH, PH036 potentiates the antibiotic, resulting in approximately a 160-fold enhanced reduction in bacterial growth (Figure 5.3.). PH036 treatment had no observable additional effect in combination with another anti-tuberculosis drug, rifampin at the concentration tested (Figure 5.3.). These data validate the transcriptional profiling results implicating the upregulation of *katG* in PH036 treated Mtb leading to potentiation of the combination of PH036 and INH against Mtb growth.

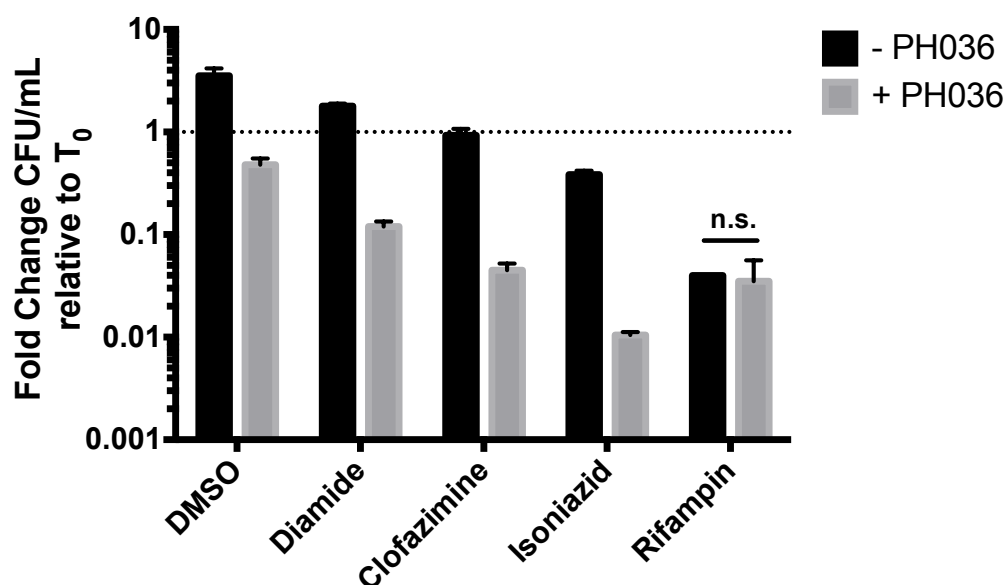


Figure 5.3. PH036 sensitizes Mtb to treatment by oxidizing agents and isoniazid. Treatment of Mtb with 10 μ M PH036 in combination with the thiol oxidizing agent diamide reduces growth ~8-fold relative to the initial inoculum. Further, the redox cycling agent clofazimine also potentiates PH036 treatment leading to a ~24-fold reduction in Mtb growth. The low molecular weight thiol containing compound DTT rescues PH036-mediated killing. Combination treatment of PH036 and INH results in potentiated bacterial killing (~160-fold reduction in bacterial growth). No effects were observed in combination with the antibiotic rifampin. Data are representative of two biological replicates and all differences are statistically significant (t-tests, multiple comparisons corrected $p < 0.05$) unless indicated otherwise. n.s. – not statistically significant. Data were generated and analyzed by Garry Coulson and Ben K Johnson.

PH036 causes accumulation of intracellular reactive oxygen species

The transcriptional profiling data and potentiation of oxidation agents prompted us to investigate whether PH036 treatment results in accumulation of intracellular reactive oxygen species (ROS). A recent study has shown that minor increases in endogenous ROS can have significant and detrimental results on Mtb growth and viability during infection (38). Further, this study showed that Mtb is particularly sensitive to perturbations in redox poise compared to the fast growing *M. smegmatis* (38). Saini et al. have recently shown that the fluorescent dye CellROX green is amenable to measuring intracellular ROS accumulation in Mtb (29). Therefore, we used this method of ROS detection for both Mtb and *S. aureus*. Mtb was grown to mid- to late-log in rich medium, pelleted, and re-suspended in either pH 7.0 or 5.7 buffered 7H9 medium. Cultures were incubated in the presence of 2 or 20 μ M PH036 or an equivalent volume of DMSO. Mtb treated with PH036 exhibited a time and pH-dependent increase of intracellular ROS (Figure 5.4. A). Mtb treated with PH036 accumulates approximately 2-fold more ROS after 24-hours relative to the 4-hour time point. To examine whether PH036 killing of *S. aureus* is due to enhanced levels of intracellular ROS, *S. aureus* was inoculated into rich medium buffered to either pH 7.0 or 5.7 and exposed to a 4-point (2-fold) dilution series of PH036, DTT, and menadione ranging from 80 – 10 μ M or an equivalent volume of DMSO. Following 6 hours incubation, cultures were assessed for accumulated ROS. PH036 caused enhanced ROS accumulation in a dose-dependent manner at pH 7.0 and 5.7 similar to the positive menadione control (Figure 5.4. B). Additionally, a superoxide dismutase deficient mutant in *S. aureus* (*ΔsodAΔsodM*) exhibits a 2-fold enhanced sensitivity to PH036 at pH 7.0 and 5.7 (Figure S5.3.). These data suggest that PH036 treatment results in accumulated intracellular ROS in Mtb and *S. aureus*, lending a potential mechanism for PH036-mediated killing. Further, enhanced levels of

ROS in Mtb by PH036 supports the potentiation of oxidizing agents on inhibiting bacterial growth (Figure 5.3.).

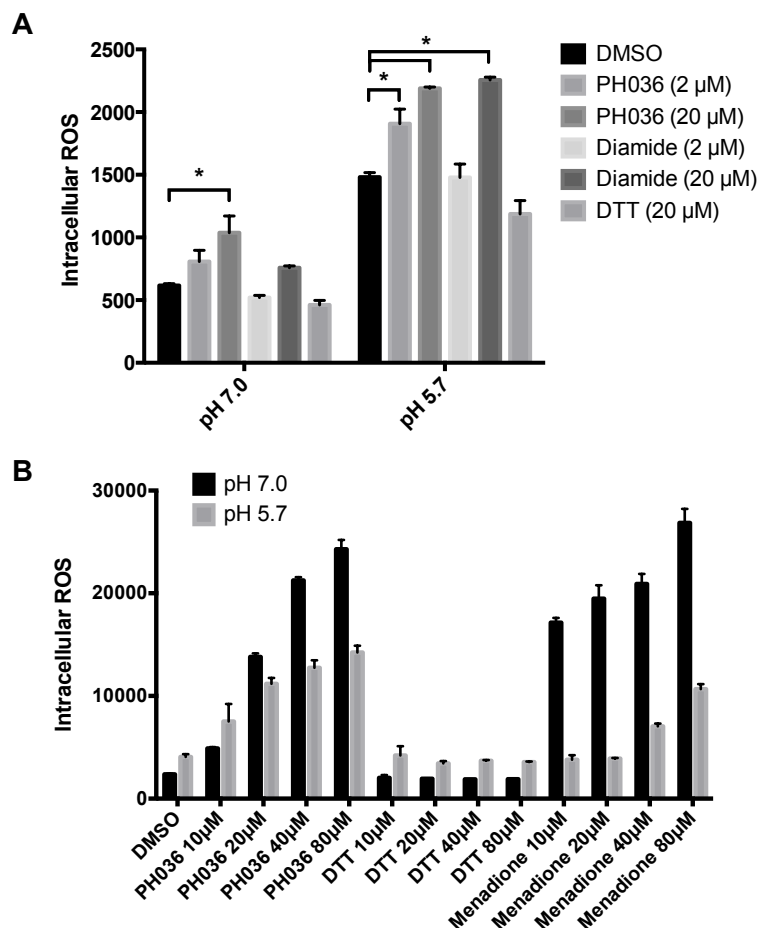


Figure 5.4. PH036 treatment leads to accumulation of reactive oxygen species. Treatment of A) *Mtb* and B) *S. aureus* with indicated concentrations of PH036 leads to a dose-dependent accumulation of reactive oxygen species (ROS). Additionally, *Mtb* accumulation of ROS is a time and pH-dependent process. *S. aureus* treated with PH036 exhibits a similar dose-dependent response to the redox cycling agent menadione. DTT had no effect on ROS accumulation at these concentrations. ROS was measured using the fluorescent dye CellROX Green (5 μM) and normalized by optical density (OD₅₉₅). * represents statistical significance (p<0.05, 2-way ANOVA). All differences in *S. aureus* are statistically significant between pH and are represented as dose-dependent trends. Data are representative of two biological replicates. Data and figures were generated by Ben K Johnson

Sensitivity to PH036 can be reversed through addition of low molecular weight thiols

We sought to investigate whether exogenous addition of other low molecular weight thiols could also restore bacterial growth in the presence of PH036. To test whether PH036-mediated killing of *S. aureus* could also be rescued with low molecular weight thiol containing compounds, *S. aureus* was inoculated into 96-well plates containing rich medium buffered to either pH 7.0 or 5.7 and incubated in the presence or absence of 80 μ M PH036 in combination with increasing levels of glutathione (GSH) or an equivalent volume of DMSO. GSH is the dominant thiol in nearly all Gram negative bacteria and eukaryotic systems to before redox stress (39). Mtb and *S. aureus* utilize either mycothiol/ergothione or bacillithiol, respectively, as thiol buffers (29, 40, 41). Therefore, we hypothesized that addition of GSH would alleviate PH036-mediated killing in *S. aureus*. GSH was incubated with *S. aureus* cultures for 20 minutes prior to addition of PH036 or DMSO. Following 6 hours incubation, bacterial growth was measured using optical density and normalized as a percent relative to the DMSO control. Addition of GSH to *S. aureus* treated with PH036 resulted in a dose-dependent recovery of bacterial growth at pH 7.0 and 5.7 (Figure 5.5.). Further, addition of GSH alone did not significantly affect bacterial growth (Figure 5.5.). Therefore, low molecular weight thiols like GSH can counteract bacterial growth inhibition by PH036 in *S. aureus*.

With the enhanced sensitivity to oxidative stress, rescue of growth with low molecular weight thiol (GSH), and strong upregulation of the thioredoxins and thioredoxin reductase in Mtb, we reasoned that PH036 may modulate thioredoxin reductase activity. A recent study has implicated the therapeutic auranofin as a thioredoxin reductase inhibitor in Mtb (42). *E. coli* encodes both the GSH and thioredoxin reductase pathways to maintain redox balance and is resistant to auranofin-mediated killing. However, if the GSH synthesis pathway is disrupted

through a mutation in the first synthetic step, *E. coli* become sensitive to auranofin as the only pathway available to maintain redox balance is through the thioredoxin reductase. However, we did not observe enhanced sensitivity of GSH synthesis or thioredoxin reductase deficient *E. coli* to PH036 treatment (Figure 5.6.). Together, this result suggests that PH036 is not acting as a thioredoxin reductase inhibitor and is likely a more general inhibitor of free thiols. However, it is possible that additional mechanisms may be leading to low activity in *E. coli* such as an inability to pass through the outer membrane or efflux out of the cell. Additional experiments are needed to assess these possibilities.

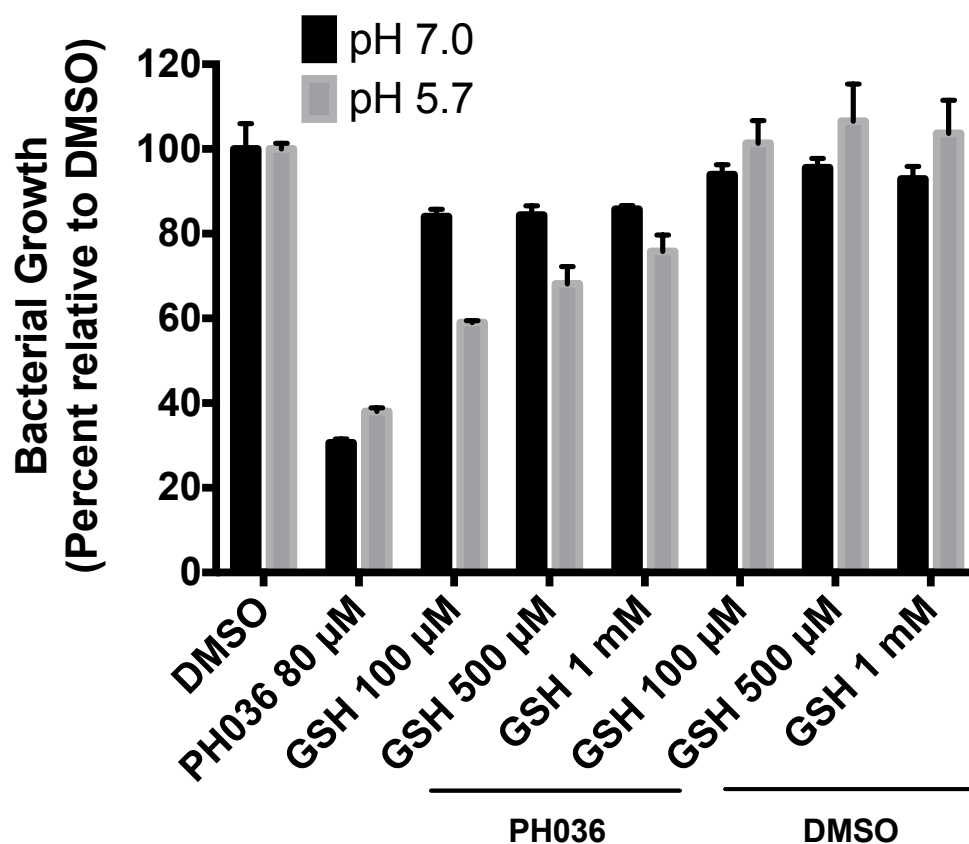


Figure 5.5. Exogenous addition of glutathione rescues PH036-mediated growth inhibition. Treatment of *S. aureus* with 80 μ M PH036 results in growth inhibition. Addition of the low molecular weight thiol glutathione (GSH) results in a dose-dependent rescue of bacterial growth in the presence of 80 μ M PH036. GSH alone minimally impacts *S. aureus* growth. Data are representative of at least two biological replicates. Data and figure were generated by Ben K Johnson.

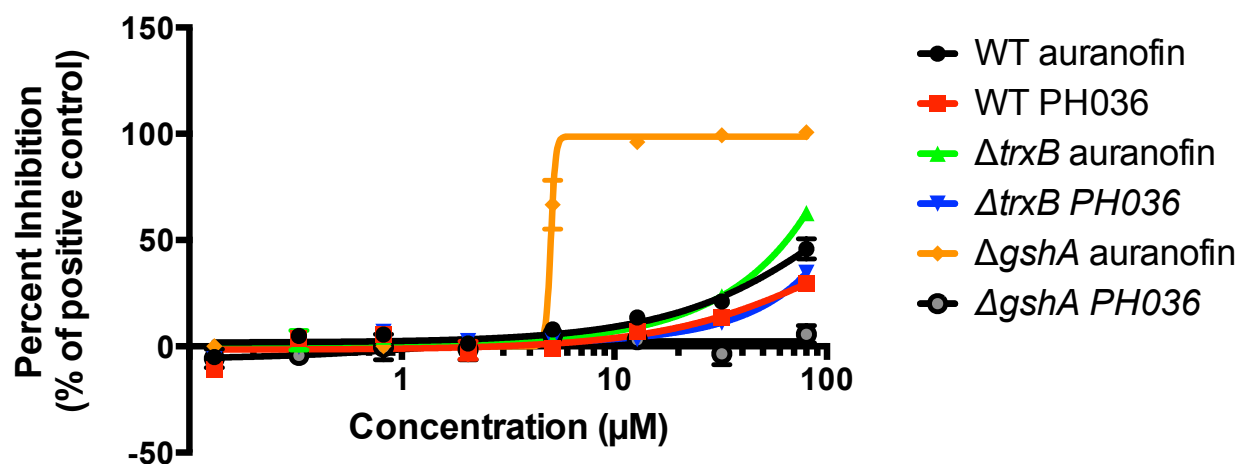


Figure 5.6. Thioredoxin (Trx) or glutathione synthesis (GSH) pathway *E. coli* mutants do not exhibit enhanced sensitivity to PH036. *E. coli* mutants and *E. coli* wild-type strains were inoculated into rich medium buffered to pH 7.0 or pH 5.7 and incubated in the presence of an 8-point dilution series (2.5-fold) of PH036 or auranofin ranging from 80 – 0.13 μM. Auranofin exhibits activity against *E. coli* lacking the GSH synthesis pathway, while PH036 does not display enhanced activity in either mutant. Data and figure were generated by Ben K Johnson.

PH036 depletes intracellular thiol pools

PH036 promotes enhanced reductive and thiol stress and sensitivity to oxidizing agents, therefore we sought to understand how PH036 impacts thiol pools in a pH-dependent manner. We hypothesized that due to pH-driven adaptations and an endogeneous reducing environment at acidic pH, PH036 would have a greater impact on thiol pools relative to neutral pH. To directly measure intracellular free thiol pools, Mtb was inoculated into rich medium buffered at pH 7.0 and pH 5.7 in the presence of either 2 μ M PH036, 20 μ M PH036, 20 μ M auranofin, INH, or an equivalent volume of DMSO. Following 24 hours incubation, cultures were analyzed for total intracellular thiol pools. Previous work has shown that auranofin depletes free thiols in Mtb and *S. aureus*; therefore it was used as a positive control (42). Additionally, a known antibiotic like INH was used as another control as it does not directly reduce total free thiols (36). Indeed, auranofin depleted free thiols relative to the DMSO treated control and INH had comparable thiol concentrations as the untreated cultures (Figure 5.7.). Notably, PH036 depleted thiol pools at both pH 7.0 and 5.7. At pH 5.7, 20 μ M PH036 depleted free thiols ~16 fold to ~80 nM as compared to ~1.3 μ M in the DMSO treated samples (Figure 5.7.). Together, this work suggests that Mtb is more sensitive to PH036-mediated thiol stress at pH 5.7 compared to 7.0 and appears to be acting by: i) promoting enhanced reductive stress at acidic pH, ii) increasing intracellular ROS, and iii) depleting free thiol pools leading to an inability to maintain its redox pool, resulting in pH-dependent bacterial killing.

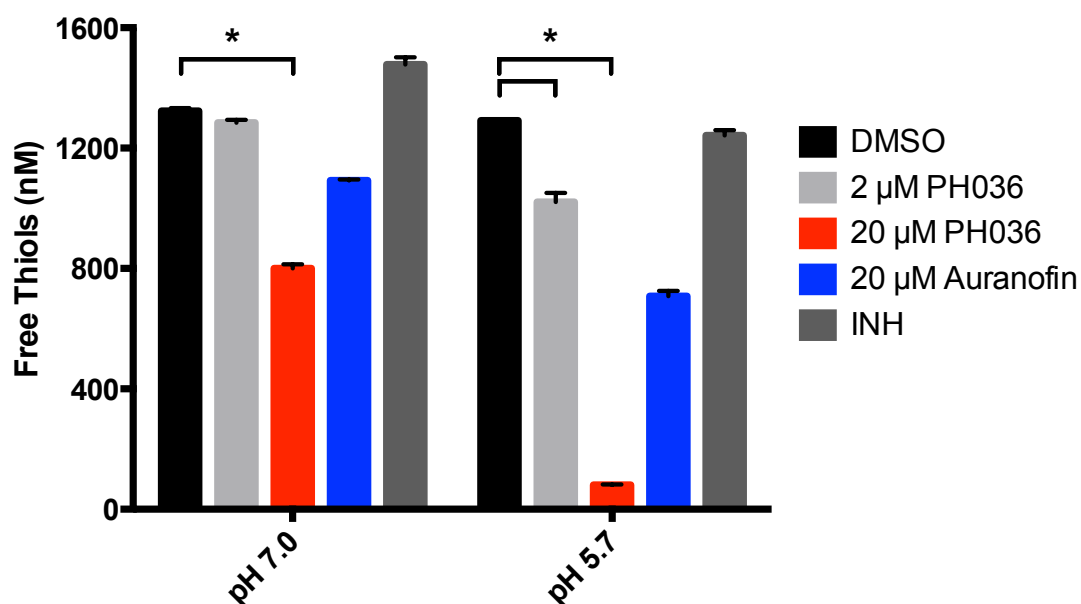


Figure 5.7. PH036 depletes intracellular free thiols. Mtb treated with indicated concentrations of PH036 results in depleted thiol pools relative to the DMSO control. Auranofin is a known inhibitor that decreases the concentrations of free thiols while isoniazid (INH) is an anti-tuberculosis antibiotic that does not directly deplete free thiols. Statistical significance was calculated based on a two-tailed t-test (*, $p < 0.05$). Data are representative of two biological replicates. Data and figure were generated by Ben K Johnson.

Discussion

We identified PH036 as a pH-dependent inhibitor of Mtb and *S. aureus* by conducting two Mtb whole-cell HTS of an identical compound library at neutral and acidic pH. Together, the data suggest that PH036 depletes intracellular thiol pools (Figure 5.7.) and enhances accumulation of ROS (Figure 5.4. A), and these activities may cause inhibition of bacterial growth. Mtb is killed at pH 5.7 in combination with PH036 (Figure 5.1. C), suggesting enhanced sensitivity to ROS or that intracellular thiol pools are required for Mtb viability at acidic pH. Indeed, inactivation of low molecular weight mycothiol synthesis results in non-viable cells (43). However, the final acetylation step in mycothiol synthesis (*mshD*) is dispensable for growth in rich medium likely owing to the redox capacity of the cysteine-containing un-acetylated substrate (43). Recently, auranofin was shown to be active against Mtb and *S. aureus* by depleting free thiol pools through inhibition of thioredoxin reductase, an essential enzyme for recycling oxidized thiols (42). Mtb and *S. aureus* lack the canonical glutathione (GSH) synthesis pathways and possess the thioredoxin (Trx) system exclusively (44). In place of GSH, Mtb and *S. aureus* synthesize mycothiol/ergothioneine and bacillithiol as low molecular weight thiols, respectively (29, 39-41, 44). Auranofin was shown to inhibit *E. coli* growth in mutants deficient in GSH synthesis and possessing only the Trx system (42). In contrast to the auranofin result, PH036 treatment does not significantly affect growth of *E. coli* mutants defective in either the Trx or GSH pathways, suggesting an alternative mechanism of action for PH036 (Figure 5.6.).

The core chemical scaffold of PH036 (5-chloro-2-methylsulfonylpyrimidine-4-carboxamide) has been researched previously in the organic chemistry literature for synthesizing derivative scaffolds of aminopyrimidine-containing drugs (45). Notably, the anionic nucleophile thiolate was shown to selectively react with the C-2 carbon almost exclusively depending on the

bound electron-withdrawing group (45). In the case of a methylsulfone moiety, this chemical group is a strong electron-withdrawing group, promoting a partial positive charge at the C-2 carbon allowing the electron rich thiolate anion to attack and displace the methylsulfone (46). Based on the known chemistry, a speculative reaction mechanism is proposed to occur for PH036 in Mtb and *S. aureus*, covalently modifying free thiols and reduced disulfides (Figure 5.8.). The NADPH-dependent reduction of the disulfide can also occur with NADH. Additionally, during the covalent modification of free thiols by PH036, either methanesulfinic acid or a highly reactive methanesulfinate are evolved. Free thiols can be overoxidized to sulfinic or sulfonic acid during oxidative stress. These reactions can lead to protein inactivation and as a result, a potent stress response to counteract the oxidative damage (47). Therefore, it is possible that PH036-dependent modification of free thiols leads to production of sulfinic acid and the bacterium may adapt to dissipate the oxidative damage and maintain redox poise through producing additional thiol containing macromolecules. Consequently, this leads to further damage by generating additional targets for PH036 to react with and is detrimental at acidic pH. Additionally, owing to the high reactivity of methanesulfinate, it is tempting to speculate that this reaction byproduct could rapidly react with nearby macromolecules leading to additional oxidative damage. However, the exact mechanism of action remains to be determined.

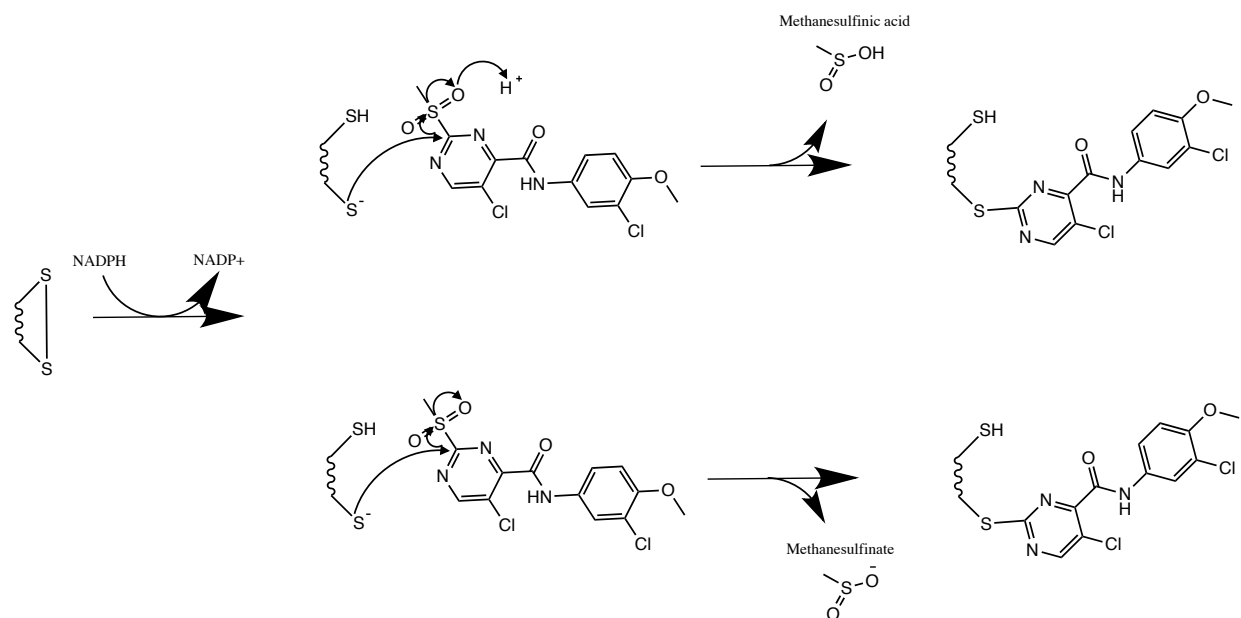


Figure 5.8. Speculative reaction mechanism of PH036 with a general disulfide. NADPH-dependent activation of the general disulfide to a thiol and thiolate anion allows for the thiolate to undergo anionic nucleophilic attack of the C-2 carbon on the pyrimidine ring of PH036, leading to a covalent modification and releasing either methanesulfinic acid or methanesulfinate. Figure was generated by Ben K Johnson

The strong induction of many of the genes within the alternative sigma factor *sigH* regulon suggests that Mtb is experiencing thiol stress when treated with PH036 (31). This group of genes was identified based on comparing the thiol oxidizing agent diamide compared to a diamide treated *sigH* mutant. By identifying genes induced in the wild-type treated with diamide and uninduced in the mutant, a thiol-dependent *sigH*-mediated stress regulon could be identified (31). The genes that comprise this regulon include induction of the thioredoxins and thioredoxin reductase, as well as cysteine biosynthesis. Thioredoxins and the thioredoxin reductase are key enzymes in the process of maintaining redox homeostasis in Mtb. If the ability to recycle thiols through the thioredoxin reductase is inhibited, Mtb is attenuated for growth (42). However, it appears that PH036 is acting in a manner independent of inhibiting thioredoxin reductase exclusively as it is a pH-independent essential enzyme for Mtb growth (Figure 5.6.) (42). The observed upregulation of the thioredoxins and thioredoxin reductase at both pH 7.0 and 5.7 suggests that PH036 is potentially blocking the ability to recycle its thiol pool to maintain redox balance, though we have no direct evidence for this. Additionally, the upregulation of cysteine biosynthesis has been implicated in maintaining redox balance in Mtb strains deficient in the low molecular weight thiol ergothioneine and the redox sensor WhiB3 (29). However, we did not observe upregulation of either mycothiol or ergothioneine biosynthetic operons at either pH, suggesting that PH036 activity does not directly promote increased levels of low molecular weight thiols as a countermeasure. Taken together, the transcriptional profiling data suggest that PH036 likely promotes thiol stress at both neutral and acidic pH, independent of modulating low molecular weight thiol synthesis in Mtb.

PH036 treatment of Mtb and *S. aureus* at acidic pH results in enhanced sensitivity to the compound relative to neutral pH (Table 5.1.). Previous work has shown that mycothiol pools

increase approximately two-fold at acidic pH (pH 5.5) (43). Intriguingly, the thiol pool assays performed in this work did not observe enhancement of thiol pools at acidic pH. This difference may be accounted for due to the previous study examining extended exposure to an acidic environment and using a more sensitive method of detection (43). Further Mtb promotes a reducing environment at acidic pH (Figure 4.1. D) (5). It is tempting to speculate that the enhanced sensitivity to PH036 at pH 5.7 in Mtb is the result of the combination of enhanced levels of mycothiol and a greater proportion of thiol pools being in a reduced (sulfhydryl) state that PH036 can covalently modify (Figure 5.8.), inhibiting their ability to be re-oxidized. This mechanism is supported based on the redox active GFP data indicating a reductive environment by PH036 treatment, the transcriptional profiling results indicating thiol and pH-dependent PH036-mediated enhanced reductive stress, and greater depletion of thiol pools at acidic pH relative to neutral pH. Alternatively, since we did not observe enhanced levels of free thiols at acidic pH, it is possible that the reductive intracellular environment is sufficient to maintain thiol pools in a reduced/susceptible state to PH036 (Figure 5.9.). This is possible because reduction of disulfides to thiols can be accomplished by NADPH or NADH, and higher levels of reducing equivalents by definition are referred to as reductive stress (33). However, higher levels of intracellular NADH or NADPH at acidic pH have not yet been directly observed despite the presence of reductive stress as indicated by the redox active GFP (5). Conversely, it is tempting to speculate that the previously reported increase in reduced mycothiol pools at acidic pH occurs by increasing the reductive pool while maintaining a balanced NAD(P)H/NAD(P)^+ ratio, though no changes in free thiols were observed during the time scales evaluated in this study (43). Therefore, using compounds like PH036 and other thiol-targeting molecules, may perturb the redox poise enough to disrupt the NAD(P)H/NAD(P)^+ ratio enhancing the proportion of reducing

equivalents, causing Mtb to engage additional means to oxidize reduced cofactors (e.g. *katG*, *narK2* and *narX* from the transcriptional profiling data).

In the absence of a canonical oxidative stress response, the upregulation of the multi-functional catalase/peroxidase *katG*, may be explained in part by oxidation activity of NADH to maintain redox balance and counteract PH036 activity (48). However, the reverse reaction of *katG* is also potentially detrimental to the cell as hydrogen peroxide is produced in the process of consuming reducing equivalents (33, 48). Further, upregulation of *katG* indicates enhanced susceptibility to the prodrug INH that is activated through the catalase/peroxidase. Indeed, we observe both enhanced accumulation of ROS and potentiation of INH when Mtb is treated with PH036. Finally, in light of the *sigH* regulon induction, cysteine synthesis is upregulated and can react with hydrogen peroxide (perhaps through *katG*-mediated production) driving oxidative stress via the Fenton reaction (49). As a result, the pathogen would not be able to adequately deal with oxidative stress at acidic pH, resulting in bacterial killing. Alternatively, the accumulation of ROS when Mtb is treated with PH036 may be the result of normal aerobic respiration and the pathogen is unable to defend against the oxidative stress due to the depletion of its thiol pools. Currently, it is unknown whether similar mechanisms may occur in *S. aureus* and additional experiments are needed.

The discovery of PH036 as a pH-dependent inhibitor of Mtb and *S. aureus* has facilitated the ability to probe Mtb thiol-mediated physiology and stress response at acidic pH. PH036 enhanced sensitivity at acidic pH may be the result of increased proportions of free thiols relative to oxidized disulfides through the generally reducing intracellular environment of Mtb at low pH. Perturbing Mtb intracellular redox poise and endogenous ROS has been proposed to be particularly detrimental relative to the related fast-growing saprophytic bacterium *M. smegmatis*

(38). Further, it has been shown that the total available redox buffers in *M. smegmatis* are approximately 4-fold higher than in slow-growing *Mycobacterium* sp (50). These results may partially explain the sensitivity of Mtb and relative resistance of *M. smegmatis* to PH036. The potential mechanism for PH036 suggests that the compound is likely generally thiol-reactive and would also target eukaryotic thiol pools. This possibility is highlighted with the cytotoxic effects of PH036 against eukaryotic macrophages (Table 5.2.). However, the eukaryotic cytotoxicity is likely the result of the R2 group of the compound and additional analogs of the J analog lacking the R2 moiety could be synthesized to improve activity against Mtb with diminished cytotoxic effects against mammalian cells. Further, in light of the known chemistry surrounding this scaffold, it may be possible to develop inhibitors of Mtb and *S. aureus* thiol pools that act as a pro-drug, resulting in activation only inside the bacterium.

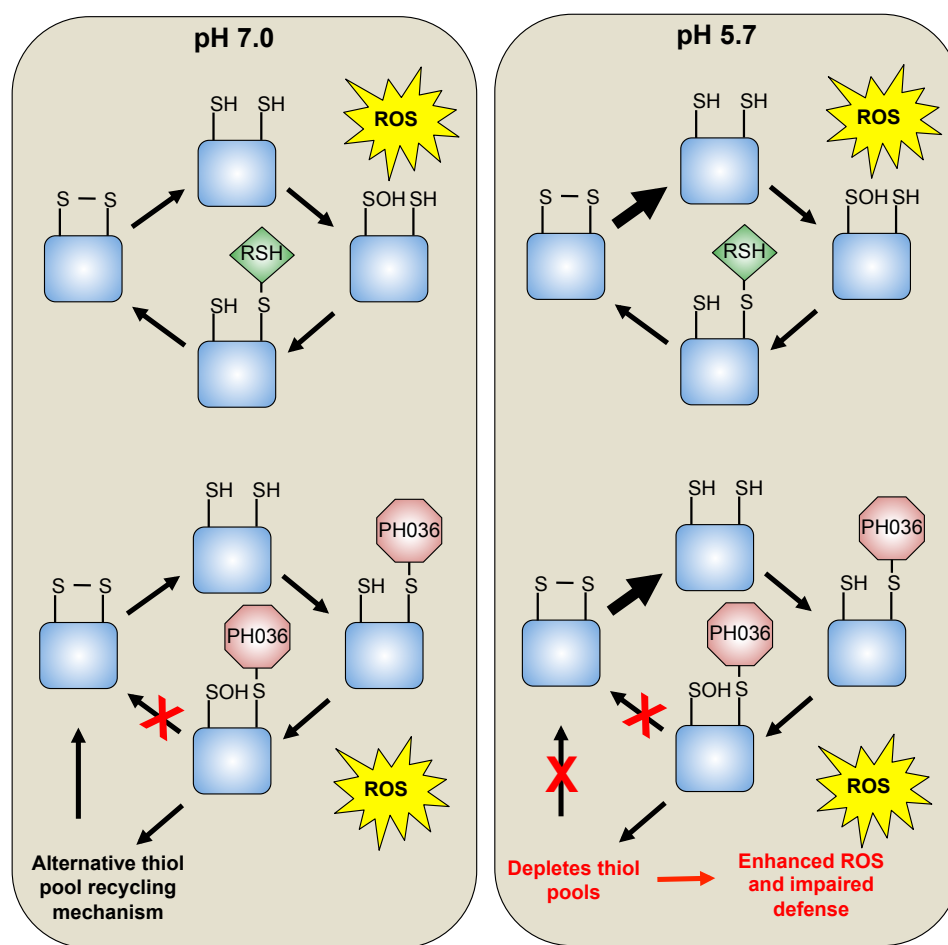


Figure 5.9. Speculative model for the mechanism of PH036. Normal responses of Mtb to reactive oxygen species (ROS) stress at neutral and acidic pH through recycling oxidized thiol pools via a low molecular weight thiol (RSH) and mycoredoxin/thioredoxin (not shown) to regenerate a disulfide bond (top half of models). At neutral pH (pH 7.0), PH036 depletes thiol pools but Mtb possesses the ability to maintain/regenerate thiol pools to defend against ROS. However, during acidic pH adaptation, Mtb promotes a reduced cytoplasm resulting in an enhanced ratio of reduced thiols to oxidized disulfides (larger black arrow). Treatment with PH036 depletes reduced thiol pools and Mtb is not able to maintain or regenerate intracellular thiol pools due to reductive stress. PH036 causes enhanced reductive stress at acidic pH through accumulation of reductants as thiol pools are depleted. As a result, Mtb is unable to defend against oxidative damage, leading to cell death. Figure was generated by Ben K Johnson.

APPENDIX

APPENDIX

Supplemental materials and methods

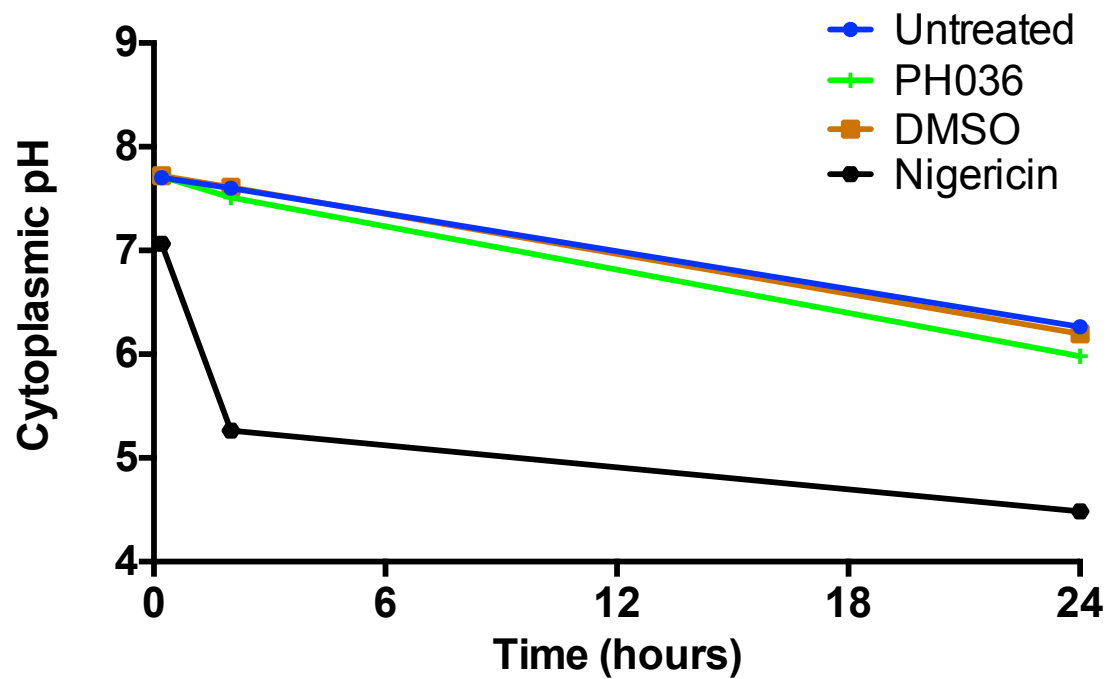


Figure S5.1. PH036 does not affect the cytoplasmic pH of *Mtb* at pH 5.7. Time-dependent changes to cytoplasmic pH. DMSO and nigericin are added as negative and positive controls. Data are representative of two independent experiments.

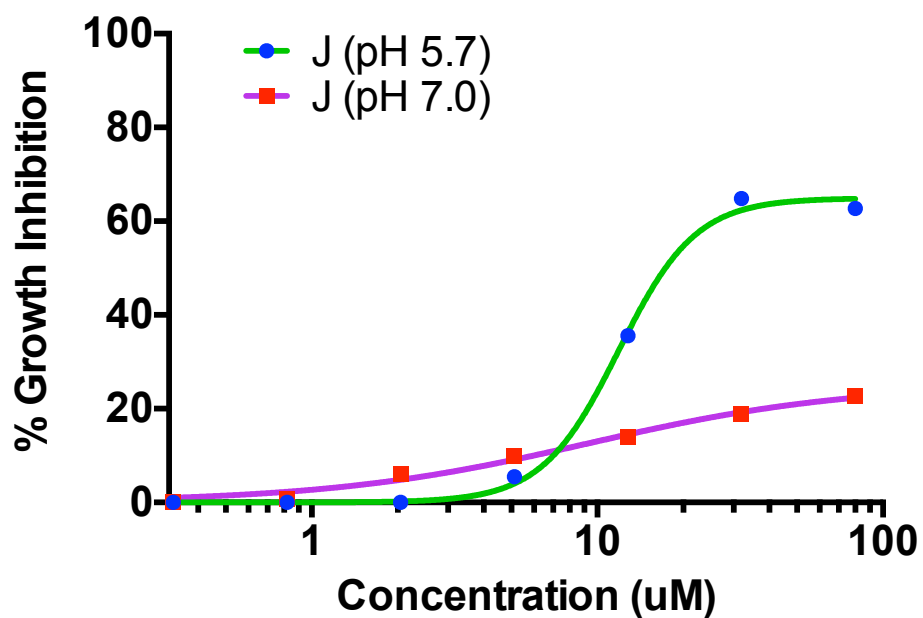


Figure S5.2. The J analog of PH036 represents the core chemical scaffold required for pH-dependent activity. Mtb was incubated in the presence of rich medium buffered to pH 7.0 or 5.7 in the presence of an 8-point dilution series (2.5-fold) ranging from 80 – 0.13 μM . At pH 5.7 the J analog retains pH-dependent activity in a dose-dependent manner. Data are representative of two independent experiments.

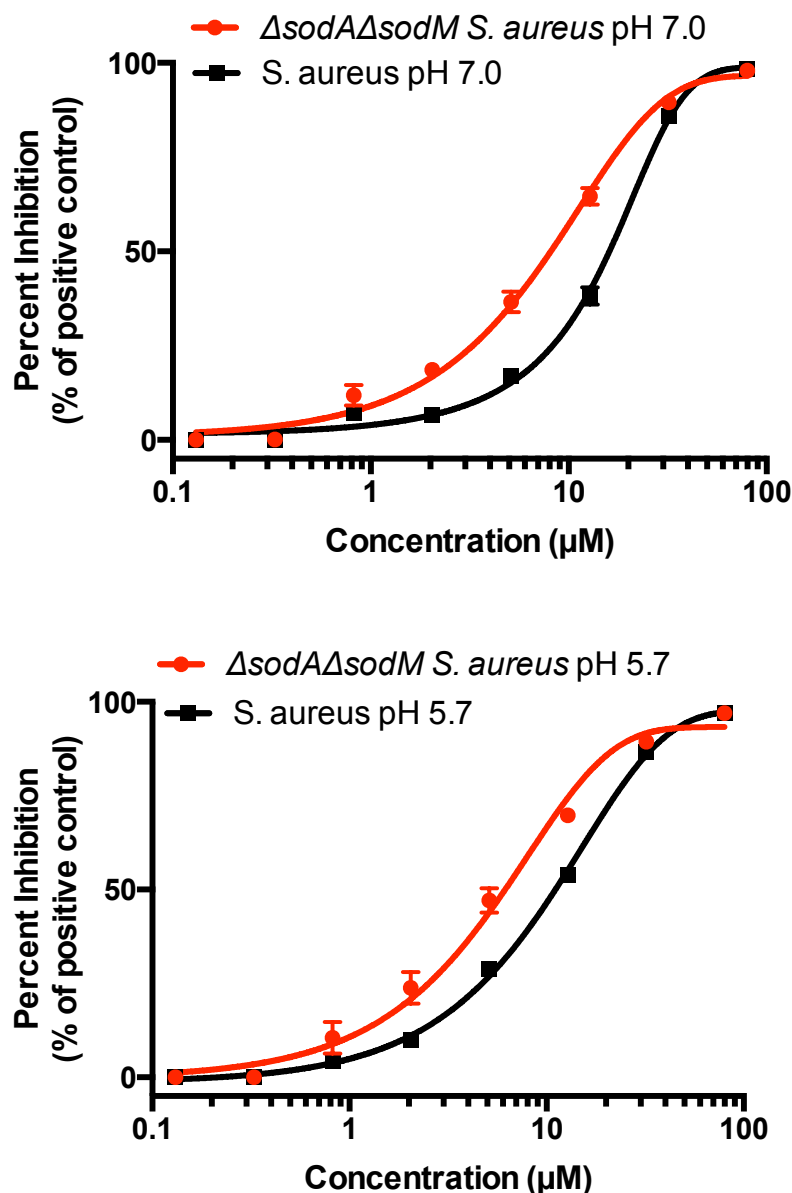


Figure S5.3. Superoxide dismutase deficient *S. aureus* exhibit enhanced sensitivity to PH036. *S. aureus* superoxide dismutase (SOD) deficient mutants and *S. aureus* wild-type strains were inoculated into rich medium buffered to pH 7.0 or pH 5.7 and incubated in the presence of an 8-point dilution series (2.5-fold) of PH036 ranging from 80 – 0.13 μM. SOD mutants exhibit a ~2-fold lower EC₅₀ compared to the wild-type strain.

REFERENCES

REFERENCES

1. **Paulson T.** 2013. Epidemiology: A mortal foe. *Nature* **502**:S2-3.
2. **WHO.** 2015. Global Tuberculosis Report.
3. **Boshoff HI, Barry CE, 3rd.** 2005. Tuberculosis - metabolism and respiration in the absence of growth. *Nat Rev Microbiol* **3**:70-80.
4. **Wayne LG, Sohaskey CD.** 2001. Nonreplicating persistence of mycobacterium tuberculosis. *Annu Rev Microbiol* **55**:139-163.
5. **Baker JJ, Johnson BK, Abramovitch RB.** 2014. Slow growth of *Mycobacterium tuberculosis* at acidic pH is regulated by *phoPR* and host-associated carbon sources. *Mol Microbiol* **94**:56-59.
6. **Betts JC, Lukey PT, Robb LC, McAdam RA, Duncan K.** 2002. Evaluation of a nutrient starvation model of *Mycobacterium tuberculosis* persistence by gene and protein expression profiling. *Mol Microbiol* **43**:717-731.
7. **Vandal OH, Nathan CF, Ehrt S.** 2009. Acid Resistance in *Mycobacterium tuberculosis*. *Journal of Bacteriology* **191**:4714-4721.
8. **Clemens DL.** 1996. Characterization of the *Mycobacterium tuberculosis* phagosome. *Trends Microbiol* **4**:113-118.
9. **Clemens DL, Horwitz MA.** 1995. Characterization of the *Mycobacterium tuberculosis* phagosome and evidence that phagosomal maturation is inhibited. *J Exp Med* **181**:257-270.
10. **Armstrong JA, Hart PD.** 1971. Response of cultured macrophages to *Mycobacterium tuberculosis*, with observations on fusion of lysosomes with phagosomes. *J Exp Med* **134**:713-740.
11. **Vergne I, Chua J, Lee HH, Lucas M, Belisle J, Deretic V.** 2005. Mechanism of phagolysosome biogenesis block by viable *Mycobacterium tuberculosis*. *Proc Natl Acad Sci U S A* **102**:4033-4038.
12. **Vergne I, Chua J, Deretic V.** 2003. *Mycobacterium tuberculosis* phagosome maturation arrest: selective targeting of PI3P-dependent membrane trafficking. *Traffic* **4**:600-606.

13. **Fratti RA, Chua J, Vergne I, Deretic V.** 2003. Mycobacterium tuberculosis glycosylated phosphatidylinositol causes phagosome maturation arrest. *Proc Natl Acad Sci U S A* **100**:5437-5442.
14. **Deretic V, Singh S, Master S, Harris J, Roberts E, Kyei G, Davis A, de Haro S, Naylor J, Lee HH, Vergne I.** 2006. Mycobacterium tuberculosis inhibition of phagolysosome biogenesis and autophagy as a host defence mechanism. *Cell Microbiol* **8**:719-727.
15. **Sturgill-Koszycki S, Schlesinger PH, Chakraborty P, Haddix PL, Collins HL, Fok AK, Allen RD, Gluck SL, Heuser J, Russell DG.** 1994. Lack of acidification in Mycobacterium phagosomes produced by exclusion of the vesicular proton-ATPase. *Science* **263**:678-681.
16. **MacMicking JD, Taylor GA, McKinney JD.** 2003. Immune control of tuberculosis by IFN-gamma-inducible LRG-47. *Science* **302**:654-659.
17. **Via LE, Fratti RA, McFalone M, Pagan-Ramos E, Deretic D, Deretic V.** 1998. Effects of cytokines on mycobacterial phagosome maturation. *J Cell Sci* **111 (Pt 7)**:897-905.
18. **Schaible UE, Sturgill-Koszycki S, Schlesinger PH, Russell DG.** 1998. Cytokine activation leads to acidification and increases maturation of Mycobacterium avium-containing phagosomes in murine macrophages. *J Immunol* **160**:1290-1296.
19. **Ramakrishnan L.** 2012. Revisiting the role of the granuloma in tuberculosis. *Nat Rev Immunol* **12**:352-366.
20. **Vandal OH, Pierini LM, Schnappinger D, Nathan CF, Ehrt S.** 2008. A membrane protein preserves intrabacterial pH in intraphagosomal *Mycobacterium tuberculosis*. *Nat Med* **14**:849-854.
21. **Raynaud C, Papavinasasundaram KG, Speight RA, Springer B, Sander P, Bottger EC, Colston MJ, Draper P.** 2002. The functions of OmpATb, a pore-forming protein of Mycobacterium tuberculosis. *Mol Microbiol* **46**:191-201.
22. **Via LE, Savic R, Weiner DM, Zimmerman MD, Prideaux B, Irwin SM, Lyon E, O'Brien P, Gopal P, Eum S, Lee M, Lanoix JP, Dutta NK, Shim T, Cho JS, Kim W, Karakousis PC, Lenaerts A, Nuermberger E, Barry CE, 3rd, Dartois V.** 2015. Host-Mediated Bioactivation of Pyrazinamide: Implications for Efficacy, Resistance, and Therapeutic Alternatives. *ACS Infect Dis* **1**:203-214.

23. **Prideaux B, Via LE, Zimmerman MD, Eum S, Sarathy J, O'Brien P, Chen C, Kaya F, Weiner DM, Chen PY, Song T, Lee M, Shim TS, Cho JS, Kim W, Cho SN, Olivier KN, Barry CE, 3rd, Dartois V.** 2015. The association between sterilizing activity and drug distribution into tuberculosis lesions. *Nat Med* **21**:1223-1227.
24. **Cannon MB, Remington SJ.** 2006. Re-engineering redox-sensitive green fluorescent protein for improved response rate. *Protein Sci* **15**:45-57.
25. **Hanson GT, Aggeler R, Oglesbee D, Cannon M, Capaldi RA, Tsien RY, Remington SJ.** 2004. Investigating mitochondrial redox potential with redox-sensitive green fluorescent protein indicators. *Journal of Biological Chemistry* **279**:13044-13053.
26. **Rohde KH, Abramovitch RB, Russell DG.** 2007. *Mycobacterium tuberculosis* invasion of macrophages: linking bacterial gene expression to environmental cues. *Cell Host Microbe* **2**:352-364.
27. **Johnson BK, Scholz MB, Teal TK, Abramovitch RB.** 2016. SPARTA: Simple Program for Automated reference-based bacterial RNA-seq Transcriptome Analysis. *BMC Bioinformatics* **17**:1-4.
28. **Johnson BK, Abramovitch RB.** 2015. Macrophage Infection Models for *Mycobacterium tuberculosis*. *Methods Mol Biol* **1285**:329-341.
29. **Saini V, Cumming BM, Guidry L, Lamprecht DA, Adamson JH, Reddy VP, Chinta KC, Mazorodze JH, Glasgow JN, Richard-Greenblatt M, Gomez-Velasco A, Bach H, Av-Gay Y, Eoh H, Rhee K, Steyn AJ.** 2016. Ergothioneine Maintains Redox and Bioenergetic Homeostasis Essential for Drug Susceptibility and Virulence of *Mycobacterium tuberculosis*. *Cell Rep* **14**:572-585.
30. **Li XZ, Zhang L, Nikaido H.** 2004. Efflux Pump-Mediated Intrinsic Drug Resistance in *Mycobacterium smegmatis*. *Antimicrobial Agents and Chemotherapy* **48**:2415-2423.
31. **Manganelli R, Voskuil MI, Schoolnik GK, Dubnau E, Gomez M, Smith I.** 2002. Role of the extracytoplasmic-function sigma factor sigma(H) in *Mycobacterium tuberculosis* global gene expression. *Mol Microbiol* **45**:365-374.
32. **Nambi S, Long JE, Mishra BB, Baker R, Murphy KC, Olive AJ, Nguyen HP, Shaffer SA, Sassetti CM.** 2015. The Oxidative Stress Network of *Mycobacterium tuberculosis* Reveals Coordination between Radical Detoxification Systems. *Cell Host Microbe* **17**:829-837.
33. **Farhana A, Guidry L, Srivastava A, Singh A, Hondalus MK, Steyn AJC.** 2010. Reductive Stress in Microbes: Implications for Understanding *Mycobacterium*

- tuberculosis Disease and Persistence. *Advances in Microbial Physiology*, Vol 57 **57**:43-117.
34. **Tan MP, Sequeira P, Lin WW, Phong WY, Cliff P, Ng SH, Lee BH, Camacho L, Schnappinger D, Ehrt S, Dick T, Pethe K, Alonso S.** 2010. Nitrate respiration protects hypoxic *Mycobacterium tuberculosis* against acid- and reactive nitrogen species stresses. *PLoS One* **5**:e13356.
 35. **Boshoff HI, Myers TG, Copp BR, McNeil MR, Wilson MA, Barry CE, 3rd.** 2004. The transcriptional responses of *Mycobacterium tuberculosis* to inhibitors of metabolism: novel insights into drug mechanisms of action. *J Biol Chem* **279**:40174-40184.
 36. **Timmins GS, Deretic V.** 2006. Mechanisms of action of isoniazid. *Mol Microbiol* **62**:1220-1227.
 37. **Lechartier B, Cole ST.** 2015. Mode of Action of Clofazimine and Combination Therapy with Benzothiazinones against *Mycobacterium tuberculosis*. *Antimicrob Agents Chemother* **59**:4457-4463.
 38. **Tyagi P, Dharmaraja AT, Bhaskar A, Chakrapani H, Singh A.** 2015. *Mycobacterium tuberculosis* has diminished capacity to counteract redox stress induced by elevated levels of endogenous superoxide. *Free Radical Biology and Medicine* **84**:344-354.
 39. **Masip L, Veeravalli K, Georgiou G.** 2006. The many faces of glutathione in bacteria. *Antioxid Redox Signal* **8**:753-762.
 40. **Newton GL, Rawat M, La Clair JJ, Jothivasan VK, Budiarto T, Hamilton CJ, Claiborne A, Helmann JD, Fahey RC.** 2009. Bacillithiol is an antioxidant thiol produced in Bacilli. *Nat Chem Biol* **5**:625-627.
 41. **Newton GL, Arnold K, Price MS, Sherrill C, Delcardayre SB, Aharonowitz Y, Cohen G, Davies J, Fahey RC, Davis C.** 1996. Distribution of thiols in microorganisms: mycothiol is a major thiol in most actinomycetes. *J Bacteriol* **178**:1990-1995.
 42. **Harbut MB, Vilcheze C, Luo X, Hensler ME, Guo H, Yang B, Chatterjee AK, Nizet V, Jacobs WR, Jr., Schultz PG, Wang F.** 2015. Auranofin exerts broad-spectrum bactericidal activities by targeting thiol-redox homeostasis. *Proc Natl Acad Sci U S A* **112**:4453-4458.
 43. **Buchmeier NA, Newton GL, Fahey RC.** 2006. A mycothiol synthase mutant of *Mycobacterium tuberculosis* has an altered thiol-disulfide content and limited tolerance to stress. *J Bacteriol* **188**:6245-6252.

44. **Lu J, Holmgren A.** 2014. The thioredoxin antioxidant system. *Free Radic Biol Med* **66**:75-87.
45. **Moon Y-C, Baiazitov R, Du W, Lee C-S, Hwang S, Almstead N.** 2013. Chemoselective Reactions of 4,6-Dichloro-2-(methylsulfonyl)pyrimidine and Related Electrophiles with Amines. *Synthesis* **45**:1764-1784.
46. **Bebbington D, Binch H, Charrier J-D, Everitt S, Fraysse D, Golec J, Kay D, Knegtel R, Mak C, Mazzei F, Miller A, Mortimore M, O'Donnell M, Patel S, Pierard F, Pinder J, Pollard J, Ramaya S, Robinson D, Rutherford A, Studley J, Westcott J.** 2009. The discovery of the potent aurora inhibitor MK-0457 (VX-680). *Bioorganic & Medicinal Chemistry Letters* **19**:3586-3592.
47. **Antelmann H, Helmann JD.** 2011. Thiol-based redox switches and gene regulation. *Antioxid Redox Signal* **14**:1049-1063.
48. **Singh R, Wiseman B, Deemagarn T, Donald LJ, Duckworth HW, Carpena X, Fita I, Loewen PC.** 2004. Catalase-peroxidases (KatG) exhibit NADH oxidase activity. *J Biol Chem* **279**:43098-43106.
49. **Park S, Imlay JA.** 2003. High levels of intracellular cysteine promote oxidative DNA damage by driving the fenton reaction. *J Bacteriol* **185**:1942-1950.
50. **Ung KS, Av-Gay Y.** 2006. Mycothiol-dependent mycobacterial response to oxidative stress. *FEBS Lett* **580**:2712-2716.

CHAPTER 6 – Development of the computational analysis programs SPARTA and HAARP for evaluation of RNA-sequencing and high-throughput screening data

The SPARTA software presented in this chapter has been published previously:

Johnson, B.K., Scholz, M.B., Teal, T.K., Abramovitch, R.B. (2016). SPARTA: Simple Program for Automated reference-based bacterial RNA-seq Transcriptome Analysis. ***BMC Bioinformatics*** 17:66 doi: 10.1186/s12859-016-0923-y

Preface

High-throughput approaches to interrogate biological systems have become widely used in research and teaching laboratories. As a result, data intensive biology approaches require computational tools capable of analyzing the large data sets produced from these types of experiments. However, advanced bioinformatics training is required to use many of the existing analysis tools, in addition to the requirement for computer hardware not commonly found in traditional laboratories. Thus, turn-key, easy to use software packages that can be executed on personal and high performance computers and tailored to a researcher's specific needs are both lacking and necessary. Accessible bioinformatics software, such as the programs presented in this chapter, can enable researchers to take full advantage of high-throughput experimental methods, such as RNA-sequencing and high-throughput screening (HTS) of small molecule libraries.

High-throughput RNA-sequencing (RNA-seq) is a next generation sequencing (NGS) method to characterize the microbial transcriptome, such as global changes in transcript abundance, operon architecture, transcriptional start sites, and expression of untranslated regions.

A common use for bacterial RNA-seq is to identify changes in gene expression between experimental conditions. However, going from raw sequencing reads to a table of differentially expressed genes requires several bioinformatics tools assembled into a workflow to analyze the data. This is not a trivial endeavor as hundreds of tools filling both general and niche use cases have been developed for each step in the analysis, underscoring the necessity for stand-alone, easy to use workflows. Thus, I developed the Simple Program for Automated reference-based bacterial RNA-seq Transcriptome Analysis (SPARTA). SPARTA seeks to provide a platform independent, easy-to-use software package capable of analyzing raw bacterial RNA-seq reads and identify differentially expressed genes on a personal or high performance computer.

With antibiotic resistance on the rise, it is imperative to identify novel targets and compounds alike. HTS drug discovery programs often screen thousands of small molecules to identify candidate compounds to be developed into a potential drug for clinical use. The resulting data set from the primary and counter-screens typically require the user to normalize the data, score and visualize positive hits, and cross-reference multiple databases to provide a more complete picture. Notably, the HTS data set is often large, exceeding the capacity of common spreadsheet software and prohibiting manual curation. Thus, I developed the High-throughput screening Automated Analysis and Retrieval of Putative hits (HAARP) software. This workflow was designed to rapidly and efficiently analyze HTS data produced by our laboratory. HAARP provides a platform to analyze any number of HTS data files in an automated fashion, producing diagnostic plots and tables containing positive hit information pooled from a variety of additional databases.

SPARTA: Simple Program for Automated reference-based bacterial RNA-seq Transcriptome Analysis

Abstract

Background: Many tools exist in the analysis of bacterial RNA sequencing (RNA-seq) transcriptional profiling experiments to identify differentially expressed genes between experimental conditions. Generally, the workflow includes quality control of reads, mapping to a reference, counting transcript abundance, and statistical tests for differentially expressed genes. In spite of the numerous tools developed for each component of an RNA-seq analysis workflow, easy-to-use bacterially oriented workflow applications to combine multiple tools and automate the process are lacking. With many tools to choose from for each step, the task of identifying a specific tool, adapting the input/output options to the specific use-case, and integrating the tools into a coherent analysis pipeline is not a trivial endeavor, particularly for microbiologists with limited bioinformatics experience.

Results: To make bacterial RNA-seq data analysis more accessible, we developed a Simple Program for Automated reference-based bacterial RNA-seq Transcriptome Analysis (SPARTA). SPARTA is a reference-based bacterial RNA-seq analysis workflow application for single-end Illumina reads. SPARTA is turnkey software that simplifies the process of analyzing RNA-seq data sets, making bacterial RNA-seq analysis a routine process that can be undertaken on a personal computer or in the classroom. The easy-to-install, complete workflow processes whole transcriptome shotgun sequencing data files by trimming reads and removing adapters, mapping reads to a reference, counting gene features, calculating differential gene expression, and,

importantly, checking for potential batch effects within the data set. SPARTA outputs quality analysis reports, gene feature counts and differential gene expression tables and scatterplots.

Conclusions: SPARTA provides an easy-to-use bacterial RNA-seq transcriptional profiling workflow to identify differentially expressed genes between experimental conditions. This software will enable microbiologists with limited bioinformatics experience to analyze their data and integrate next generation sequencing (NGS) technologies into the classroom. The SPARTA software and tutorial are available at sparta.readthedocs.org.

Background

One of the most common applications of RNA sequencing (RNA-seq) is to identify differentially expressed genes under differing experimental conditions. Before biological insights can be gained, one must process and analyze the large datasets generated from each sequencing experiment. Each sample contains millions of reads that must be trimmed and assessed for read quality, mapped back to a reference genome (or assembled *de novo* in the absence of a reference), counted for transcript abundance, and tested for differential gene expression. Many computational analysis tools have been developed specifically to work with RNA-seq data; however, a single tool is often not suitable and requires several different applications assembled into a workflow. This task can be complicated as both the tool choice and input and output file formats for a given tool need to be considered and potentially modified to meet the requirements for the subsequent analysis step. Several RNA-seq analysis workflows exist, however, most are designed for eukaryotic organisms (1-11). The goal of this work is to assemble several open-source computational tools to deliver a complete, accessible, and easy-to-use reference-based

bacterial RNA-seq analysis workflow that is amenable to both the research laboratory and undergraduate classroom.

Implementation

The SPARTA workflow (Figure 6.1.) is implemented utilizing Python for file input/output management and tool execution, combining several open-source computational tools. The SPARTA workflow analyzes data by: conducting read trimming and adapter removal with Trimmomatic (12); performing quality analysis of the data sets with FastQC (13); mapping the reads to the reference with Bowtie (14); counting transcript or gene feature abundance with HTSeq (15); and, analyzing differential gene expression with edgeR (16-18). Within the differential gene expression analysis step, batch effects can be detected and the user is warned that potentially unintended variables need to be considered. If left unaccounted for, batch effects can significantly skew the results of the data analysis, leading to inappropriate experimental conclusions (19). Following analysis, SPARTA outputs quality analysis reports, gene feature counts and differential gene expression tables and scatterplots.

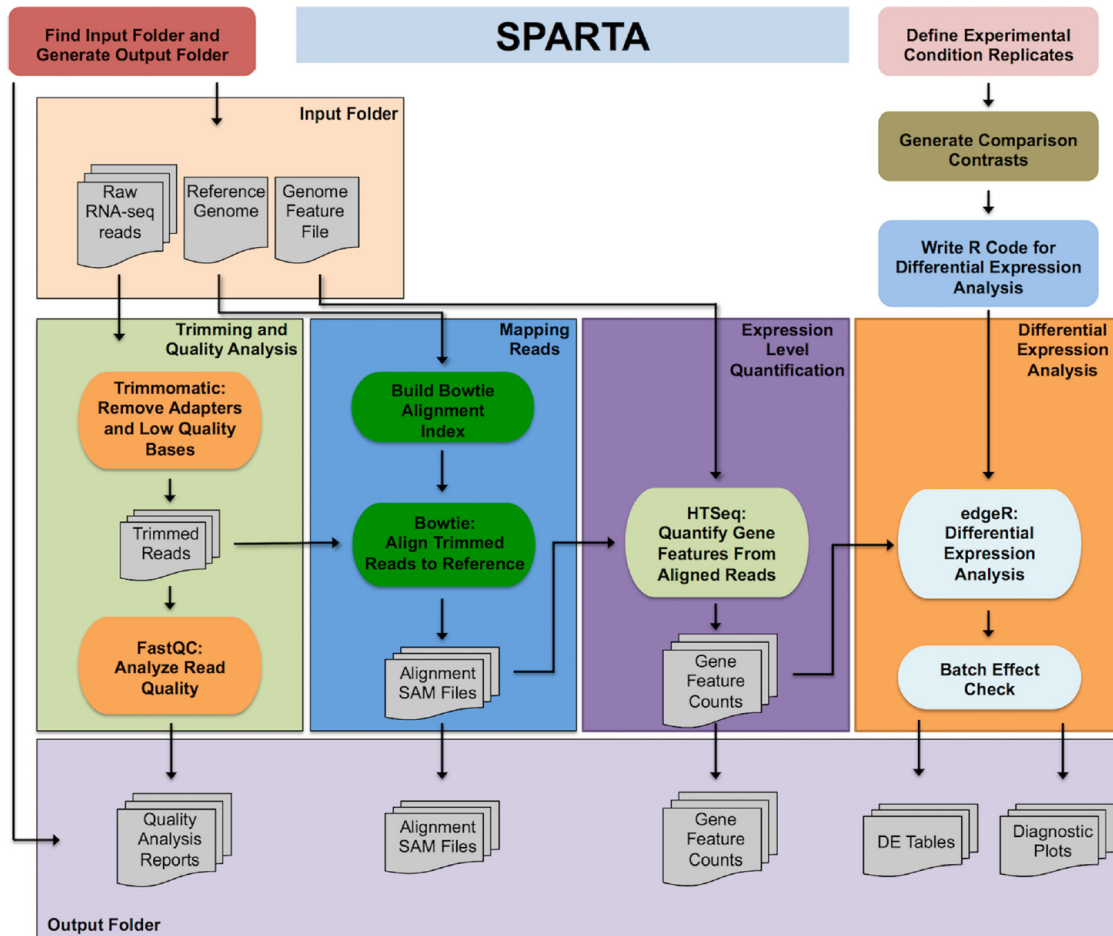


Figure 6.1. SPARTA workflow diagram. Single-end Illumina FASTQ files, a FASTA formatted reference genome, and genome feature file (GFF or GTF) are given as inputs to the workflow. Trimmomatic and FastQC perform trimming of adapters and low quality bases/reads and quality assessment reports, respectively. Bowtie maps the trimmed reads to the reference. HTSeq quantifies transcript abundance. R/edgeR tests for statistically significant genes and warns the user of potential batch effects present in the analyzed data set.

SPARTA requires Python 2, NumPy (a Python library for numerical analyses), Java and R. Once Python is installed, the user initializes SPARTA, which then checks for the necessary dependencies at runtime. If any of these dependencies are not met, SPARTA informs the user of the missing components. To reduce complex software installation, SPARTA is distributed with the required software and an online tutorial (sparta.readthedocs.org) guides the user through installation and data analysis procedures for each operating system platform. The workflow maintains analytic flexibility for specific use cases by allowing the user to tailor the options utilized for each analysis step, but can proceed without requiring option specification. Further, SPARTA will write the necessary R commands at runtime and will generate the appropriate contrasts to test all possible comparisons between user defined experimental conditions. The workflow is distributed with an example data set containing the first 100,000 reads from a previously published study (20). This data set is included to allow the user to become rapidly familiarized with the analysis procedure as well as ensure the appropriate dependencies are met.

Each stage of the analysis requires choices to be made regarding which tool will meet the user and analysis needs. For SPARTA, a variety of tools were considered and tested for each analysis step to specifically suit bacterial RNA-seq differential gene expression analysis and reduce dependency requirements. Trimmomatic is a Java-based tool and was chosen for adapter removal and read trimming as it is widely utilized throughout NGS applications, including bacterial RNA-seq. The computationally efficient methodology implemented to identify adapters and low quality reads allows the tool to be executed on a personal computing platform but can scale to multi-processor systems. FastQC is a lightweight Java application that subsets each sample file and can predictively extrapolate and identify a variety of putative read quality issues for the full sample data set. Bowtie is an analytically flexible and complex read alignment tool

that implements a Burrows-Wheeler transform of the reference genome to rapidly align experimental reads to the reference in a memory-efficient manner. Bowtie and Bowtie2 are similar tools, though the latter is capable of identifying gapped alignments while Bowtie cannot. However, Bowtie is better suited to efficiently align short (50 base pair) Illumina reads than Bowtie2. Further, the 50 base pair sequencing methodology is arguably the most common and inexpensive methodology for reference-based bacterial RNA-seq, suggesting that Bowtie is the optimal choice for the initial releases of SPARTA. Bowtie has been recompiled from source with the MAXBITS flag set to 64 for legacy support of Mac OSX systems (10.6+) and eliminate the need for the end user to have a C compiler installed on their machines. HTSeq is a flexible, Python-based NGS read analysis framework that provides a robust transcript abundance counting feature that has been established to be sensitive and fast for post-processing of read alignment files. Further, the output is an informative, two-column text file that can readily be read by statistical analysis packages to identify genes differentially expressed within a given experimental condition.

Differential gene expression analysis for RNA-seq currently utilizes two common packages within the statistical programming language R: edgeR and DESeq(2). RNA-seq reads are non-normally distributed requiring alternative considerations and are thus modeled using a variation of the Poisson distribution termed the negative binomial distribution. A recent publication analyzing 48 replicates per condition allowed the authors to visualize read distributions due to the high number of replicates, revealing that the negative binomial distribution is indeed an appropriate representation of RNA-seq read count data (21). Further, the authors were able to rigorously test both edgeR and DESeq(2) to determine whether underlying assumptions in each package led to more appropriate approximation of dispersion estimates for

each gene (22). With RNA-seq experiments still being reasonably expensive, replicate numbers often tend to be low, thus the way the gene-wise variance/dispersion estimates are made impact the ability to delineate statistically significant differences. For instance, if a few genes in one biological replicate are significantly different compared to another biological replicate, the variance will be large and must be modeled in a way to account for the increased dispersion while maintaining that they belong to the same biological condition in order to make any sort of subsequent inference regarding differential expression between experimental conditions. Taken together, edgeR was deemed the best approach because the model attempts to squeeze each gene towards a common dispersion calculated across all genes (21, 22). As a result, edgeR was chosen as the preferred package for differential gene expression analysis in the SPARTA workflow. Specifically, SPARTA takes advantage of the generalized linear model functionality in edgeR to allow for n-possible comparisons between conditions through contrast specification.

The ability to dynamically account for any number of biological and technical replicates is a necessary component to maintain analytical flexibility and ease-of-use for SPARTA. This plasticity can become further complicated during the differential gene expression step as the total number of replicates per condition may vary. To overcome this complexity, SPARTA implements a contrast matrix generator that allows for all possible comparisons to be made between experimental conditions, accounting for n-replicates per condition. Further, the contrast matrix only allows possible comparisons between non-reference conditions as the default behavior of edgeR allows for straightforward comparisons between a reference and experimental conditions through coefficient specification via the design matrix. Specifically, defining the comparison coefficient that corresponds to a given experimental condition within the design matrix relative to the reference condition is achieved by iterating over the matrix specifying the test value in a 1

+ n implementation where n represents the experimental condition matrix coefficient. If there exists more than two total conditions (e.g. reference and experimental), the contrast matrix generator will apply a series of equations, iterating over the list of user-defined experimental conditions. If we define $\varphi > M; M = \mathbb{Z} > 2$ and $\psi = N; N = 2$ and $\tau = P; P = 0$, we can dynamically construct the contrast matrix dimensions based on n-possible comparisons between experimental conditions (Equation 6.1.)

$$\left(\psi \neq \varphi \rightarrow \begin{matrix} \tau = \tau + \varphi - \psi \\ \psi + 1 \end{matrix} \right) \wedge (\psi = \varphi \rightarrow \tau > P)$$

Equation 6.1.

Further, if we let the list of weighted experimental conditions be $C = a_1\theta_1 + \dots + a_i\theta_i = 0$ it can be extended to represent the contrast vector for each comparison between condition θ_{i-1} and θ_i where $3 \geq i \leq \varphi$. Generally, the contrast vector C can be defined as Equation 4.2.

$$C = \sum_{i=1}^{\varphi} a_i\theta_i ; \text{where } \sum_{i=1}^{\varphi} a_i = 0$$

Equation 6.2.

Finally, SPARTA produces a matrix of contrast coefficients that can be expressed as $A_{\varphi,\tau}$ (Equation 6.3.). This matrix is then passed to R for generating the appropriate tests for significant differentially expressed genes between n-possible experimental conditions.

$$A = \begin{bmatrix} C_{1,1} & \cdots & C_{1,\varphi} \\ \vdots & \ddots & \vdots \\ C_{\tau,1} & \cdots & C_{\tau,\varphi} \end{bmatrix}$$

Equation 6.3.

Batch effects can be defined as additional confounding variables that are unrelated to the experimental variables being measured and can significantly skew the data, potentially leading to inappropriate conclusions regarding the biological phenomena being

observed. A common batch effect observed in RNA-seq data is that of time-dependent clustering of experimental measurements. As an example, if a sequencing library is generated on one day and another biological replicate library is made the following day, a time-dependent batch effect will likely be introduced into the experiment due to the nature of NGS sequencing methodology. In an effort to resolve and warn researchers of potential batch effects present within an RNA-seq experiment, SPARTA utilizes the multi-dimensional scaling (MDS) plot generated during the differential gene expression analysis step in edgeR. Specifically, SPARTA will test all possible pairwise comparisons for batch effects through a dynamic decision-making algorithm (Equation 6.4) post-MDS clustering. If a putative batch effect is detected, SPARTA generates a warning regarding the specific pairwise comparison and that significantly differentially regulated genes should be interpreted with caution. If we let the matrix of leading log-fold change cluster coefficients be defined as $\mathbf{B}_{\gamma,\delta}$ and the first experimental condition within the matrix as $\theta_{\gamma,\delta}$ and the second experimental condition of the pairwise comparison as $\vartheta_{\gamma,\delta}$, we can construct the dynamic decision-making algorithm by iterating over the matrix and extracting the initial biological replicate of each condition producing β the binary result (e.g. True [β_T] or False [β_F]). The assumption made is that if a batch effect is present, it will be resolved across all replicates as represented by the first replicate per condition.

$$\beta(\theta_{\gamma,\delta}, \vartheta_{\gamma,\delta}) = (sgn\theta_{\gamma,\delta} \neq sgn\vartheta_{\gamma,\delta} \rightarrow \beta_F) \wedge (sgn\theta_{\gamma,\delta} = sgn\vartheta_{\gamma,\delta} \rightarrow \beta_T)$$

Equation 6.4.

Results and Discussion

RNA-seq transcriptional profiling is becoming increasingly routine, and there is a demand for applications such as SPARTA that enable stand-alone workflows. Though several bacterial RNA-seq analysis workflows have been developed (4, 5, 11), SPARTA is currently the only workflow capable of addressing the possibility of batch effects within the data set as well as the other necessary analysis procedures to identify differentially expressed genes. Using a previously published data set (20), SPARTA was capable of analyzing 4 experimental conditions containing 8 samples with approximately 30 million reads per sample in 4 hours on an off-the-shelf iMac computer (8 GB RAM, Intel i5 2.7GHz quad-core processor). SPARTA can also be implemented in high performance computing environments utilizing the non-interactive mode functionality.

SPARTA is capable of analyzing data in both interactive and non-interactive modes. To initiate non-interactive data analysis, one can run the option `--noninteractive`. However to execute the analysis, the user is required to specify the desired options in a configuration file (`ConfigFile.txt`). SPARTA will read in the configuration file and perform the analysis with the given options specified. Such an operation is amenable to high-performance computing environments as the user may not want to perform the analysis on a personal computer due to a variety of factors including: hardware, hard disk space, and the size of the data. The recommended distribution of SPARTA for high-performance computing (HPC) execution is `SPARTA_Linux` as most HPC systems are Linux-based. To take advantage of multi-processor systems, it is necessary that the user define the number of processors required and threads to be utilized within the configuration file. The specifics of running SPARTA non-interactively on a multiprocessor system are detailed in the online tutorial.

As NGS technologies and applications continue to permeate life science research, undergraduate education must incorporate the use of contemporary sequencing techniques to address biological questions. However, despite the rapid increase in data intensive experimental biology, undergraduates receiving a life sciences degree are often not exposed to the tools and basic computational skills required to study NGS data sets. To address this shortcoming, we have developed an online tutorial to guide students through the RNA-seq analysis process (sparta-teaching.readthedocs.org). The SPARTA teaching tool was integrated into a senior level genomics course and successfully engaged students in the theory and application of RNA-seq data analysis. SPARTA can provide educators an opportunity to incorporate bacterial RNA-seq into the classroom in a practical, straightforward method to expose students to basic computational skills and contemporary sequencing applications to address biological questions. To aid in this process, the teaching website (sparta-teaching.readthedocs.org) provides a brief overview of RNA-seq technology and analysis, with basic details of the tools incorporated into SPARTA.

SPARTA and Rockhopper2 are both bacterial RNA-seq workflows that provide similar features (5). An execution time comparison was conducted between the two platforms. SPARTA was executed with default parameters and Rockhopper2 was tested with default parameters, verbose output, SAM output, and operon and untranslated region identification turned off. Further, the Rockhopper2 cache was cleared before each test to mimic an initial analysis. When SPARTA was compared to Rockhopper2 for execution time, SPARTA exhibited greater scalability (Figure 6.2.). Therefore, differentiating features of SPARTA as compared to Rockhopper2 include: improved scalability; incorporation of trimming and quality control of reads; and, a check for potential batch effects within the data set. Notably, Rockhopper2 provides

additional functions not provided by SPARTA, such as operon analysis, definition of untranslated regions, and files for visualization of the results in a genome browser.

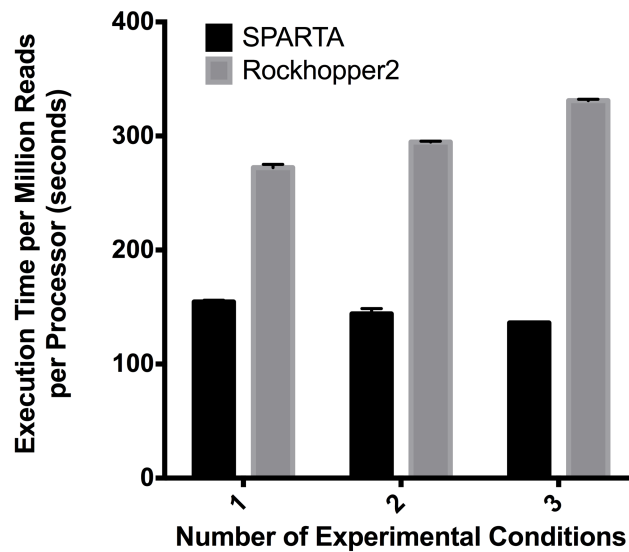


Figure 6.2. Data analysis execution time comparison between SPARTA and Rockhopper2.

The two programs were compared for execution time when processing *one*, *two*, or *three* experimental conditions as compared to a reference condition. Both SPARTA (1.0) and Rockhopper2 (2.03) were installed and tested on an off-the-shelf iMac (2.7 GHz i5, 8 GB memory, OSX 10.11.2). Dependencies: Java (1.6.0_65), Python (2.7.9), and R (3.2.2). Data are the mean of three software executions and *error bars* represent the standard deviation. Data files (100,000 reads/file) utilized were the example data bundled with SPARTA.

Future Directions and Functionality

Additional features and functionality that will be into future releases of SPARTA are listed below and will be updated at <http://sparta.readthedocs.org/en/latest/wishlist.html>. Further, to become involved into the active development of SPARTA, the current state of the code base and feature development can be found on GitHub through <http://sparta.readthedocs.org> under the “Contribute” heading. Future releases of SPARTA will include, but is not limited to: 1) automated batch effect correction, 2) additional input file format support, 3) paired-end reads support, 4) read mapping output with normalized expression values, 5) operon analysis and definition of untranslated regions, 6) files for visualization in common genome browsers, and 7) reference-free transcriptome analysis.

Conclusions

SPARTA is a bacterial RNA-seq analysis tool capable of taking raw Illumina reads to differentially expressed genes in a turn-key, stand-alone workflow format that takes advantage of existing state of the art analysis tools and warns the user of potential batch effects. By reducing the required computational proficiency to perform transcriptional profiling experiments using RNA-seq, SPARTA can enable microbiologists to accelerate their research and provide instructors the ability to incorporate a hands-on approach to NGS technologies in the classroom. Further, SPARTA maintains analytic flexibility by allowing the user to tailor the analysis through option specification but is capable of proceeding with default values.

HAARP: High-throughput screening Automated Analysis and Retrieval of Putative hits

Abstract

Background: High throughput screening (HTS) approaches cast a wide net to identify novel therapeutics against a specific malady, often screening thousands of compounds. Thus, the data sets produced from a HTS even if only one metric is measured, are large. Typical spreadsheet programs like Excel are insufficient to adequately analyze the data in an efficient manner. This shortcoming can be addressed through development and implementation of a computational workflow composed of an HTS specific set of analytic functions to automate data analysis in an unbiased manner.

Results: To accelerate data analysis of HTS efforts within the Abramovitch laboratory, I developed the High-throughput screening Automated Analysis and Retrieval of Putative hits (HAARP) software suite. HAARP is a standalone, custom analysis suite meant to rapidly assess HTS data from primary hits to follow-up secondary assays, as well as prepare the entire screening data set for submission to publically curated databases such as PubChem. HAARP is a computational workflow composed of a series of modularized analytic functions necessary to normalize the dataset, score positive hits, query additional databases for additional hit information, output diagnostic plots for visualization, and output analysis tables that can be opened in spreadsheet software packages.

Conclusions: HAARP provides an all-in-one analysis suite to analyze HTS data within the Abramovitch laboratory. Through automating the process, any number of data sets can be

analyzed and assessed in an efficient, unbiased manner. This software suite has enabled the ability to spend less time on data analysis and concentrate efforts on additional biological characterization of lead compounds.

Background

As bacterial antibiotic resistance continues to rise and few new antimicrobials are developed, novel approaches to treating bacterial infections are necessary. Conventional antimicrobial discovery campaigns often seek to identify small molecules that are bactericidal or bacteriostatic and are typically performed *in vitro*. However, many targets required for pathogenesis are only required *in vivo*. Compounds that inhibit *in vivo* essential targets are known as antivirulence therapies. Treatment of *Mycobacterium tuberculosis* (Mtb) infections requires a four-drug regimen for 6-9 months for antibiotic susceptible Mtb, and 24 months or longer for resistant strains. We sought to identify compounds that inhibit *in vivo* required adaptation pathways, potentially shortening the course of treatment when utilized as an adjunct therapy with current frontline drugs. We screened greater than 500,000 compounds, representing broad chemical diversity for inhibitors of adaptation pathways as well as general inhibitors of Mtb growth. The details regarding the screen are significantly expanded upon in Chapter 2. Manually curating the data from each of the high-throughput screens would require a significant time investment. Further, during the course of analyzing the data, one may inadvertently bias the data due to a dynamic decision as to what constitutes a positive hit. Through systematic data analysis using automation, the ability to efficiently, reproducibly, and consistently approach each step in calling positive hits for subsequent biological characterization is achieved. Thus, the goal

of this work was to develop and implement a series of functions to efficiently analyze the large data sets produced by each of the screens.

Implementation

Workflow procedure

The HAARP software suite is implemented in Python 2 and requires built-in libraries as well as the plotting library, Matplotlib. Generally, the analysis procedure is as follows: read in raw data files containing fluorescence and growth (optical density; OD₅₉₅) values, data normalization, positive hit filtering and binning, and export color-coded scatter plots for visualization (Figure 6.4.) and comma separated files containing the pertinent hit information. Raw data is converted from the plate-reader format to nested list data structures and iteratively examined following the aforementioned workflow.

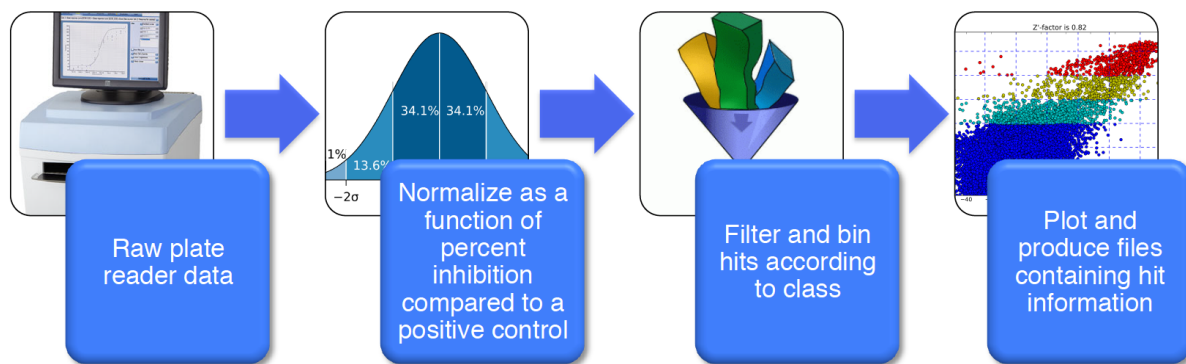


Figure 6.3. HAARP workflow diagram. Raw data files are read into HAARP and processed as comma separated files. Each plate within a given run is then assessed for effect response dynamic range of the positive and negative controls via calculating a Z' value. Data are normalized within each run if the Z' value is greater than or equal to 0.5 relative to a positive control. Positive hits are filtered and binned according to user-defined criteria. Compound libraries are queried to provide as much information as possible for each positive hit and outputted as comma separated files as well as diagnostic scatter plots. Further, the entire screen may be processed for submission to a publically curated database such as PubChem through the Harvard screening facility.

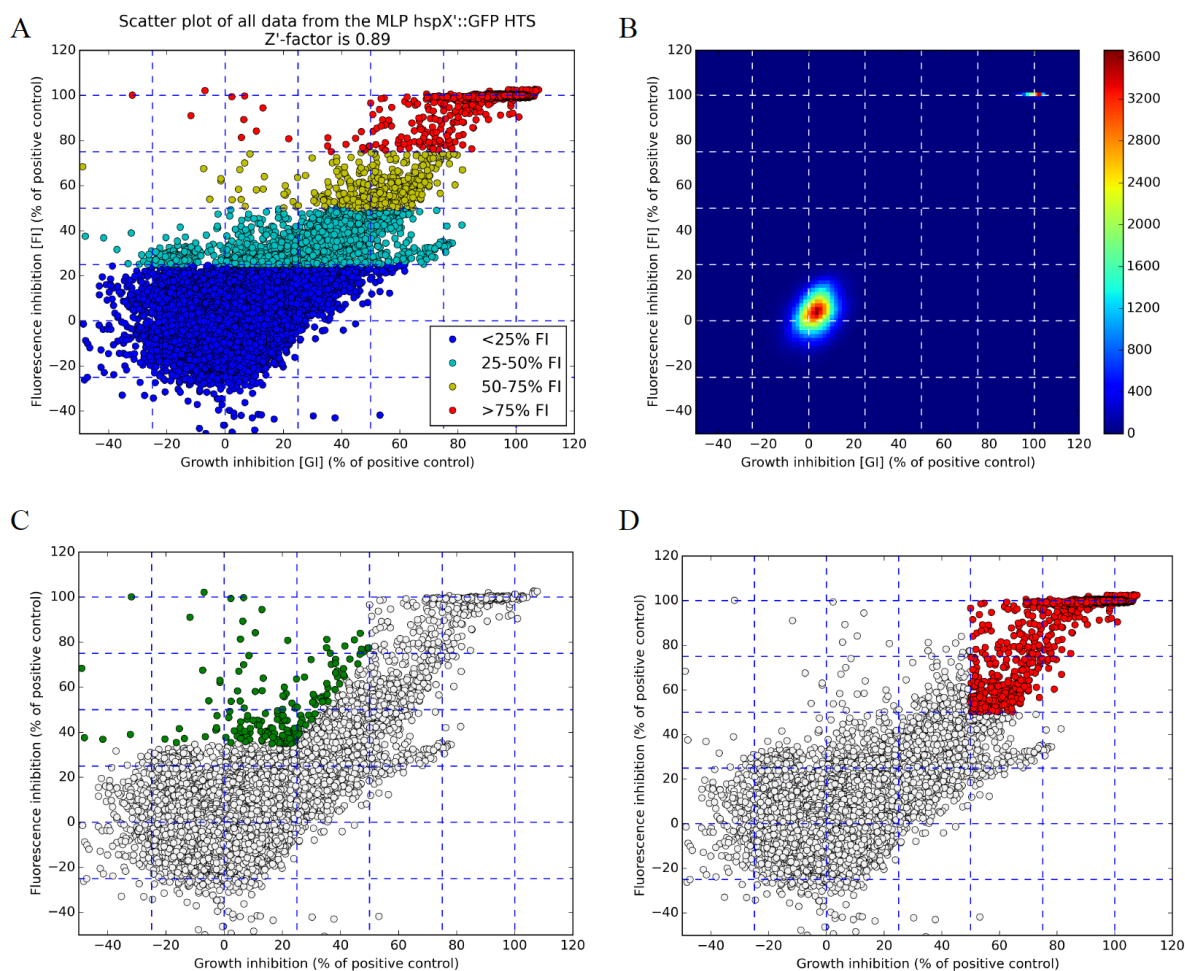


Figure 6.4. Examples of HTS screen-wide diagnostic scatter plots produced by HAARP. A) All compounds assayed and stratified by fluorescence inhibition (FI) as a percent inhibition relative to a positive control. B) Two-dimensional density plot of all compounds assayed. The coloration scale was determined based on default parameter topographical pixel density informed using the total number of experimental compounds that aggregate into a single pixel bin. Red indicates a high number and blue indicates a low number of compounds comprising the given bin. C) Positive hits that have been filtered as potential environmental sensing inhibitors (Class I). D) Positive hits that have been filtered and scored as putative general inhibitors of *Mycobacterium tuberculosis* growth (Class II).

Data normalization

The data normalization algorithm (Equation 6.5.) was developed to account for technical variability that may arise within each individual run in contrast to normalizing the data across the entire screening library. This methodology provides a more sensitive approach to identifying positive hits as well as affords the user the ability to rapidly identify and remove or filter runs that skew the overall data set due to systematic error. A measure of a high quality screen is the Z' factor (23). This value represents how large the effect response is between positive and negative controls, ranging from 0 to 1. If the value of Z' is greater than or equal to 0.5, the screen is considered to have an excellent dynamic range and able to adequately resolve positive hits. In an effort to control and sustain a large dynamic range, only plates with a Z' factor greater than or equal to 0.5 were factored into the average positive and negative control values for each set of plates within a specific run. Specifically, the mean positive and negative control values for fluorescence and growth (optical density; OD₅₉₅) are iteratively calculated as normalized percent inhibition for each assay plate within a given run and tested for the Z' value. If the value is greater than 0.5, the positive and negative control values are parsed and stored temporarily in a list data structure until the data from each plate within the run have been examined. Finally, the mean is calculated for the run and transferred to a global list data structure to be utilized later in the positive hit filtering procedure. Experimentally derived values for each of the test compounds were converted from raw fluorescence or optical density values to normalized percent inhibition based on the calculated Z' -informed positive and negative control values within the run.

$$NPI_{ijk} = \left\{ \frac{\beta_{ijk} - \bar{\mu}_{nk}}{\bar{\mu}_{nk} - \bar{\mu}_{pk}} \times 100 \mid \exists Z'_{jk} \geq 0.5; Z'_{jk} = 1 - \frac{3\sigma(\mu_{njk}) + 3\sigma(\mu_{pjk})}{\mu_{njk} - \mu_{pjk}} \right\}$$

Equation 6.5. Normalized percent inhibition algorithm. The normalized percent inhibition (NPI) for fluorescence or optical density was calculated by subtracting the mean of the negative controls within a run ($\bar{\mu}_{nk}$) from the measured experimental value (β), divided by the dynamic range and multiplied by 100. The mean of the positive and negative controls within the run ($\bar{\mu}_{nk}$, $\bar{\mu}_{pk}$) are determined if there exists at least one plate in the run with a Z' greater than or equal to 0.5. ijk subscripts represent the i th value in the j th plate within the k th run. σ represents the standard deviation from the mean.

Positive hit filtering

After data normalization, compounds that exhibit a specific fluorescence and growth inhibition profile were considered for binning into three separate classes of positive hits. All other hits that did not meet the criteria described below were discarded from further characterization by HAARP and stored in a global nested list data structure for subsequent preparation of the total dataset for submission to a public database (e.g. PubChem). The first class of hits (Class I) have greater than 35% fluorescence inhibition, growth that has not been greatly decreased, and at least a 1.5-fold selectivity fluorescence to growth inhibition ratio. These compounds may be directly or indirectly inhibiting the specific two-component regulatory system signaling (PhoPR or DosRST). The second class of hits (Class II) has greater than 50% fluorescence and growth inhibition. These compounds are likely general inhibitors of Mtb growth. The third class of hits (Class III) have exhibit less than 50% fluorescence inhibition, greater than 50% growth inhibition, and at least a 1.5-fold selectivity growth to fluorescence inhibition ratio. These compounds were specific to the screen seeking to identify inhibitors of

PhoPR-dependent signaling and may be stimulating reporter fluorescence when growth is slowed. Once a compound is determined to meet one of the three class criteria for further characterization, HAARP will retrieve additional information regarding the positive hit for more adequately informing the user about the compound in the final output. Each hit has the specific plate identification number, well location within the experimental assay plate, compound library stock plate identification, and compound name (if listed) appended. Finally, the collective information regarding the positive hit is then stored in a global nested list data structure until it is required for writing the output at the end of the analysis.

Results and Discussion

We successfully screened greater than 500,000 small molecules for inhibitors of Mtb adaptation during infection and identified several candidate compounds to follow-up for further biological characterization (Chapters 2, 3, and 5). With the massive amount of data generated from this endeavor, we implemented HAARP, a modular computational analysis approach to efficiently identify putative inhibitors. Using a subset of the total compounds screened, HAARP was capable of completely analyzing ~ 303,000 wells in 35 minutes on an off-the-shelf MacBook Pro (8 GB RAM, Intel i5 2.6 GHz quad-core processor). HAARP was primarily designed to operate on a personal computing platform but is capable of scaling to high performance-computing environments. Further, HAARP is a custom designed analysis suite to suit the specific needs of our HTS experiments; therefore the software could not adequately be benchmarked against other existing software.

REFERENCES

REFERENCES

1. **Goloseva O, Henderson R, Vaskin Y, Gabrielian A, Grekhov G, Nagarajan V, Oler AJ, Quinones M, Hurt D, Fursov M, Huyen Y.** 2014. Unipro UGENE NGS pipelines and components for variant calling, RNA-seq and ChIP-seq data analyses. *PeerJ* **2**:e644.
2. **Michalovova M, Kubat Z, Hobza R, Vyskot B, Kejnovsky E.** 2015. Fully automated pipeline for detection of sex linked genes using RNA-Seq data. *BMC Bioinformatics* **16**:78.
3. **D'Antonio M, D'Onorio De Meo P, Pallocca M, Picardi E, D'Erchia AM, Calogero RA, Castrignano T, Pesole G.** 2015. RAP: RNA-Seq Analysis Pipeline, a new cloud-based NGS web application. *BMC Genomics* **16**:S3.
4. **McClure R, Balasubramanian D, Sun Y, Bobrovskyy M, Sumby P, Genco CA, Vanderpool CK, Tjaden B.** 2013. Computational analysis of bacterial RNA-Seq data. *Nucleic Acids Res* **41**:e140.
5. **Tjaden B.** 2015. De novo assembly of bacterial transcriptomes from RNA-seq data. *Genome Biol* **16**:1.
6. **Kalari KR, Nair AA, Bhavsar JD, O'Brien DR, Davila JI, Bockol MA, Nie J, Tang X, Baheti S, Doughty JB, Middha S, Sicotte H, Thompson AE, Asmann YW, Kocher JP.** 2014. MAP-RSeq: Mayo Analysis Pipeline for RNA sequencing. *BMC Bioinformatics* **15**:224.
7. **Wang Y, Mehta G, Mayani R, Lu J, Souzaiaia T, Chen Y, Clark A, Yoon HJ, Wan L, Evgrafov OV, Knowles JA, Deelman E, Chen T.** 2011. RseqFlow: workflows for RNA-Seq data analysis. *Bioinformatics* **27**:2598-2600.
8. **Goncalves A, Tikhonov A, Brazma A, Kapushesky M.** 2011. A pipeline for RNA-seq data processing and quality assessment. *Bioinformatics* **27**:867-869.
9. **Habegger L, Shoner A, Gianoulis TA, Rozowsky J, Agarwal A, Snyder M, Gerstein M.** 2011. RSEQtools: a modular framework to analyze RNA-Seq data using compact, anonymized data summaries. *Bioinformatics* **27**:281-283.
10. **Qi J, Zhao F, Buboltz A, Schuster SC.** 2010. inGAP: an integrated next-generation genome analysis pipeline. *Bioinformatics* **26**:127-129.

11. **Forstner KU, Vogel J, Sharma CM.** 2014. READemption-a tool for the computational analysis of deep-sequencing-based transcriptome data. *Bioinformatics* **30**:3421-3423.
12. **Bolger AM, Lohse M, Usadel B.** 2014. Trimmomatic: a flexible trimmer for Illumina sequence data. *Bioinformatics* **30**:2114-2120.
13. **Anders S.** 2010. FastQC -
<http://www.bioinformatics.babraham.ac.uk/projects/fastqc/>.
<http://www.bioinformatics.babraham.ac.uk/projects/fastqc/>. Accessed
14. **Abuaita BH, Withey JH.** 2009. Bicarbonate Induces *Vibrio cholerae* virulence gene expression by enhancing ToxT activity. *Infect Immun* **77**:4111-4120.
15. **Anders S, Pyl PT, Huber W.** 2015. HTSeq--a Python framework to work with high-throughput sequencing data. *Bioinformatics* **31**:166-169.
16. **Robinson MD, McCarthy DJ, Smyth GK.** 2010. edgeR: a Bioconductor package for differential expression analysis of digital gene expression data. *Bioinformatics* **26**:139-140.
17. **Robinson MD, Oshlack A.** 2010. A scaling normalization method for differential expression analysis of RNA-seq data. *Genome Biol* **11**:R25.
18. **McCarthy DJ, Chen Y, Smyth GK.** 2012. Differential expression analysis of multifactor RNA-Seq experiments with respect to biological variation. *Nucleic Acids Res* **40**:4288-4297.
19. **Leek JT, Scharpf RB, Bravo HC, Simcha D, Langmead B, Johnson WE, Geman D, Baggerly K, Irizarry RA.** 2010. Tackling the widespread and critical impact of batch effects in high-throughput data. *Nat Rev Genet* **11**:733-739.
20. **Baker JJ, Johnson BK, Abramovitch RB.** 2014. Slow growth of *Mycobacterium tuberculosis* at acidic pH is regulated by *phoPR* and host-associated carbon sources. *Mol Microbiol* **94**:56-59.
21. **Gierlinski M, Cole C, Schofield P, Schurch NJ, Sherstnev A, Singh V, Wrobel N, Gharbi K, Simpson G, Owen-Hughes T, Blaxter M, Barton GJ.** 2015. Statistical models for RNA-seq data derived from a two-condition 48-replicate experiment. *Bioinformatics* **31**:3625-3630.
22. **Schurch NJ, Schofield P, Gierlinski M, Cole C, Sherstnev A, Singh V, Wrobel N, Gharbi K, Simpson GG, Owen-Hughes T, Blaxter M, Barton GJ.** 2015. Evaluation of

tools for differential gene expression analysis by RNA-seq on a 48 biological replicate experiment. ArXiv e-prints. **1505**(

23. **Zhang JH, Chung TD, Oldenburg KR.** 1999. A Simple Statistical Parameter for Use in Evaluation and Validation of High Throughput Screening Assays. *J Biomol Screen* **4**:67-73.

CHAPTER 7 – Conclusions

With the rise of antibiotic resistant *Mycobacterium tuberculosis* (Mtb), new strategies and targets are required to combat resistant infections. Mtb environmental sensing pathways and the associated physiological adaptations provide promise as candidates for developing novel therapeutics (Chapters 2 and 3). Inhibiting *in vivo* required targets or virulence factors provides several advantages over traditional antibiotic therapy, including reducing off-target effects against the resident microbiota and potentially lower selective pressure for resistance. Further, by disrupting Mtb virulence or adaptive physiologies, it is possible to make the pathogen more susceptible to antibiotic treatment (Chapter 5). Therefore, identification and characterization of inhibitors of environmental sensing pathways and adaptive physiologies can serve a dual purpose to the larger Mtb community: 1) provide therapeutic lead scaffolds and targets to follow-up for further development and 2) act as chemical probes for a deeper understanding of Mtb physiology during infection.

The Mtb two-component regulatory system (TCS) PhoPR has been studied extensively. However, the precise environmental signals remain to be biochemically defined. It is clear that PhoPR-regulated gene expression is induced at acidic pH *in vitro* and in acidified compartments *in vivo*, strongly suggesting that pH is a relevant cue sensed by this TCS. Further, Mtb lacking PhoPR are highly attenuated during infection, providing evidence that PhoPR-mediated pH-driven adaptation is required for Mtb pathogenesis. My research has taken a high-throughput screening approach to identify inhibitors of PhoPR-mediated pH-driven adaptation and identified a potential candidate compound for further development as an adjunct treatment for Mtb infections (Ethoxzalamide [ETZ], Chapter 3). Additionally, the discovery of the carbonic anhydrase (CA) inhibitor ETZ establishes a previously unrecognized link between carbon

dioxide, CA, pH-sensing, and PhoPR. Mtb encodes three CA enzymes and two (*Rv1284* and *Rv3588c*) are required for survival *in vivo* suggesting that the ability to respond to changes in carbon dioxide is required for growth during infection. I have proposed a model where the histidine kinase (HK) PhoR directly senses changes in pH through environmental fluctuations in carbon dioxide mediated by CA (Figure 3.7). A CA deficient strain of Mtb would be invaluable to show that CA is indeed the target of ETZ and required for PhoPR induction at acidic pH. Unfortunately, due to the redundancy and difficulty to make knockout mutants in Mtb, this work does not include characterization of a CA knockout, though this is actively being investigated in the laboratory. Further, despite the demonstration that ETZ inhibits Mtb CA (Figure 3.1. C) and no inhibition of PhoPR-signaling from an ETZ analog predicted to be deficient in binding the CA active site (Figure 4.3.), additional targets could exist that are targeted by ETZ. An approach that could be used to screen for additional factors that alleviate ETZ-mediated inhibition of PhoPR-signaling at acidic pH is through a genetic screen of Mtb possessing a plasmid with the promoter of the PhoPR-regulated gene *aprA* fused to an antibiotic resistance cassette (e.g. hygromycin) in the presence of ETZ. Predicted results include cells unable to circumvent inhibition of ETZ would be antibiotic sensitive, while bacteria possessing a mutation that gives Mtb resistance to ETZ-mediated inhibition of PhoPR-signaling would be antibiotic resistant. Whole genome sequencing could be used to identify ETZ resistant mutations. Additional studies would be required to validate the mutation (e.g. gain- or loss-of-resistance complementation). Further, with this approach it may be possible to discover additional regulators of PhoPR and *aprA* expression at acidic pH.

Characterization of the mechanism PhoR uses to sense environmental pH would provide the first definitive study of a signal directly sensed by this HK. I have proposed that histidine

residues conserved only in the slow-growing pathogenic Mtb complex PhoR sensor loop may play a role in directly sensing protons (Figures 3.7., 4.5., 4.6.). Specifically, a His72Pro substitution exhibits pH-dependent activity in induction of PhoPR-regulated genes at acidic pH. However, the result is mild and it is possible that additional His residues (e.g. His114) need to be substituted in combination with His72 for a more dramatic reduction in PhoPR-regulated gene expression at acidic pH. This represents a targeted approach, but untargeted approaches also exist to define amino acids required for sensing acidic pH. Deep mutational scanning is an emerging approach to define regions of proteins that contribute to a phenotype of interest (1). In the case of PhoPR sensing acidic pH, several regions could be targeted: the sensor loop of PhoR, full length PhoR, and full length PhoP. The general idea of deep mutational scanning is to generate a library of mutated DNA sequences through either error-prone PCR or site-directed mutagenesis. Then, this library is ligated into an expression vector system, followed by transformation of the library into the desired system (e.g. Mtb). Next, mutants are selected that disrupt the phenotype of interest. For the purposes of understanding how Mtb senses acidic pH through PhoPR, the expression library could be generated by mutagenizing a copy of PhoPR expressed by the native promoter on an integrative plasmid. The mutagenized plasmid library would be transformed into the PhoPR knockout strain of Mtb that contains a hygromycin resistance cassette driven by the *aprA* promoter. Transformants that are hygromycin sensitive at acidic pH could contain mutations in key regions of PhoPR required for sensing acidic pH. To define which mutated copies of PhoPR are lost during selection, next generation sequencing approaches can be utilized to sequence the pre- and post-selection pools. Finally, using software to predict how each mutation affects transcription, protein structure, etc. can be used to categorize mutations/regions of interest for further follow-up. Ultimately, to show whether PhoR directly

responds to protons, the HK will need to be reconstituted in vesicles with an acidic internal pH and monitor ATPase or phosphotransfer activity in response to changes in pH (2). This approach is currently underway in the laboratory and could benefit from the deep mutational scanning method to test specific mutations.

Data intensive biology is becoming increasingly common and easy-to-use software is required to allow widespread use of methods that leverage these “big data” approaches. I have developed a turn-key software package that can rapidly analyze RNA sequencing (RNA-seq) experiments and produce relevant output to determine differentially expressed genes under a specific condition (Chapter 6). This software has enabled our lab and others to define differentially expressed genes under an experimental treatment that has guided additional follow-up experiments to investigate specific hypotheses. It is possible that another version of this software will be required soon to incorporate these new long read methods. Specifically, technologies like the Oxford Nanopore and Pacific Biosciences sequencing methods will revolutionize microbial pathogenesis, as we will be able to sequence and assemble sequences in our own laboratory in the case of the Oxford Nanopore. Further, these technologies will allow real-time monitoring of an outbreak and could be applicable for Mtb drug resistance surveillance. Though these technologies can rapidly produce high quality sequences, it will be the software that is required to make sense of the data and guide researchers and epidemiologists for further follow-up studies.

A deeper understanding of Mtb pH-dependent adaptations will provide new targets for developing therapeutics. The discovery that PH036 disrupts thiol pool maintenance, promoting a reduced cytoplasm at acidic pH builds on previous work suggesting that Mtb encounters reductive stress at low pH (3). Together, these data suggest that an imbalance in the redox pool at

low pH will potentially sensitize Mtb to oxidative killing. In contrast, Mtb treated with PH036 at neutral pH does deplete thiol pools, but to a lesser degree, suggesting that alternative metabolism is available to Mtb at pH 7.0 and restricted at acidic pH. Additionally, it has been suggested that the catalase/peroxidase *katG* also exhibits NADH oxidase activity (4). Indeed, at both neutral and acidic pH, *katG* is upregulated in PH036 treated cultures, suggesting that Mtb may be attempting to balance its redox pools through oxidation of reducing equivalents. However, this process also can generate hydrogen peroxide that may be particularly detrimental to Mtb at acidic pH owing to enhanced metabolic stress from loss of thiol pools when treated with PH036 (5). The normal thiol stress response has been attributed to *sigH* (6). PH036 treated cultures induce the *sigH* regulon, including cysteine synthesis and thioredoxin reductase. Both systems are used to defend against oxidative stress (7, 8). However, each system also contains a moiety that is likely targeted by PH036. To elucidate the biochemical mechanism and additional physiological changes that occur at acidic pH when treated with PH036, we will need to take several approaches. A key experiment would be to identify whether PH036 modified sulfhydryls can be re-reduced through exogenous addition of a reductant such as glutathione or if addition of the low molecular weight thiol can aid in recycling oxidized thiols. The predicted result would be that Mtb would not be as sensitive to oxidative stress/PH036 at acidic pH. Further, it will be necessary to define whether *katG* is contributing to oxidative damage. This could be accomplished by treating a *katG* mutant and the complemented strain in a dose-dependent manner with PH036 and observe whether the mutant is less sensitive to PH036. Finally, to define the chemistry of PH036, it will be necessary to modify the two nitrogens on the pyrimidine ring (Chapter 5). This is because they act as additional electron withdrawing groups to allow for the thiolate anion to attack the C-2 carbon. A predicted result would be that loss of the nitrogens

would make the methylsulfone a poorer leaving group. Taken together, these experiments can provide insight for additional studies to define the necessity of maintaining redox homeostasis through thiol pools in Mtb at acidic pH.

Understanding how Mtb senses and responds to host cues, such as acidic pH, is of paramount importance to develop new targets and tactics to treat Mtb infections. I have demonstrated that the PhoPR TCS can be inhibited by small molecules and defined a previously unrecognized link between carbonic anhydrase and PhoPR. Further, Mtb's ability to maintain redox homeostasis at acidic pH through its thiol pools is critical for survival and resistance to reactive oxygen species (Chapter 5). This work has furthered our understanding of PhoPR-mediated pH-driven adaptation and Mtb physiological requirements for survival at acidic pH, providing a foundation for future studies.

REFERENCES

REFERENCES

1. **Fowler DM, Stephany JJ, Fields S.** 2014. Measuring the activity of protein variants on a large scale using deep mutational scanning. *Nature Protocols* **9**:2267-2284.
2. **Prost LR, Daley ME, Le Sage V, Bader MW, Le Moual H, Klevit RE, Miller SI.** 2007. Activation of the bacterial sensor kinase PhoQ by acidic pH. *Mol Cell* **26**:165-174.
3. **Baker JJ, Johnson BK, Abramovitch RB.** 2014. Slow growth of *Mycobacterium tuberculosis* at acidic pH is regulated by phoPR and host-associated carbon sources. *Mol Microbiol* **94**:56-59.
4. **Singh R, Wiseman B, Deemagarn T, Donald LJ, Duckworth HW, Carpena X, Fita I, Loewen PC.** 2004. Catalase-peroxidases (KatG) exhibit NADH oxidase activity. *J Biol Chem* **279**:43098-43106.
5. **Farhana A, Guidry L, Srivastava A, Singh A, Hondalus MK, Steyn AJC.** 2010. Reductive Stress in Microbes: Implications for Understanding *Mycobacterium tuberculosis* Disease and Persistence. *Advances in Microbial Physiology*, Vol 57 **57**:43-117.
6. **Manganelli R, Voskuil MI, Schoolnik GK, Dubnau E, Gomez M, Smith I.** 2002. Role of the extracytoplasmic-function sigma factor sigma(H) in *Mycobacterium tuberculosis* global gene expression. *Mol Microbiol* **45**:365-374.
7. **Harbut MB, Vilcheze C, Luo X, Hensler ME, Guo H, Yang B, Chatterjee AK, Nizet V, Jacobs WR, Jr., Schultz PG, Wang F.** 2015. Auranofin exerts broad-spectrum bactericidal activities by targeting thiol-redox homeostasis. *Proc Natl Acad Sci U S A* **112**:4453-4458.
8. **Hatzios SK, Bertozzi CR.** 2011. The regulation of sulfur metabolism in *Mycobacterium tuberculosis*. *PLoS Pathog* **7**:e1002036.